TESIS DE LA UNIVERSIDAD DE ZARAGOZA
2024
355

Giuseppe Lattanzio

La deficiencia de hierro en plantas: un enfoque proteómico y basado en nuevas tecnologías

Director/es
López Millán, Ana Flor
Rodríguez Celma, Jorge

ISSN 2254-7606

Prensas de la Universidad
Universidad Zaragoza

Universidad de Zaragoza
Servicio de Publicaciones

ISSN 2254-7606

Universidad Zaragoza
1542

Tesis Doctoral

LA DEFICIENCIA DE HIERRO EN PLANTAS: UN ENFOQUE PROTEÓMICO Y BASADO EN NUEVAS TECNOLOGÍAS

Autor

Giuseppe Lattanzio

Director/es

López Millán, Ana Flor
Rodríguez Celma, Jorge

UNIVERSIDAD DE ZARAGOZA
Escuela de Doctorado

Programa de Doctorado en Bioquímica y Biología Molecular

2024

Universidad Zaragoza
1542

Tesis Doctoral

LA DEFICIENCIA DE HIERRO EN PLANTAS: UN ENFOQUE PROTEÓMICO Y BASADO EN NUEVAS TECNOLOGIAS

Autor

Giuseppe Lattanzio

Director/es

Jorge Rodríguez Celma
Ana Flor López Millán

UNIVERSIDAD DE ZARAGOZA
Escuela de Doctorado

Programa de Doctorado en Bioquímica y Biología Molecular

2023

CONSEJO SUPERIOR DE INVESTIGACIONES CIENTÍFICAS (CSIC)
ESTACIÓN EXPERIMENTAL DE AULA DEI

Departamento de Nutrición Vegetal

Grupo de Fisiología de Estrés Abiótico en Plantas

Tesis Doctoral:

La deficiencia de hierro en plantas: un enfoque proteómico y basado en nuevas tecnologías

Memoria presentada por **Giuseppe Lattanzio**, Licenciado en Química y Tecnología Farmacéuticas, para optar al grado de Doctor en Ciencias.

Zaragoza, diciembre de 2023

AUTORIZACIÓN DE LOS DIRECTORES

El Dr. JORGE RODRÍGUEZ CELMA, Doctor en Ciencias y Profesor de Investigación del CSIC, y la Dra. ANA FLOR LÓPEZ MILLÁN, Doctora en Ciencias y Científica Titular del CSIC en situación de excedencia,

AUTORIZAN

La presentación de la Tesis Doctoral titulada "**LA DEFICIENCIA DE HIERRO EN PLANTAS: UN ENFOQUE PROTEÓMICO Y BASADO EN NUEVAS TECNOLOGIAS**", elaborada por el Licenciado en Química y Tecnología Farmacéuticas D. GIUSEPPE LATTANZIO, para optar al Grado de Doctor por la Universidad de Zaragoza, y certifican que ha sido realizada bajo su dirección en la Estación Experimental de Aula Dei del Consejo Superior de Investigaciones Científicas (EEAD-CSIC).

Y para que conste a los efectos oportunos, expiden la presente autorización.

Zaragoza, diciembre de 2023

Fdo. Jorge Rodriguez Celma

Fdo. Ana Flor López Millán

Financiación

Los trabajos incluidos en esta Tesis Doctoral fueron financiados por los proyectos de investigación del Ministerio de Economía y Competitividad (MINECO; AGL2011-25379, AGL2012-31988 y AGL2013-42175-R, co-financiados con FEDER), y el Grupo Consolidado de la Diputación General de Aragón (grupo A03).

La Tesis de Giuseppe Lattanzio ha sido financiada por una beca-contrato FPI del MINECO (BES-2008-005834).

Agradecimientos

Todo el mundo dice que la redacción de una tesis doctoral no es el fruto del esfuerzo de una única persona. Lo había leído muchas veces y me parecía una frase un poco retórica, pero es totalmente cierto.

Personalmente, esta tesis no es solo un registro de experimentos y de análisis, sino un testimonio de mi experiencia intelectual y emocional a lo largo de más de una "década" desde mi llegada al CSIC de "Aula Dei".

La "gestación" de este proyecto, por circunstancias de la vida, ha sido extensa y se han ido entrelazando nuevos caminos a lo largo de su recorrido, y unos cuantos años después estoy aquí sentado escribiendo mis "agradecimientos".

Nunca olvidaré aquel agosto del 2008, cuando Zaragoza con más de 40ºC celebraba su Expo y yo esperaba el autobús 28 para ir por primera vez a "Aula Dei" a sembrar la semilla de mi tesis.

Muchas cosas han pasado desde entonces marcando el rumbo de mi vida actual. Siempre recordaré esta etapa tan importante de mi vida.

Agradezco todos aquellos, que sin su ayuda y esfuerzos este proyecto seguirá en mi cajón de cosas pendientes.

La primera persona a quien debo todo esto es a mi mentor, mi "director" de tesis el Prof. Javier Abadía quien fue en todo momento una guía, un modelo a seguir y donde el término "jefe" encuentra su reencarnación. Javier siempre serás "mi jefe", con tu forma de ser tan cercana, tus sabios consejos y tus palabras de apoyo. Siempre has sabido estar ahí, sobre todo en mis momentos de más frustración, recuerdo cuando me estuve peleando, casi un año, para poner a punto el "Nano y Trampa", que sin ellos esta tesis tampoco existiría. Te estaré eternamente agradecido, por cada llamada donde me decías "venga acabala…que te falta solo escribirla" y puedo asegurar que sin ti este trabajo no existiría.

La segunda persona a quien me gustaría agradecer, es a mi "codirectora" la Dra. Ana Flor Lopez-Millan. He tenido la suerte de poder trabajar con ella, siempre guiándome y aconsejándome incluso desde la larga distancia.

Realmente me he sentido un "becario" afortunado y feliz, por haber podido formar parte del grupo *Plant Stress Physiology*. Siempre recordaré la sabiduría de la Profa. Anunciación Abadía (Monona), y la Técnico Aurora Poc, cuerpo y alma del laboratorio "Abadía", y a los demás miembros del grupo, el Dr. Fermín Morales y la Dra Ana Álvarez. Gracias por vuestros consejos.

Gracias a mis compañeros de “proteínas”, mi nuevo “director” el Dr. Jorge Rodríguez-Celma y el Dr. Elain Gutiérrez-Carbonell. Jorge, que fue el primero en explicarme como hacer un gel en condiciones y Elain a quien le salían mucho mejor que a mí. Sin olvidarme del Dr. Rubén Rellán-Álvarez fuente inagotable de inquietudes científicas. Sin ellos los cimientos de esta tesis no existirían. ¡Un agradecimiento extra a Jorge por ayudarme a dar forma a este trabajo…mil gracias!!!

Un gracias a todas las personas que he conocido a través de Aula Dei, que han sido muchas, y que han tenido directa o indirectamente un papel importante para mí. Me gustaría dar un agradecimiento especial, al Dr. Manuel Matamoros y a mi querido “George” el Dr. Jorge Álvaro-Fuentes, sabios amigos que han estado presentes en mi vida zaragozana.

Gracias a mi tesis, además de “Aula Dei”, he tenido la suerte de conocer nuevos laboratorios. Estas estancias han sido lo mejor que me ha pasado a nivel profesional. Parte importante de esta tesis es fruto de mi etapa en Alemania en el *Leibniz Institute of Plant Genetics and Crop Plant Research* (IPK) de Gatersleben. Agradezco al Dr. Hans-Peter Mock y al laboratorio de *Applied Biochemistry* con una mención especial a la Dra. Andrea Matros y a la Dra. Manuela Peukert por haberme introducido en el mundo del “MALDI *Imaging*”. Fueron 6 meses muy formativos e intensos, donde he tenido la posibilidad de aprender muchísimo. Un gracias a tod@s mis amig@s italianos e hispanos del IPK que entre cervezas y charlas amenizaron mi estancia.

Sobre mi breve paréntesis en Australia, agradezco al Prof. Paul Haynes en la *Macquarie University* de Sídney por haberme dado la oportunidad de conocer su laboratorio y por supuesto agradecer a mi “jedi proteómico” el Dr. Mehdi Mirzaei. Además, pude disfrutar de ese lugar único como es Australia, que jamás en mi vida pensé poder llegar a visitar.

A mi familia aragonesa, a Lourdes y Andrés, gracias por estar ahí cuando os necesitamos. A mis dos hijos Nico y Claudia, con la esperanza que este trabajo sea de alguna manera un ejemplo en vuestras vidas. También doy las gracias a mis queridos amigos Susana y Luis siempre presentes y por haber sido desde el principio mi punto de referencia y mi apoyo en todos estos años.

Me gustaría dedicar esta tesis a mi padre Francesco, faro de mi vida y a mi atenta madre Antonietta quien me enseñaron el valor de las cosas y que con esfuerzo y sacrificio se pueden alcanzar nuestras metas. Y *dulcis in fundo* agradecer las dos personas más importantes de mi vida, a mi paciente hermana Francesca siempre aconsejándome y que sin ella no habría ni empezado a escribir la primera página de esta tesis, y a mi dulce pelirroja Raquel, el amor de mi vida y la parte racional de mi ser, hartándose de repetirme a lo Jennifer López “…y la tesis pa cuándo?”. Sin ella no estaría aquí sentado escribiendo estas palabras.

Gracias a tod@s!

A mi dulce pelirroja, a mis padres y a mi paciente hermana

A la memoria de mi querido mentor, Javier, quien fue mi guía, una fuente inagotable de inspiración y mi mayor apoyo a lo largo de los años

Suceden cosas que son como preguntas. Pasa un minuto, o tal vez años, y después la vida responde.

Alessandro Baricco (Tierra de cristal)

Abreviaturas

1-DE	One-dimensional electrophoresis
2-DE	Two-dimensional electrophoresis
BLAST	Basic Local Alignment Search Tool
CCD	Charge-coupled device
CHAPS	3-[(3-cholamidopropyl)dimethylammonio]-1-propanesulfonate
CHCA	α-Cyano-4-hydroxycinnamic acid
CHCA	α-Cyano-4-hydroxycinnamic acid
CID	Collision-induced dissociation
Da	Dalton
DAP	Days after pollination
DHB	2,5-Dihydroxybenzoic acid
DMAN	1,8-Bis (dimethylamino) naphthalene
DTCB	2-((2E)-3- (4-tert-butylphenyl)-2-methylprop-2-enylidene) malononitrile
DTT	Dithiothreitol
ESI	Electrospray ionization
Ferene	3-(2-pyridyl)-5,6-bis (2-[5-furylsulfonic acid])-1,2,4-triazine disodium salt
GC-MS	Gas chromatography-mass spectrometry
GO	Gene Ontology
HCCA	α-Cyano-4-hydroxycinnamic acid
HPLC	High-performance liquid chromatography
IEF	Isoelectric focusing
IMAC	Immobilized metal affinity chromatography
IMS	Imaging mass spectrometry
IPG	Immobilized pH gradient
ITO	Indium tin oxide
LC-MS	Liquid chromatography-mass spectrometry
m/z	Mass/charge
MALDI	Matrix-assisted laser desorption/ionization
MALDI-MSI	MALDI Mass spectrometry Imaging
MS	Mass spectrometry
MS/MS	Tandem mass spectrometry
MSI	Mass spectrometry imaging
nESI	Nano electrospray ionization
nHPLC	Nano high-performance liquid chromatography
nLC	Nano liquid chromatography
OCT	Optimal cutting temperature
PAGE	Polyacrylamide gel electrophoresis

PCA	Principal component analysis
PMSF	Phenylmethylsulfonyl fluoride
PVDF	Polyvinylidene Fluoride
Py-GC-MS	Pyrolysis Gas Chromatography Mass Spectrometry
SDS	Sodium dodecyl sulfate
SDS-PAGE	Sodium dodecyl sulfate polyacrylamide gel electrophoresis
ß-DDM	N-Dodecyl-Beta-D-Maltoside
TFA	Trifluoroacetic acid
TOF	Time of flight

ÍNDICE

RESUMEN

El objetivo general de esta tesis doctoral es incrementar el conocimiento acerca de la homeostasis del hierro (Fe) en relación con la nutrición vegetal desde un punto de vista proteómico. El estudio pretende poner un énfasis particular en los cambios inducidos por el Fe en diferentes especies vegetales utilizadas como modelo [*Lupinus texensis*, *Medicago truncatula* y un patrón híbrido de *Prunus* (*P.dulcis x P. pérsica*)] y en distintos sub-proteomas (savia de floema, tallo y raíz). Este enfoque ha permitido obtener una visión global sobre las complejas adaptaciones metabólicas implicadas en la nutrición férrica en plantas. El trabajo pretende además utilizar nuevas herramientas tecnológicas como el *MALDI- Mass Spectrometry Imaging* (MALDI-MSI), un potente instrumento analítico muy utilizado en biomedicina, pero aún poco usado en el mundo vegetal. Esta herramienta nos ha permitido ahondar en la caracterización anatomo-morfológica, analizando las distribuciones espaciales de pequeñas moléculas y proteínas en diferentes tejidos de las plantas, abriendo así futuros estudios relacionados con la nutrición vegetal, tanto a nivel del proteoma como de los procesos metabólicos implicados en el transporte y la absorción de nutrientes.

Este tipo de aproximaciones ayudará a desarrollar mejores sistemas agrícolas basados en el conocimiento de las posibles alteraciones metabólicas producidas por estreses nutricionales en los cultivos, evitando por lo tanto perdidas de productividad y calidad, incrementando el conocimiento global existente sobre la hemostasis de este metal en las plantas.

Se plantearon los siguientes objetivos específicos: 1- Optimización de diferentes parámetros analíticos para el estudio de la distribución espacial de pequeñas moléculas en diferentes tejidos funcionales vegetales, utilizando la técnica del MALDI-*Mass Spectrometry Imaging* (MALDI-MSI). 2- Caracterización de los cambios producidos por la deficiencia y el reabastecimiento de Fe en el perfil proteico de la raíz de un patrón híbrido melocotonero/almendro (*P. dulcis* × *P. persica*). 3- Caracterización del proteoma de la savia del floema de *Lupinus texensis* y estudio de las proteínas implicadas en la unión con el Fe y el Zn. 4- Caracterización de los efectos de la deficiencia de Fe en los perfiles proteicos y la composición de lignina del tallo de *Medicago truncatula* en ausencia o presencia de carbonato cálcico en el medio de cultivo.

The general aim of this doctoral thesis is to increase understanding of iron (Fe) homeostasis in relation to plant nutrition from a proteomic perspective. The study aims to emphasize the changes induced by Fe in different plant species used as models [*Lupinus texensis*, *Medicago truncatula*, and a Prunus hybrid rootstock (*P.dulcis x P. persica*)] and in different sub-proteomes (phloem sap, stem, and root). This approach has provided a comprehensive view of the complex metabolic adaptations involved in ferric nutrition in plants. Additionally, the work aims to utilize novel technological tools such as MALDI-Mass Spectrometry Imaging (MALDI-MSI), a powerful analytical instrument widely used in biomedicine but still underutilized in the plant world. This tool has allowed us to deepen into the anatomical-morphological characterization, analyzing spatial distributions of small molecules and proteins in different plant tissues, thus opening up future studies related to plant nutrition, both at the proteome level and in the metabolic processes involved in nutrient transport and absorption.

Such approaches will help develop better agricultural systems based on understanding the potential metabolic alterations caused by nutritional stresses in crops, thereby avoiding productivity and quality losses, and increasing the overall knowledge of metal homeostasis in plants.

The following specific objectives were proposed: 1- Optimization of different analytical parameters for studying the spatial distribution of small molecules in different functional plant tissues using the MALDI-Mass Spectrometry Imaging (MALDI-MSI) technique. 2- Characterization of the changes produced by Fe deficiency and Fe resupply in the protein profile of the root of a peach-almond hybrid rootstock (*P. dulcis* × *P. persica*). 3- Characterization of the phloem sap proteome of *Lupinus texensis* and study of the proteins involved in binding with Fe and Zn. 4- Characterization of the effects of Fe deficiency on the proteomic profiles and lignin composition of the stem of *Medicago truncatula* in the absence or presence of calcium carbonate in the culture medium.

Capítulo 1

INTRODUCCIÓN

1.1. Prologo

La génesis de esta tesis doctoral se remonta al año 2008, cuando tuve la fortuna de iniciar mi trayecto en el seno de la Estación Experimental de Aula Dei (EEAD-CSISC) con una beca doctoral en el laboratorio del Profesor Javier Abadía Bayona.

En aquel entonces, la homeostasis de metales y la fisiología vegetal eran un territorio inexplorado para mí, y al mismo tiempo un desafío apasionante que ansiaba abordar. Mi formación académica en Química y Tecnologías Farmacéuticas, adquirida en Italia, sentaron las bases de esta travesía, adentrándome en los secretos de la relación entre las plantas y las proteínas mediante la fascinante lente de la proteómica y de la espectrometría de masas. A lo largo de este proceso investigador, atravesado por momentos de incertidumbres y de avances, he enfrentado innumerables desafíos, llevándome a explorar no solo la complejidad de la proteómica vegetal y las múltiples facetas de la espectrometría de masas, sino también a sumergirme en una amalgama de culturas científicas en estancias internacionales en centros de investigación en Alemania y Australia. Estas experiencias enriquecieron mis perspectivas, ampliando y reforzando mi compromiso con la investigación y la pasión por el conocimiento.

Un punto de inflexión crucial ocurrió en 2013, cuando mi formación y conocimientos adquiridos me condujeron a desempeñar un puesto de técnico especializado en una unidad de proteómica en Zaragoza. Este nuevo camino fue un giro significativo en mi trayectoria y me brindó la oportunidad de consolidar y aplicar mis conocimientos en este campo prometedor. Sin embargo, este giro también alargó la duración de la tesis, ya que equilibrar las demandas profesionales y académicas resultó un reto en sí mismo.

Desde la finalización de la parte experimental de esta tesis, hace ya una década, el mundo de la espectrometría de masas y la proteómica vegetal han experimentado transformaciones asombrosas. La espectrometría de masas, que en ese entonces se consideraba ya una técnica avanzada, ha evolucionado a pasos agigantados, proporcionando herramientas más precisas y potentes para analizar los complejos perfiles proteicos en las plantas. Este desarrollo ha ampliado nuestro entendimiento de la fisiología vegetal y la respuesta de las plantas a diversos estímulos y condiciones ambientales, sentando las bases necesarias para contribuir a la mejora de cultivos, la comprensión de sus respuestas a estrés ambiental y la búsqueda de soluciones sostenibles en la agricultura.

Esta tesis, aunque realizada hace una década, sigue siendo relevante en el contexto de estos avances y espero que este prólogo sirva como un puente entre el pasado y el presente en la investigación de proteómica vegetal. Esta tesis no es solo una colección de datos, es un testimonio

de una travesía intelectual y emocional, y ha sido moldeada por la colaboración, el apoyo y la inspiración de colegas y de mi querido mentor a lo largo de estos años.

Por lo tanto, invito al lector de tener en cuenta estos registros de experimentos y de análisis, leyéndolo con un enfoque crítico, con la pretensión de que este trabajo pueda ayudar a profundizar en la comprensión de las homeostasis de metales en plantas, confiando en que aporte un pequeño granito de arena en el mundo de la proteómica vegetal.

1.2. La proteómica: descifrando el lenguaje de las proteínas

La proteómica es un campo científico interdisciplinario que se centra en el estudio y análisis de las proteínas presentes en un sistema biológico específico (Aizat and Hassan, 2018). Las proteínas son moléculas fundamentales en la biología, cumpliendo una variedad de funciones cruciales en el organismo. La proteómica busca comprender la estructura, función y expresión de todas las proteínas en un sistema biológico dado, así como sus interacciones y modificaciones (Aslam *et al.*, 2017). Se podría decir que la proteómica es el complemento de la genómica (Tyers and Mann, 2003), ya que se centra en la identificación, cuantificación, caracterización y análisis funcional de las proteínas, que son los productos finales de la información genética contenida en el ADN (Peng and Gygi, 2001; Tyers and Mann, 2003). Esta disciplina es esencial para comprender la complejidad de los sistemas biológicos y ha revolucionado la investigación en biología y medicina en las últimas décadas (Al-Amrani *et al.*, 2021).

Los orígenes de la proteómica se remontan a la década de 1970, cuando se desarrollaron las técnicas de electroforesis bidimensional y la espectrometría de masas (Pandey and Mann, 2000). Estos avances tecnológicos permitieron a los científicos separar y analizar una gran cantidad de proteínas de manera eficiente. Sin embargo, la proteómica como campo consolidado comenzó a tomar forma en la década de 1990, con la creación de bases de datos de secuencias proteicas y el desarrollo de instrumentos más sofisticados para el análisis de proteínas (Williams *et al.*, 2014; Humphery-Smith, 2015). El término "proteómica" se acuñó por primera vez en 1994 por Marc Wilkins, un científico australiano, para describir esta nueva disciplina que se centraba en el estudio global de las proteínas (Wasinger *et al.*, 1995; Wilkins *et al.*, 1996). Desde entonces, la proteómica ha evolucionado rápidamente y se ha convertido en una herramienta fundamental para una amplia gama de aplicaciones en biología y medicina (Shah and Misra, 2011).

El objetivo principal de la proteómica es comprender cómo las proteínas interactúan entre sí y con otros componentes celulares para llevar a cabo las funciones biológicas. Esto implica la identificación y caracterización de proteínas, la determinación de sus niveles de expresión, la detección de modificaciones post-traduccionales y la elucidación de sus interacciones (Peng and Gygi, 2001). Para lograr esto, se utilizan diversas técnicas, como la espectrometría de masas, la cromatografía líquida y la electroforesis bidimensional, entre otras.

La proteómica desempeña un papel fundamental en la investigación. Por ejemplo, en la medicina personalizada, permite identificar biomarcadores que pueden usarse para diagnosticar enfermedades, predecir la respuesta de un paciente a un tratamiento específico y monitorizar la progresión de una enfermedad. Además, la proteómica también se utiliza en la investigación de enfermedades complejas como el cáncer, la diabetes y las enfermedades neurodegenerativas,

contribuyendo a la identificación de dianas terapéuticas potenciales (Husi and Albalat, 2014). En la agricultura y la biotecnología, la proteómica se utiliza para mejorar la producción de cultivos y el desarrollo de organismos genéticamente modificados. También desempeña un papel importante en la investigación de alimentos, ayudando a garantizar la seguridad y la calidad de los productos alimentarios.

En resumen, la proteómica es una disciplina científica que se centra en el estudio integral de las proteínas y desempeña un papel crucial en la comprensión de los sistemas biológicos, la medicina, la agricultura y muchas otras áreas. Gracias a avances tecnológicos constantes (Aebersold, Nature and 2003; Thikekar *et al.*, 2023) y a la colaboración entre investigadores de diferentes disciplinas, la proteómica sigue evolucionando y revelando secretos cada vez más profundos sobre la biología y la salud humanas.

1.2.1. La proteómica vegetal

Las proteínas desempeñan un papel fundamental dentro de los procesos biológicos de las plantas y poder comprender su composición y estudiar sus funciones tiene un enorme potencial tanto a nivel de la investigación científicas como agrícolas, esenciales para una variedad de aplicaciones (López-Millán *et al.*, 2013a).

Una de las aplicaciones más notables de la proteómica vegetal es la identificación y caracterización de proteínas involucradas en la respuesta de las plantas al estrés abiótico y biótico (Kaur *et al.*, 2021; Halder *et al.*, 2022). Esto incluye la exposición a condiciones adversas como sequía, salinidad, temperaturas extremas y patógenos. Al identificar las proteínas que se expresan o se regulan en respuesta a estos factores, los científicos pueden desarrollar estrategias para mejorar la resistencia de las plantas a estas condiciones y, por lo tanto, aumentar la productividad agrícola (Zhang *et al.*, 2022). Otra aplicación importante de la proteómica vegetal es la mejora de la calidad nutricional de los cultivos. Mediante el análisis de las proteínas presentes en diferentes variedades de plantas, los investigadores pueden identificar aquellas relacionadas con la acumulación de nutrientes esenciales como vitaminas, minerales y proteínas de alto valor nutricional. Esto ha llevado al desarrollo de cultivos biofortificados que son más ricos en nutrientes y pueden ayudar a abordar deficiencias nutricionales en las poblaciones humanas (Garg *et al.*, 2018; Jorrin Novo, 2021). Además de las numerosas aplicaciones agrícolas, los estudios proteómicos en vegetales también son esenciales en la investigación de la biología vegetal básica (Carpentler *et al.*, 2008). Estos estudios han permitido la identificación de proteínas implicadas en procesos fundamentales, como la fotosíntesis, la respiración, el desarrollo de órganos, la senescencia y la regulación del crecimiento.

Las técnicas utilizadas en proteómica vegetal incluyen la electroforesis bidimensional, la espectrometría de masas y la espectroscopía de resonancia magnética nuclear, entre otras. Estas herramientas han permitido a los científicos realizar análisis a gran escala de las proteínas vegetales, identificar modificaciones post-traduccionales, como la fosforilación y la glicosilación, y cuantificar las diferencias en la expresión de proteínas en diferentes condiciones experimentales (Jorrín-Novo *et al.*, 2015; Jorrin Novo, 2021).

La homeostasis de metales es un aspecto crítico de la fisiología vegetal, ya que los metales desempeñan un papel vital en una serie de procesos biológicos (Bashir *et al.*, 2016). La aplicación de la proteómica en este contexto ha permitido la identificación y caracterización de proteínas clave relacionadas con la absorción, transporte, almacenamiento y regulación de la homeostasis del hierro en las plantas (López-Millán *et al.*, 2013). Estos cambios proteómicos también proporcionan información valiosa sobre cómo las plantas reasignan recursos y regulan vías metabólicas para sobrevivir en condiciones de deficiencia de hierro (Abadía *et al.*, 2011). Esta información es esencial para el desarrollo de estrategias de mejora de cultivos, entendiendo los efectos de la deficiencia de hierro en la producción y la nutrición de las plantas (Garg *et al.*, 2018).

1.2.2. Mapeo y proteómica diferencial

En esta tesis doctoral, se pretende abordar el estudio del efecto de la deficiencia de hierro mediante la proteómica descriptiva y de expresión diferencial. Según el enfoque empleado podemos diferencias dos grandes grupos de estudios: el *mapping* y la proteómica diferencial, siendo dos herramientas esenciales en la identificación de proteínas y el análisis de su expresión en sistemas biológicos vegetales (Agrawal *et al.*, 2011; Tauseef *et al.*, 2021).

Por un lado, el mapeo proteómico se centra en la caracterización de manera exhaustiva del mayor número de las proteínas presentes en una muestra, generando un perfil proteico de una muestra biológica (Amagliani *et al.*, 2017). Por otro lado, la proteómica diferencial se enfoca en comparar las proteínas presentes en una muestra biológica en diferentes condiciones, estudiando la expresión diferencial de las proteínas identificadas. Esta técnica busca identificar proteínas que se expresen de manera diferencial en las condiciones analizadas, revelando información acerca de los procesos biológicos ocasionados por dichas condiciones (McWhite *et al.*, 2020). Ambos enfoques son complementarios y desempeñan un papel crucial en la evolución de los estudios de los diferentes proteómas y sub-proteómas en plantas, siempre teniendo en mente que el proteoma es muy dinámico en el tiempo y en el espacio (Mergner and Kuster, 2022). Además, el mapeo y la proteómica diferencial nos dan un mapa global de la expresión proteica (Baerenfaller *et al.*, 2008) describiendo la muestra analizada a diferentes niveles de complejidad, como tejido, celular o componente subcelular (Hu, Rampitsch and Bykova, 2015; Fuchs *et al.*, 2020; Mergner and Kuster, 2022).

1.3. Herramientas en proteómica

La instrumentación para la investigación en proteómica presenta un hoy en día un desafío importante en el laboratorio, donde técnicas y métodos analíticos avanzados desempeñan un papel destacado en la separación y caracterización de compuestos, particularmente en el análisis de proteínas y péptidos (Panicker, Chattopadhaya and Yao, 2006). El estudio de la proteómica implica una variedad de técnicas avanzadas, que incluyen, la electroforesis bidimensional, la cromatografía líquida y la espectrometría de masas. Estas herramientas permiten analizar la composición proteica de una muestra, sus modificaciones y la dinámica de su expresión (Jorrin Novo, 2021).

1.3.1. Electroforesis bidimensional

La electroforesis bidimensional (2-DE) es una técnica ampliamente utilizada en la investigación proteómica para separar y analizar proteínas en una muestra biológica. Fue desarrollado por O'Farrell y Klose en 1975 y ha sido una herramienta esencial en el estudio de proteínas en diversas disciplinas (Klose, 1975; O'Farrell, 1975). Implica dos etapas de separación de las proteínas. En la primera dimensión, se utiliza la focalización isoeléctrica (IEF) para separar las proteínas según su punto isoeléctrico (pI) (Klose, 1975). En esta etapa las proteínas se mueven en un gradiente de pH inmovilizado en un soporte físico (tiras "IPG"; *inmobilized pH gradient*) (Bjellqvist *et al.*, 1982; Görg *et al.*, 1995) y se detienen cuando alcanzan el pH que coincide con su pI, lo que resulta en una separación en función de la carga eléctrica de cada una de las proteínas contenidas en la muestra. En la segunda dimensión, las proteínas separadas previamente se someten a una electroforesis en gel de poliacrilamida (SDS-PAGE), en presencia de dodecil sulfato sódico con como agente desnaturalizante (Klose, 1975). Esta segunda dimensión separa las proteínas únicamente en función de su masa molecular, lo que da como resultado un mapa bidimensional de manchas proteicas o "*spots*" dibujado a lo largo de las dos dimensiones. Cada "*spot*" representa una proteína específica y su posición en el gel está determinada por su pI y su masa molecular (Jorrin-Novo *et al.*, 2019). Una vez finalizada la separación, los spots tienen que ser visualizados. Se emplean varios métodos de tinciones con diferentes características de sensibilidad, linealidad o reproducibilidad. Entre ellos las tinciones visibles con colorantes como la tinción con nitrato de plata o el coomassie coloidal G-250 (Dyballa and Metzger, 2009) y las tinciones fluorescentes como en el caso del Deep Purple o el Sypro Ruby (Patton, 2000).

Las ventajas de la 2-DE son notables. Esta técnica permite la separación simultánea desde centenares hasta miles de proteínas individuales en un solo experimento, dependiendo del tamaño del gel y otros factores (Görg *et al.*, 1995), proporcionando además información cuantitativa sobre las mismas (Abdallah *et al.*, 2012). Además, la 2-DE aporta una alta resolución, lo que facilita la

separación e identificación de isoformas proteicas y modificaciones post-traduccionales (O'Farrell, 1975). La capacidad de visualizar directamente el perfil proteico de una mezcla complejas de proteínas en único estudio es una ventaja significativa. La 2-DE es una manera efectiva de fraccionar y reducir la complejidad de las muestras potente en comparación con otros métodos de fraccionamiento cromatográfico (Righetti, Castagna and Herbert, 2001), que generalmente incluye columnas como podrían ser la cromatografía de exclusión molecular, de afinidad o de intercambio iónico (Righetti *et al.*, 2005). Una limitación clave de esta técnica es la dificultad para visualizar proteínas minoritarias, ya que pueden quedar enmascaradas por proteínas más abundantes (Fey and Larsen, 2001). Además, la solubilización de proteínas hidrofóbicas, como las proteínas de membrana, en la primera dimensión de IEF puede ser un desafío (Rabilloud, 1998). Estas proteínas, con propiedades de solubilidad más cercanas a los polímeros orgánicos convencionales, a menudo no se detectan mediante 2-DE. Las proteínas con pI muy ácido o básico también pueden ser difíciles de focalizar en la primera dimensión (Görg, Weiss and Dunn, 2004). Estas limitaciones han llevado al desarrollo de otras técnicas en proteómica avanzada (Righetti *et al.*, 2005).

A pesar de estas desventajas, la electroforesis bidimensional sigue siendo una técnica valiosa en la investigación proteómica, especialmente en la identificación de proteínas y en estudios de proteómica comparativa. Su capacidad resolutiva y su capacidad para proporcionar información detallada sobre las proteínas en una muestra la convierten en una herramienta esencial en el análisis de proteomas (Vadivel, 2015; Jorrin-Novo *et al.*, 2019).

1.3.2. La cromatografía liquida

La aplicación de técnicas cromatográficas ha demostrado ser una herramienta muy potente y versátil para la separación, análisis y purificación de mezclas complejas, tanto a nivel de laboratorio como industrial. Las técnicas más "convencionales", como la cromatografía de intercambio iónico (IEC), la cromatografía de exclusión de tamaño (SEC) y la cromatografía de afinidad, han dejado puesto a técnicas más avanzadas debido a la diversidad y complejidad de proteínas y péptidos en los diferentes sistemas biológicos (Righetti *et al.*, 2005; Panicker, Chattopadhaya and Yao, 2006).

Los fundamentos de la cromatografía líquida se basan en la distribución de componentes entre una fase estacionaria y una fase móvil, permitiendo la separación de mezclas complejas de analitos. En el contexto del análisis de proteínas, la cromatografía líquida, y más específicamente la cromatografía de fase reversa (RP-HPLC), ha demostrado ser una herramienta clave (Josic and Kovac, 2010). Desde la implantación en proteómica de la cromatografía líquida clásica (LC), se han ido incorporando nuevas variantes técnicas como la cromatografía líquida de alto rendimiento (HPLC; *high-performance liquid chromatography*) y la cromatografía líquida de ultra

rendimiento (UPLC; *ultra-performance liquid chromatography*), también conocida como cromatografía líquida de ultra-alto rendimiento (UHPLC; *ultrahigh-performance liquid chromatography*), generalmente acoplada a espectrometría de masas (MS) como detector (Nahar, Onder and Sarker, 2020). Los sistemas que constituyen la LC como herramienta analítica en proteómica no difiere en términos de instrumentación con otros campos de investigación (Koçak, Eylem and Nemutlu, 2023). Los sistemas de bombeo, las columnas de separación y los detectores utilizados en la investigación de proteómica son los mismos que se utilizan en el análisis convencional. La diferencia, sin embargo, radica en la magnitud de la velocidad de flujo, de las presiones de trabajo y, por lo tanto, de las columnas (Mitulović and Mechtler, 2006; Nahar, Onder and Sarker, 2020).

La RP-HPLC se utiliza comúnmente para la separación de proteínas en función de sus propiedades hidrofóbicas, lo que permite la identificación y cuantificación precisa de los analitos. Además, esta técnica se ha aplicado con éxito en la separación de proteomas completos, permitiendo un análisis exhaustivo de las proteínas en una muestra dada. En comparación con la electroforesis bidimensional en geles, la cromatografía líquida ofrece ventajas significativas, como una mayor capacidad de resolución y la posibilidad de separar proteínas en un rango más amplio de masas y propiedades químicas. Además, la miniaturización de la técnica en nano-HPLC ha mejorado la sensibilidad y precisión en el análisis de péptidos en aplicaciones de proteómica, superando las limitaciones de la electroforesis bidimensional en geles. Esta evolución ha permitido un análisis más detallado y preciso de las muestras biológicas, desempeñando un papel crucial en la investigación vegetal (Wilson *et al.*, 2015).

1.4. Espectrometría de masas

La espectrometría de masas se ha convertido en una herramienta esencial para el estudio de proteomas y subproteomas permitiendo la identificación de proteínas con alta precisión y brindando información crucial para desentrañar las funciones que desempeñan en los diferentes sistemas biológicos (Dupree *et al.*, 2020). Diversos tipos de espectrómetros de masas se utilizan en este contexto, dependiendo de la naturaleza de la muestra y los objetivos del estudio. Estos instrumentos tienen la capacidad generar espectros de masas únicos (MS1) y, en función de tecnología analítica que los constituyen, también permiten la fragmentación de estos espectros (MS/MS o MS^2) a través de la espectrometría en tándem.

La espectrometría de masas en tándem (MS/MS) es una técnica avanzada que desempeña un papel crucial en la identificación y caracterización de proteínas en proteómica vegetal, y en más campos de la investigación biomolecular. A diferencia de la espectrometría de masas convencional (MS1), que se centra en la medición de masas moleculares de iones generados a partir de una muestra, la MS/MS va un paso más allá al permitir la fragmentación controlada de los iones previamente seleccionados en la etapa de MS1 (Abdul-Khalek *et al.*, 2023). Esta fragmentación proporciona mucha más información sobre la secuencia de aminoácidos y las modificaciones post-traduccionales de los péptidos, lo que facilita abordar la complejidad de las muestras, al permitir la identificación de proteínas con mayor precisión y confianza en mezclas biológicas complejas, contribuyendo significativamente al entendimiento de los procesos biológicos (Mergner and Kuster, 2022).

En la actualidad, para mejorar aún más la resolución y la precisión en la identificación de proteínas en proteómica vegetal, se utiliza la cromatografía líquida de alta resolución (HPLC) acoplada a la espectrometría en tándem (HPLC-MS/MS). Este enfoque permite separar las proteínas de una mezcla biológica compleja, previa digestión enzimática (por ejemplo, con tripsina) y, posteriormente, analizar los péptidos generados mediante cromatografía líquida en fase reversa antes de su introducción en el espectrómetro de masas. Este acoplamiento facilita la identificación de proteínas al reducir la complejidad de la muestra y proporciona información adicional sobre la composición y las modificaciones de los péptidos (Mergner and Kuster, 2022; Abdul-Khalek *et al.*, 2023).

1.4.1. Las fuentes de ionización

En espectrometría de masas, una de las condiciones necesarias es la ionización de los analitos, es decir, la producción de iones en fase gaseosa adecuados para poder ser detectados en el analizador de masas. La ionización se produce en la fuente de iones. Hay varias fuentes de iones disponibles; cada una tiene ventajas y desventajas para aplicaciones particulares (Awad,

Khamis and El-Aneed, 2015). Para el análisis de péptidos y proteínas basados en la espectrometría de masas, las dos técnicas de ionización más ampliamente empleadas son el *ElectroSpray Ionization* (ESI) y el *Matrix-Assisted Laser Desorption/Ionization* (MALDI), cada una con su propio origen y aplicaciones específicas (Nadler *et al.*, 2017).

El MALDI fue desarrollado en la década de 1980 por Koichi Tanaka, galardonado con el Premio Nobel de Química en 2002. Destaca por su capacidad de lograr una ionización suave (*soft ionization*) (Wang *et al.*, 2018) de muestras sólidas o liquidas depositadas en una matriz. La energía láser es directamente aplicada en dicha matriz, que es capaz de absorberla y pasarla directamente a la muestra, permitiendo la liberación de los analitos en forma de iones gaseosos (Tanaka *et al.*, 1988).

El ESI, concebido en la misma década por John B. Fenn, también premio Nobel en 2002 (Fenn *et al.*, 1989; Cox and Mann, 2007), se diferencia al permitir una ionización suave de las moléculas en solución. En este caso, las muestras liquidas pasan al estado de iones gaseosos gracias a la aplicación de un alto voltaje directamente a la solución que contiene el analito. La generación de iones a partir de las proteínas en solución facilita la obtención de espectros de masas detallados (El-Aneed, Cohen and Banoub, 2009).

Ambas fuentes de ionización siguen teniendo un enorme impacto en muchas ramas de la investigación. El ESI sigue siendo un elemento fundamental para aplicaciones avanzadas en proteómica como el *single-cell proteomics* (Wu *et al.*, 2023) y también la fuente MALDI en la investigación clínica (por ejemplo, el MALDI biotyper) (Rychert, 2019) o en el estudio de las nuevas técnicas "-omicas" como en el caso del MALDI *Imaging Mass Spectrometry* (Zhu *et al.*, 2022).

1.4.2. Analizadores de masas: el tiempo de vuelo y la trampa iónica

La parte más importante de un espectrómetro de masas reside el analizador. Este es el corazón pulsante capaz de analizar los iones que entran en el MS y separarlos en función de la ratio masa-carga (m/z) de cada uno de los iones sometidos a un determinado campo eléctrico y magnético (Haag, 2016). En el mercado existen diferentes tipos de analizadores para diferentes tipos de aplicaciones y la elección del analizador dependerá de las propiedades del analito y de los requisitos del experimento a realizar (Li *et al.*, 2021).

Para el estudio de la proteómica, en esta tesis, se han utilizado dos tipos de analizadores: de masas de tiempo de vuelo o TOF (*Time of Flight*); y la trampa iónica o IT (*Ion Trap*).

El tiempo de vuelo (Time of Flight, TOF)

El analizador TOF (en castellano "tiempo de vuelo") fue desarrollado por primera vez por J. Wiley y I. McLaren en la década de 1950, utilizándose en el campo de la proteómica desde la década de 1990 (Price, 2023).

Se basa en la medición del tiempo que tarda un ion en recorrer una distancia conocida en un campo eléctrico. Proporciona una alta resolución de masas y precisión en la identificación de proteínas. Es conocido por su rapidez en la adquisición de datos, lo que lo hace adecuado para el análisis de analitos como metabolitos, péptidos o proteínas en muestras complejas, particularmente cuando se acopla a la fuente de ionización MALDI (*Matrix-Assisted Laser Desorption/Ionization*). Dependiendo de su configuración pueden trabajar en modalidad MS o MS/MS. Si la adquisición de datos por parte de analizador se realiza en un único paso (MS1), los iones son acelerados y separados en un tobo de vuelo en función de su velocidad (por ejemplo, MALDI-TOF). Si el análisis de la muestra se realiza en dos pasos, esto ocurre mediante la introducción de una celda de colisión (CID, *Collision-induced dissociation*) entre dos tubos de vuelos, hablaremos de masas en tándem (MS^2), específicamente de TOF/TOF (por el ejemplo MALDI-TOF/TOF) (Leung and Pitts, 2008). Esta configuración permite la identificación de péptidos y proteínas a través de la espectrometría de masas de fragmentación. El sistema CID-MS/MS es unos de los métodos de fragmentación más robustos y empleados en espectrometría de masas (Zhu *et al.*, 2017).

Las principales ventajas del analizador TOF son su rapidez, su bajo coste, su alta sensibilidad y su automatización. Además, es un analizador muy versátil que permite gastar un volumen muy reducido de muestra, permitiendo analizar cientos de muestras en minutos. Además, es versátil a la hora de elegir la ventana de adquisición de las señales, permitiendo analizar tanto pequeños péptidos como proteínas de alto peso molecular (Beretov *et al.*, 2014; Brais *et al.*, 2021).

La trampa iónica (Ion trap, IT)

El analizador de IT (en castellano "trampa de iones") tiene su origen en la década de 1980 y fue desarrollado principalmente por Ronald Macfarlane en los laboratorios de la Universidad de Washington (Holzscheiter, 1995).

El IT se ha convertido en una herramienta fundamental en espectrometría de masas en general y ha sido ampliamente utilizado en la proteómica desde la década de 1990 (March, 1999). La IT es capaz de atrapar iones en un campo electromagnético tridimensional durante un determinado tiempo. Durante este tiempo es capaz de acumular, excitar y fragmentar estos iones de manera rápida y eficiente, lo que resulta especialmente útil para la secuenciación de péptidos

y la caracterización de proteínas (Nolting, Malek and Makarov, 2019). Su alta sensibilidad y rapidez en el análisis lo convierte en una elección acertada cuando se acopla a la fuente de ionización ESI (*ElectroSpray Ionization*) para analizar péptidos y proteínas en solución, lo que es beneficioso en estudios proteómicos.

La elección entre el TOF y el IT, depende de los objetivos específicos de la investigación y el tipo de muestras, con el TOF destacando por su resolución en tiempo, velocidad y automación, mientras que el IT sobresale en capacidad de fragmentación y su mayor sensibilidad.

1.5. Estrategias en proteómica

Las dos principales estrategias para identificar y caracterizar proteínas mediante espectrometría de masas son las metodologías "*top-down*" y *bottom-up*" (Baysal, 2017). En el caso del *bottom-up proteomics* (de abajo arriba), las proteínas presentes en una muestra son digeridas en péptidos mediante enzimas proteolíticos (tripsina u otras proteasas), que posteriormente son identificados mediante cromatografía líquida y espectrometría de masas en tándem. En el caso de la aproximación *top-down proteomics*, se evita la digestión en péptidos, y la identificación de proteínas se obtiene directamente a partir de la fragmentación de las proteínas intactas (Smith *et al.*, 2013).

1.5.1. *Top-down proteomics*

En la proteómica *top-down* (de arriba abajo), las proteínas son analizadas "intactas" mediante la espectrometría de masas, permitiendo la caracterización de las modificaciones (interacciones proteínas-proteínas, isoformas o modificaciones postraduccionales) para cada proteoforma (Khoranhlai, 2015). Esta aproximación tiene la ventaja de que todas las modificaciones en la misma molécula se pueden medir juntas, permitiendo una identificación precisa de la proteoforma (Smith *et al.*, 2013). Sin embargo, este procedimiento es complejo a nivel experimental y presenta un desafío a nivel computacional (Aebersold and Mann, 2016). Una de las limitaciones técnicas es que las proteínas intactas son difíciles de separar por cromatografía, y el análisis por espectrometría de masas en tándem (MS/MS) es mucho menos sensible para proteínas intactas que para péptidos (Dupree *et al.*, 2020). Además la misma proteína puede presentar múltiples proteoformas que pueden varias funciones biológicas (Smith *et al.*, 2013). A pesar de las dificultades, el análisis de mezclas de proteínas intactas por *top-down* es actualmente un campo intenso de investigación.

1.5.2. *Bottom-up proteomics*

Por otro lado, en la proteómica *bottom-up*, las proteínas se descomponen en fragmentos peptídicos mediante la digestión enzimática mediante una proteasa específica. Los péptidos generados se separan por cromatografía de fase reversa (RP-HPLC) y se ionizan por electroespray (ESI) antes de ser analizados por un espectrómetro de masas, donde los iones peptídicos se fragmentan para generar espectros de MS/MS (MS^2). Este proceso proporciona información para la identificación y cuantificación de péptidos específicos (Aebersold and Mann, 2016) y los datos resultantes se analizan mediante herramientas y programas bioinformáticos diseñados *ad-hoc* (Khoranhlai, 2015).

Este tipo de análisis posee numerosas ventajas, como la posibilidad de emplear proteasas de altamente selectivas y con una alta especificidad de corte para la digestión de proteínas, permitiendo la combinación de diferentes tipos de enzima en el mismo experimento (por ejemplo, tripsina/Lys-C). Además, los flujos de trabajo en proteómica se pueden aplicar fácilmente a diferentes organismos en función de su comportamiento, y los protocolos establecidos en el campo de mamíferos se pueden aplicar fácilmente a otros sistemas, como los vegetales. Por último, los avances en la metodología de fraccionamiento como la LC de micro y nano flujo, además del uso de espectrómetros de masas más modernos, han permitido el análisis de miles de proteínas en un solo análisis ("s*ingle-shot*") (Bian *et al.*, 2021). Estos avances han llevado a poder medir >100,000 péptidos que representan >10,000 proteínas en prácticamente cualquier tejido o especie estudiada (Mergner and Kuster, 2022).

Para el desarrollo de esta tesis, se ha optado por la estrategia del *bottom-up* para explorar en detalle el perfil proteómico, centrándose en comprender las complejas interacciones subyacentes en el sistema vegetal estudiado.

1.6. Herramientas para la identificación de proteínas

Las enormes potencialidades de la espectrometría de masas, no sólo en la investigación proteómica, sino también en muchas otras áreas de las ciencias de la vida, ha tenido un rápido desarrollo en términos de tanto de hardware, software y de herramientas para la gestión de datos (Zengin *et al.*, 2017) Estos avances han dado lugar a numerosos instrumentos, algoritmos de análisis, múltiples formatos de datos, programas informáticos, y bases de datos en continuo desarrollo (McHugh and Arthur, 2008).

Por lo tanto, en investigación y en particular en la proteómica tiene un papel fundamental elegir bien el enfoque, la metodología y las herramientas más adecuadas para un determinado estudio.

1.6.1. La identificación de proteínas: PMF vs PFF

La identificación de proteínas en estudios proteómicos, se lleva a cabo utilizando dos enfoques principales: la huella peptídica (PMF, "*Peptide Mass Fingerprinting*") obtenida a partir de un espectro de masas (MS) y la huella del espectro de fragmentación o PFF ("*Peptide Fragment Fingerprinting*") mediante la secuenciación de fragmentos de péptidos mediante MS/MS (Zengin *et al.*, 2017).

PMF (Peptide Mass Fingerprinting)

El PMF fue el primer método disponible para la identificación de proteínas mediante espectrometría de masas, y sigue siendo ampliamente utilizado (Henzel, Watanabe and Stults, 2003). Su eficacia reside en la rapidez con que calcula las puntuaciones de las identificaciones obtenidas por huella peptídicas frente a una base de datos. Cada proteína deja una firma única en términos de masas de péptidos, lo que permite la identificación de la proteína a partir de esta "huella digital". En este método, los espectros “experimentales”, compuestos por las masas de los fragmentos de las proteínas digeridas, se comparan con los espectros “teóricos” generados a partir de las masas esperadas resultantes de la digestión enzimática de cada secuencia de proteína en una base de datos de referencia. Herramientas informáticas, como MASCOT, MS-Fit, Profound y PeptIdent, (Joo *et al.*, 2007) son muy conocidas por su facilidad de uso para el análisis de datos de este tipo de enfoque (McHugh and Arthur, 2008).

Esta metodología, aunque puede producir identificaciones de proteínas con alta confianza en organismos bien caracterizados, presenta algunas limitaciones cuando los espectros no se asemejan lo suficiente a los espectros teóricos. Esto puede deberse a diversos factores como modificaciones post-traduccionales o variantes de secuencia de proteínas, entre otros. Otra

posible limitación del PMF es su sensibilidad al tamaño de la base de datos, lo que afecta la confianza estadística en las identificaciones. A menudo, los investigadores utilizan PMF como un primer paso y, en caso de fallo, recurren a métodos como de fragmentación por MS/MS (Zhang and Chait, 2000).

PFF (Peptide Fragment Fingerprinting)

El enfoque conocido como *Peptide Fragment Fingerprinting* (PFF) analiza los fragmentos de péptidos generados por la fragmentación controlada de las moléculas en el espectrómetro de masas. Después de la digestión enzimática de las proteínas, los fragmentos peptídicos obtenidos, una vez ionizados entran en el espectrómetro de masas, donde se seleccionan los péptidos de manera individual para someterlos a una fragmentación adicional, generando espectros de PFF. Estos espectros de fragmentación, además de aportar la información de la masa principal de los péptidos fragmentados, proporciona información sobre la secuencia de aminoacídica de los péptidos, permitiendo una mayor confianza y precisión a la hora de identificar las proteínas en comparación con el enfoque PMF tradicional. También en es este caso, es importante el uso de paquetes y softwares bioinformáticos a la hora de analizar los resultados. Entre los paquetes populares de PFF se encuentran MASCOT, SEQUEST y X!Tandem (McHugh and Arthur, 2008).

En resumen, mientras que el PMF se centra en la huella "dactilar" de masas de los péptidos para la identificación de proteínas, el PFF se basa en la secuenciación de los péptidos mediante la fragmentación por MS/MS. Ambos enfoques son herramientas complementarias en estudios proteómicos, brindando flexibilidad en función de la disponibilidad y tipo de datos espectrales (Sinha and Mann, 2020).

1.6.2. Motores de búsqueda: MASCOT

En esta tesis, para el análisis de los datos de espectrometría de masas se ha empleado el software MASCOT (https://www.matrixscience.com). El MASCOT es un motor de búsqueda (Perkins *et al.*, 1999) y es una herramienta clave en la identificación de péptidos. Utiliza su propio algoritmo de puntuación (*score*), basado en el algoritmo MOWSE descrito por primera vez en 1993 (Pappin, Hojrup and Bleasby, 1993). Este software tiene la tarea de calcular la probabilidad de coincidencias aleatorias al analizar la distribución de las longitudes de péptidos trípticos en la base de datos empleada. Perkins et al. proporcionan una visión general de su enfoque probabilístico (Perkins *et al.*, 1999). La probabilidad más baja se considera la mejor coincidencia, cuya significancia depende también del tamaño de la base de datos. En búsquedas en bases de datos pequeñas (menor tamaño en términos de entradas), las puntuaciones umbral (*threshold*) de confianza son generalmente más bajas, mientras que, en bases de datos más grandes como en el

caso de organismos superiores, son más altas. MASCOT ajusta automáticamente el umbral de puntuación, considerando espectros experimentales ruidosos y posibles picos adicionales que contribuyen a la posibilidad de coincidencias aleatorias, elevando así el umbral de confianza. MASCOT (Chen *et al.,* 2019) devuelve un umbral de puntuación con resultados calculados para representar un nivel de confianza de $p < 0,05$ (Perkins *et al.,* 1999).

El MASCOT se puede emplear tanto en análisis por PMF como por PFF, integrando búsquedas en la base de datos de secuencias, búsqueda de pesos moleculares de péptidos y datos de MS/MS. Su algoritmo de puntuación probabilístico permite una determinación sencilla de la significancia de los resultados, comparaciones con otros tipos de búsquedas y la optimización de parámetros. Aunque presenta limitaciones, como la falta de detalles específicos sobre el proceso preciso de puntuación del MASCOT, la dificultad en la interpretación de resultados o la sensibilidad del software al tamaño de la base de datos empleadas, sigue siendo una herramienta fundamental.

1.6.3. Bases de datos de proteínas

La principal finalidad de un estudio proteómico es la caracterización e identificación de los péptidos y proteínas presentes en un determinado experimento. Para ello se recurre a base de datos biológica de secuencia de proteínas. En la actualidad, disponemos de numerosos repositorios de acceso público (genéricamente llamados bases de datos) que permiten recuperar información sobre las proteínas (Riffle and Eng, 2009).

El acceso puede llevarse a cabo directamente utilizando el "nombre" de la proteína o a través de la llave primaria o identificador interno de la entrada ("*accession number*"), contenidos en cada base de datos. Sin embargo, es crucial tener en cuenta que tanto el nombre como el identificador de la proteína varían según la base de datos que se emplea para la búsqueda, lo que subraya la necesidad constante de hacer referencia a la fuente de datos correspondiente para garantizar la precisión y comprensión de la información asociada a una proteína identificada.

En el contexto de las identificaciones, tanto basadas en huella de masa peptídica (PMF) como por las huellas de fragmentación peptídica (PFF), resulta indispensable contar con bases de datos actualizadas que incluyan las secuencias de aminoácidos de las proteínas buscadas. Estas bases de datos, en su mayoría, ofrecen secuencias de proteínas en su forma original, es decir, sin modificaciones, obtenidas directamente de la traducción del gen que codifica la proteína.

A pesar de la amplia variedad de bases de datos de proteínas, es importante señalar que no todos almacenan la misma categoría de información (Zengin *et al.,* 2017). Algunos repositorios, como SwissProt (http://www.uniprot.org/) o NCBIprot (http://www.ncbi.nlm.nih.gov/), contienen además de los datos sobre la secuencia de aminoácidos

de la proteína, información sobre anotaciones funcionales y bibliográficas publicadas (Morales *et al.*, 2022; Bateman *et al.*, 2023). Por otro lado, existen repositorios más específicos, como PDB (http://www.rcsb.org/pdb/home/home.do), que se especializan en datos relativos a la estructura tridimensional obtenidos mediante difracción de rayos X (Riffle and Eng, 2009; Zardecki *et al.*, 2022).

En esta tesis, para la identificación y caracterización de proteínas vegetales se han empleado tres distintos bases de datos como Swiss-Prot, NCBInr (antigua definición de la actual NCBIprot) y la EST (*expressed sequence tag*), esta última importante recurso para las identificaciones de proteínas en plantas (PLANT EST) (Dong *et al.*, 2005).

1.7. Avances tecnológicos: el MALDI Mass Spectrometry Imaging

La tecnología del MALDI *Mass Spectrometry Imaging* (MALDI-MSI), es una extensión de MALDI que combina la sensibilidad la selectividad de la espectrometría de masas con el análisis espacial, aportando una nueva dimensión revelando la distribución exacta de las biomoléculas en los tejidos (Gessel, Norris and Caprioli, 2014).

Han pasado casi 20 años desde las primeras publicaciones científicas (Spengler B., Hubert M., 1994; Gusev *et al.*, 1995) y desde entonces el MALDI-MSI ha ganado interés en el análisis de compuestos con un amplio rango de masas, desde el análisis de moléculas pequeñas como metabolitos o fármacos (Reyzer *et al.*, 2003), pasando por el análisis de péptidos (Groseclose *et al.*, 2007) hasta proteínas de alto peso molecular (Karas *et al.*, 1989). El MALDI-MSI permite el estudio de biomoléculas directamente en el tejido preservando la información espacial, clave para entender procesos biológicos. Aunque persisten desafíos, las mejoras en métodos e instrumentación han elevado la eficacia del MALDI-MSI en diversas aplicaciones biológicas en sus casi 20 años de existencia (Caprioli, Farmer and Gile, 1997).

Optimización de los protocolos a la muestra y analitos a analizar

El flujo de trabajo experimental se compone de estas etapas: cortes de tejido congelado, recubrimiento con matriz MALDI y generación de espectros de masas para cada coordenada x-y, obteniéndose de esta manera imágenes digitales de los espectros adquiridos. Gracias al sistema de coordenadas dentro del área de tejido seleccionado podemos visualizar la intensidad de cada ion y su ubicación exacta en la superficie del corte de tejido.

La adaptación de un determinado tipo de muestra a su análisis mediante MALDI-MSI se desarrolla en cuatro etapas cruciales: (i) desarrollo de protocolos estandarizados para la preparación de muestras (McDonnell *et al.*, 2012), (ii) mejora de la resolución espacial (Yang and Caprioli, 2011), (iii) identificación eficiente de los analitos para ampliar el rango dinámico (Stoeckli *et al.*, 2001), y (iv) desarrollo de algoritmos avanzados de procesamiento de datos (Gessel, Norris and Caprioli, 2014).

Las etapas de preparación de muestras se ajustan antes del análisis de MALDI-MSI, optimizando el grosor de la sección y la aplicación de matriz para maximizar la sensibilidad y resolución espacial (McDonnell *et al.*, 2012). La elección precisa de la resolución espacial en MALDI-MSI es crucial, especialmente para aplicaciones celulares de alta resolución (<20 μm). Los instrumentos actuales alcanzan resoluciones cercanas a los 20 μm, pero el uso de técnicas como el sobremuestreo (*oversampling*) permiten mejorar la calidad de la imagen y la intensidad de la señal (Jurchen *et al.*, 2005). La forma de aplicación de matriz y sublimación es un factor

crítico que influye en la resolución de la señal durante la adquisición (Hankin *et al.*, 2007). Otros factores a tener en cuenta es el tamaño de las áreas de adquisición de los datos. La selección de áreas más pequeñas reduce el tiempo de análisis (Shimma and Sugiura, 2014).

Desafíos de la tecnología

La imagen de alta resolución en MALDI-MSI plantea desafíos, como tiempos extensos y desgaste del instrumento. Evaluar la resolución necesaria es crucial, y el desarrollo instrumental se enfoca en mejorar la velocidad y las capacidades de almacenamiento y procesamiento de datos. El tamaño de un archivo de MALDI-MSI, incluso para imágenes de baja resolución, es considerable y se carece de herramientas de reducción de datos comerciales. A mayor resolución, la necesidad de reducción de datos se vuelve vital (Jones *et al.*, 2012; Xiong *et al.*, 2012).

Aunque la identificación *in situ* de lípidos y moléculas pequeñas con MALDI MS/MS es rutinaria, la identificación de proteínas y péptidos presenta desafíos significativos (Mascini and Heeren, 2012). En el uso de MALDI-MSI para proteómica y la identificación de proteínas existen dos enfoques. El primero utiliza un espectrómetro TOF para imágenes de proteínas, comparándolas con datos MS de tejido fraccionado. Aunque limitado a proteínas grandes, este método guía experimentos LC MS/MS. El segundo enfoque implica la hidrólisis trípsica in situ seguida de análisis MS/MS directo, pero la resolución limitada y la superposición de señales pueden complicar el análisis de los datos. La MSI de alta resolución con analizadores versátiles como por ejemplo el timsTOF fleX de Bruker (Chen *et al.*, 2023) o el MALDI-LTQ-Orbitrap de Thermo (Moreno-Gordaliza *et al.*, 2017) aborda estos problemas, aunque con tiempos de adquisición más largos y archivos grandes. Además de los desafíos técnicos, la falta de automatización en la adquisición de datos MS/MS, la limitación en el número de análisis debido a la ablación de matriz y la eficiencia de fragmentación de péptidos afectada por sus estados de carga ($z = +1$), son otras limitaciones de la técnica (Li *et al.*, 2012; Gessel, Norris and Caprioli, 2014).

El análisis y procesado de datos de MSI está en constante desarrollo. La complejidad de los datos de MSI ha dado lugar a diversos métodos de pre-procesamiento y análisis, que requieren una comprensión adecuada para obtener resultados precisos (Jones *et al.*, 2012). Sin embargo, muchos de estos métodos no están disponible comercialmente, lo que limita su accesibilidad. La falta de integración con software libres dificulta para la interpretación de los datos crudos (*RAW DATA*) generando una barrera a la hora de visualizar los resultados lo que, en muchas ocasiones, obliga a los investigadores buscar la asesoría de expertos en bioinformática para evaluar la fiabilidad de los hallazgos científicos y aplicar estas herramientas computacionales de manera efectiva. Aunque hay software comercial y de código abierto disponible, su especificidad y la falta de transparencia en el tratamiento estadístico llevan a la dependencia de soluciones internas.

Se necesita más desarrollo para facilitar la interpretación clara de los resultados y estandarizar el análisis de datos de MALDI-MSI (Jones *et al.*, 2012; Xiong *et al.*, 2012). Las aplicaciones clínicas de MALDI-MSI se beneficiarán enormemente cuando estén disponibles enfoques estandarizados para el análisis y la clasificación de estos datos.

El enorme desarrollo tecnológico y su versatilidad ha convertido rápidamente el MALDI-MSI en una herramienta robusta para el estudio de tejidos biológicos de múltiples especies (Buchberger *et al.*, 2018; Müller *et al.*, 2021) y extremamente versátil permitiendo analizar metabolitos, lípidos, péptidos u proteínas (Fuchs et al., 2020)(Fuchs *et al.*, 2020; Müller *et al.*, 2021; Salviati, Sommella and Campiglia, 2022; Wittek, Jahreis and Römpp, 2023), llegando a hablar de técnicas de *Spacial multi-omics* (Wang *et al.*, 2023). En la última década la espectrometría de masas por imágenes (MSI) se está consolidando como una de las tecnologías utilizadas en fisiología vegetal (Berin A Boughton *et al.*, 2016; Sarabia *et al.*, 2018; Ajith *et al.*, 2022; Maia *et al.*, 2022; Horn and Chapman, 2023; Wang *et al.*, 2023). En esta tesis, se pretende estudiar y aplicar el MALDI *Mass Spectrometry Imaging*, como técnica avanza para el estudio de la distribución espacial de los metabolitos en diferentes tejidos u órganos vegételas, y permitiendo entender mejor sus papeles y respuestas frente a distintos fenómenos fisiológicos.

1.8. La homeostasis de metales en plantas

La "homeostasis" es un concepto fundamental en la biología que se refiere a la regulación de las condiciones internas de un organismo para mantener un equilibrio constante y óptimo en las propiedades físico-químicas de su medio interno (Cannon, 1929).

Las plantas al igual que los animales, necesitan de ciertos elementos indispensables para su desarrollo y crecimiento. Estos nutrientes esenciales se dividen en dos categorías: macronutrientes y micronutrientes (Martin and Horst Marschner, 1988; Mengel K., Kosegarten H., 2001). Los macronutrientes (como N, K, P, Ca, Mg y S) son necesarios en cantidades elevadas (de 1% a 6% del peso seco), mientras que los micronutrientes (como Fe, Mn, Cu, Zn, Ni, Mo, Cl y B) son vitales en cantidades muy pequeñas (de 1 a 200 ppm).

La regulación de la homeostasis de micronutrientes es un proceso altamente controlado en las plantas que debe adaptarse a las fluctuaciones en la disponibilidad y necesidad de estos elementos, que varían según la especie vegetal, el tejido y las condiciones de crecimiento (Martin and H. Marschner, 1988). La absorción, el transporte y el almacenamiento de estos elementos se rigen por mecanismos específicos que aseguran que los micronutrientes se mantengan dentro de un rango fisiológico estrecho. Mantener los niveles óptimos de micronutrientes es crucial para el crecimiento de las plantas. Tanto la deficiencia (cuando los niveles son muy bajos) como la toxicidad (cuando son excesivos) pueden dañar las plantas (Schützendübel and Polle, 2002; White and Brown, 2010).

Se define como condiciones de "deficiencia" de un micronutriente a aquellas condiciones en las que la una concentración de un micronutriente impide que el crecimiento del cultivo alcance el 90% de su rendimiento máximo. Ante una deficiencia de micronutrientes, las plantas activan mecanismos que aumentan su capacidad de adquisición. Por otro lado, se utiliza el término "toxicidad" cuando la concentración de un micronutriente es excesiva y provoca una disminución en el crecimiento de la planta superior al 10% (White and Brown, 2010). Tanto la deficiencia como la toxicidad de los micronutrientes pueden tienen un impacto significativo en el crecimiento y la producción de cultivos (Macnicol and Beckett, 1985; Martin and Horst Marschner, 1988; Mengel K., Kosegarten H., 2001; Álvarez-Fernández *et al.*, 2003).

La investigación en nutrición vegetal busca comprender los mecanismos de asimilación y distribución de los nutrientes y cómo se mantiene su homeostasis, lo que tiene implicaciones significativas en la agricultura y la seguridad alimentaria (Vigani, Maffi and Zocchi, 2009).

1.9. El hierro es un elemento esencial para las plantas

El hierro (Fe) es un elemento esencial para el crecimiento de las plantas, al igual que para otros organismos. Es necesario para una serie de procesos celulares críticos, como la respiración, la biosíntesis de la clorofila y la fotosíntesis, y sirve como cofactor en enzimas implicadas en la transferencia de electrones u oxígeno.

Es el cuarto elemento más abundante en el suelo y se encuentra generalmente en forma de óxido de hierro, tanto en forma ferrosa (Fe^{+2}) como férrica (Fe^{+3}) en función del pH del suelo (Abadía *et al.*, 2011; Colombo *et al.*, 2014). A pesar de su abundancia en los suelos minerales, la mayor parte del Fe se encuentra en forma de férrica [Fe(III)], que tiene una baja solubilidad en el rango de pH fisiológico en condiciones aeróbicas. Como resultado, la baja disponibilidad de Fe en suelos con un pH elevado es un desafío importante en la agricultura a nivel mundial, afectando negativamente a la producción en aproximadamente el 30% de las tierras de cultivo (Colombo *et al.*, 2014; Tripathi *et al.*, 2018).

Las plantas superiores, han desarrollado al menos dos estrategias para adquirir Fe del suelo, a pesar de su baja disponibilidad. Las plantas no gramíneas emplean una estrategia de reducción, conocida como Estrategia I, que involucra la excreción de protones desde las raíces hacia la rizosfera, la conversión de Fe(III) en la forma más soluble de Fe(II) y el transporte del ion ferroso (Fe^{2+}) a través de la membrana celular de la raíz mediante el transportador de Fe^{2+}, IRT1 (Eide *et al.*, 1996; Vert *et al.*, 2002; Xu *et al.*, 2024). Por otro lado, las plantas gramíneas utilizan una estrategia de quelación, denominada Estrategia II, y liberan fitosideróforos de la familia del ácido mugineico (MAs) desde sus raíces para quelar el Fe(III) en el suelo (Takagi, 1976; Takagi, Nomoto and Takemoto, 1984). Los complejos Fe(III)-MAs son posteriormente absorbidos a través de los transportadores de hierro-fitosideróforo como el YS1 y de los trasportadores de metal-nicotianamina como el YSL (Curie *et al.*, 2001). Los MAs se sintetizan a partir de L-metionina a través de la nicotianamina (NA) (Mori and Nishizawa, 1987; Shojima *et al.*, 1990). La NA es un aminoácido no proteico sintetizado en todas las plantas, incluyendo las plantas de Estrategia I (Shojima *et al.*, 1989). La NA es un quelante de varios metales micronutrientes y se ha sugerido que está involucrado en el movimiento de micronutrientes en toda la planta (Takahashi *et al.*, 2003).

Los genes que codifican las enzimas involucradas en la biosíntesis de MAs se identificaron por primera vez en cebada (Higuchi *et al.*, 1999; Takahashi *et al.*, 1999; Nakanishi *et al.*, 2000; Bashir *et al.*, 2006) y posteriormente en otras plantas gramíneas (Inoue *et al.*, 2003) (Inoue *et al.*, 2008). En arroz es inusual entre las plantas gramíneas porque también muestra aspectos del mecanismo de captación de Fe de estrategia-I. Además de la secreción de MAs, las

raíces deficientes en Fe del arroz muestran una mayor expresión de un transportador tipo IRT, OsIRT1, que permite la captación de Fe^{2+} del entorno reductor común en los campos de arroz inundados (Ishimaru *et al.*, 2006).

Para facilitar la solubilidad y transporte del Fe y evitar su toxicidad una vez adquirido, las plantas han desarrollado pequeños metabolitos capaces de quelar el hierro, como la NA, la familia de fitosideróforos del ácido mugineico y el citrato (Suzuki *et al.*, 2021), además de diversos tipos de transportadores para estos agentes quelantes, los complejos de hierro-quelato o iones de hierro libres (Kobayashi, Nozoye and Nishizawa, 2019).

Estudios recientes han descrito que la expresión de varios genes involucrados en la captación y translocación del hierro se induce en situaciones de deficiencia de hierro a través de redes de factores de transcripción (Kobayashi, Nozoye and Nishizawa, 2019). Estos factores de transcripción se regulan de manera negativa por una pequeña familia de E3 ubiquitin-ligasas [HRZ (Hemerythrin RING Zinc finger) en arroz; BTS (BRUTUS) y BTSL (BRUTUS-LIKE) en *Arabidopsis*]. Estas proteínas que se encuentran en algas verdes y plantas, desempeñan un papel importante para evitar la sobrecarga tóxica de Fe (Rodríguez-Celma *et al.*, 2019).

Capítulo 2

OBJETIVOS

El objetivo general de esta tesis doctoral es el estudio de los cambios inducidos por el Fe en distintos sub-proteomas (savia de floema, tallo y raíz) en diferentes especies vegetales utilizadas como modelo [*Lupinus texensis*, *Medicago truncatula* y un patrón híbrido de *Prunus* (*P.dulcis x P. persica*)]. El trabajo pretende además utilizar nuevas herramientas tecnológicas como el *MALDI-Mass Spectrometry Imaging* (MALDI-MSI), un potente instrumento analítico muy utilizado en biomedicina, pero aún poco usado en el mundo vegetal. Este tipo de aproximaciones ayudará a desarrollar mejores sistemas agrícolas basados en el conocimiento de las posibles alteraciones metabólicas producidas por estreses nutricionales en los cultivos, evitando por lo tanto perdidas de productividad y calidad, incrementando el conocimiento global existente sobre la hemostasis de este metal en las plantas.

Se plantearon los siguientes objetivos específicos:

1. Optimización de diferentes parámetros analíticos para el estudio de la distribución espacial de pequeñas moléculas en diferentes tejidos funcionales vegetales, utilizando la técnica del MALDI-*Mass Spectrometry Imaging* (MALDI-MSI)

2. Caracterización de los cambios producidos por la deficiencia y el reabastecimiento de Fe en el perfil proteico de la raíz de un patrón híbrido melocotonero/almendro (*P. dulcis* × *P. persica*)

3. Caracterización del proteoma de la savia del floema de *Lupinus texensis* y estudio de las proteínas implicadas en la unión con el Fe y el Zn.

4. Caracterización de los efectos de la deficiencia de Fe en los perfiles proteicos y la composición de lignina del tallo de *Medicago truncatula* en ausencia o presencia de carbonato cálcico en el medio de cultivo

Capítulo 3

RESULTADOS

3.1. Spatially resolved analysis of small molecules by matrix-assisted laser desorption/ionization mass spectrometric imaging (MALDI-MSI)

Manuela Peukert[1], Andrea Matros[1], Giuseppe Lattanzio[2], Stephanie Kaspar[1], Javier Abadía[2] and Hans-Peter Mock[1]

[1]*Applied Biochemistry Group, Leibniz Institute of Plant Genetics and Crop Plant Research (IPK), Corrensstrasse 3, D-06466 Gatersleben, Germany*

[2]*Department of Plant Nutrition, Estación Experimental de Aula Dei (CSIC), Av. Montañana 1005, Campus de Aula Dei, E-50059 Zaragoza, Spain*

Published in New Phytologist (2012) 193, 806-815 (doi: 10.1111/j.1469-8137.2011.03970.x).

Additional supporting information may be found in the online version of this article at the publisher's web-site.

SUMMARY

Matrix-assisted laser desorption/ionization mass spectrometric imaging (MALDI-MSI) of tissues provides the means to analyse the spatial distributions of small molecules and proteins within tissues. This imaging technique is commonplace in medicinal and pharmaceutical research, but its application in plant science is very recent. Broader introduction requires specific adaptations for plant tissues. Sample preparation is of paramount importance in order to obtain high-quality spectra providing sufficient spatial resolution for compounds. Optimization is required for sectioning, choice of matrix and means of matrix deposition. Here, we present our current protocols for the detection of small molecules in cryodissected immature barley (*Hordeum vulgare*) grains and tobacco (*Nicotiana tabacum*) roots. Examples of MALDI-MSI measurements are provided, and the level of reproducibility across biological replicates is addressed. Furthermore, our approaches for the validation of distribution patterns and for the identification of molecules are described. Finally, we discuss how MALDI-MSI can contribute to applied plant research.

3.1.1. Introduction

Substantial progress has been made over recent years in the parallel analysis of transcripts, gene products and metabolites, with a major impact on plant science (Yuan *et al.*, 2008; Saito and Matsuda, 2010; Kaufmann *et al.*, 2011). At present, the most well-developed platform targets mRNA, whereas those aimed at the analysis of proteins and metabolites remain more challenging, largely because the chemical composition of these analytes is much more

heterogeneous. Nonetheless, these two classes of molecules are important, as they carry information which cannot be addressed by transcript analysis – for example, many proteins are post-translationally modified and, for the cell, this represents a critical component of its control machinery. A particular priority area is to develop ways to improve the spatial resolution of measurements, as higher organisms, including plants, comprise an array of functionally specialized tissues within every organ (in plants, the root, leaf or seed). Furthermore, the molecular content of many tissues responds to both development and cues from the external environment.

However, methods for untargeted comprehensive analyses of specific tissues are lacking. The deployment of pressure probe glass capillaries or laser capture microdissection has been pioneered for the isolation of specific tissues (Amantonico, Urban and Zenobi, 2010), and tissue-specific transcriptome profiling can be facilitated by either the incorporation of tagged ribosomal proteins (Zanetti *et al.*, 2005; Mustroph *et al.*, 2009), or the labelling of particular protoplast subpopulations to allow their sorting (Dinneny *et al.*, 2008a; Dinneny, 2010; Tsukagoshi, Busch and Benfey, 2010). The latter approach may also be feasible for proteomic or metabolomic analyses, although it is unclear to what extent the protoplast preparation process per se may induce cellular reactions likely to alter protein and metabolite composition.

Innovative instrumentation and sample preparation protocols have facilitated matrix-assisted laser desorption ⁄ ionization mass spectrometric imaging (MALDI-MSI) of large and varied molecules at both the whole-tissue and single-cell level (Caprioli, Farmer and Gile, 1997; Stoeckli *et al.*, 2001; Gardel *et al.*, 2008). The versatility of the approach has been well demonstrated in the clinical field, in which, for example, it has been used to define certain complex molecular interactions occurring in various carcinomas (Chaurand *et al.*, 2004; Schwartz *et al.*, 2005; Cornett *et al.*, 2006). Several excellent reviews describing the applications of MALDI-MSI have been published in recent years (Rohner, Staab and Stoeckli, 2005; Burnum, Frappier and Caprioli, 2008; Goodwin, Pennington and Pitt, 2008; Amstalden van Hove, Smith and Heeren, 2010; Svatoš, 2010; Zaima *et al.*, 2010b), but its potential in plant biology has yet to be widely explored, even though the spatial distribution of specific molecules is a critical component of compartmentalized cellular processes. Among the few plant-based examples to date, as recently reviewed (Kaspar *et al.*, 2011), are, for example, a study of the distribution of glucosinolates following insect feeding on *Arabidopsis thaliana* leaves (Shroff *et al.*, 2008) and a description of epicuticular lipid metabolites on the surface of A. *thaliana* flower and root (Jun *et al.*, 2010). Only rare use has been made of MALDI-MSI to analyse sectioned plant material, but it has been effective, for example, in demonstrating the uneven distribution of specific amino acids, sugars and phosphorylated metabolites within the wheat grain (Burrell, Earnshaw and Clench, 2007), and in being able to distinguish between various organ and tissue types present in

the rice grain (Zaima *et al*, 2012a). The MALDI-MSI approach has been shown to be as sensitive as the well-established liquid chromatography-mass spectrometry (LC-MS) method for the detection of wheat stem oligosaccharides (Robinson *et al.*, 2007), and has been successfully deployed to describe the distribution of both c-aminobutyric acid in the seed of eggplant (Goto-Inoue, Setou and Zaima, 2010) and pesticides in soybean (Mullen *et al.*, 2005) and sunflower (Anderson *et al.*, 2010). No comparable analysis of polypeptide distribution has been published to date, but the potential of the technology has been demonstrated by the identification of a 12-residue oligopeptide in the stem of *A. thaliana* (Kondo *et al.*, 2006).

The quality of MALDI-MSI is strongly influenced by the complexity of the target, especially where there are structural differences between distinct tissue types in the sample. Careful sample treatment is essential to ensure signal quality and to avoid lateral displacement of the analytes (Schwartz and Caprioli, 2010), as artefacts can arise at any stage between sample collection and MSI analysis (Goodwin, Pennington and Pitt, 2008). Here, we present a viable strategy for the MALDI-MSI analysis of metabolites in cryodissected barley grains and tobacco roots. Although much has been learned regarding grain development in barley using laser capture microdissection (Thiel *et al.*, 2008), in general, the sample size is too small for certain analytical procedures. Instead, we have focused on an LC-MS-based label-free quantitative approach to underpin a proteomic description of the content of the internal structures of the developing grains (Kaspar *et al.*, 2010). Furthermore, we aim to investigate the metabolite composition in several tissue types. MSI measurements have reproducibly displayed either tissue-specific or co-localized metabolite expression patterns. As a contrast, we have also studied the root, an organ heavily involved in plant–environment interactions (e.g., nutrient transport and sensing). In addition, roots differ totally in tissue composition from seed material with regard to, for example, the intercellular spaces of cortex tissue, high water content and lignin comprising central tissues.

3.1.2. Materials and Methods

Plant material

Barley (*Hordeum vulgare* L. cv 'Barke') plants were raised under controlled conditions as described by Weschke et al. (2000) (Weschke *et al.*, 2000). During the reproductive phase, the plants were subjected to a 16-h photoperiod, with an 18°C day: 10°C night temperature regime. Grains were harvested at between 1 and 20 d after pollination (DAP) and frozen in liquid nitrogen. Three replicate grains were analysed for each experiment. Tobacco plants (*Nicotiana tabacum* L. cv 'Samsun' NN) were grown in a glasshouse held at 20°C with additional illumination (300 mmol m^{-2} s^{-1} as measured at the top of the plants) provided to give a 16-h photoperiod. Roots were sampled from 8–10-wk-old plants. All samples were stored at −80°C.

Cryosectioning

Samples were frozen in liquid nitrogen, transferred to a cryostat cooled to −20°C and fixed to a sample plate via either a droplet of water (ice) or of optimal cutting temperature (OCT) medium. Longitudinal and cross-sections of varying thickness were cut from the developing barley grains and from the main and lateral tobacco roots with a razor blade. These were immediately thaw mounted on indium tin oxide (ITO)-coated glass slides (Bruker Daltonics, Bremen, Germany), which were transferred into a desiccator for 0.5–1.0 h until completely dried. The time until complete dryness varied and was longest for the tissues with high water content (roots). Microscopic images were captured with a stereomicroscope (Leica MZ6, Wetzlar, Germany) connected to a digital camera (AxioCam ICc1, Zeiss, Jena, Germany).

Matrix deposition

Matrix solutions were deposited via sensor-controlled vibrational vaporization utilizing the ImagePrep instrument (Bruker Daltonics) according to the manufacturer's instructions. For this purpose, spray protocols are provided by the manufacturer specific for the particular matrix substance. Dilutions of particular matrices were prepared as stated below after adaptation to the various tissues. 2,5-Dihydroxybenzoic acid (DHB) was diluted to 30 mg ml^{-1} in 50% v⁄v methanol, 0.2% v⁄v trifluoroacetic acid (TFA), and α-cyano-4-hydroxycinnamic acid (HCCA) to 7 mg ml^{-1} in 60% v⁄v acetonitrile, 0.2% v/v TFA. DHB and HCCA were applied in the recommended cycles of deposition, incubation and drying, controlled by the optical sensor of the instrument. High-purity HCCA, DHB, 1,8-bis (dimethylamino) naphthalene (DMAN) and 2-((2E)-3- (4-tert-butylphenyl)-2-methylprop-2-enylidene) malononitrile (DTCB) were obtained from Sigma-Aldrich (St Louis, MO, USA) and formulated as described in Supporting Information Fig. 3.1.S1.

MALDI-MSI measurement

Slides were fitted into a Slide Adapter II MALDI target (Bruker Daltonics). MSI measurements were performed in positive ionization mode using an ultrafleXtreme MALDI time-of-flight (TOF) ⁄TOF device (Bruker Daltonics), equipped with a smartbeam-II laser with a repetition rate of 1000 Hz. The resulting images were loaded into flexImaging software v2.1 (Bruker Daltonics), and auto execute sequences were generated, according to the manufacturer's instructions. The auto execute parameters were adjusted by flexControl software v3.3 (Bruker Daltonics). The laser power and laser raster (resolution) were selected manually, according to the needs of the experiment. The laser power was adjusted to obtain a relative signal intensity of 25 000 based on measurements from the tissue section before the automated MSI measurement. The laser raster (resolution) was set between 15 and 35 µm depending on the size of the tissue section.

As an example, for very small sections (such as young seeds, crosssection), a 15 µm laser raster was used in order to obtain sufficient representation of the various tissues. An *m/z* range of 80–1300 was chosen for small metabolites and the sample rate was set to 0.5 Gs s^{-1}. The laser width was set to 10 µm, and 1000 shots per raster spot were acquired. The measurement of the spots was carried out in random order to eliminate influences of measurement order.

Data processing and data analysis

FlexImaging and flexAnalysis software were used to evaluate the MSI data. Unprocessed spectra were loaded into flexImaging software and a baseline subtraction was performed. The sum spectra generated were manually evaluated by comparing a blank region with the sample measurement region. For small molecules, the mass range filter to be displayed in the ion images was set to 0.1 Da. For the determination of exact masses, manual measurements of distinct sample areas were performed and examined using flexAnalysis software.

MALDI-MSI analysis of manually dissected grain tissues

Longitudinal and cross-sections, 30 µm thick, from barley grains were cut as already described. The samples were thaw mounted on MembraneSlide 1.0 PET (Zeiss) and transferred into a desiccator for 0.5–1.0 h. Laser microdissection was carried out using a PALM Laser Microbeam instrument (Carl Zeiss Micro-Imaging GmbH, Jena, Germany), according to Kaspar et al. (2010) (Kaspar *et al.*, 2010). The isolated tissues were extracted using 7 µl hexane : isopropanol (1 : 1, v/v) or 60% methanol. Extracts were transferred directly to an AnchorChip 800 target plate (Bruker, Bremen, Germany) with a final volume of 2 µl per spot. One microlitre of DHB (diluted to 30 mg ml^{-1} in 50% v/v methanol, 0.2% v/v TFA) was added to each sample spot. In addition, the manual dissection of barley grain tissues was performed using a precooled (in liquid nitrogen) stainless steel plate. Pericarp, chlorenchyma layer, endosperm, scar and embryo region were isolated with a razor blade and fórceps using a Stemi DV4 stereomicroscope (Zeiss). The extraction of compounds was carried out as mentioned above, but with a volume of 50 µl on a shaker for 30 min. After 5 min of centrifugation, 1 µl of each sample was spotted onto an AnchorChip 800 target and 1 µl of DHB solution was added. MALDI-MS measurements were performed as described in the MALDI-MSI measurement section.

Identification of L-a-lysophosphatidylcholine (LPC) and L-a-phosphatidylcholine (PC) by MALDI MS/MS

Standard mixtures of LPC and PC from soybean were obtained from Sigma-Aldrich and diluted to 100 lg ml^{-1} for PC and 1% for LPC in chloroform. One microlitre of each standard was spotted onto an AnchorChip 800 target together with 1 µl of DHB solution. Collision-induced dissociation (CID) spectra of standard compounds and corresponding precursor ions from barley grain sections were acquired in 'LIFT' mode using argon as a collision gas on an ultrafleXtreme MALDI TOF/TOF device (Bruker Daltonics).

3.1.3. Results and Discussion

Both the barley grain and the tobacco root comprise a mixture of tissue types (e.g., parenchymal, collenchymal and vascular tissues), so that sample preparation had to preserve, as closely as possible, the three-dimensional structure of the tissues. During the early stage of development, the barley grain contains a high proportion of water, making sample preparation fairly straightforward; however, more mature grains contain much less free water, so that their sectioning requires particular attention. Specific optimization targets were tissue section preparation, choice of matrix and matrix application, and MALDI-MSI measurement parameters and data analysis.

Tissue section preparation

Thin tissue slices were cut with a conventional cryotome, but the preparation of sections cannot follow the standard histological procedures, for example, slice preparation for immunostaining or dye staining, because embedding in polymeric compounds, such as synthetic resin (HM20), or the use of OCT medium would result in ionization suppression of the analytes during MS measurements. OCT is a polymeric alcohol composed of polyvinyl alcohol and polyethylene glycol (PEG), and is widely used for the embedding of samples before cryosectioning processes (Turbett and Sellner, 1997). Therefore, samples were fixed in the desired orientation with a small droplet of fixation medium on the cutting block of the instrument. For fixation, we tested two compounds: OCT and water (ice). A series of cross-sections was made from both the main and lateral roots of tobacco, and from barley grains harvested at various DAP (Fig. 3.1.1a,b). Because it was impossible to avoid contamination with OCT in barley grains younger than 6 DAP and in longitudinal tobacco root sections, water (ice) was used as the fixation medium. However, the use of water resulted in a considerable degree of diffusion of analyte during thaw mounting, visible as a smear around the section (Fig. 3.1.1c,d). There are also other plant organs, such as leaves, small seeds and root tips, which have proven to be difficult to section.

The film sectioning method (Kawamoto, 2003) generates significantly less distortion and dislocation than occurs in the absence of any supporting material, and has been successfully used for the analysis of rice grains (Zaima, Goto-Inoue, *et al.*, 2010). However, this approach proved to be impractical for the very small samples used.

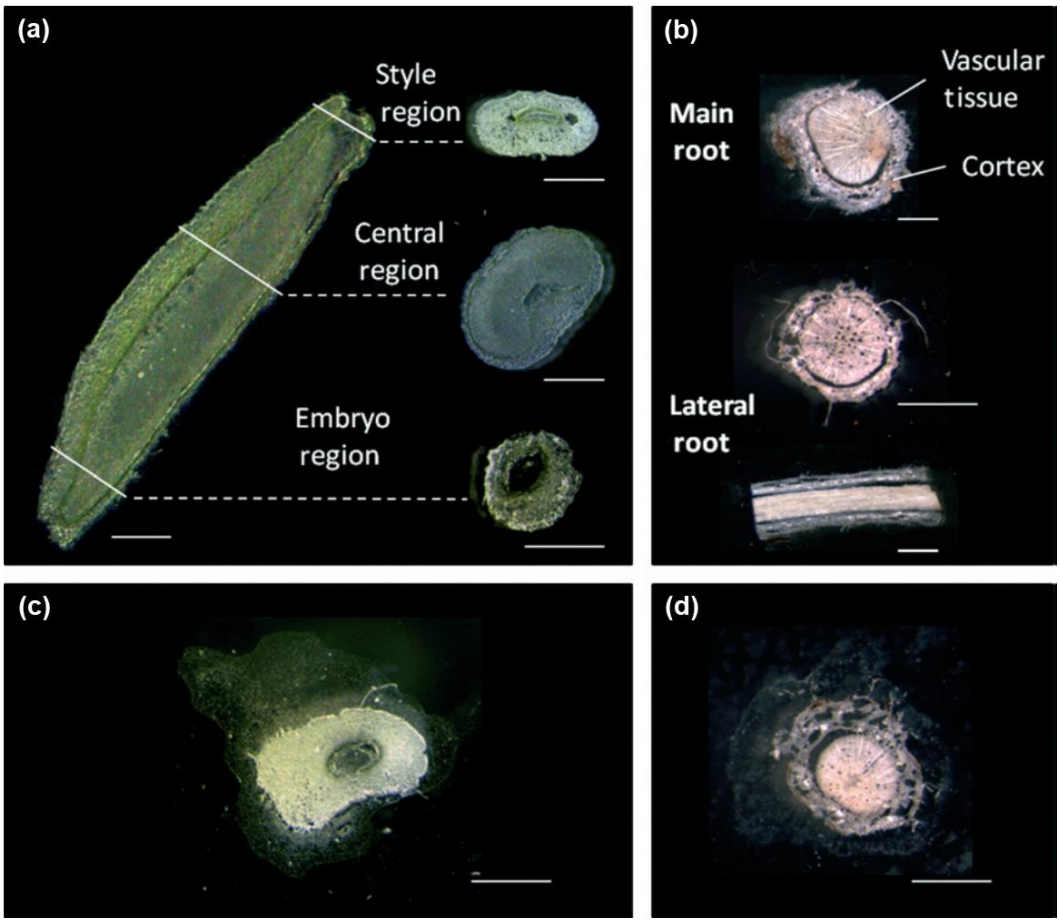

Figure 3.1.1. *Tissue sectioning. (a) Representative optimal cutting temperature (OCT) medium-fixed 30-µm longitudinal and cross-sections cut from various regions of a 7-d after pollination (DAP) developing barley (Hordeum vulgare) grain. (b) Water-fixed 55-µm longitudinal section of a lateral root, and cross-sections from a main (55 µm) and a lateral (40 µm) tobacco (Nicotiana tabacum) root. (c) 30-µm cross-section from the scar region of a 3-DAP developing barley grain (water-embedded tissue). (d) 55-µm cross-section from a lateral tobacco root (water-embedded tissue). Delocalized metabolites are visible as a smear surrounding the sections after thaw mounting on indium tin oxide-coated slides. Bars, 1 mm.*

The optimal thickness range for tobacco root sections was 35–55 µm. Fig. 3.1.1b shows a 55-µm longitudinal section of a lateral root, and cross-sections from a main (55 µm) and lateral (40 µm) root, from 8-wk-old tobacco plants. These sections are thicker than those commonly used for MSI experiments to avoid disruption caused by the large intercellular spaces in the parenchymal cortex. The influence of root section thickness on MALDI-MSI output is depicted in Fig. 3.1.2a, which shows images of four molecular adduct ions from 35-, 45- and 55-µm cross-sections of a tobacco lateral root. A slice thickness above 45 µm led to a notable deterioration in measurement sensitivity, particularly when analysing distribution patterns in the central root. The

loss of MS signal in this root region probably reflects matrix absorption effects, as the signal intensities for root cortex were rather independent of sample thickness.

For young (1–7 DAP) barley grains, 20 µm slices were effective, but, as the grain developed, the accumulating starch (associated with a loss of water content) forced the section thickness to be increased to 30–40 µm (Fig. 3.1.1a). The effect of section thickness on the resulting MALDI-MSI is shown in Fig. 3.1.2b, which presents ion images of four molecular masses from a 7-DAP grain. The signal intensities from 20 and 30 µm sections were consistent, but the detection sensitivity was reduced in 40 µm sections, because of the higher matrix absorption by the tissue. Therefore, the section preparation of barley grains was set to 30 µm. Unlike in the root, there were less tissue type-dependent matrix effects observed for barley grains and the less fragile structure of the grain allowed very thin sections to be used. Sample preparation is particularly demanding when an array of highly differentiated tissues is present. The use of nonembedded frozen sections requires a high degree of technical proficiency. Conventionally, the majority of sections used for MSI are 10–20 µm thick (Goodwin, Pennington and Pitt, 2008; Amstalden van Hove, Smith and Heeren, 2010), a thickness which provides a reasonable compromise between MSI performance and practicality (Zaima *et al.*, 2010b), particularly when a large number of samples are to be analysed. However, the optimal slice thickness is very much dependent on the kind of tissue under investigation.

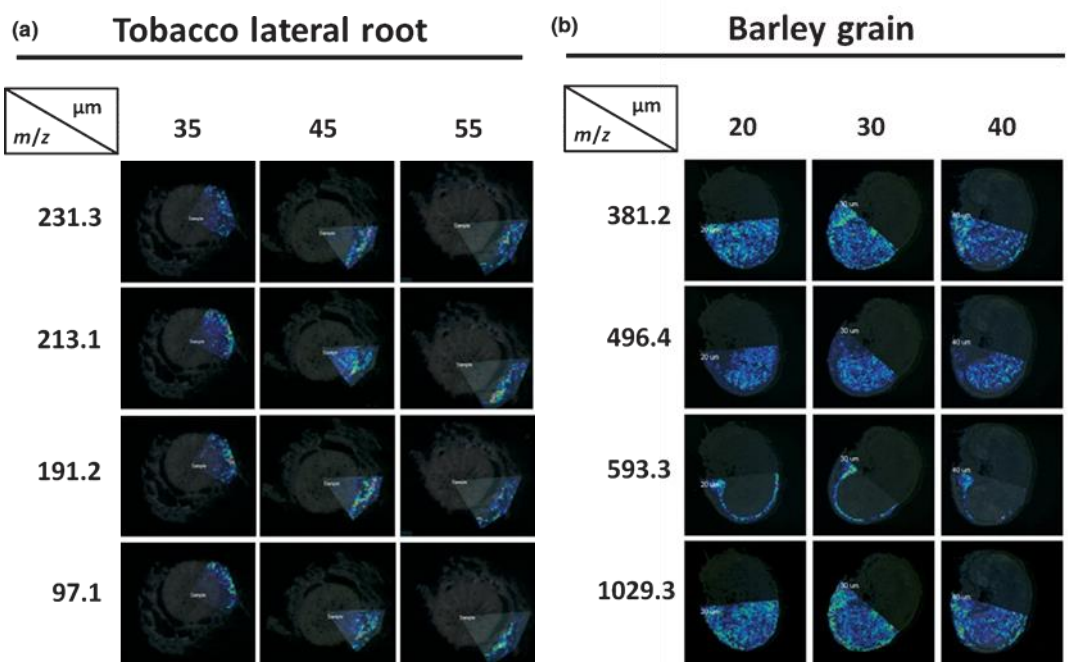

Figure 3.1.2. *The influence of section thickness. Ion images obtained from matrix-assisted laser desorption / ionization mass spectrometric imaging (MALDI-MSI) of cross-sections of three thicknesses of a tobacco (Nicotiana tabacum) lateral root (a) and a 9-d after pollination (DAP) developing barley (Hordeum vulgare) grain (b). Measurements were conducted at a resolution of 30 µm (tobacco root) and 25 µm (barley grain). Some signal intensities proved to be dependent on the section thickness.*

Choice of matrix and matrix application

Depending on the alterations in ionizing capacity of the different substrate groups to be analysed, various matrix compounds have been proposed (Svatoš, 2010; Kaspar *et al.*, 2011). We chose to test HCCA, DHB, DMAN and DTCB. DMAN, which belongs to the so-called 'proton sponges', is a new matrix introduced by Shroff & Svatoš (Shroff and Svatoš, 2009). According to its strong basicity, this matrix is useful for the analysis of anions. Of the tested matrices, DHB gave the most reproducible results, given the choice of application strategy, matrix-derived background (Supporting Information Fig. 3.1.S1) and MALDI-MSI reproducibility (Fig. 3.1.5). One of the most challenging aspects of MSI relates to the reproducibility in the application of the matrix compound (Gustafsson, McColl and Hoffmann, 2008). The most widely used deposition techniques are spraying with a simple airbrush and the use of a dedicated instrument to obtain vibrational vaporization. Here, the latter approach was adopted, based on an instrument able to apply a series of matrix layers with an incubation and drying period between each deposition step. Reproducible layers were obtained for HCCA, DCTB and DHB, but the DMAN matrix could not be deposited by vibrational vaporization, as its chemistry hindered adequate crystal formation. Image- Prep spray plates can normally be used for several cycles of matrix deposition, but we noted that, after a number of cycles, larger droplets started to form, and these led to a loss in the achievable spatial resolution. Fine layers of matrix crystals could still be obtained, but this required manual intervention during the spraying process. Thus, for optimal reproducibility, fresh spray plates should be used. An alternative approach is to use either microchip spotting technology (<20 µm spatial resolution) or sublimation (1 µm resolution), compared with the 10–100 µm resolution achieved by spray application (Kaletas *et al.*, 2009; Agar *et al.*, 2010).

A critical consideration in the choice of matrix is the frequency of matrix-derived MALDI-MSI signals caused by matrix fragmentation and cluster formation. To distinguish matrix- and sample-derived *m/z* values, every MSI experiment includes the measurement of a blank region with matrix only. During data analysis, sum mass spectra of both measurement regions are then overlaid and compared. The interference of DHB with the signals generated from a barley grain sample is illustrated in Fig. 3.1.3, which represents a sum mass spectrum from one MSI experiment in which the matrix-derived and barley grain signals in two specific mass regions are shown in detail. Comparison of the mass signals generated from the barley grain section and blank region revealed *m/z* 758.6 and 851.5 as being potential grain tissue-related signals, but also showed interference with DHB related signals for *m/z* 758.6. Another example of matrix interference is presented in Supporting Information Fig. 3.1.S2, which shows the mass spectra and corresponding ion images for two particular *m/z* values. These peaks can only be assigned to the tissue by their distinct distribution pattern in the sample or by comparison of the isotope pattern. Many of the signals in the low mass region (*m/z* <400) could be associated with DHB

fragmentation and cluster formation, and so these needed to be subtracted from MSI sample sets as part of the data evaluation process. The mass spectra obtained from HCCA, DHB, DMAN and DTCB were compared in both positive and negative ionization mode. In the positive ionization mode, DHB and DMAN produced the fewest peaks, whereas the HCCA spectrum was well populated at *m/z* <400 and, similarly for DCTB, in the range *m/z* 400–800. In the negative ionization mode, few peaks were generated by DHB, and even fewer by DMAN. However, more complex spectra were observed for HCCA and DCTB (Supporting Information Fig. 3.1.S1). Other ionization-enhancing reagents, such as silver or gold nanoparticles (Hua *et al.*, 2007; Wu *et al.*, 2009), colloids and graphite have been introduced recently (Svatoš, 2010); these appear to have advantages in the context of lipid detection, and also tend to produce fewer and less intense signals, thereby improving the spatial resolution. However, the use of these matrices requires the adaptation of application strategies and the consideration of target compound classes.

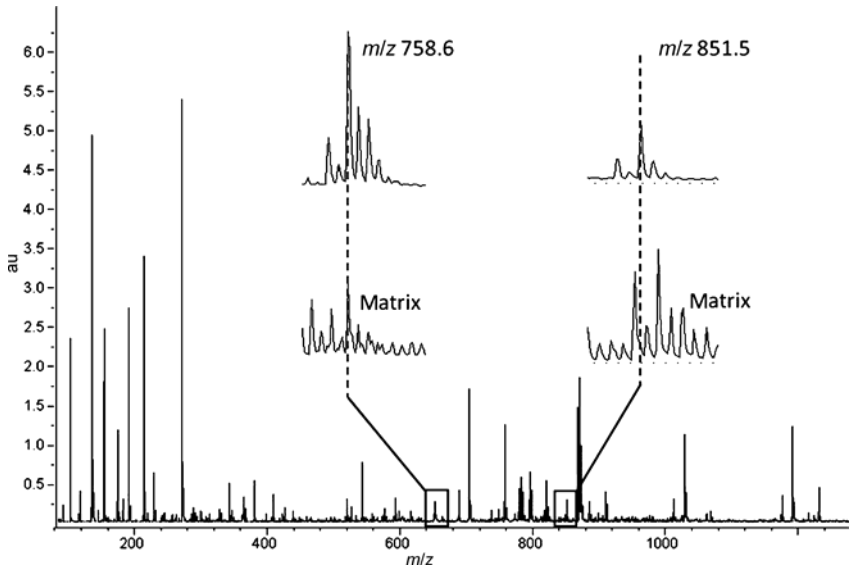

Figure 3.1.3. *The assessment of the background signal generated by the matrix. A representative sum spectrum from one matrix-assisted laser desorption / ionization mass spectrometric imaging (MALDI-MSI) run of a 7-d after pollination (DAP) developing barley (Hordeum vulgare) grain, together with the detail of the mass spectrum for the matrix alone and for the barley grain alone at m/z 759 and m/z 852. au, arbitrary units.*

MALDI-MSI parameters and data analysis

The size of the barley grain longitudinal sections increases from a length of c. 2 mm and a diameter of c. 1 mm at 2 DAP to a length of >1 cm and a diameter of c. 3 mm by 14 DAP. Thus, depending on the sample size, we must adapt the measurement resolutions to extract biologically relevant information, but also to limit the size of the dataset. Metabolite distributions in barley grains appear at the tissue level rather than at the single-cell level, and cellularization levels vary strongly from very young grains (1–6 DAP) to grains in the seed filling or mature stage (7– 20 DAP). Some tissues require a higher resolution measurement than others – for example, the

aleurone layer is only two to three cell layers thick (Garrett *et al.*, 2011). As a result, the resolution adopted for 1–6-DAP grains were 10–20 µm and, for 7–20-DAP grains, 20–35 µm (for details, see Supporting Information Table 3.1.S1). It should be noted that most of the current literature describing MALDI-MSI analyses of plant material describes spatial resolutions in the range 100–200 µm (see review by Kaspar et al., 2011 (Kaspar *et al.*, 2011)). The exceptions are an investigation of eggplant seed with a resolution of 25 µm (Goto-Inoue, Setou and Zaima, 2010), and a study of the *A. thaliana* flower, stem and root with measurement resolutions of 12, 25 and 50 µm (Jun *et al.*, 2010). The highest spatial resolution reported so far for plant material (*A. thaliana* and *Hypericum* species), 10 µm, was achieved by matrix-free UV-laser ionization mass spectrometry for the analysis of UV-absorbing secondary metabolite distributions (Hölscher *et al.*, 2009).

The reproducibility of MALDI-MSI results is reflected by the same distribution pattern of *m/z* values through independent experiments. In our experiments, MALDI-MSI-derived metabolite distributions were verified through both biological replication and by comparing the outcomes from longitudinal and cross-sections of different seed parts. At least three replicates were conducted to derive spatial and temporal distribution patterns. Thus, it is possible to describe the specific arrangement of molecules both histologically and within a developmental context. In addition, MALDI-MSI spectra of extracts from manually dissected barley grain tissues revealed *m/z* values with the same distribution pattern as detected by MALDI-MSI experiments. Fig. 3.1.4 presents a set of ion images of longitudinal and cross-sections of a 7-DAP barley grain. The multi-ion image on the left is from a longitudinal section, the corresponding images from cross-sections are in the centre and the various spectra are on the right. The abundance of the *m/z* 773.4 product was specific to the scar region of the developing grain (Fig. 3.1.4, top), whereas the region surrounding the developing endosperm (in both the longitudinal and cross-sections) featured the *m/z* 593.3 product (Fig. 3.1.4, centre), and the *m/z* 816.5 analyte was largely localized within the region of the developing embryo (Fig. 3.1.4, bottom). Fig. 3.1.5 presents ion images for two products of different *m/z* showing their tissue-specific localization (593.3 and 520.4) across three replicates (top part of the figure); the bottom panel illustrates examples for two co-localized molecular masses (*m/z* 104.1 and 820.5) across three replicates. The data demonstrate the feasibility of generating reproducible, high-resolution MALDI-MSI profiles from thin barley grain sections, once sample preparation, matrix application and MS measurement have all been optimized.

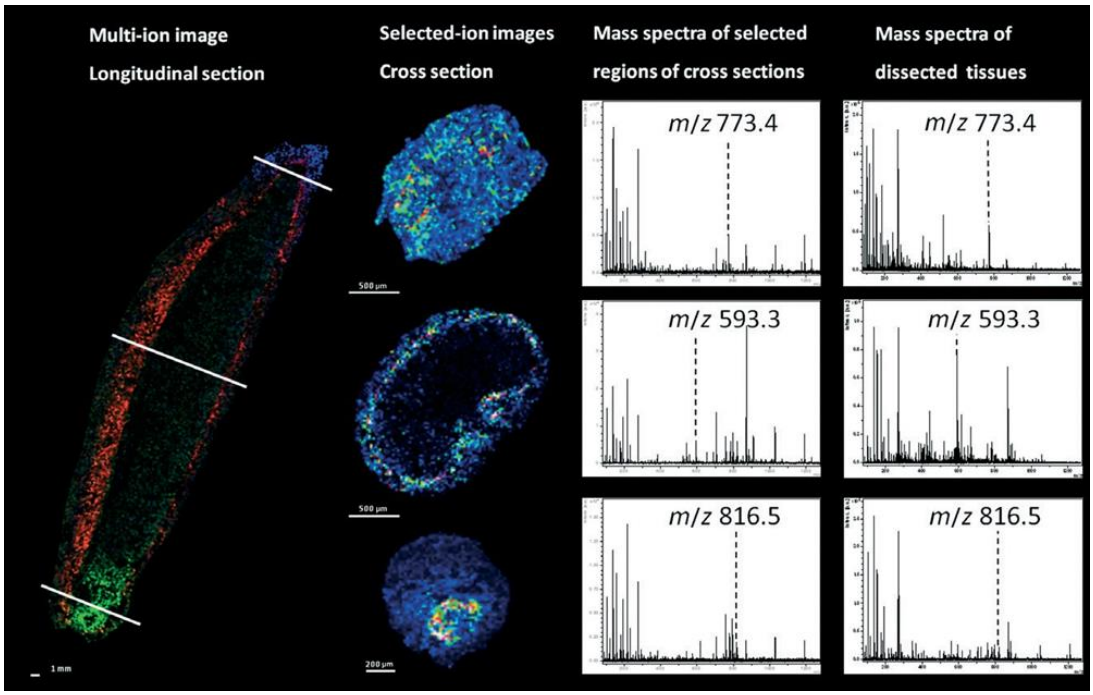

Figure 3.1.4. *Reproducibility of matrix-assisted laser desorption/ionization mass spectrometric imaging (MALDI-MSI) across tissues, showing the spectra obtained from 30-µm sections of a 7-d after pollination (DAP) developing barley (Hordeum vulgare) grain. The multi-ion image shows molecular masses m/z 773.4 (blue), m/z 593.3 (red) and m/z 816.5 (green) from a longitudinal section (left), the corresponding selected-ion images (centre) and the respective mass spectra with molecular masses indicated by a dotted line (right). The resolution was 25 µm for the longitudinal section, the cross-section of the scar and the central region, and 20 µm for the embryo cross-section.*

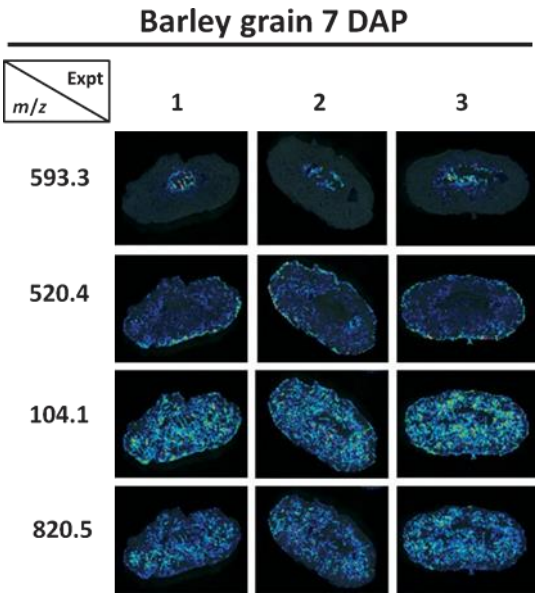

Figure 3.1.5. *Reproducibility of matrix-assisted laser desorption/ionization mass spectrometric imaging (MALDI-MSI) across biological individuals. Ion images from cross-sections of the scar region of three 7-d after pollination (DAP) developing barley (Hordeum vulgare) grains. Measurements were conducted at a resolution of 20 µm.*

Once the MS data collection is completed, processing and visualization methods for the evaluation of intensity distributions and statistical comparison are applied. FlexImaging software was used for the evaluation of a sum spectrum of the complete dataset, and to visualize multi-ion and selected-ion images within tissue sections. Baseline subtraction was included in the data acquisition, but additional subtraction of the matrix-derived signal was not possible. As a result, the tissue-derived sum spectra had to be manually compared with the spectra derived from the matrix alone (an example is given in Fig. 3.1.3). A number of MALDI-MSI software packages (both open-source and commercial) offer data processing algorithms and statistical analysis (Kaspar *et al.*, 2011), but software-driven subtraction of the matrix background in the low *m/z* range is not yet available. Furthermore, current software packages designed to statistically analyse MALDI-MSI datasets are unable to handle large datasets, for which prior data reduction is required. Depending on the number of single spectra per MALDI-MSI dataset, this type of data reduction implies a loss of resolution. The number of spectra routinely acquired in our experiments varied from 2500 to 18 000 per tissue section (Supporting Information Table 3.1.S1). This scale of data is beyond the analytical capacity of current software, underlining the need for development in this direction, as exemplified by BioMap analysis software (http://www.maldi-msi.org/).

Great effort is needed for the identification of compounds detected with MALDI-MSI. To reveal almost exact *m/z* values, we carried out manual measurements on the tissue surface. Several online databases (http://metlin.scripps.edu/), KNApSack (http://kanaya.naist.jp/KNApSAcK/) and Lipidomics Gateway (http://www.lipidmaps.org/), as well as literature data, were used to classify products on the basis of their measured *m/z*. Additional information was obtained from MS/MS measurements. Diagnostic fragment ions allowed an assignment of precursor masses as molecular species of PC and LPC. These phospholipid classes are expected to produce fragment ions of *m/z* 104 and 184 and a neutral loss of *m/z* 59 (Xu *et al.*, 2009; Garrett *et al.*, 2011; Murphy and Gaskell, 2011). The fragmentation is based on CID, a technique designed to control the fragmentation of selected precursor ions. For example, CID of molecular ion *m/z* 520.4 from barley grain tissue generated fragment ions of *m/z* 104 and 184. A comparison with the MS⁄MS spectrum of *m/z* 520.4 from LPC standard solution showed the same fragment ions (Fig. 3.1.6). This protonated ion was identified as an 18:2 LPC species with linoleic acid as unsaturated fatty acid residue.

However, as the mass accuracy of MALDI TOF⁄TOF instrumentation is insufficient at present to determine the molecular formulae of selected compounds, a targeted analysis based on gas chromatography-mass spectrometry (GC-MS) and⁄or LC-MS is still required to achieve identification. Improvements in analytical software are still required to enhance the mass accuracy of the sum spectra and to avoid peak shifts during the simultaneous acquisition of different regions

of interest. In our protocol, the instrument was calibrated in the positive ionization mode with PEG200 + 600 before the start of an automatic acquisition, but a calibration in between individual measurements is currently not supported by the vendor's software. The development of software solutions for external calibration during automatic MALDI-MSI runs remains a strong priority.

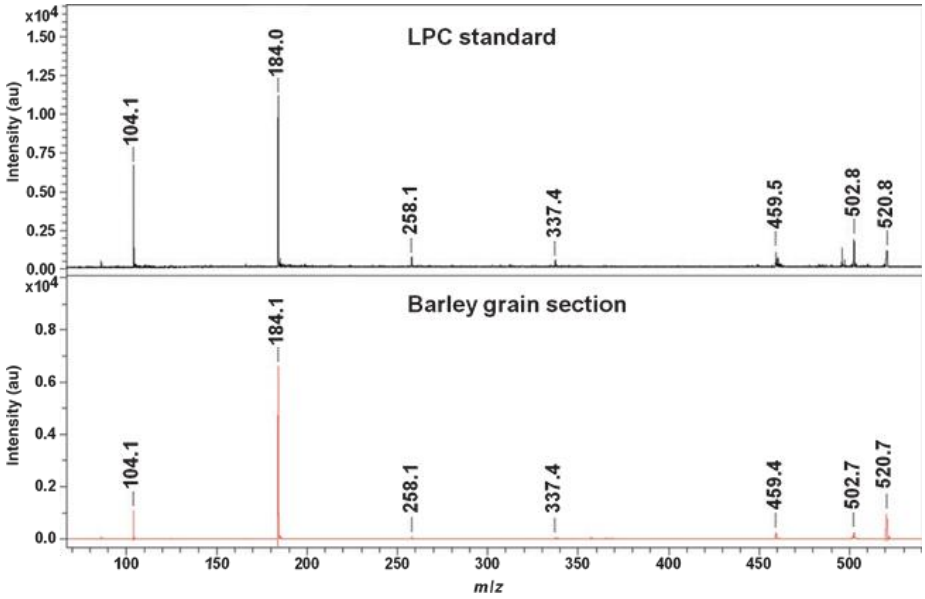

***Figure 3.1.6**. Comparison of collision-induced dissociation (CID) spectra of molecular adduct ion m/z 520.4 from L-alysophosphatidylcholine (LPC) standard solution (1% in chloroform) and barley (Hordeum vulgare) grain section (pericarp region). au, arbitrary units.*

3.1.4. Conclusions

The data presented here have demonstrated that MALDI-MSI measurements can reliably illuminate the spatial distribution of small molecules in barley grain and tobacco root sections, once sample preparation protocols have been optimized. The metabolite and protein composition of an organ (and of the individual tissues within) depends on the organ's function. Sampling strategies producing a range of spatial resolutions have been trialled in plants, including manual and laser capture-assisted dissection in conjunction with micropipetting approaches (Table 3.1.1). More recently, protoplast labelling and ribosome tagging have been proposed as a means of obtaining a nontargeted analysis of the content of specific tissues (Dinneny *et al.*, 2008b; Mustroph *et al.*, 2009). An alternative platform, involving liquid extraction surface analysis (LESA) coupled to MS detection, has been suggested for the direct analysis of tissues. MALDI-MSI has the particular advantage that the distribution of compounds can be assessed from direct measurements of the sample at high spatial resolution. An appropriate choice of experimental protocol, particularly for sample preparation, is critical. However, once established, MALDI-MSI can provide highly selective, rapid and parallel acquisition of many compounds. Thus, MALDI-MSI should find applications in various fields of plant research, including development, host–pathogen interactions, abiotic responses, nutrition and symbiotic interactions, and varietalspecific gene expression. The relevance of development lies in the changes affecting tissues during the

process, as these affect the distribution of cellular components. In the interaction between the host and its pathogens, the host's production of antimicrobials is a key part of host defence. Similarly, the abiotic response, including nutrient stress (e.g., inadequate nitrogen or excess trace elements), involves the induction of a range of molecules in a tissue-specific manner. Finally, the establishment of the effect of single genes is often attempted by making comparisons between isogenic lines, or between mutants (or transformants) and the wild-type, so that the capacity to identify primary or secondary gene products is becoming increasingly important. As observed previously for the barley grain (Bollenbeck *et al.*, 2009; Kaspar *et al.*, 2011), the identification of metabolites or proteins and the confirmation of tentatively assigned *m/z* signals constitute major challenges for MSI. We suggest that improvements in both sample preparation strategy and the analytical platform (both for spectrum acquisition and post-acquisition analysis) will enhance the relevance of MALDI-MSI technology in plant research. The implementation of tandem mass spectrometry will encourage MALDI-MSI applications in plant research by enabling the identification of metabolites and, via on-tissue digestion, N-terminal peptide derivatization and CID tandem MS, by facilitating the identification of polypeptides. Much of our current effort is focused on data integration. The most widely applied approach is tissue-specific characterization, which requires the integration of the data into existing histological models (Bollenbeck *et al.*, 2009) or into metabolic networks in the case of transcript and metabolite profiling (Thiel *et al.*, 2009). An understanding of the molecular events unfolding during development will be much aided by a knowledge of the localization and abundance of key molecules present in specific tissues. Despite the growing impact of molecular imaging, MALDI-MSI technology is likely to complement, rather than to replace, targeted profiling approaches typified by forward functional genomics.

Table 3.1.1. *An overview of sampling strategies used to obtain spatially resolved profiling in plant materials*

Sampling technique	Resolution	Analysis targets	Analysis approach	Selected references
Manual dissection	Organs, tissues	RNA, metabolites, proteins	Targeted/untargeted	Amantonico et al.(2010)
LCM[1]	Tissues, cells	RNA, metabolites, proteins	Targeted/untargeted	Thiel *et al.* (2008); Kaspar *et al.* (2010)
Micropipetting	Cells	RNA, metabolites, proteins	Targeted/untargeted	Amantonico et al. (2010)
Protoplast sorting	Tissues, cells	RNA, metabolites, proteins	Targeted/untargeted	Dinneny *et al.* (2008); Tsukagoshi *et al.* (2010)
Tagged ribosomal proteins	Tissues, cells	RNA	Untargeted	Zanetti *et al.* (2005); Mustroph *et al.* (2009)
Cryosectioning[2]	Tissues, cells	Metabolites, proteins	Targeted/untargeted	Burrell *et al.* (2007); Zaima *et al.* (2010a)
Direct surface analysis[3]	Surfaces, tissues	Metabolites, proteins	Untargeted	Shroff *et al.* (2008); Jun *et al.* (2010)

[1]Laser capture microdissection.
[2]Direct analysis of cryosections by matrix-assisted laser desorption/ionization mass spectrometric imaging (MALDI-MSI) approaches.
[3]Direct analysis by liquid extraction surface analysis (LESA) coupled to mass spectrometry

Acknowledgements

This research was funded by the German Research Foundation (DFG; MA 4814/1-1) and by the Spanish Ministry of Science and Innovation (AGL2010-16515). Financial support from the EU (COST Action FA0603) is gratefully acknowledged. The authors have declared no conflict of interest.

Supporting Information for Chapter 3.1

All the additional supporting information may be found in the online version of this article (doi: 10.1111/j.1469-8137.2011.03970.x).

- ***Figure 3.1.S1.*** *Matrix background.*

- ***Figure 3.1.S2.*** *Exclusion of matrix derived signals.*

- ***Table 3.1.S1.*** *Representative numbers.*

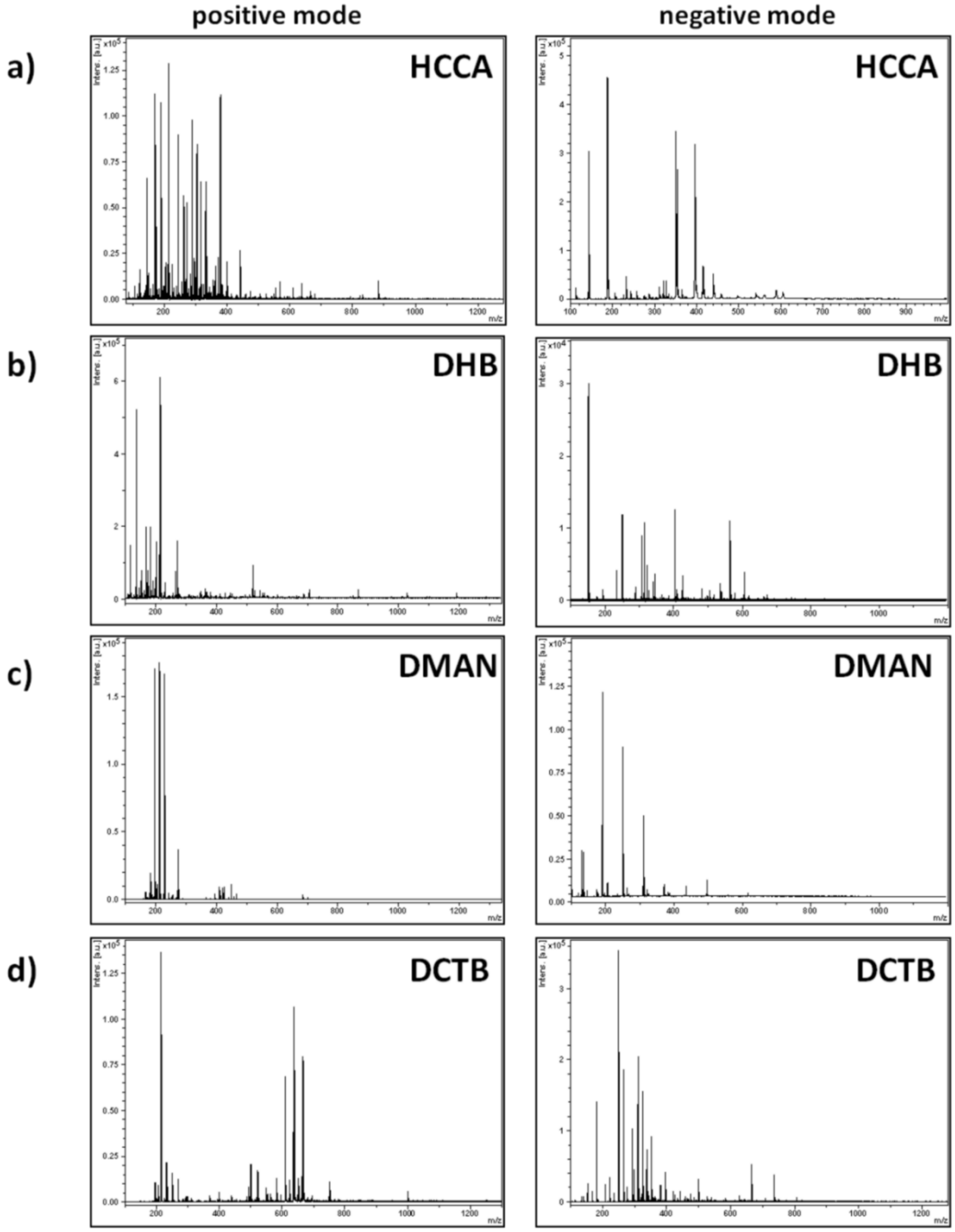

Figure 3.1.S1. *Matrix background. Variation between matrix compounds in the background signal generated. Representative sum spectra from MALDI-MS runs for (a) α-cyano-4-hydroxycinnamic acid (HCCA), (b) 2,5-dihydroxybenzoic acid (DHB), (c) 1,8-bis(dimethylamino)naphthalene (DMAN), and (d) 2-((2E)-3-(4-tert-butylphenyl)-2-methylprop-2-enyliden) malononitrile (DTCB) in positive and negative ionization mode. Measurements were perfomed on stainless steel anchor chip targets (MTP AncorChip™ 800/384 TF, Bruker Daltonics, Bremen, Germany) as follows: (a) 7 mg ml^{-1} in 60% acetonitrile and 0.2% TFA, (b) 30 mg ml^{-1} in 50% methanol and 0.2% TFA, (c) 1 mg ml^{-1} in ethanol, (d) 10 mg ml^{-1} in 80% acetonitril.*

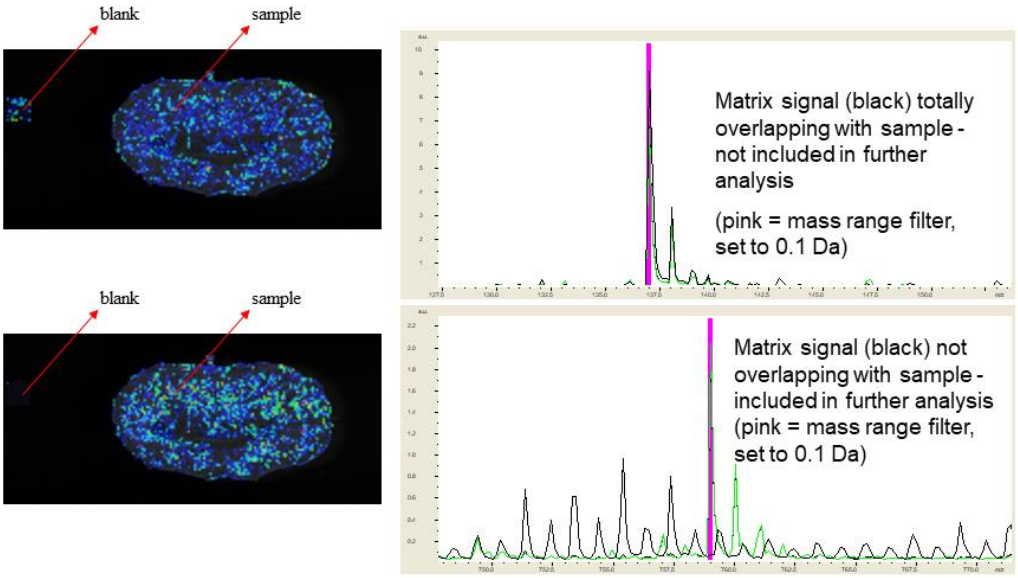

Figure 3.1.S2. *Exclusion of matrix derived signals. In every MSI experiment independent blank regions with just matrix (square) are included. During analysis sum spectra of both regions are overlaid to compare matrix derived (black) signals with those from the sample (green).*

Table 3.1.S1. *Representative numbers of individual spectra from MALDI-MS imaging runs at various spatial resolutions for longitudinal and cross sections of barley grains harvested at a range of developmental stages.*

	Longitudinal section			**Transversal section**		
	2 DAP	**7 DAP**	**10–20 DAP**	**2 DAP**	**7 DAP**	**10–20 DAP**
Resolution (µm)	20	30	35	15–20	20–25	20–30
Spectra number	4,500	7,500	13,000–18,000	2,500–6,000	4,000–6,000	4,000–8,000

DAP, days after pollination. The *m/z* range of all MSI experiments for low molecular weight measurements was 80–1,300.

3.2. Changes induced by Fe deficiency and Fe resupply in the root protein profile of a peach-almond hybrid rootstock

Jorge Rodríguez-Celma[1], Giuseppe Lattanzio[1], Sergio Jiménez[2], Jean-Francois Briat[3], Javier Abadía[1], Anunciación Abadía[1], Yolanda Gogorcena[2] and Ana-Flor López-Millán[1]

[1]*Plant Nutrition, Aula Dei Experimental Station (CSIC), P.O. Box 13034, E-50080, Zaragoza, Spain*

[2]*Pomology Departments, Aula Dei Experimental Station (CSIC), P.O. Box 13034, E-50080, Zaragoza, Spain*

[3]*Biochimie et Physiologie Moléculaire des Plantes, Centre National de la Recherche Scientifique, Institut National de la Recherche Agronomique, Université Montpellier 2, SupAgro. Bat 7, 2 place Viala, 34060 Montpellier cedex 1, France*

Published in the Journal of Proteome Research (2013) 12, 1162-1172 (doi: 10.1021/pr300763c).

Additional supporting information may be found in the online version of this article at the publisher's web-site.

SUMMARY

The changes in the root extract protein profile of the Prunus hybrid GF 677 rootstock (*P. dulcis* × *P. persica*) grown in hydroponics as affected by Fe deficiency and short-term (24 h) Fe resupply have been studied by 2-dimensional gel electrophoresis-based techniques. A total of 335 spots were consistently found in the gels. Iron deficiency caused above 2-fold increases or >50% decreases in the relative abundance in 10 and 6 spots, respectively, whereas one spot was only detected in Fe-deficient plants. Iron resupply to Fe-deficient plants caused increases and decreases in relative abundance in 15 and 16 spots, respectively, and one more spot was only detected in Fe-resupplied Fe-deficient plants. Ninety-five percent of the proteins changing in relative abundance were identified using nanoliquid chromatography-tandem mass spectrometry. Defense responses against oxidative and general stress accounted for 50% of the changes in Fe-deficient roots. Also, a slight induction of the glycolysis-fermentation pathways was observed in GF 677 roots with Fe-deficiency. The root protein profile of 24 h Fe-resupplied plants was similar to that of Fe-deficient plants, indicating that the deactivation of Fe-deficiency metabolic responses is slow. Taken together, our results suggest that the high tolerance of GF 677 rootstock to Fe deficiency may be related to its ability to elicit a sound defense response against both general and oxidative stress.

3.2.1. Introduction

Iron deficiency is a common nutritional disorder in many fruit tree orchards growing in the Mediterranean basin (Rombolà and Tagliavini, 2006; Abadía *et al.*, 2004). Fruit crops affected include peach, pear, quince, kiwi, and citrus (Tagliavini and Rombolà, 2001). In these orchards, Fe deficiency causes leaf yellowing (chlorosis), delayed fruit ripening (Álvarez-Fernández *et al.*, 2003), decreased fruit yield and quality (Álvarez-Fernández *et al.*, 2011), and increased orchard management costs (Abadía *et al.*, 2004). The most prevalent cause of Fe deficiency in this area is the presence of high $CaCO_3$ in soils. In these basic pH conditions, Fe availability for plants is low, due to its poor solubility in the rhizosphere.

When Fe is scarce, plants induce several mechanisms to increase the Fe acquisition capacity. Strategy I plants, including dicotyledonous and non-graminaceous monocots, induce a multistep mechanism for root Fe acquisition that includes the induction of an Fe(III)-reductase (FRO, Ferric Reductase Oxigenase) (Robinson *et al.*, 1999), an Fe(II) transporter (IRT, Iron Regulated Transporter) (Eide *et al.*, 1996), and an enhanced proton extrusion capacity by a plasma-membrane H+-ATPase (Santi and Schmidt, 2009). These plants also elicit changes at the metabolic level to sustain the high energy requirements for Fe uptake (G. Zocchi, 2006; López-Millán *et al.*, 2009). These include an accumulation of organic acids, mainly malate and citrate, throughout the plant (Abadía *et al.*, 2002), shifts in the redox state of the cytoplasm (Lopez-Millan, Morales, Andaluz, *et al.*, 2000) and increases in the activity of phosphoenolpyruvate carboxylase and other enzymes of the Krebs cycle and of the glycolytic and pentose phosphate pathways (G. Zocchi, 2006). This metabolic reprogramming constitutes an anaplerotic carbon source, which compensates partially for the low photosynthetic rates occurring in Fe-deficient plants (López-Millán *et al.*, 2009).

Although many studies have focused on the physiological responses to Fe deficiency in roots, the root responses to Fe fertilization have been less explored. Iron resupply leads to a rapid (within 24 h) deactivation of genes associated to root Fe acquisition mechanisms, including FRO and IRT (Enomoto *et al.*, 2007; Gonzalo, Moreno and Gogorcena, 2011), whereas the enzymatic activities of Fe reductase and PEPC were reported to decrease more gradually (López-Millán *et al.*, 2001; Abadía *et al.*, 2011). A considerable decrease in the capacity to lower the pH of the nutrient solution was also observed upon Fe resupply to Fe-deficient *Cucumis sativus* (Dell'Orto *et al.*, 2000). Organic acid concentrations and metabolite profiles reached control levels only within a few days after Fe resupply (Rellán-Álvarez, Andaluz, *et al.*, 2010; Abadía *et al.*, 2011). Also, Fe resupply leads to progressive decreases in the concentration of organic acids at the whole plant level (López-Millán *et al.*, 2001).

Recently, 2-DE proteomic profiling techniques have been used to study Fe deficiency responses in roots of different herbaceous plant species, including *Lycopersicon esculentum* (Brumbarova *et al.*, 2008; Li *et al.*, 2008), *Beta vulgaris* (Rellán-Álvarez, Andaluz, *et al.*, 2010), *C. sativus* (Donnini *et al.*, 2010), and *Medicago truncatula* (J Rodríguez-Celma *et al.*, 2011). These studies not only confirmed the general changes in root carbon metabolism induced by Fe deficiency, but also unraveled previously unknown root responses elicited by Fe shortage. These include the induction of the riboflavin synthesis pathway in *B. vulgaris* (Rellán-Álvarez, Andaluz, *et al.*, 2010) and *M. truncatula* (J Rodríguez-Celma *et al.*, 2011), and a reprogramming of the N metabolism, via protein turnover, in *C. sativus* (Donnini *et al.*, 2010) and *M. truncatula* (J Rodríguez-Celma *et al.*, 2011) Information on the effects of Fe deficiency on the root proteome has arisen mostly from studies on Fe-deficient herbaceous species, whereas little information on this topic is available in fruit trees (Wang *et al.*, 2010) and none after Fe resupply.

Fruit tree species such as *Prunus persica* (peach) respond to Fe deficiency by using typical Strategy I responses (Gogorcena, Abadía and Abadía, 2000). Fruit trees in production are usually composed of two parts, a rootstock that provides adaptation to the soil and a grafted scion that determines the fruit characteristics. The peach-almond hybrid GF 677 (*P. dulcis* × *P. persica*) is one of the most widely used rootstock in peach and nectarine orchards in the Mediterranean area. This vigorous rootstock has high tolerance to Fe chlorosis and drought (Cinelli and Loreti, 2004; Cinelli, Iacona and Tamantini, 2004; Giorgi *et al.*, 2005). When challenged with Fe deficiency, GF 677 displays an induction of the Fe reductase and proton extrusion activities, as well as an increase in PEPC activity (Gogorcena, Abadía and Abadía, 2004; Molassiotis *et al.*, 2006; Jiménez *et al.*, 2008, 2011). When woody species (fruit trees and others) become Fe-deficient, younger leaves become progressively chlorotic while a significant part of the canopy remains green, due to the slow growth rates of these species (Gogorcena *et al.*, 2001; Jiménez *et al.*, 2009). This contrasts with Fe-deficient herbaceous plant species, where a large part of the foliage rapidly develops Fe-chlorosis symptoms.

A proteomic approach study in a fruit tree species will reveal metabolic changes induced by Fe deficiency in a holistic way that may allow for comparisons with herbaceous species. However, Fe resupply studies will also provide an overview of root behavior after fertilization practices. A better understanding of the mechanisms involved in Prunus root Fe homeostasis may strengthen our ability to select for tolerant rootstocks and tackle fertilization practices. Therefore, the aim of this work was to investigate the changes in the root protein profiles of the commonly used Prunus hybrid GF 677 rootstock with Fe-deficiency and upon short-term Fe resupply to Fe-deficient plants.

3.2.2. Materials and methods

Plant Material and Culture

Micropropagated Prunus hybrid GF 677 plants [*Prunus dulcis* (Mill.) D.A. Webb × *P. persica* (L.) Batsch] were obtained from Agromillora Iberia S.A. (Subirats, Barcelona, Spain). Plants were grown for two weeks in 300 mL pots containing a peat substrate. Then, plants were transferred to 10 L plastic boxes (30 plants per container) filled with continuously aerated, half-strength Hoagland solution, containing (in mM) 2.5 Ca-$(NO_3)_2$, 2.5 KNO_3, 1 $MgSO_4$, 1 KH_2PO_4, and (in μM) 46.2 H_3BO_3, 9.2 $MnCl_2$, 0.38 $CuSO_4$, 2.4 $ZnSO_4$, 0.12 Na_2MoO_4, and 90 μM Fe(III)-EDTA, pH 6.0. Plants were pre-grown for two weeks in a growth chamber with a photoperiod of 16 h light (220−250 μmol photon m^{-2} s^{-1} at the leaf level) at 23°C/8 h darkness at 20°C, and 70−75% relative humidity. The pH of the nutrient solution was adjusted daily to 6.0 with 1 N HCl. Nutrient solutions were changed every week. After the two weeks pre-growth period, plants were transferred (by then roots were about 10 cm long) to new 10 L boxes (30 plants/ box) containing either 0 μM (-Fe) or 90 μM Fe(III)-EDTA (+Fe). After 14 d without Fe, a subset of -Fe plants was resupplied with 180 μM Fe(III)-EDTA (-FeR) and grown in these conditions for 1 d. In the −Fe and +Fe treatments, solutions were renewed every 4 days. At the end of the 15 d experiment, lateral roots and root tips (approximately 1 cm long) were harvested separately from six plants per treatment for proteomic analyses. These root sections were chosen in order to study the effects of Fe deficiency and short-term resupply in those areas actively participating in Fe uptake and growth. The whole experiment was repeated twice.

Protein Extraction

For protein extraction, approximately 0.5−1 g of root tip material (from 2 plants of a given treatment) was ground in liquid N_2 with mortar and pestle, and then homogenized in 6 mL of phenol, saturated with Tris-HCl 0.1 M (pH 8.0) containing 5 mM β-mercaptoethanol, by stirring for 30 min at 4°C. After incubation, the homogenate was filtered (PVDF, 0.45 μm) and centrifuged at 5000g for 15 min. The phenol phase was re-extracted for 30 min with one volume of phenolsaturated Tris-HCl 0.1 M (pH 8.0) containing 5 mM β- mercaptoethanol, and centrifuged as described above. The phenol phase was collected, and proteins precipitated by adding four volumes of 0.1 M ammonium acetate in cold methanol, followed by overnight incubation at −20 °C. Samples were then centrifuged at 5000g for 15 min, and the pellet was washed three times with cold methanol, dried with N2 gas and resuspended in sample rehydration buffer containing 8 M urea, 2% (w/v) CHAPS, 50 mM DTT, 2 mM PMSF and 0.2% (v/v) 3−10 ampholytes (Amersham, Uppsala, Sweden). After rehydration, samples were incubated at 38°C for 1.5 h and then centrifuged at 15 000g for 10 min at 20°C. Samples were analyzed immediately by 2-DE.

Protein concentration in the samples was measured with the Bradford method using microtiter plates and an Asys UVM 340 (Biochrom Ltd., Cambridge, U.K.) spectrophotometer. The protein extraction yield (ca. 800 μg protein g^{-1} root FW; Table 3.2.1) is within the range obtained in roots of herbaceous plants such as tomato(Rodríguez-Celma *et al.*, 2010).

Table 3.2.1. *Summary of Protein Profiling Results from Root extracts of Prunus Hybrid GF 677*[a]

	+Fe	−Fe	−FeR
root FW (g root−1)	0.58 ± 0.09	0.44 ± 0.03	0.66 ± 0.14
protein yield (μg protein g^{-1} root FW)	867 ± 169	708 ± 139	826 ± 221
number of spots	338 ± 5	339 ± 1	336 ± 5
	−Fe vs +Fe	−FeR vs +Fe	−FeR vs −Fe
spots with significant intensity changes	17 (17)	32 (30)	8 (8)
number of new spots	1 (1)	1 (1)	0
number of spots with increased abundance	10 (10)	15 (14)	5 (5)
number of spots with decreased abundance	6 (6)	16 (15)	3 (3)

[a]*Root fresh weight (g root^{-1}), protein yield (μg protein g^{-1} root FW), average number of spots, number of spots changing significantly in intensity (Student t-test at $p < 0.10$) and above a two-fold threshold, and number of spots newly detected, showing increased and decreased intensities. Numbers in brackets indicate identified proteins. Results are means ± SD of five replicates.*

Protein 2-DE Separation

Preliminary 2-DE experiments were carried out using a first dimension IEF separation with a linear pH gradient 3−10; under these conditions, most of the spots were concentrated in the central region of the 2-DE gel (results not shown); therefore, to prevent protein comigration and improve resolution a narrower pH gradient was chosen. A first dimension IEF separation was carried out on 7 cm ReadyStrip IPG Strips (BioRad) with a linear pH gradient pH 5−8 using a Protean IEF Cell (BioRad, Hercules, CA, U.S.). Strips were rehydrated for 16 h at 20°C in 125 μL of rehydration buffer containing 60 μg of root extract proteins and a trace of bromophenol blue, and then transferred onto a strip tray. IEF was run at 20°C, for a total of 14 000 V h (20 min with a 0−250 V linear gradient, 2 h with a 250−4000 V linear gradient and 4000 V until 10 000 V h). After IEF, strips were equilibrated for 20 min in equilibration solution I [6 M urea, 0.375 M Tris-HCl, pH 8.8, 2% (w/v) SDS, 20% (v/v) glycerol, 2% (w/v) DTT] and for another 20 min in equilibration solution II [6 M urea, 0.375 M Tris-HCl pH 8.8, 2% (w/v) SDS, 20% (v/v) glycerol, 2.5% (w/v) iodoacetamide].

For the second dimension SDS-PAGE, equilibrated IPG strips were placed on top of vertical 12% SDS-polyacrylamide gels (8 × 10 × 0.1 cm) and sealed with melted 0.5% agarose in 50 mM Tris HCl, pH 6.8, containing 0.1% SDS. SDS-PAGE was carried out at 20 mA per gel for approximately 1.5 h, until the bromophenol blue reached the plate bottom, in a buffer containing

25 mM Tris, 192 mM glycine, and 0.1% SDS, at 4°C. Gels were subsequently stained with Coomassie-blue R-250 (Sigma-Aldrich, St. Louis, MO, U.S.). For each treatment, gels were made from six independent root preparations, each from two different plants (three independent root preparations per treatment per batch, and two different batches of plants). Five gels of each treatment were selected for image analysis (n = 5).

Gel Image and Statistical Analysis

Stained gels were scanned with an Epson Perfection 4990 at 600 dpi. Spot detection, gel matching, and interclass analysis were performed with PDQuest 8.0 software (BioRad). First, normalized spot volumes based on total intensity of valid spots were calculated for each 2-DE gel and used for statistical calculations of protein abundance; for all spots present in the gels, pI, Mr, and normalized volumes (mean values, SD, and CV) were determined. Only spots consistently present in at least 80% of the replicates (four out of five gels) from at least one class were considered and used in further analysis; missing spot volumes were estimated from the data set by a sequential K-Nearest Neighbor algorithm using an R 2.7.0 environment. After the input of missing values, a second normalization based on total intensity of valid spots per gel was used to compensate for gel replicate variations. The spots were also manually checked, and a consistent reproducibility between normalized spot volumes was found in the different replicates (Supporting Information Table 3.2.S1).

Univariate and multivariate statistical analyses were carried out. Protein response ratios were defined as the relative abundance in a given treatment divided by the relative abundance in the controls; when ratios were lower than one the inverse was taken and the sign changed. Only proteins with mean response ratios above 2.0 or below −2.0 were considered relevant and are discussed in this study. Spots changing in relative abundance were defined using a Student t test and a significance level of $p < 0.10$. Partial Least Square (PLS) analysis and ANOVA test were carried out using Statistica software (v. 10.0).

Protein in Gel Digestion

Spots were excised automatically using an EXQuest spot cutter (BioRad), transferred to 500 µL Protein LoBind Eppendorf tubes, destained in 400 µL of 40% [v/v] acetonitrile (ACN) and 60% [v/v] 200 mM NH_4HCO_3 for 30 min and dehydrated in 100% ACN for 10 min. Gel pieces were dried at room temperature and then in gel digested with 15 µL Trypsin solution (Sequencing grade Modified Trypsin V511, Promega, Madison, WI, U.S.A.; 0.1 µg/µL in 40 mM NH4HCO3/9% ACN). After incubation for 5 h at 37°C, the reaction was stopped by adding 1 µL of 1% TFA. The peptide solution was finally analyzed using mass spectrometry (MS).

Protein Identification by Nanoliquid Chromatography-Tandem Mass Spectrometry (nLC−ESI−MS/MS)

Peptides present in 5 μL of sample were preconcentrated on line onto a 300 μm i.d. × 5 mm, 5 μm particle size ZORBAX 300SB-C18 trap column (Agilent Technologies, Waldbronn, Germany), using a 100 μL min−1 flow rate of 3% ACN, 0.1% formic acid, in a nano-HPLC system 1200 series (Agilent Technologies). Backflow elution of peptides from the trap column was carried out, and separation was done with a 75 μm i.d. × 150 mm, 3.5 μm particle size ZORBAX 300SB-C18 column (Agilent Technologies), using a 300 nL min−1 nanoflow rate and a 55 min linear gradient from solution 97% A (0.1% formic acid) to 90% of solution B (90% ACN, 0.1% formic acid). The nano-HPLC was connected to a HCT Ultra high-capacity ion trap (Bruker Daltoniks, Bremen, Germany) using a PicoTip emitter (50 μm i.d., 8 μm tip i.d., New Objective, Woburn, MA, U.S.) and an on line nanoelectrospray source. Capillary voltage was −1.8 kV in positive mode and a dry gas flow rate of 10 L min^{-1} was used with a temperature of 180°C. The scan range used was from 300 to 1500 *m/z*. The mass window for precursor ion selection was ±0.2 Da and the rest of parameters were those recommended by the manufacturer for MS/MS proteomics work. Peak detection, deconvolution. and processing were performed with Data Analysis 3.4 software (Bruker Daltoniks).

Protein identification was carried out using the Mascot search engine (Matrix Science; London, U.K.) and the nonredundant databases NCBInr 20120303 (17378729 sequences; 5967463365 residues), SwissProt 2012_02 (534695 sequences; 189667883 residues) and Plants_EST_109 (149929128 sequences; 26337522384 residues). Search parameters were: monoisotopic mass accuracy, peptide mass tolerance ±0.2 Da, fragment mass tolerance ±0.6 Da; one allowed missed cleavage; allowed fixed modification carbamidomethylation (Cys), and variable modification oxidation (Met). Positive identification was assigned with Mascot scores above the threshold level ($p < 0.05$), at least 2 identified peptides with a score above homology, 10% sequence coverage and similar experimental and theoretical molecular weight and pI values. We used the GO biological process annotation (http://www.geneontology.org) of the individual identified proteins for classification.

3.2.3. Results

After 14 days of Fe deficiency, shoot growth was significantly reduced by Fe deficiency, whereas root growth was unaffected when compared to that of Fe-sufficient control plants (Jiménez *et al.*, 2009). Fe-deficient plants showed the typical yellowing of the young leaves with the remaining canopy being similar to that of Fe-sufficient control plants (Fig. 3.2.1A,B). The short-term Fe-resupply did not induce major visual differences in Fe-deficient plants (Fig. 3.2.1B,C).

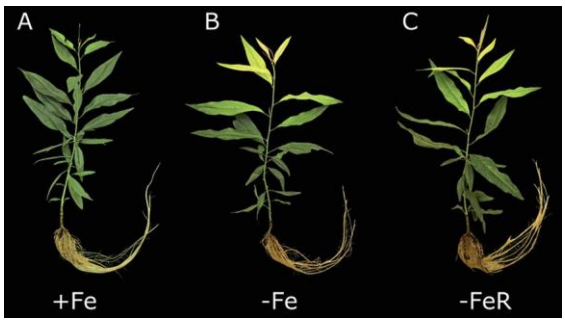

Figure 3.2.1. *Prunus hybrid GF 677 plants. General overview of Fe-sufficient (A), Fe-deficient (B), and Fe-resupplied Fe-deficient (-FeR) plants at the end of the 15 d experiment.*

Changes in Protein Profiles

Changes in the protein profile of root extracts of Prunus GF 677 plants induced by Fe deficiency and short-term Fe resupply were studied by 2-D IEF-SDS PAGE electrophoresis. Typical real scans of 2-DE gels obtained from protein extracts of roots from Fe-sufficient (+Fe), Fe-deficient (−Fe), and Fe-resupplied Fe-deficient (−FeR) plants are shown in Fig. 3.2.2A-C, respectively. The average number of detected spots (mean ± SD; n = 5) was 338 ± 5, 339 ± 1 and 336 ± 5 in +Fe, −Fe, and −FeR, respectively (Table 3.2.1). The total number of spots consistently detected in the whole experiment (present in at least 80% of the gels of one treatment) was 335. A composite averaged virtual map containing all spots present in all 15 gels (5 per treatment) is shown in Fig. 3.2.2D.

When compared to Fe-sufficient controls, approximately 5 (17) and 10% (32) of the spots showed significant changes in relative abundance (Student t test, $p < 0.10$) with mean response ratios above 2.0 or below −2.0 as a result of Fe deficiency or Fe resupply to Fe deficient plants (spots are highlighted in Fig. 3.2.2E,F).

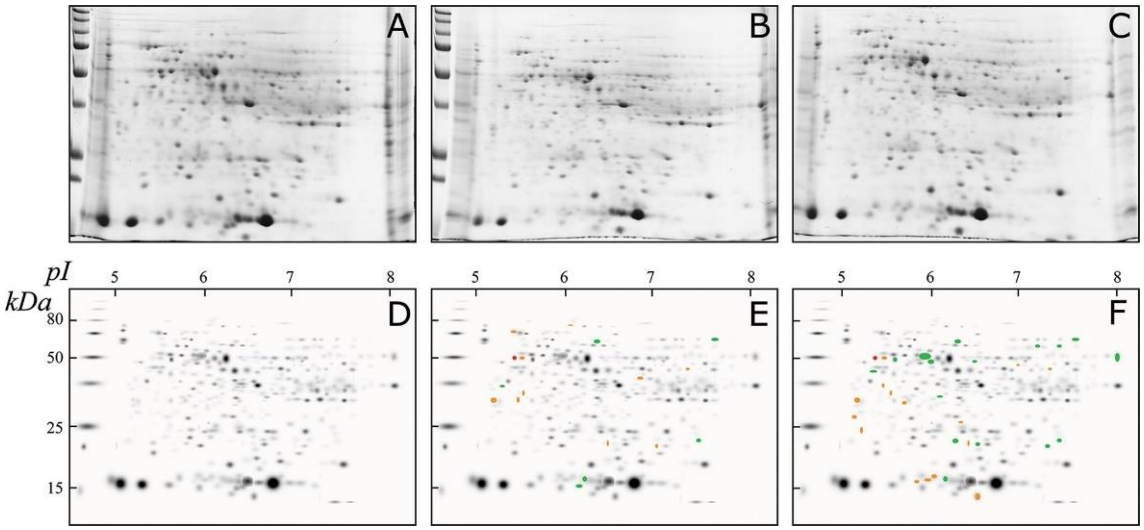

Figure 3.2.2. *2-D IEF-SDS PAGE electrophoresis protein profile maps of whole root extracts from Prunus hybrid GF 677 plants, and changes in spot relative abundance taking the Fe-sufficient roots as controls. Proteins were separated in the first dimension in linear IPG pH 5−8 gel strips and in the second dimension in 12% acrylamide vertical gels. Scans of typical gels of root extracts from Fe-sufficient (+Fe), Fe-deficient (−Fe) and Fe-resupplied Fe-deficient (−FeR) plants are shown in A, B, and C, respectively. To facilitate visualization of the studied spots, a virtual composite image (D) was created containing all spots present in the real gels A, B, and C. Panels E and F show spots whose relative abundance changed in –Fe and −FeR plants when compared to the +Fe plants. Spots that decreased when compared to control maps were marked with green symbols, and those with increased abundance or newly detected ones were marked with orange and red symbols, respectively.*

When a second comparison was carried out with the same criteria between the Fe resupplied and Fe deficient plants, only 2% (8) of the spots showed changes (spots are highlighted in Fig. 3.2.3).

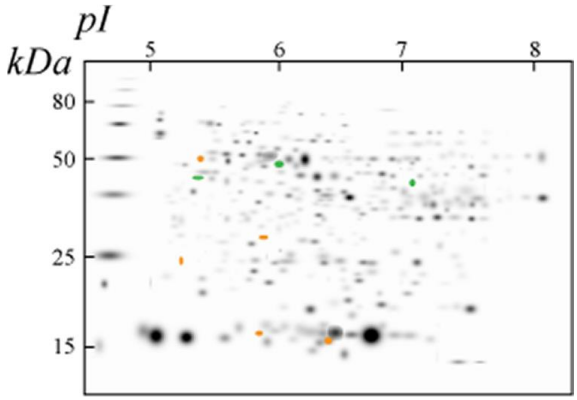

Figure 3.2.3. *Changes in spot relative abundance in the 2-D IEF−SDS PAGE electrophoresis protein profile maps of whole Prunus hybrid GF 677 root extracts from Fe-resupplied (-FeR) plants taking the Fe-deficient (-Fe) roots as controls. Spots whose relative abundance decreased when compared to control maps were marked with Green symbols, and those with increased abundance or newly detected ones were marked with orange and red symbols, respectively.*

The total number of spots having consistent changes between all treatments was 42 (Supporting Information Fig. 3.2.S2), and 95% of them (40) were identified by MS. Details on the identification and characteristics of these protein species are shown in Table 3.2.2, and the location of these proteins in the composite averaged virtual map is shown in Fig. 3.2.4. The PLS analysis showed a good separation between treatments when using all consistent spots (Supporting Information Fig. 3.2.S1A), and similar results were obtained when the analysis was carried out using only identified spots (Supporting Information Fig. 3.2.S1B).

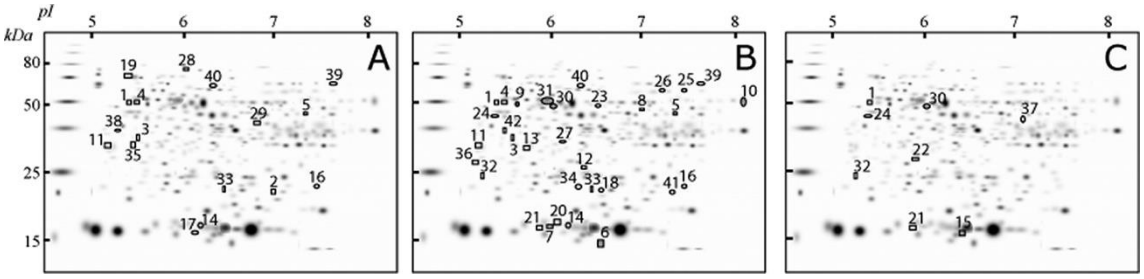

Figure 3.2.4. *Protein species identified in extracts of Prunus hybrid GF 677 roots. Proteins exhibiting significant and over 2-fold changes in response ratios and with significant homologies to proteins present in databases (using nLC-ESI-tandem MS and MASCOT, described in detail in Table 3.2.2) were annotated on the virtual composite gel images. (A) Changes in Fe-deficient (−Fe) using Fe-sufficient (+Fe) as controls; (B) Changes in Fe-resupplied plants (−FeR) using Fe-sufficient (+Fe) ones as controls; (C) Changes in Fe-resupplied (−FeR) plants using Fe-deficient (−Fe) ones as controls. Increases and decreases in relative abundance are marked by circles and squares, respectively.*

Table 3.2.2. Proteins Identified in 2-D IEF-SDS PAGE Gels from Root Extracts of Prunus Hybrid GF 677[a]

Spot	**−Fe vs +Fe/ −FeR vs +Fe**	−FeR vs −Fe	p-value −Fe vs +Fe/−FeR vs +Fe/−FeR vs-Fe	ANOVA P <0.1	Protein name	Species	ID	Score/pep/ ion	% Sq	M_w/pI th	M_w/pI exp	Function	GO:P
					Oxidative stress								
1	**new/new**	2.3	0.061/0.000/0.057	+	Peroxidase	*Phaseolus lunatus*	Q3S615	390/8/6	17	32.3/8.1	49.7/5.4	Cell redox homeostasis	45459
2	**2.8/1.7**	−1.7	0.084/−/−		manganese superoxide	*Prunus persica*	Q9G2T0	295/8/6	22	26.1/8.6	20.3/7.0	Cell redox homeostasis	45462
3	**2.5/2.6**	1.0	0.085/0.024/−	+	L-Galactose dehydrogenase	*Prunus persica*	B6ZL95	118/2/2	10	35.2/5.5	35.2/5.6	Ascorbic a. biosynthesis	19853
4	**2.2/2.3**	1.0	0.053/0.094/-		Peroxidase	*Phaseolus lunatus*	Q3S615	411/23/6	17	32.3/8.1	49.4/5.5	Cell redox homeostasis	45457
5	**2.0/2.1**	1.0	0.009/0.071/−	+	peroxidase	*Vigna angulariz*	Q43854	287/13/4	10	39.6/8.5	43.6/7.3	Cell redox homeostasis	45455
6	**1.8/2.2**	1.2	−/0.001/−	+	Copper/Zinc superoxide dismutase	*Nicotiana tabacum*	A8UDS9	120/4/2	29	9.0/5.3	11.0/6.5	Cell redox homeostasis	45461
7	**1.7/2.0**	1.2	−/0.001/−	+	Thioredoxin H	*Prunus persica*	Q93WZ3	403/12/7	39	14.7/5.6	16.1/6.0	Cell redox homeostasis	45454
8	**1.6/2.0**	1.3	−/0.077/−		Peroxidase	*Prunus persica*	Q94IQ1[p]	229/3/3	20	21.3/8.6	45.6/6.9	Cell redox homeostasis	45456
9	**−2.0/−2.5**	−1.3	−/0.015/−	+	Peroxidase	*Prunus persica*	Q94IQ1[p]	229/9/4	28	25.6/8.5	48.7/5.6	Cell redox homeostasis	45458
10	**−1.7/−2.5**	−1.4	−/0.002/−	+	Catalase	*Prunus persica*	Q7XTK8	822/23/16	41	57.3/7.0	50.4/8.0	Cell redox homeostasis	45460
					Plant stress and defense								
11	**2.0/2.4**	1.2	0.002/0.017/−	+	(+)-Neomenthol dehydrogenase-like	*Prunus persica*	D7UC32[p]	609/23/11	39	27.0/5.5	31.9/5.2	Defense response	6952
12	**2.0/2.2**	1.1	−/0.010/−	+	Glutathione-s-transferase omega,	*Prunus persica*	B9SGT4[p]	638/19/11	67	20.8/8.4	26.1/6.3	Stress response	6950
13	**1.5/2.3**	1.5	−/0.030/−	+	Adenine nucleotide alpha	*Prunus armeniaca*	G5DW21[p]	295/7/4	23	26.1/4.8	31.1/5.7	Stress response	6950
14	**−3.3/−5.0**	−1.7	0.006/0.001 /−	+	Major allergen Pru av 1	*Prunus persica*	O24248	351/19/7	37	17.6/5.9	16.3/6.2	Defense response	6952
15	**−3.3/−1.7**	2.0	−/−/0.059		Putative allergen Pru du 1.04	*Prunus dulcis x Prunus persica*	B6CQS3	864/71/13	84	17.7/5.6	15.4/6.4	Defense response	6952
16	**−3.3/−2.5**	1.7	0.054/0.100/−/−	+	Glutathione S-transferase	*Prunus persica*	Q06FE1[p]	140/3/2	11	22.3/5.7	21.4/7.4	Stress response	6950
17	**−2.5/−1.7**	1.7	0.010/−/−	+	Putative allergen Pru du 1.04	*Prunus dulcis x Prunus persica*	B6CQS3	590/24/10	67	17.7/5.6	15.5/6.1	Defense response	6952

Table 3.2.2. continued

spot	**−Fe vs +Fe/ −FeR vs +Fe**	−FeR vs −Fe	p-value −Fe vs +Fe/−FeR vs +Fe/−FeR vs-Fe	ANOVA P <0.1	Protein name	Species	ID	Score/pep/ ion	% Sq	M_w/pI th	M_w/pI exp	Function	GO:P
18	**−1.3/−2.5**	−2.0	−/0.028/−	+	Glutathione S-transferase F1	*Prunus cerasus*	Q6XX18[p]	366/19/6	22	23.3/8.7	20.6/6.5	Stress response	6950
					Protein synthesis/modification								
19	**2.4/2.7**	1.1	0.087/−/−		Putative luminal-binding protein	*Isatis tinctoria*	Q0ZUG6	872/22/14	23	73.9/5.1	77.7/5.4	Protein folding	6457
20	**1.7/2.0**	1.2	−/0.034/−	+	Translation initiation factor 5A	*Euphorbia esula*	Q9M5P9	260/6/5	37	17.3/5.8	16.4/6.1	Translation	6412
21	**1.0/2.4**	2.4	−/0.059/0.046	+	40S Ribosomal protein S12	*Prunus persica*	D3Y1 × 9[p]	285/5/5	27	25.8/6.7	16.0/5.9	Translation	6412
22	**−1.4/2.2**	2.9	−/−/0.091		Alpha chain of nascent polypeptide associated complex	*Prunus persica*	Q9M612[p]	127/3/2	14	25.0/4.4	27.9/5.9	Protein transport	15031
23	**−1.1/−2.0**	−2.0	−/0.069/−		Calreticulin-3	*Prunus persica*	G7KRL3[p]	231/4/4	29	22.5/5.0	48.2/6.5	Protein folding	6457
					Nitrogen metabolism								
24	1.4/−5.0	−10.0	−/0.000/0.100		Putative plastidic glutamine synthetase	*Crataegus crus-galli*	Q8GUZ6	160/3/3	11	47.9/6.6	42.6/5.4	Glutamine biosynthesis	6542
25	−2.0/−2.0	−1.1	−/0.001/−	+	Nitrite reductase	*Prunus persica*	Q93XS0	894/26/18	42	60.2/6.4	59.9/7.4	Nitrate assimilation	42128
26	−1.4/−2.5	−1.7	−/0.006/−	+	Ferredoxin-nitrite reductase, putative	*Ricinus communis*	B9RYH9	279/9/4	10	66.6/6.1	60.3/7.2	Nitrate assimilation	42128
27	−1.3/−2.0	−1.7	−/0.084/−		Isoflavone reductase-like protein 6	*Vitis vinifera*	Q3KN67	230/6/5	17	33.9/6.0	32.6/6.1	Phytoalexin biosynthesis	52315
					Carbon metabolism								
28	2.3/1.5	−1.4	0.011/−/−	+	Enolase	*Prunus*	Q1 × 8N5	229/3/3	36	16.0/5.1	90.0/6.0	Glycolysis	6096
29	2.2/1.8	−1.2	0.025/−/−	+	Alcohol dehydrogenase	*Prunus dulcis x Prunus persica*	F6K5 V5	825/30/16	48	43.0/6.0	39.1/6.8	Oxidoreductase activity	16491
30	1.2/−2.0	−2.5	−/0.093/0.046	+	Dihydrolipoamide acetyltransferase	*Cucumis melo subsp. melo*	E5GB89	483/11/8	16	58.4/8.0	47.5/6.0	Pyr metabolic process	6090
31	−1.3/−2.5	−2.0	−/0.011/−	+	Enolase	*Jatropha curcas*	E6NU46	658/18/10	28	52.7/6.3	51.1/6.0	Glycolysis	6096
32	−1.1/2.0	2.2	−/0.035/0.027	+	Ribose 5-phosphate isomerase A	*Prunus persica*	Q9S726[p]	557/17/8	34	31.4/5.1	24.6/5.3	Pentose phosphate shunt	9052

Table 3.2.2. continued

spot	**−Fe vs +Fe/ −FeR vs +Fe**	−FeR vs −Fe	p-value −Fe vs +Fe/−FeR vs +Fe/−FeR vs-Fe	ANOVA P <0.1	Protein name	Species	ID	score/pep/ ion	% Sq	M_w/pI th	M_w/pI exp	Function	GO:P
					Energy metabolism								
33	2.3/2.9	1.3	0.064/0.068/−		Flavodoxin-like quinone reductase 1	*Arabidopsis lyrata subsp. lyrata*	D7MUA0	172/3/3	20	21.9/6.2	20.8/6.4	Electron carrier	9055
34	−1.4/−3.3	−2.5	−/0.002/−	+	Quinone reductase family protein	*Prunus persica*	D7MEH6[p]	89/2/2	22	24.0/7.2	21.3/6.3	Electron carrier	9055
					Secondary metabolism								
35	3.0/1.8	−1.7	0.042/−/−	+	Phenazine biosynthesis protein, putative	*Prunus persica*	B9S448[p]	202/3/3	17	24.5/4.6	32.0/5.5	Biosynthetic process	9058
36	2.3/2.5	1.1	−/0.031/−		Isopentenyl-diphosphate delta-isomerase I	*Camptotheca acuminata*	O48964	159/7/5	20	27.2/5.3	27.3/5.2	Isoprene biosynthesis	8299
37	1.2/−1.7	−2.0	−/−/0.054		Chalcone synthase	*Prunus persica*	Q76K34	158/4/4	12	43.1/6.1	40.9/7.0	Flavonoid biosynthesis	9813
					Others								
38	−5.0 / −1.4	3.5	0.023/−/−		Plastid-dividing ring protein similar to HSP70	*Solanum tuberosum*	Q6J4T5	436/7/6	18	44.1/5.8	36.0/5.3	Microtubule organization	7017
39	−2.5 / −2.5	1.2	0.060/0.100/−	+	BU042094 (Poly(A)-binding protein, partial)	*Prunus persica*	Q9M6E4[p]	139/4/3	33	22.3/5.3	68.0/7.6	Unknown-nucleotide binding	166
40	−2.0 / −3.3	−1.4	0.083/0.008/−	+	β-Glucosidase, putative	*Ricinus communis*	B9RIY8	486/16/8	11	84.7/6.2	65.3/6.3	Cell wall organization	7047
					Unidentified								
41	−2.5/−5.0	−1.7	−/0.034/−	+									
42	2.5/2.4	−1.1	−/0.083/−										

[a]Positive identification was assigned with Mascot scores (Score) above the threshold level ($p < 0.05$), at least 2 identified peptides (ion) with a score above homology, 10% sequence coverage (%Sq) and similar experimental and theoretical molecular weight and pI. Function was inferred from GO:P annotation. The second column indicates relative spot intensity changes (in −fold, relative to the +Fe control treatment) in the −Fe and −FeR treatments, respectively, and the third column indicates relative spot intensity changes in Fe resupplied relative to Fe-deficient plants. Bold figures mark statistically significant changes and p-values are presented in the fourth column. "New" indicates spots that have been newly detected. The p superindex next to protein ID indicates identification was achieved using the Plants_EST_109, when no superindex is present identification was achieved using NCBInr 20120303 database.

Comparison of Root Proteome of Fe-Deficient vs Fe-Sufficient Plants

The statistical analysis of averaged maps indicated that the Fe deficiency treatment caused increases in the relative abundance of 10 spots (orange symbols in Fig. 3.2.2E), whereas one spot was present in the −Fe treatment but absent in the control (red symbol in Fig. 3.2.2E). All 11 spots were identified (spots labeled 1−5, 11, 19, 28, 29, 33, and 35 in Fig. 3.2.4) and their functions assessed according to their GO terms (Table 3.2.2). Five spots matched reliably to known protein species related to cell redox homeostasis, including several peroxidases (spots 1, 4, and 5), MnSOD (spot 2) and a L-galactose dehydrogenase (spot 3) involved in ascorbic acid synthesis. One (spot 11) was identified as a neomenthol dehydrogenase-like with a role in plant defense response against pathogens, whereas three more spots matched to protein species participating in protein folding (spot 19), glycolysis (spot 28), and fermentation (spot 29). One more spot was identified as a protein involved in electron transport, a flavodoxin-like quinone reductase (spot 33), and ascribed to energy metabolism. Finally, one spot (35) was identified as a phenazine biosynthesis protein and assigned to the secondary metabolism category. On the other hand, six spots showed decreases in relative abundance in the –Fe treatment when compared to controls (green symbols in Fig. 3.2.2E). All of them were identified (spots labeled 14, 16, 17, and 38−40 in Fig. 3.2.4 and Table 3.2.2). Three of them were protein species related to plant stress response, including two major allergen proteins (spots 14 and 17) and a glutathione S-transferase (spot 16), whereas the other three were involved in microtubule organization (spot 38), nucleotide binding (spot 39) and cell wall reorganization (spot 40).

Comparison of Root Proteome of Fe-Resupplied vs Fe-Sufficient Plants

When comparing the averaged map of the Fe resupply treatment with that of Fe-sufficient controls, 15 spots showed relative increases in abundance (orange symbols in Fig. 3.2.2F) and one more was detected de novo (red symbol in Fig. 3.2.2F). Among them, 15 were identified (spots *1*, *3−8*, *11−13*, *20*, *21*, *32*, *33*, and *36* in Fig. 3.2.4 and Table 3.2.2). Metabolic pathways containing proteins with increases in relative abundance in the resupply treatment included response to oxidative stress (spots *1* and *3−8*), plant stress and defense (spots *11−13*), protein metabolism (spots *20* and *21*), and energy and secondary metabolism (spots 33 and 36, respectively). One of the protein species showing increases in abundance, spot *42*, was not identified. Sixteen spots showed decreases in relative abundance (green symbols in Fig. 3.2.2F) in the Fe resupply treatment when compared to controls. Among them, 15 protein species were identified (spots *9*, *10*, *14*, *16*, *18*, *23−27*, *30*, *31*, *34*, *39*, and *40* in Fig. 3.2.4 and Table 3.2.2) and assigned to oxidative stress response (spots *9* and *10*), plant defense (spots *14*, *16*, and *18*), protein metabolism (spot *23*), N metabolism (spots *24−27*), C metabolism (spots *30* and *31*), energy (spot

34), and others (spots *39* and *40*). One of the protein species showing decreases in abundance, spot *41*, was not identified.

Comparison of Root Proteome of Fe Resupplied vs Fe-Deficient Plants

When comparing the averaged map of the Fe resupply treatment with that of Fe-deficient plants, five spots showed relative abundance increases above 2-fold (orange symbols in Fig. 3.2.3). All of them were identified (spots 1, 15, 21, 22, and 32 in Fig. 3.2.4 and Table 3.2.2). Identified protein species included a peroxidase (spot 1) involved in cell redox homeostasis, an allergen related to plant defense mechanisms (spot 15), two proteins related to protein metabolism, a 40S ribosomal protein (spot 21) and a polypeptide complex (spot 22), and a ribose 5-P-isomerase (spot 32) from the pentose phosphate shunt. Three spots showed decreases in relative abundance (green symbols in Fig. 3.2.3) in the Fe resupply treatment when compared to the Fe-deficient one. These three spots (spots 24, 30, and 37 in Fig. 3.2.4 and Table 3.2.2) were identified as a glutamine synthetase related to N metabolism (spot 24), a dihydrolipoamide acetyltransferase (spot 30) from the pyruvate metabolic process and a chalcone synthase involved in flavonoid biosynthesis (spot 37).

The information on the changes in protein abundance occurring in the different treatments is summarized in Venn diagrams (Fig. 3.2.5). When the Fe-sufficient control was used for comparison, some of the changes are specific of one Fe-deficiency treatment, whereas others are common (Fig. 3.2.5A). A group of six proteins (spots 1, 3−5, 11, and 33) and another of four proteins (spots 14, 16, 39, and 40) exhibited increases and decreases, respectively, in relative abundance in both Fe-deficient and Fe-resupplied plants compared to the controls. Among these common spots, only one (spot 1) showed significant differences between Fe-deficient and Fe-resupplied plants. Also, when the Fe resupply treatment was compared to the Fe deficiency treatment only five (spots 1, 15, 21, 22, and 32) and three (spots 24, 30, and 37) protein species exhibited increases and decreases, respectively, in relative abundance (Fig. 3.2.5B).

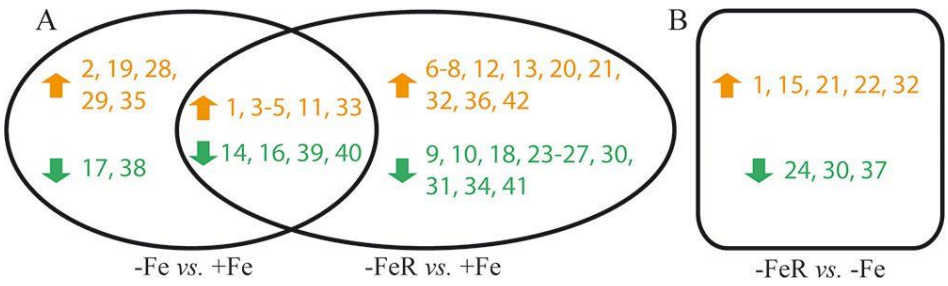

Figure 3.2.5. *Venn diagram indicating major changes in Prunus hybrid GF 677 root proteins. A: changes in relative abundance in roots of Fe-deficient and Fe-resupplied plants using Fe-sufficient roots as control; B: changes in relative abundance in roots of Fe-resupplied plants using Fe-deficient roots as control. Only proteins with response ratios over 2-fold are shown (values are shown in Table 3.2.2). Increases and decreases are depicted in orange and green, respectively.*

3.2.4. Discussion

In the present study, we have assessed the changes in the root protein profiles of the Prunus hybrid GF 677 rootstock grown in hydroponics as affected by Fe deficiency and short-term Fe resupply. The number of spots consistently found was 335, in the range of those found in recent root protein profile 2-DE studies (Rellán-Álvarez, Andaluz, *et al.*, 2010; Rodríguez-Celma *et al.*, 2010; J Rodríguez-Celma *et al.*, 2011). Overall, results indicate that stress and defense and carbohydrate metabolism are the metabolic pathways more affected by Fe deficiency; upon short-term Fe resupply, stress and defense still accounted for most of the changes, and a slight down accumulation of glycolysis and N-related protein species was observed (Fig. 3.2.6).

Changes in Fe Deficient Roots

Iron deficiency caused significant changes in the relative abundance of approximately 5% (17 spots) of the total number of protein species separated by 2-DE in GF 677 root extracts. This percentage is lower than those found in similar 2-DE studies describing changes with Fe deficiency in sugar beet, tomato, cucumber, and *M. truncatula* (13, 11, 14, and 7% of the total, respectively) (Li *et al.*, 2008; Rellán-Álvarez, Andaluz, *et al.*, 2010; J Rodríguez-Celma *et al.*, 2011). This low number of changes may be associated either to the peculiarities of the effect of Fe deficiency in woody plants (see below)(Jiménez *et al.*, 2009), to the especially high Fe deficiency tolerance previously described for this rootstock (Cinelli, Iacona and Tamantini, 2004) or both.

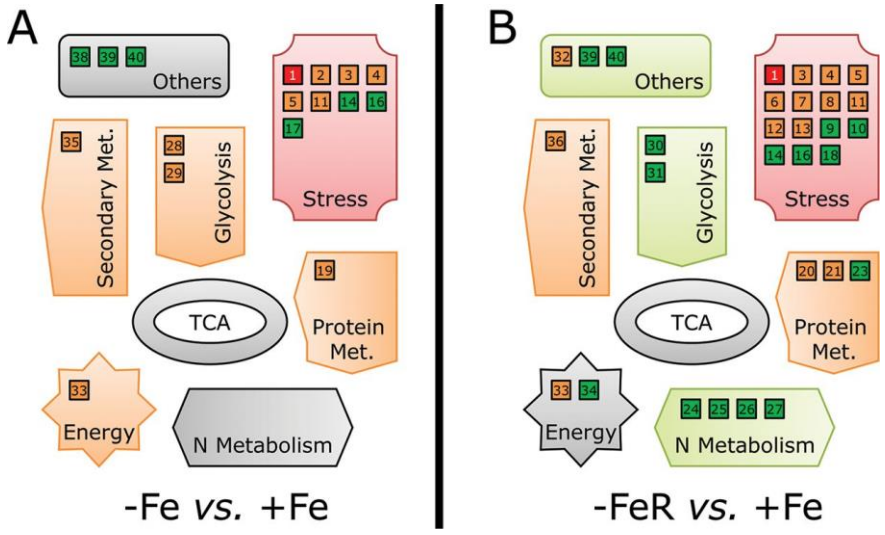

Figure 3.2.6. *Changes in metabolic pathways as affected by Fe deficiency (A) and short-term Fe-resupply to Fe-deficient plants (B) when compared to Fe-sufficient plants. Pathways related to the identified proteins were integrated according to the GO annotation. A statistical Student t test was performed to show relevant changes between samples. Red symbols mark newly detected proteins in Fe-deficient and Fe-resupplied roots, and orange symbols mark proteins with increased relative abundance compared to controls (using a 2-fold threshold change). The same threshold (decreases larger than 50%) was selected for proteins with decreased intensity (green symbols). Numbers correspond to those in Table 3.2.2.*

When comparing changes in the root protein profile of the Prunus hybrid GF 677 rootstock as affected by Fe-deficiency with those reported in herbaceous species, the most striking difference is the absence of major increases in protein species involved in TCA and the pentose phosphate shunt (Fig. 3.2.6A). In GF 677 roots, only two protein species associated to these processes showed relative abundance increases with Fe-deficiency: enolase (spot 28) and alcohol dehydrogenase (spot 29). These enzymes are involved in the glycolysis and fermentation pathways, and increases in their activities, as well as in their protein and transcript abundances, have also been reported in Fe deficient roots of several plant species (Lopez-Millan, Morales, Andaluz, *et al.*, 2000; Thimm *et al.*, 2001; López-Millán *et al.*, 2009; Donnini *et al.*, 2010).

Our results support than in Fe-deficient GF 677 roots the enhancement in glycolysis was moderate. In this rootstock, the shift of pyruvate to an anaerobic metabolism could be more relevant that the extensive metabolic reprogramming involving PEPC and TCA described for herbaceous species (G. Zocchi, 2006; Vigani, 2012). This is also in line with the relatively small increases in root carboxylates in this rootstock upon Fe shortage (Jiménez *et al.*, 2011). It is also worth mentioning that in GF 677 roots the increase in PEPC activity with Fe-deficiency is only 4-fold, a value much lowerthan the 10- to 60-fold increase found in herbaceous species (Abadía *et al.*, 2002; Jiménez *et al.*, 2011). The increases in root sucrose concentration found in this genotype when Fe-deficient (Jiménez *et al.*, 2011) also supports a metabolic shift toward fermentation (less efficient than aerobic metabolism). On the other hand, the results may also reflect the high tolerance to Fe-deficiency of this rootstock that in these growth conditions shows relatively high SPAD values and photosynthesis rates (Jiménez *et al.*, 2009, 2011). In contrast, in Fe-deficient herbaceous species the strong decrease in chlorophyll and photo-synthesis triggers a C deficiency that leads to the elicitation of metabolic reprogramming (López-Millán *et al.*, 2009).

A second major difference between this rootstock and herbaceous plants is that stress-related protein species account for a large part (50%) of the protein species showing significant changes in abundance (with 33 and 17% involved in oxidative stress and plant defense, respectively; Fig. 3.2.6A). As mentioned above, these findings contrast with studies in other plant species where changes in C and N metabolism accounted for the largest differences (Li *et al.*, 2008; Donnini *et al.*, 2010; Rellán-Álvarez, Andaluz, *et al.*, 2010; J Rodríguez-Celma *et al.*, 2011), and support that the major response to Fe deficiency in this rootstock is a defense strategy rather than a metabolic reprogramming. Oxidative stress-related enzymes showing significant changes in Fe-deficient roots included peroxidases (spots *1*,*4*,*5*), galactose dehydrogenase (spot *3*), and MnSOD (spot *2*). Oxidative stress is a common consequence of Fe deficiency across the plant kingdom (Iturbe-Ormaetxe *et al.*, 1995; Zaharieva, Gogorcena and Abadía, 2004), including fruit trees (Molassiotis *et al.*, 2006), and the level of elicitation of the defense mechanisms has been associated to Fe-deficiency tolerance (Molassiotis *et al.*, 2006; M'sehli *et al.*, 2009). The

increases in root Mn concentrations found in GF677 upon Fe shortage (Jiménez, 2006) may be behind the increase found in MnSOD. However, increases in peroxidase activity may indicate modifications in cell wall, such as an increased root lignification, as a consequence of Fe deficiency. This hypothesis is further supported by the decrease in *β*-glucosidase (spot *40*), an exocellulase with specificity for *β*-D-glucoside substrates. A similar peroxidase-driven root lignification process has been described for Fe-deficient pear and quince (Donnini, Dell'Orto and Zocchi, 2011).

The stress related proteins decreasing with Fe-deficiency included two allergen proteins, *Pru av* 1 and *Pru du* 1.04, and a glutathione S-transferase. The abundance of allergen proteins is known to increase upon biotic or abiotic stresses, and some of them are lipid transfer proteins although the specific functions in plant metabolism are still poorly known (Scheurer *et al.*, 1997; Sánchez-Monge *et al.*, 1999). Glutathione S-transferases conjugate glutathione to cytotoxic products and the decrease found here with Fe-deficiency is similar to that found in tomato (Li *et al.*, 2008) but contrasts with the increases observed in roots of *M. truncatula*, a flavin accumulator species. Increases in the root glutathione pools were found in sugar beet with Fe-deficiency (Zaharieva and Abadía, 2003; Zaharieva, Gogorcena and Abadía, 2004). An increase in the relative abundance of a putative protein related to phenazine biosynthesis was also detected with Fe-deficiency. Phenazines are a large group of N-containing heterocyclic compounds produced by a diverse range of bacteria that serve as electron shuttles capable to modify cell redox homeostasis (Mavrodi *et al.*, 2010; Pierson and Pierson, 2010).

Changes after Short-Term Resupply When Compared to Fe-Sufficient Plants

When comparing 24 h Fe-resupplied plants to the Fe-sufficient controls, relative abundance changes were found in only approximately 10% of the root protein species. As it occurs in Fe-deficient roots, oxidative stress and plant defense were the largest categories, accounting for 45% of the total (with 24 and 21% involved in oxidative stress and plant defense, respectively; Fig. 3.2.6B). Most of the proteins showed changes in the same direction (relative abundance increases or decreases) than those occurring in Fe-deficient plants, suggesting that the major oxidative stress and plant defenses were still active after shortterm Fe resupply.

Several N-metabolism associated protein species decreased upon short-term Fe-resupply. It is remarkable that glutamine synthetase (GS, spot *24*) showed the largest decrease in relative abundance (10-fold) upon Fe resupply. This cytosolic enzyme is key in controlling the use of N inside the cell (Eisenberg *et al.*, 2000). The Sharp decrease in GS relative abundance after Fe resupply suggests that this enzyme could be one of the first sensors of Fe nutritional status, responding to the decreased needs for N compounds after Fe resupply. When Fe-deficient GF677 roots are compared to the controls, both the GS relative abundance (1.4-fold; Table 3.2.2) and the

Glu+Gln pool (Jiménez *et al.*, 2011) increase, and this is in line with the GS increase reported in Fe-deficient cucumber roots (Donnini *et al.*, 2010; Borlotti, Vigani and Zocchi, 2012). Increases in GS in Fe-deficient roots have been associated to the decrease in nitrite reductase (spot *25*) and the consequent need for N recycling (Donnini *et al.*, 2010; J Rodríguez-Celma *et al.*, 2011). Nitrite reductase, an Fe-containing enzyme located in plastids, was found in our 2-DE study but did not change in abundance to short-term Fe resupply. A similar behavior is observed for catalase (spot *10*), an Fe containing enzyme located in peroxisomes.

Some changes in protein metabolism-related processes found after short-term Fe resupply were already present in the Fe-deficient plants (although the values were not statistically significant in that treatment). Increases in translation factor 5A (spot *20*) and a 40S ribosomal protein (spot *21*) indicate that *de novo* protein synthesis is enhanced in response to Fe resupply. With regard to C metabolism, the decreases in two enzymes of the glycolytic pathway and pyruvate metabolism (enolase and dihydrolipoamide acetyltransferase) and the increase in one protein of the pentose phosphate shunt (ribose 5-P-isomerase, spot *32*) indicate that the slight Fe deficiency induced C metabolism reprogramming is already being deactivated in the short term after Fe resupply (Fig. 3.2.6B). This is also supported by the decrease in relative abundance (although not significant) in alcohol dehydrogenase in Fe-resupplied roots.

Other changes occurring worth mentioning in Fe-resupplied GF 677 roots with respect to control plants include the changes in opposite directions (increases/decreases) in the relative abundances of two quinone reductases (spots *33* and *34*, respectively), which suggest the occurrence of a compensatory mechanism (this is also observed in roots of Fe-deficient plants). Also, the relative abundance decrease in β-glucosidase (spot *40*) that occurs in Fe-deficient roots is also observed in Fe-resupplied roots, suggesting that cell wall modifications may still be in place after short-term Fe resupply.

Changes after Short-Term Resupply When Compared to Fe Deficient Plants

Comparison of Fe-resupplied and Fe-deficient roots clearly indicates that Fe-resupplied plants are still behaving mostly as Fe-deficient, since only eight proteins showed changes in relative abundance (five and three showing increases and decreases, respectively). These proteins may be considered as the first responders to the new Fe nutritional status. Two spots related to protein biosynthesis and transport increased in abundance, supporting that de novo protein synthesis is one of the first steps for stress recovery. The increase in one protein from the phosphate shunt would reflect the need of energy and reducing power for this process. However, the relative abundance increases in a peroxidase and the allergen *Pru du* 1.04 in Fe-resupplied roots when compared to Fe-deficient ones confirm that plants are facing an additional stress.

When focusing on the three proteins showing decreases in relative abundance, the largest one was observed for glutamine synthetase, confirming its sensitivity to Fe status and the decrease in N recycling needs. The deactivation of metabolic changes is also supported by the decrease in the enzyme dihydrolipoamide acetytransferase. Finally, chalcone synthase, an enzyme that catalyzes the synthesis of chalcone-derived metabolites in the phenylpropanoid pathway (PAL), decreased in abundance when Fe was resupplied. This enzyme can be involved in defense and a role in protection against oxidative stress (Haraguchi *et al.*, 1998; Choi, Kim and Kim, 2010) but it is also involved in lignin biosynthesis. The responsiveness of this protein species to Fe resupply further supports that deactivation of root responses to Fe-deficiency is occurring after short-term Fe resupply, and points toward a role of this enzyme (or the PAL pathway) in the early stress recovery response. Future research will be needed to study the effects of long-term Fe resupply when plants undergo regreening.

3.2.5. Conclusions

Three major conclusions can be derived from this study. First, the main responses elicited by Fe deficiency in the protein profile of *Prunus* GF 677 rootstock are associated to oxidative and general stress. This is in contrast to what happens in herbaceous species, where in addition to these, C/N metabolic reprogramming is one of the major metabolic adaptations taking place. Only a moderate induction of the glycolysis-fermentation path is observed in GF 677 roots, compared to the preferred shift toward glycolysis-PEPC-TCA observed in herbaceous species. Second, after short-term Fe resupply, in GF677 rootstock the deactivation of many of the Fe-deficiency root metabolic responses is slow, at least when considered at the protein level. Glutamine synthetase seems to play an important role in this early stage. Third, taken together, our results suggest that the high tolerance to Fe deficiency of GF 677 rootstock may be related to its ability to elicit a sound defense response against both general and oxidative stress.

Acknowledgments

Supported by the Spanish Ministry of Economy and Competitivity (MINECO; Projects AGL2009-09018 and AGL2010-16515, cofinanced with FEDER) and the Aragón Government (Groups A03 and A44). This work was also supported in the framework of the European Transnational Cooperation (Germany, France, Spain) within the PLANTKBBE Initiative funded by (i) the Spanish Ministry of Science and Innovation (MICINN EUI2008-03618 to J.A.), and (ii) the Agence Nationale de la Recherche (ANR-08-KBBE-009-01 to J-F.B.). S.J. was supported by a JAE-Doc contract from CSIC/ FSE (Spanish Council for Scientific Research/European Social Fund).

Supporting Information for Chapter 3.2

All the additional supporting information may be found in the online version of this article (doi: 10.1021/pr300763c).

- ***Figure 3.2.S1.*** *Partial Least Square (PLS) analysis.*

- ***Figure 3.2.S2.*** *Column charts representing volumes (mean ± SE) of all spots*. This Figure is not included here due to the size of the file; the online version is at doi: 10.1021/pr300763c.

- ***Table 3.2.S1.*** *Spot volumes in all samples*. This Table is not included here due to the size of the file; the online version is at doi: 10.1021/pr300763c.

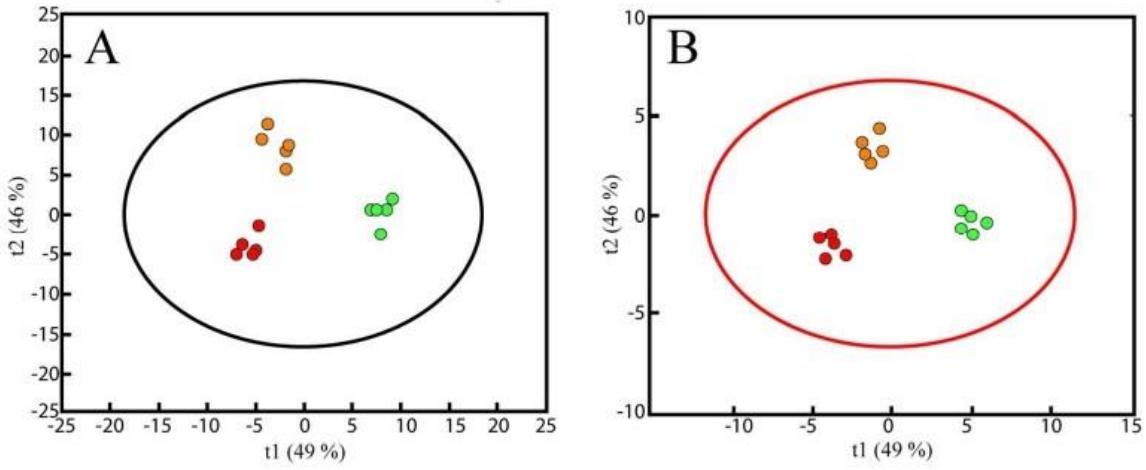

Figure 3.2.S1. *Partial Least Square (PLS) analysis of Prunus hybrid GF 677 consistently detected (A) and identified (B) proteins in whole root extracts. Score scatter plot of PLS vector 1 (v1) vs. PLS vector 2 (v2) of all identified proteins in Fe-sufficient (green), Fe-deficient (orange), and Fe-resupplied (red) plants. The percentage of variability explained by each vector is indicated in parenthesis in the corresponding axes.*

3.3. Protein profile of Lupinus texensis phloem sap exudates: searching for Fe- and Zn-containing proteins

Giuseppe Lattanzio[1], Sofía Andaluz[1], Andrea Matros[2], Juan José Calvete[3], Julia Kehr[4], Anunciación Abadía[1], Javier Abadía[1] and Ana-Flor López-Millán[1]

[1]*Department of Plant Nutrition, Aula Dei Experimental Station (CSIC), Zaragoza, Spain*

[2]*Leibniz Institute of Plant Genetics and Crop Plant Research (IPK), Gatersleben, Germany*

[3]*Instituto de Biomedicina de Valencia, C.S.I.C., Valencia, Spain*

[4]*Centro de Biotecnología y Genómica de Plantas (UPM-INIA), Campus de Montegancedo, Madrid, Spain*

Published in Proteomics (2013) 13, 2283-2296 (doi: 10.1002/pmic.201200515).

Additional supporting information may be found in the online version of this article at the publisher's web-site.

SUMMARY

The aim of this study was to obtain a comprehensive overview of the phloem sap protein profile of *Lupinus texensis*, with a special focus on proteins binding Fe and Zn. *L. texensis* was chosen as model plant given the simplicity to obtain exudates from sieve elements. Protein profiling by 2-DE revealed 249 spots, and 54 of them were unambiguously identified by MALDI-MS and ESI-MS/MS. The largest number of identified protein species belongs to protein modification/turnover and general metabolism (19–21%), followed by redox homeostasis (9%) and defense and cell structural components (7%). This protein profile is similar to that reported in other plant species, suggesting that the phloem sap proteome is quite conserved. Staining of 2-DE gels for Fe-containing proteins and affinity chromatography experiments revealed the presence of two low molecular weight Fe-binding proteins in phloem sap: a metallothionein-like protein type 2B identified in the Fe-affinity chromatography, and a second protein identified with both Fe staining methods. This protein species had a molecular weight of 13.5 kDa, a p*I* of 5.6 and 51% homology to a phloem-specific protein from *Medicago truncatula*. Zinc affinity chromatography revealed four Zn-binding proteins in phloem sap, one belonging to the dehydrin family and three Zn finger proteins.

3.3.1. Introduction

In vascular plants, phloem is a living tissue involved in the long-distance transport of a diverse range of compounds, including photosynthates and others, from source to sink tissues. The phloem tissue is composed of an intimately associated complex of two cell types, sieve elements that form the sieve tube, a cellular conduit that extends throughout the plant, and companion cells that nourish and support the sieve elements (Oparka and Santa Cruz, 2000; Van Bel, 2003). Mature sieve elements undergo a selective cytoplasmic degradation, with the remaining organelles residing in a thin layer of cytoplasm located close to the cell wall and containing smooth endoplasmic reticulum, starchstoring plastids, and a small number of mitochondria (Evert and Elements, 1990). Companion cells synthesize the macromolecules needed to maintain the functionality of both cell types (Oparka and Santa Cruz, 2000). Sieve elements are connected by perforated end walls known as sieve plates, and connection between sieve elements and companion cells occurs through branched plasmodesmata, which allow loading and unloading the sieve tubes with macromolecules (Fisher, Wu and Ku, 1992).

The phloem sap is rich in sugars, and contains minerals, other organic compounds, and small signaling molecules such as hormones, systemic wound signals, and even herbicides and pathogens (Thompson and Schulz, 1999; Fiehn, 2003; Van Bel, 2003). Endogenous mRNAs are also transported in the phloem sap (Lucas, Yoo and Kragler, 2001; Doering-Saad *et al.*, 2006; Omid *et al.*, 2007; Deeken *et al.*, 2008) and could play a role in the long-distance regulation of gene-specific expression patterns (Lough and Lucas, 2006). Recently, studies have revealed the presence of microRNAs in phloem sap from different plant species (Yoo *et al.*, 1979; Buhtz *et al.*, 2008; Varkonyi-Gasic *et al.*, 2010). The movement of all these components through the sieve tubes most likely occurs by mass flow driven by the pressure gradient between source and sink regions of the plant (Münch, 1932; Turgeon, 2010).

The mature, functional sieve tube system in higher plants is dependent upon protein import from companion cells to sieve elements to maintain a functional long-distance transport system (Oparka and Santa Cruz, 2000; Atkins, Smith and Rodriguez-Medina, 2011). To characterize these proteins, proteomic studies have been conducted in phloem sap using 1-DE approaches in different plant species (Fisher, Wu and Ku, 1992; Schobert *et al.*, 1998; Walz *et al.*, 2002). More recently, 2-DE and LC-MS/MS have been used to separate soluble polypeptides from phloem sap obtained either by using aphids (in *Triticum aestivum* (Fisher, Wu and Ku, 1992) and rice (Aki *et al.*, 2008)), or by sap exudation after incision [in *Cucurbita maxima* (Haebel and Kehr, 2001; Lin *et al.*, 2009), *Ricinus communis* (Krüger *et al.*, 2002; Barnes *et al.*, 2004), *Brassica napus* (Giavalisco *et al.*, 2006), *Cucumis sativus* (Walz *et al.*, 2004), poplar (Dafoe *et al.*, 2009) and *Lupinus albus* (Rodriguez-Medina *et al.*, 2011)]. More than a hundred polypeptides

have been detected using these approaches (Atkins, Smith and Rodriguez-Medina, 2011), with the identified proteins being grouped into different classes, including sugar metabolism, signal transduction, redox regulation, protein metabolism, macromolecular trafficking, defense, and cell structure (Hayashi *et al.*, 2000; Atkins, Smith and Rodriguez-Medina, 2011). However, many of the proteins present in the phloem sap still remain unidentified, mainly due to the limitations in sequence information and genomic resources for those plant species that allow obtaining sufficient phloem sap quantities for comprehensive proteomic studies.

Although recent research has allowed drawing a comprehensive picture of the phloem sap protein profile, very few studies have focused on proteins related to metal transport. Metal mobility in phloem sap depends on the plant species, the nutritional status of the plant and other factors (Martin and H. Marschner, 1988). The compounds that are associated with phloem Fe transport are not well established yet, although Fe chelation is mandatory due to Fe redox properties that cause the generation of highly reactive oxygen species. Moreover, if Fe was present as free ions, either as Fe(III) or Fe(II), the neutral to basic pH values of the sieve element sap would lead to Fe precipitation (Rellán-Álvarez, Abadía and Álvarez-Fernández, 2008). The general thought is that Fe and Zn could be transported in the phloem sap as complexes with nicotianamine (NA), since the pH values of phloem sap are suitable for metal-NA formation (Rellán-Álvarez, Abadía and Álvarez-Fernández, 2008; Curie *et al.*, 2009; Harris, Sammons and Grabiak, 2012). Accordingly, Zn–NA and Fe(III)-2'-deoxymugineic acid complexes have been recently identified in phloem sap from rice (Nishiyama *et al.*, 2012). Mutants defective in NA production display lower Mn, Zn, Fe, and Cu concentrations in reproductive organs (Curie *et al.*, 2009). Also, a protein capable to bind Fe, ITP (iron transporter protein), was described to occur in the phloem sap of *R. communis* (Krüger *et al.*, 2002).

The aim of this study was to obtain a comprehensive overview of the phloem exudate protein profile in *Lupinus texensis*, with a special focus on proteins binding Fe and Zn. *L. texensis* was chosen as model plant because of the simplicity to obtain phloem exudates. We have used Zn and Fe affinity chromatography, followed by 1-DE of the fractions obtained, and 2-DE to separate soluble proteins from phloem sap. Specific staining methods were also used to find putative Fe-binding proteins. Subsequently, MALDI-MS and ESI-MS/MS were used to identify the protein species found.

3.3.2. Materials and methods

Plant material

Seeds of *L. texensis* were imbibed overnight in distilled water and germinated on filter paper for 5 days in darkness with 100% humidity. Five seedlings were transferred to a 10 L container and grown in a controlled environment chamber with a photosynthetic photon flux density at leaf height of 350 µmol m^{-2} s^{-1} photosynthetically active radiation, 80% relative humidity and a 16 h (22°C)/8 h (20°C), day/night regime. The standard solution for hydroponically grown plants contained: (in mM) 0.6 K_2SO_4, 0.5 $Ca(NO_3)_2$, 1.0 NH_4NO_3, 0.3 KH_2PO_4, 0.2 $MgSO_4$, and (in µM) 25 $CaCl_2$, 25 H_3BO_3, 2 $MnSO_4$, 2 $ZnSO_4$, 0.5 $CuSO_4$, 0.5 H_2MoO_4, 0.1 $NiSO_4$, and 45 Fe(III)-EDTA. All hydroponic solutions were buffered by the addition of 1 mM MES, and the pH was set at 5.5. Plants were maintained for 1 month in 10 L of standard solution and solutions were changed weekly. After this time, each plant was transferred to plastic pots containing 1:1, vermiculite:potting soil (Floradur, Oldenburg, Germany) mix, and grown for approximately 1 month until inflorescence development. Plants were fertilized with a modified Hoagland-type nutrient solution (Marentes and Grusak, 1998). Two independent batches of plants were used for the analyses.

Phloem sap collection

Phloem exudates, also referred to as "phloem sap," were collected every other day for 2 wk after the emergence of the inflorescence (approximately 2 months after sowing). Shallow incisions were made with a lancet device (BD, NJ, USA; using number 6 depth setting), at the base of the attached inflorescence 3 h after the light onset, and exuded droplets were collected for approximately 20 min using a plastic micropipette. The first droplets were discarded to minimize contamination with other plant fluids. Samples were kept on ice during the entire collection period. pH values were measured, aliquots for carboxylate and sugar analyses taken, and samples stored at −80°C.

Protein extraction

Phloem sap exudates from different plants were pooled, and proteins present in 1 mL aliquots were precipitated by adding four volumes of a solution containing 80% acetone and 0.07% ß-mercaptoethanol. Samples were incubated for at least 4 h at −20°C and centrifuged at 10 000 × *g* for 10 min. The pellet was washed thrice with cold methanol, dried with N_2 gas, and resuspended in sample rehydration buffer containing 2 M thiourea, 8 M urea, 20 mM Tris, 4% w/v CHAPS, 50 mM DTT, 0.05% ß-DDM, 2 mM PMSF, and 0.5% v/v IPG buffer pH 3–10 (GE

Healthcare, Uppsala, Sweden). After rehydration, samples were incubated at 28°C for 1.5 h and then centrifuged at 15 000 × *g* for 10 min at 20°C. Protein concentration was measured with the RC DC Protein Assay BioRad (BioRad, Hercules, CA, USA) based on the Lowry method.

2-DE

Preliminary 2-DE experiments were carried out using a 1-D IEF separation with a linear pH gradient 3–10. With these conditions, most of the spots were located in the central region of the 2-DE gel (results not shown). Therefore, a narrower pH gradient was chosen to prevent protein comigration and to improve resolution. A 1-D IEF separation was carried out on 7 cm ReadyStrip IPG Strips (BioRad) with a linear gradient pH 5–8 in a Protean IEF Cell (BioRad). Strips were passively rehydrated for 16 h at 20°C in 125 µL of rehydration buffer containing 50 µg of phloem sap proteins and a trace of bromophenol blue, and then transferred onto a strip electrophoresis tray. IEF and 2-D polyacrylamide gel electrophoresis (SDS- and native-PAGE) were performed as described elsewhere (Krüger *et al.*, 2002; J Rodríguez-Celma *et al.*, 2011). 2-DE gels were subsequently silver stained (Blum, Beier and Gross, 1987). Gels were made from independent phloem sap exudates from two different batches of plants with three technical replicates each.

Gel image and statistical analysis

Silver stained gels were scanned with a Bluescan48 Scanner (LaCie, Portland, OR, USA). Experimental *M*r and p*I* values were calculated by comparison with a 2-DE SDS-PAGE standard (BioRad) run in a separate gel. Spot detection, gel matching, and interclass analysis were performed with PDQuest 8.0 software (BioRad). First, normalized spot volumes based on total quantity were calculated for each 2-DE gel and used for statistical calculations of protein abundance; for all spots present in the gels, p*I*, *M*r, and normalized volumes (mean values, SD, and CV) were determined. Only spots present in all the six replicates were considered as consistent and used in further analysis. A second normalization based on total spot intensity per gel was used to compensate for gel replicate variations. The spots were also manually checked, and a high level of reproducibility between normalized spot volumes was found in all six different replicates.

Protein in-gel digestion

All consistently detected spots (249) in silver-stained gels were excised automatically using a spot cutter EXQuest (BioRad), transferred to Protein LoBind Eppendorf tubes, destained twice in 400 µL of 40% v/v ACN and 60% v/v 200 mM NH_4HCO_3 for 30 min and dehydrated in 100% ACN for 10 min. Gel pieces were dried at RT and then in-gel digested with 15 µL trypsin

solution (Sequencing Grade Modified Trypsin V511, Promega, Madison, WI, USA; 0.1 µg/µL in 40 mM NH_4HCO_3/9% ACN). After incubation for 5 h at 37°C, the reaction was stopped by adding 1 µL 1% TFA.

MALDI analysis

For MALDI-TOF MS, 0.5 µL of the matrix solution (5 mg CHCA in 50% v/v ACN and 0.25% w/v TFA) were placed onto the MALDI target and dried at RT. Then, 2 µL of the digested sample were applied on top, allowed to dry and topped with 0.5 µL of the matrix solution. Tryptic peptides were analyzed with a SHIMADZU AXIMA-CFR mass spectrometer (Shimadzu Scientific Instruments, Columbia, USA). Spectra acquisitions were done using AXIMA software (Shimadzu).

For MALDI-TOF/TOF MS, 1µL of the digested sample was placed onto the MALDI target, dried at RT and 0.5 µL of the matrix solution (5mg α-CHCA in 80% v/v ACN and 0.1% w/v TFA) were placed on top. Tryptic peptides were analyzed in an UltrafleXtreme MALDI TOF/TOF device (Bruker, Bremen, Germany) using FlexControl software v3.3 (Bruker).

Protein identification was performed by searching in the nonredundant NCBInr 20120226 (17406376 sequences; 5965441494 residues), SwissProt 2012_02 (534695 sequences; 189667883 residues) and Plants_EST EST_110 (151512996 sequences; 26700120026 residues) databases, using the Mascot search engine (Matrix Science, London, UK) and the following parameters: monoisotopic mass accuracy, fragment mass tolerance ±0.6 Da; missed cleavages, 0 and 1; allowed variable modifications, oxidation (Met), and carbamidomethylation (Cys). Positive identification was retained with MASCOT scores above the threshold level ($p < 0.05$), at least five peptides matched, sequence coverage above 20% and similar experimental and theoretical molecular weight and p*I*. We used the GO biological process annotation (http://www.geneontology.org) of the individual identified proteins for classification.

Protein identification by nano-LC-MS/MS

Peptides (5 µL) were preconcentrated online onto a 300 µm id × 5 mm, 5 µm particle size ZORBAX 300SB-C18 trapcolumn (Agilent Technologies, Waldbronn, Germany), using a 100 µL/min flow rate of 3% ACN, 0.1% formic acid, in a nano-HPLC system 1200 series (Agilent Technologies). Sequential elution of peptides from the trap column was accomplished in the same instrument with a 75 µm id × 150 mm, 3.5 µm particle size ZORBAX 300SB-C18 column (Agilent), using a 300 nL/min nanoflow rate with a linear gradient from solution 97% A (0.1% formic acid) to 90% of solution B (90% ACN, 0.1% formic acid) for 55 min. The nano-HPLC was connected using a PicoTip emitter (50 µm id, 8 µm tip id, New Objective, Woburn, MA, USA) and an online nanoelectrospray source to a HCTUltra™ high-capacity ion trap (Bruker).

Capillary voltage was −1.8 kV in positive mode and a dry gas flow rate of 10 L/min was used with a temperature of 180°C. The scan range used was from 300 to 1500 *m/z*. Peak detection, deconvolution, and processing was performed with Data Analysis 3.4 software (Bruker).

Protein identification was performed using the databases indicated above. The search parameters were: monoisotopic mass accuracy, peptide mass tolerance ±0.2 Da, fragment mass tolerance ±0.6 Da; one allowed missed cleavage; allowed fixed modification carbamidomethylation (Cys), and variable modification oxidation (Met). Positive identification was retained with MASCOT scores above the threshold level ($p < 0.05$), at least two identified peptides with a score above homology, and similar experimental and theoretical molecular weight and p*I*. The GO biological process annotation of the identified proteins was used for classification.

Comparison of phloem proteomes of different plant species

A comparison of the phloem sap proteome of *L. texensis* with those of rice, pumpkin, rape, and white lupin was performed by creating a reference "non-redundant phloem proteome" from Arabidopsis based on the protein species found in *L. texensis*, as described in (Lin *et al.*, 2009). Briefly, BLAST searches of the unambiguously identified protein species in *L. texensis* were done in Arabidopsis, retaining those matches with E-values below e-30, and then duplicates were deleted. These proteins were compared to the reference Arabidopsis phloem proteomes reported for pumpkin, rice, rape, and castor bean (Lin *et al.*, 2009).

Protein blotting and staining

For electroblotting to PVDF membranes (Immobilon PSQ; Millipore), proteins were transferred from the 2-DE (IEF-native PAGE) gel using a semidry transfer unit (Hoefer scientific instruments, San Francisco, USA) with a transfer buffer containing 25 mM Tris pH 8.3, 0.192 M glycine, 25% v/v methanol. Two different staining methods were used. The Ferene S method, based on the formation of a Fe colored complex, was used to detect Fe-containing proteins(Krüger *et al.*, 2002). The blotted membrane was incubated overnight in darkness at room temperature in a freshly prepared solution containing 0.75 mM Ferene [3-(2-pyridyl)-5,6-bis (2-[5-furylsulfonic acid])-1,2,4-triazine disodium salt; SIGMA, St Louis, MO, USA], 15 mM thioglycolic acid, and 2% v/v acetic acid. After incubation, the membrane was washed twice with water.

A second method based on the catalytic ability of Fe to participate in redox processes(Krüger *et al.*, 2002) was used with some modifications. The blotting membrane was incubated at 35°C for 2 h with 50 mM Na acetate/acetic buffer pH 5.5 containing 80 mM diaminobenzoic acid dihydrochloride. After this period, 100 mM H2O2 was added and the membrane was incubated at 35°C overnight. The membrane was washed twice with water and then destained with 7% v/v acetic acid. Myoglobin was used as a positive staining control in both

methods. Stained membranes were scanned with a Bluescan48 Scanner (LaCie, Portland,OR, USA). In both methods, a myoglobin standard was run in parallel to phloem sap samples as a positive control (Supporting Information Fig. 3.3.S1).

Protein Fe/Zn affinity purification

For affinity purification of metal (Zn/Fe)-chelating proteins, a Hi-TRAP chelating HP column (bed volume, 1 mL; Amersham Biosciences, Uppsala, Sweden) containing chelating Sepharose was rinsed with 5mL of water before the matrix was loaded with either Fe(III) or Zn(II) using 0.5 mL of 0.1M $FeCl_3$ or $ZnCl_2$ according to the manufacturer's instructions. Excess metals were removed by washing with 5 mL of water, and the column was equilibrated with elution buffer (2.5 mM phosphate buffer, 62.5 mM NaCl, 10mM imidazole, pH 7.4). One milliliter of phloem sap pooled from different plants was diluted with 2.5 mL 20 mM HEPES, pH 7.2, 0.15 mM NaCl, filtered and loaded to the column by recirculation for 30 min using a peristaltic pump with a rate of 1 mL/min. The column was washed with 5 mL of elution buffer and proteins were eluted with 1 mL each of increasing concentrations of imidazole in the elution buffer (50, 100, 150, 200, and 250 mM), and finally with 5mL of 400 M imidazole. Proteins in the different fractions were precipitated overnight with 80% acetone and 0.07% ß-mercaptoethanol at −20°C. After centrifugation at 10 000 × *g* for 10 min, the pellet was washed twice with cold methanol and dried with N_2. The sample rehydration buffer consisted on 2 M thiourea, 8 M urea, 20 mM Tris, 4% w/v CHAPS, 50 mM DTT, 0.05% ß-DDM, and 2 mM PMSF. After rehydration, samples were incubated at 29°C for 1.5 h, centrifuged at 15000×*g* for 10 min at 20°C, separated by 1-DE SDS-PAGE (containing 12 and 16.5% acrylamide for Fe and Zn experiments, respectively), and gels were silver stained.

Carboxylate analysis

Carboxylate analyses in phloem sap exudates were conducted by liquid chromatography-electrospray ionization TOF MS as described elsewhere (Rellan-Alvarez *et al.*, 2011).

Sugar analysis

Sugar analyses in phloem sap exudates were performed with an HPLC device (Waters, Milford, MA, USA) equipped with a 515 pump and a differential refractive index detector (Waters 2410). Sugars were separated in an Aminex HPX-87C (300 × 7.8 mm) column at 85°C. Chromatographic separations were performed isocratically at a solvent flow rate of 0.6 mL/min, using MilliQ water as mobile phase. Peaks were identified by comparison of the retention time with those of known standards from Sigma and quantification was made with known amounts of the standards using peak areas.

3.3.3. Results

Protein profile of phloem sap exudate

The phloem sap exudation yield was 660 ± 165 µL per plant during the 2 wk collection period, and the protein extraction yield was 0.15 ± 0.03 µg/µL. A typical real scan of 2-DE gels obtained from phloem sap exudates is shown in Fig. 3.3.1A.

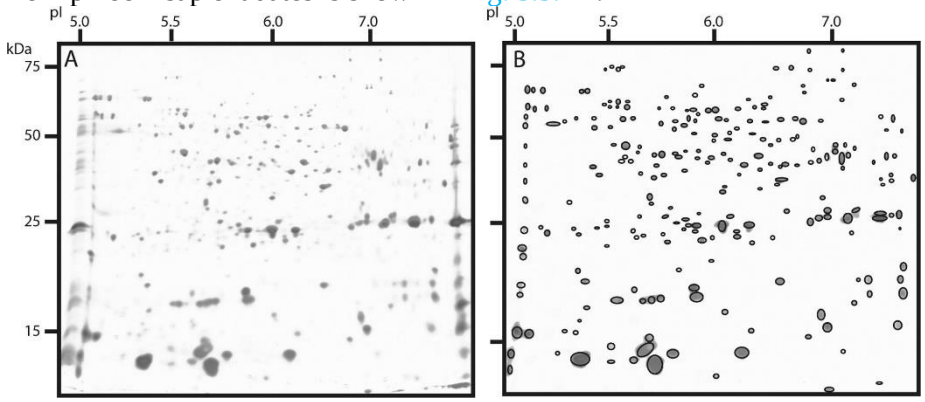

Figure 3.1.1. *2-DE IEF-SDS-PAGE protein map of phloem sap from Lupinus texensis plants. Proteins were separated in the first dimension in linear IPG pH 5–8 gel strips and in the second dimension in 12% acrylamide vertical gels. (A) Scan of a typical gel. (B) Virtual composite image with spots consistently detected and further analyzed by MS.*

Approximately 90% of spots were consistently found in all six replicates, and the total number of spots consistently detected in the whole experiment (present in all gels) was 249. A composite averaged virtual map containing spots present in all six gels is shown in Fig. 3.3.1B. All 249 spots were excised and analyzed by MS (spots circled in Fig. 3.3.1B). From the 249 spots analyzed, 54 protein species (22% of the total) were unambiguously identified (proteins complying with all the identification requirements; marked by squares and labeled 1 to 54 in Fig. 3.3.2A and described in Table 3.3.1), whereas 44 protein species (18% of the total) were tentatively assigned (only positive Mascot score; marked by squares and labeled 55 to 98 in Supporting Information Fig. 3.3.S2 and described in Supporting Information Table 3.3.S1).

The protein species unambiguously identified were classified according to their GO biological process annotation (Fig. 3.3.2B). Among them, 12 (19%) were related to different aspects of protein metabolism (spots 1–12, Fig. 3.3.2A, Table 3.3.1). Proteins identified include: two chaperones involved in protein folding (spots 1–3), three eukaryotic initiation factors (eIF-A1, 2 and 5; spots 4–7), and three proteolysis-related enzymes, two of them involved in the ubiquitination pathway (spots 8 and 9) and one cystatin (spots 10–12). Four spots were related to cytoskeleton organization, two identified as actin (spots 13 and 14), and two as depolymerizing factors 1 and 2 (spots 15 and 16, respectively), whereas four corresponded to Rubisco, three to the small chain (spots 17–19), and one to the large chain (spot 20). Five spots were identified as ascorbate peroxidase (spot 21), glutathione peroxidase (spot 22), and thioredoxin (spots 23–25),

all of them involved in cellular redox homeostasis, whereas three spots, identified as LEA2, PR10.2C, and leucine-rich-repeat (LRR) disease resistance protein (spots 26–28, respectively), were related to plant defense mechanisms.

Two protein species (spots 29 and 30) were identified as enoyl-ACP reductase involved in lipid biosynthesis, and two as proteins involved in glycolysis: phosphoglycerate kinase (spot 31) and fructose-biphosphate aldolase (spot 32). Two spots (33 and 34) were identified as malate dehydrogenase from the TCA cycle, one (spot 35) as a 6-phosphogluconolactonase-4 from the pentose phosphate shunt, and two (spots 36 and 37) were identified as cell division cycle protein 48 homolog.

Eight protein species were identified as related to different metabolic processes, including metal transport (spot 38), amino acid, and nucleotide biosynthesis (spots 39 and 40, respectively), DNA and RNA processing (spots 41 and 42), one carbon and secondary metabolic processes (spots 43 and 44, respectively) and signal transduction (spot 45). Finally, nine spots (21% of the total identified) were identified as hypothetical proteins (spots 46–54). It is worth mentioning that spot 53 corresponded to a phloem-specific protein from *L. albus* (Supporting Information Table 3.3.S3).

Comparison of phloem exudate of L. texensis with those of other species

Based on the BLAST results, 35 non-redundant Arabidopsis phloem proteins were identified for *L. texensis*, while seven spots did not yield any match (Supporting Information Table 3.3.S2). A Venn diagram comparing the nonredundant Arabidopsis reference proteins for pumpkin, rice, rape, and *L. texensis* species is shown in Fig. 3.3.2C and the data used for the comparison are provided in Supporting Information Table 3.3.S3.

When comparing the nonredundant phloem Arabidopsis reference proteome from *L. texensis* with those from pumpkin, rape, and rice (Giavalisco *et al.*, 2006; Aki *et al.*, 2008; Lin *et al.*, 2009), we found only 13 protein species that had not been previously reported; from these, one protein was previously described in castor bean (Krüger *et al.*, 2002; Barnes *et al.*, 2004) (spot 40) and two in several plant species including *L. albus* (Rodriguez-Medina *et al.*, 2011; Barnes *et al.*, 2004; Walz *et al.*, 2004; Batailler *et al.*, 2012) (spots 27, 33, and 34). The remaining ten novel protein species included two hypothetical proteins (spots 46 and 47) of unknown function, two proteins involved in RNA processing, a maturase and a histone (spots 41 and *42*), and six protein species with nonredundant identifiers but with assigned functions similar to other protein species already described in phloem from other plant species: a putative chaperonin (spot 3), an actin (spot 14), a LEA (late-embryogenesis-abundant) protein (spot 26), a LRR protein

(spot 28), an enoyl-ACP-reductase (spots 29 and 30), and a putative phosphoglycerate dehydrogenase (spot 39).

Eleven nonredundant Arabidopsis protein species were consistently detected in the phloem sap of *L. texensis*, pumpkin, and rape; six of them were also common when a monocot, rice, was included in the comparison (Fig. 3.3.2C). Common proteins found among monocotyledonous and dicotyledonous species included translation initiation factors (spots 4–7), cysteine proteases (spots 10–12), actin, and actin depolymerizing factors (spots 13 and 15), HSP70 (spot 2), and a ran-related guanosine-5'-triphosphate (GTP)-binding protein (spot 45). In addition to these, the phloem sap of the dicotyledonous plants compared shared the presence of two ubiquitin-related proteins (spots 8 and 9), a fructose biphosphate aldolase (spot 32), S-adenosylmethionine synthetase (spot 43), and a fragment of Rubisco (spot 20).

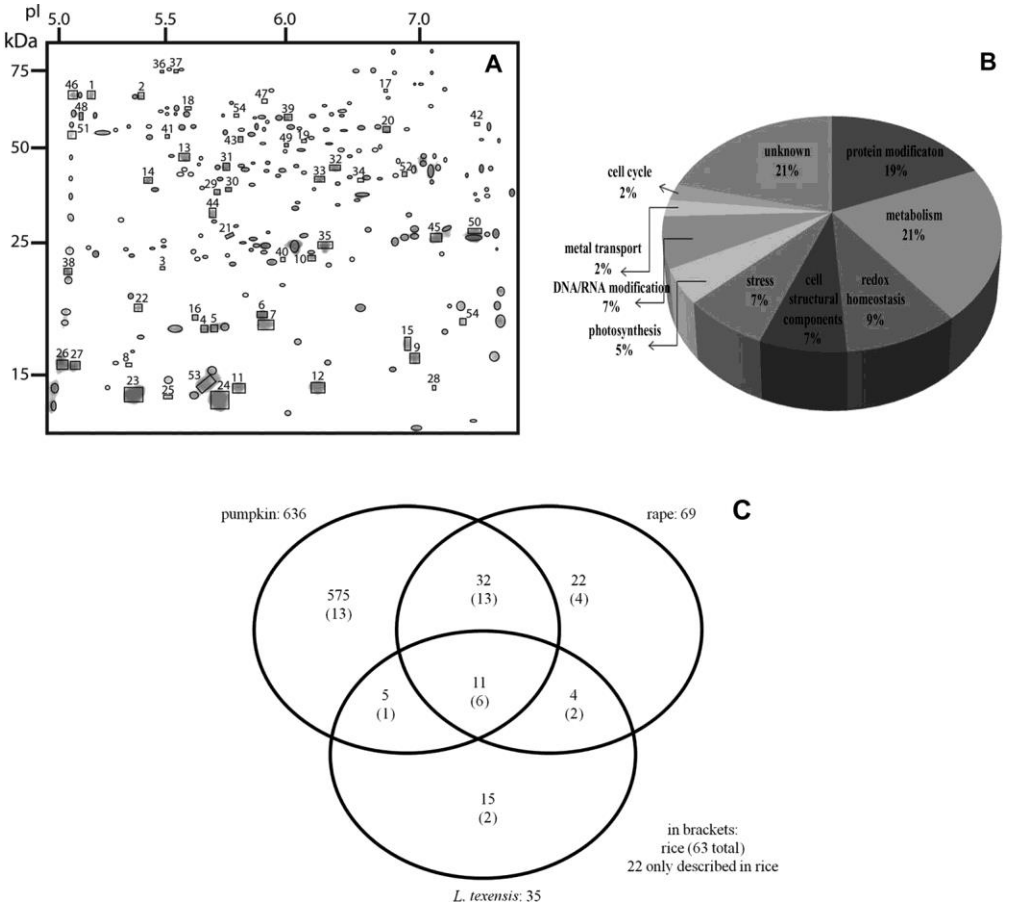

Figure 3.3.2. *Polypeptides identified in phloem sap from Lupinus texensis. (A) Polypeptides with significant homologies to proteins present in databases are marked by squares and numbered as in Table 3.3.1. (B) Distribution of identified proteins in phloem sap according to their GO (biological process) term. (C) Venn diagram showing the comparison of nonredundant phloem Arabidopsis reference proteome from L. texensis in this study with those from pumpkin, rape, and rice (data from* (Lin *et al.*, 2009)*; numbers in brackets in the different areas are those also common for rice.*

Table 3.3.1. *Protein species identified in 2-DE IEF-SDS PAGE gels. Protein score is –10*Log (P), where P is the probability that the observed match is a random event. Homology identification was retained with a probability set at 95%. Identifications were validated with at least five peptides matched and sequence coverage above 20% for MS data, and at least two identified peptides with a score above homology and similar experimental MW and pI for MS/MS data. Function was inferred from GO biological process annotation.*

Spot	**Protein**	***Plant species***	***ID***	***Score/pep/ion***	***% coverage***	***Mw/pI th***	***Mw/pI exp***	***Function***	***GO (BP)***
1	Heat shock protein 70	*Cucumis sativus*	gi|1143427	*277/4/4*	*7*	*75.5/5.2*	*64.0/5.1*	*Protein folding*	*GO:0006457*
2	Heat shock protein 70	*Ocimum basilicum*	DY336109	*98/2/2*	*10*	*24.8/8.9*	*64.0/5.3*	*Protein folding*	*GO:0006457*
3	Chaperonin, putative	*Quercus robur*	FP024807	*80/2/2*	*10*	*25.0/8.3*	*22.2/5.4*	*Protein folding*	*GO:0006457*
4	Initiation factor eIF-A5	*Manihot esculenta*	gi|13094963	*42/2/1*	*6*	*17.8/5.6*	*17.0/5.6*	*Protein biosynthesis*	*GO:0006412*
5	Initiation factor eIF-5A2	*Lupinus albus*	FG090639	*110/3/2*	*12*	*19.9/5.5*	*17.0/5.7*	*Protein biosynthesis*	*GO:0006412*
6	Eukaryotic initiation factor 5A-1	*Plantago major*	*gi|53748427*	*134/5/-*	*35*	*17.0/5.3*	*18.0/5.8*	*Protein biosynthesis*	*GO:0006412*
7	Eukaryotic initiation factor 5A-5	*Solanum tuberosum*	*gi|2225885*	*145/5/-*	*26*	*17.0/5.7*	*17.0/5.8*	*Protein biosynthesis*	*GO:0006412*
8	Ubiquitin-like protein	*Arabidopsis thaliana*	gi|1707372	*121/2/2*	*22*	*11.8/5.3*	*13.8/5.3*	*Ubiquitin-dependent proteolysis*	*GO:0006511*
9	Ubiquitin-conjugating enzyme	*Arabidopsis thaliana*	*gi|30699363*	*139/5/-*	*33*	*13.0/9.3*	*14.0/6.9*	*Ubiquitin-dependent proteolysis*	*GO:0006511*

10	Cysteine proteinase inhibitor	*Manihot esculenta*	*gi|8099682*	*67/2/1*	*12*	*11.0/4.9*	*23.0/6.1*	*Proteolysis*	*GO:0006508*
11	Cysteine proteinase inhibitor	*Vigna unguiculata*	gi|1169196	*81/3/2*	*19*	*10.8/6.1*	*13.3/5.7*	*Proteolysis*	*GO:0006508*
12	Cysteine proteinase inhibitor	*Vigna unguiculata*	*gi|288188*	*78/2/1*	*11*	*11.0/9.1*	*13.3/6.1*	*Proteolysis*	*GO:0006508*
13	Actin	*Setaria italica*	*gi|9965319*	*191/6/-*	*25*	*42.0/5.3*	*46.0/5.5*	*Cytoskeleton organization*	*GO:0007010*
14	Actin	*Zea mays*	gi|226510460	*267/5/5*	*15*	*42.4/5.2*	*37.0/5.4*	*Cytoskeleton organization*	*GO:0007010*
15	Actin depolymerizing factor 2 (ADF2)	*Arabidopsis thaliana*	gi|7339501	*105/3/3*	*11*	*15.4/5.2*	*15.0/6.8*	*Cytoskeleton organization*	*GO:0007010*
16	Actin-depolymerizing factor 1	*Petunia x hybrida*	gi|17366768	*105/7/3*	*18*	*16.3/5.8*	*18.0/5.6*	*Cytoskeleton organization*	*GO:0007010*
17	Rubisco small chain	*Medicago truncatula*	gi|217071562	*145/54/4*	*21*	*20.2/8.7*	*67.5/6.6*	*Photosynthesis*	*GO:0015979*
18	Rubisco small chain	*Medicago truncatula*	gi|217071562	*111/34/3*	*17*	*20.2/8.7*	*60.0/5.5*	*Photosynthesis*	*GO:0015979*
19	Rubisco small chain	*Medicago truncatula*	gi|217071562	*114/54/3*	*17*	*20.2/8.7*	*49.0/6.0*	*Photosynthesis*	*GO:0015979*
20	Rubisco large chain	*Lupinus albifrons*	*CAA93912.1.*	*195/5/5*	*11*	*50.7/6.2*	*52.5/6.6*	*Photosynthesis*	*GO:0015979*
21	L-Ascorbate peroxidase	*Arabidopsis thaliana*	*gi|1523789*	*67/2/1*	*10*	*28.0/5.9*	*25.0/5.7*	*Cell redox homeostasis*	*GO:0045454*

22	Glutathione peroxidase 1	*Lotus japonicus*	gi|37930463	*130/2/2*	*9*	*26.4/8.8*	*20.0/5.3*	*Cell redox homeostasis*	*GO:0045454*
23	Thioredoxin	*Ricinus communis*	*gi|1255954*	*88/2/1*	*13*	*13.0/5.6*	*13.0/5.3*	*Cell redox homeostasis*	*GO:0045454*
24	Thioredoxin H	*Prunus persica*	*gi|16588843*	*70/2/2*	*6*	*14.5/5.6*	*13.0/5.7*	*Cell redox homeostasis*	*GO:0045454*
25	Thioredoxin H	*Prunus persica*	Q93WZ3	*86/2/2*	*15*	*19.7/8.3*	*13.0/5.5*	*Cell redox homeostasis*	
26	LEA-2 protein	*Bupleurum chinense*	gi|209980062	*56/2/1*	*9*	*17.0/4.9*	*13.8/5*	*Plant defense*	*GO:0006952*
27	PR10.2C protein	*Lupinus luteus*	gi|12958727	*121/2/2*	*15*	*16.8/4.8*	*13.8/5*	*Plant defense*	*GO:0006952*
28	Putative LRR disease resistance protein	*Pinus strobus*	PS4_PINST	*31/2/1*	*100*	*0.9/9.7*	*13.5/7.0*	*Plant defense*	*GO:0006952*
29	Enoyl-ACP reductase	*Nicotiana tabacum*	gi|2204236	*113/4/3*	*8*	*41.9/8.9*	*34/5.7*	*Lipid biosynthesis*	*GO:0008610*
30	Enoyl-ACP reductase	*Nicotiana tabacum*	gi|2204236	*89/2/2*	*6*	*41.9/8.9*	*34.5/5.7*	*Lipid biosynthesis*	*GO:0008610*
31	Cytosolic phosphoglycerate kinase	*Pisum sativum*	gi|9230771	*190/3/3*	*9*	*42.3/5.7*	*39.2/5.7*	*Glycolysis*	*GO:0006096*
32	Fructose-bisphosphate aldolase	*Cicer arietinum*	*gi|3021338*	*193/7/-*	*41*	*39.0/6.2*	*39.0/6.2*	*Glycolysis*	*GO:0006096*
33	Malate dehydrogenase	*Lupinus albus*	gi|27462764	*254/6/4*	*14*	*35.9/6.0*	*37.0/6.2*	*TCA cycle*	*GO:0006099*

34	Cytosolic malate dehydrogenase	*Lupinus angustifolius*	GD001384	*264/5/4*	*18*	*26.7/6.6*	*37.0/6.5*	*TCA cycle*	*GO:0006099*
35	Probable 6-phosphogluconolactonase 4	*Oryza sativa*	gi|115480295	*128/5/2*	*6*	*38.7/4.5*	*24.5/6.2*	*Pentose-phosphate shunt*	*GO:0006098*
36	Cell division cycle protein 48 homolog	*Glycine max*	gi|1705678	*97/2/2*	*2*	*90.5/5.2*	*72.5/5.4*	*Cell cycle*	*GO:0007049*
37	Cell division cycle protein 48 homolog	*Glycine max*	gi|1705678	*101/2/2*	*2*	*90.5/5.2*	*72.5/5.5*	*Cell cycle*	*GO:0007049*
38	Copper chaperone homolog CCH	*Lupinus albus*	FG090635	*82/2/1*	*7*	*19.5/5.0*	*22.0/5.0*	*Metal ion transport*	*GO:0030001*
39	d-3-Phosphoglycerate dehydrogenase, putative	*Ricinus communis*	gi|255555301	*151/3/3*	*5*	*63.4/7.6*	*56.0/6.0*	*L-Serine biosynthetic process*	*GO:0006564*
40	Uridylate kinase	*Medicago truncatula*	gi|217075148	*78/2/1*	*7*	*23.2/5.6*	*23.0/5.9*	*Pyrimidine biosynthesis*	*GO:0006221*
41	Histone H3 methyltransferase complex	*Physcomitrella patens*	gi|168001870	*44/2/1*	*2*	*53.8/8.8*	*50.1/5.4*	*Histone H3-K4 methylation*	*GO:0051568*
42	Maturase	*Acacia blakelyi*	gi|22725553	*48/2/2*	*25*	*9.8/9.0*	*54.9/7.4*	*mRNA processing*	*GO:0006397*
43	S-Adenosylmethionine synthetase	*Arabidopsis thaliana*	gi|166872	*87/2/2*	*5*	*43.6/5.5*	*50.0/5.7*	*One-carbon metabolic process*	*GO:0006730*

44	Lactoylglutathione lyase	*Gossypium hirsutum*	gi|211906514	*113/3/2*	*8*	*32.6/5.7*	*29.0/5.6*	*Secondary metabolic process*	*GO:0019748*
45	Ran-related GTP binding protein	*Zea mays*	*gi|4336905*	*125/7/-*	*36*	*20.0/6.3*	*25/7.2*	*Signal transduction*	*GO:0007264*
46	Predicted protein	*Populus trichocarpa*	gi|224120086	*417/6/5*	*9*	*75.4/5.2*	*64.0/5.0*	*Unknown*	
47	Hypothetical protein	*Vitis vinifera*	gi|147805930	*47/2/2*	*4*	*69.6/8.5*	*62.5/5.8*	*Unknown*	
48	Hypothetical protein	*Vitis vinifera*	gi|147778524	*47/3/3*	*1*	*71.8/9.1*	*57.3/5.1*	*unknown*	
49	Hypothetical protein	*Arabidopsis thaliana*	gi|110740271	*45/2/1*	*1*	*49.5/8.7*	*48.2/5.9*	*Unknown*	
50	Hypothetical protein	*Vitis vinifera*	gi|147859203	*45/4/2*	*2*	*51.8/9.0*	*26.0/7.4*	*Unknown*	
51	Conserved hypotetical protein	*Ricinus communis*	*gi|255544349*	*72/4/4*	*42*	*14.0/8.8*	*21.0/7.6*	*Unknown*	
52	Unknown	*Panicum virgatum*	*FL852282*	*94/7/7*	*34*	*24.8/8.4*	*38.0/6.8*	*Unknown*	
53	Unknown	*Lupinus albus*	*FG090187*	*154/4/2*	*7*	*20.6/6.5*	*13.5/5.6*	*Unknown*	
54	Hypothetical protein	*Vitis vinifera*	A5BP68	*70/2/2*	*2*	*34.7/7.7*	*7.5/7.3*	*Unknown*	

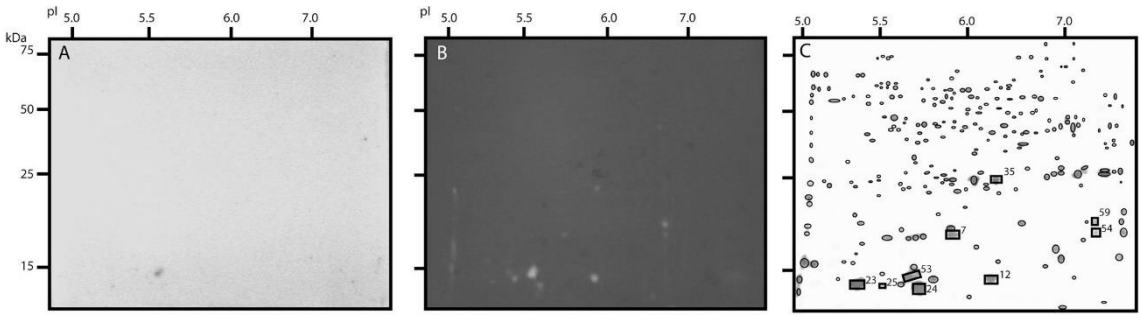

Figure 3.3.3. *Membrane blots from similar gels as shown in Fig. 3.3.1, stained with Ferene (A) and with a second method based on redox properties (B) and a 2-D gel with corresponding stained spots marked by squares and numbered as in Table 3.3.1 (C).*

Protein blotting and Fe staining

Protein species from phloem sap exudates were separated by 2-DE and blotted to PVDF membranes. Putative Fe-binding proteins were studied by two different staining methods: Ferene S and a method based on the catalytic properties of Fe in redox processes. The Ferene S staining method revealed the presence of one major spot with Fe-binding capacity (Fig. 3.3.3A), which corresponded to a protein in the 2-DE gel with an experimental molecular weight of 13.5 kDa and a p*I* of 5.6 (the phloem-specific protein species spot 53 in Fig. 3.3.2A and Table 3.3.1).

A less specific staining method, the oxidation of diaminobenzoic acid in the presence of H_2O_2, causes a destaining of the transfer membrane at locations corresponding to redox-active, metal-binding proteins (Krüger *et al.*, 2002). Nine destained spots were found in the blot from phloem sap (Fig. 3.3.3B). Comparisons of the blotted membrane and the 2-DE gel showed that they corresponded to spots 7, 12, 23–25, 35, and 53–54 (squared spots in Fig. 3.3.3C, Table 3.3.1), and spot 59 (Fig. 3.3.3C and Supporting Information Table 3.3.S1). Three of the spots were identified as thioredoxin (spots 23–25), two as eukaryotic initiation factor 5-A1 (spots 7 and 59), spot 12 was a cystatin, spot 35 a putative probable 6-phosphoglucolactonase-4, one spot was the phloem-specific protein species indicated above (spot 53), and another spot corresponded to an unknown protein (spot 54).

nLC-Tandem MS analysis of Fe-binding protein

The spot of 13.5 kDa and a p*I* of 5.6 corresponding to a putative Fe-binding protein detected by both staining methods (Fig. 3.3.3A–B, spot 53 in Fig. 3.3.2A and Table 3.3.1) was further analyzed by nLC-ESI-MS/MS. Double or triple charged precursor ions shown in Table 3.3.2 were fragmented and the spectra obtained were interpreted manually in addition to the online form of the MASCOT program using the Plant_EST database. Partial sequences of peptides found

are shown in Table 3.3.2 and manually interpreted spectra are provided in Supporting Information Fig. 3.3.S3.

Table 3.3.2. *Peptide ions used for de novo sequencing of spot 53 and peptide sequences derived from the* analyses

m/z	z	MS/MS-derived sequence	Method
532.2	3+	KVVYEEEEIEGLR	Manually assigned
623.6	3+	VSEVVYEDVVDI/LETDR	Manually assigned
726.3	2+	VVYEEDEIEGLR	Manually assigned
732.6	2+	VVYEEEEIEGLR	Manually assigned
797.3	2+	KVVYEEEEIEGLR	Manually assigned
905.4	2+	EEFNNGYNTEVQ/KR	Manually assigned
934.5	2+	VSEVVYEDVVDI/LETDR	Manually assigned
733.2	2+	VVYEEEEIEGLR	MASCOT assigned
797.3	2+	KVVYEEEEIEGLR	MASCOT assigned

The sequences deduced from these peptides were blasted against NCBI Plant_EST database and resulted in significant matches to an EST from *L. albus* roots (FG090187) that displayed the highest homology (E value: 4e-05) to a protein from *Medicago truncatula* annotated as phloem-specific (XP_003601185), and lower homologies to other phloem-specific proteins from *Pisum sativum* (EF372612.1) and *Vicia faba* (X89207.1). A manual alignment of the translated sequence of the EST and deduced peptide sequences is shown in Supporting Information Fig. 3.3.S4.

Protein Fe/Zn affinity purification

Affinity chromatography with immobilized Fe and silver staining of the subsequent 1-DE SDS-PAGE revealed a weakly retained band that was eluted from the column in the first step (50 mM imidazole) of the elution gradient. This band had a very low intensity and a molecular weight of 16.5 kDa (Fig. 3.3.4A). MS analyses of the band, after excision and in-gel digestion, revealed a mixture of protein species. Two identified protein species were a photosystem I iron-sulphur center and a metallothionein-like protein type 2 B (Table 3.3.3). Both of them are Fe-containing proteins.

Seven different bands were detected in the SDS-PAGE gels after Zn affinity Hi-Trap chromatography (Fig. 3.3.4B). The first eluted fraction (50 mM imidazole) resulted in five bands (bands Zn3 to Zn7) with molecular weights of 23.1, 19.5, 15.6, 15.5, and 15.4 kDa, respectively. Bands Zn3 and Zn4 eluted in fractions one to four, whereas bands Zn5, Zn6, and Zn7 eluted in fractions one to three. Another two tightly bound proteins corresponding to molecular weights of 23.6 and 23.3 kDa were detected in the second to fourth fractions (bands Zn1 and Zn2, respectively).MS analyses of the bands, after excision and in-gel digestion, provided positive

identification for band Zn1 as an EST from *L. albus* (Table 3.3.3), and bands Zn2, Zn4, Zn6, and Zn7 as Zn finger proteins (Table 3.3.3).

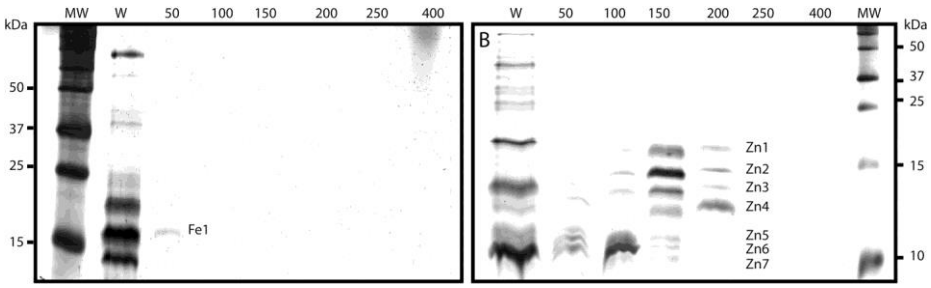

Figure 3.3.4. *1-DE of fractions from Fe- affinity (A) and Zn-affinity (B) Hi-Trap chromatography. MW and W stand for molecular weight markers and washes, and 50–400 refers to the imidazole concentration in mM in the subsequent elution steps. Acry-lamide concentration for SDS-PAGE was 12% for Fe and 16.5% for Zn experiments.*

Carboxylate and sugar analysis

To assess the purity of phloem sap samples, sugar concentrations were measured. Sucrose was the major sugar detected in phloem sap, as would be expected from pure phloem sap samples, with a concentration of 227 mM (Table 3.3.4). The concentrations of the reducing sugars glucose and fructose were much lower, approximately 4–5 mM. Total concentration of carboxylates in phloem sap was 15.4 mM, with malate, succinate, ascorbate, and citrate being the most abundant ones (Table 3.3.4).

Table 3.3.4. *Concentrations (in mM) of carboxylates and sugars in phloem sap obtained from Lupinus texensis plants. Data are means ± SD of 6 replicates.*

	concentration (mM)
Malic	5.47 ± 1.45
Succinic	5.38 ± 1.03
Ascorbic	1.95 ± 0.30
Citric	1.10 ± 0.28
2-Oxoglutaric	0.44 ± 0.07
Dehydroascorbic	0.31 ± 0.06
Oxalacetic	0.18 ± 0.03
Cis-aconitic	0.18± 0.01
Fumaric	0.18 ± 0.06
Oxalic	0.10 ± 0.03
Gliceric	0.05 ± 0.01
Malonic	0.02 ± 0.01
Mitramalic	0.01 ± 0.00
Sucrose	227 ± 26
Glucose	4.58 ± 1.44
Fructose	4.09 ± 2.95

Table 3.3.3. *Protein species identified in 1-DE SDS-PAGE gels obtained from the Fe/Zn affinity chromatography fractions. Protein score is –10*Log (P), where P is the probability that the observed match is a random event. Homology identification was retained with a probability set at 95%. Identifications were validated with at least five peptides matched and sequence coverage above 20% for MS data, and at least two identified peptides with scores above homology and similar Mws for MS/MS data.*

Band	ID	Plant species	ID	Score/pep/ion	% coverage	Mw th	Mw exp	sequence
Zn1	Similar to dehydrin family protein	*Lupinus albus*	GW583364	95/2/2	5	25.1	23.6	K.IGDALHVGGHK.KK
Zn2	Putative RING-H2 finger protein ATL71	*Arabidopsis thaliana*	Q9FG21	78/5/-	33	22	23.3	IGDALHVGGHKK.E
Zn3	No id	--	--	--	--	--	23.1	
Zn4	Zn finger AN1 domain-containing stress-associated protein 17 (SAP17)	*Oryza sativa*	Q6H595	105/9/-	43	19.9	19.5	
Zn5	No id	--	--	--	--	--	15.6	
Zn6	Zn finger AN1 domain-containing stress-associated protein 17	*Oryza sativa*	Q6H595	69/5/-	28	19.9	15.5	
Zn7	RING-H2 zinc finger protein RHA1b	*Arabidopsis thaliana*	Q9SUS5	76/7/-	35	18	15.4	
Fe1	Photosystem I iron-sulfur center	*Ostreococcus tauri*	Q0P3P1	84/6/-	65	8.7	16.4	
Fe1	Metallothionein-like protein type 2 B	*Solanum lycopersicum*	Q40158	99/7/-	92	8.3	16.4	

3.3.4. Discussion

Sieve tube exudates from *L. texensis* plants have been used to study the protein profile of phloem sap, with the particular aim to identify putative Fe- and Zn-binding proteins in this plant compartment. The 2-DE proteomic approach allowed us to resolve 249 polypeptides in phloem exudates of *L. texensis*, with 54 of them (22%) being identified. These results are similar to those reported in *L. albus*, where 200 spots were detected and 52 of them (26%) identified (Rodriguez-Medina *et al.*, 2011). A similar studyusing larger gels and *B. napus* revealed 600 spots from which 135 (23%) were identified (Giavalisco *et al.*, 2006). Protein distribution according to the biological process in *L. texensis* (Fig. 3.3.2B) is very similar to that reported for *L. albus*, with general metabolism (24 and 21% in *L. texensis* and *L. albus*, respectively) and protein modification/turnover (19 and 9% in *L. texensis* and *L. albus*, respectively) being the groups containing the largest number of proteins, followed by redox homeostasis (9% in both), defence (7% in both), and cell structural components (7% in both).

The Venn diagram comparing the nonredundant phloem Arabidopsis reference proteome from *L. texensis* with those from pumpkin, rape, and rice (Fig. 3.3.2C) shows the presence of 13 proteins not previously reported in these species. From these, the most interesting ones are a histone metyltransferase (spot 41) and a maturase (spot 42). The presence in phloem sap from *L. texensis* of RNA/DNA processing protein species is in consistent with the proposed existence of an RNA-based signaling network in the phloem sap that may control many plant processes (Lough and Lucas, 2006; Atkins, Smith and Rodriguez-Medina, 2011), and warrants further investigation. Both novel proteins were identified in low intensity spots as it could be expected from signaling molecules; however, one should keep in mind the issue of the purity of phloem sap obtained by the incision method as discussed below. On the other hand, the ubiquitous presence in phloem sap from different plant species of RNA-binding proteins such as the eukaryotic initiation factors and the ran-GTPbinding protein also points toward an RNA-based signaling network (Supporting Information Table 3.3.S3). Furthermore, the presence of a histone methyltransferase might suggest that it could play a role in epigenetic regulation in the phloem sap of *L. texensis*. The presence of a histone-binding protein in the phloem sap from pumpkin(Lin *et al.*, 2009) would be in line with this hypothesis.

Six proteins have been consistently found in phloem sap of mono and dicotyledonous species, and the presence among them of several eukaryotic initiation factors (spots 4–7) supports the hypothesis that sieve elements contain components necessary for protein biosynthesis(Lin *et al.*, 2009). Cystein proteinases, suggested to play a role in the stability of proteins in the phloem (Rodriguez-Medina *et al.*, 2011; Giavalisco *et al.*, 2006), were three of the most intense spots

(spots 10–12) in *L. texensis*, suggesting a conserved role among plant species. Also, the presence of actin and actin-depolymerizing factors (spots 13 and 15) may reflect the existence of basic cellular components within the enucleate sieve elements (Lin *et al.*, 2009) and indicate that actin-related processes are also conserved among species. In addition to these, the phloem sap of the dicotyledonous plants compared shared the presence of two ubiquitin-related proteins (spots 8 and 9) in agreement with the idea that sieve elements have the machinery for protein degradation via the ubiquitin/proteasome 26 pathway (Lin *et al.*, 2009). The finding of the glycolytic enzyme fructose biphosphate aldolase (spot 32) in all dicotyledonous species tested may support the existence of an active carbohydrate metabolism in sieve elements and feeds the debate of the role of reducing sugars in phloem sap (Rodriguez-Medina *et al.*, 2011; Van Bel and Hess, 2008; Lin *et al.*, 2009). Finally, the presence of S-adenosylmethionine synthetase (spot 43) in all dicotyledonous species tested may be related to the synthesis of nicotianamine, a chelator proposed to have an essential role in metal translocation in the phloem (Curie *et al.*, 2009), which also may provide methyl groups for protein modification.

A general overview of the proteins identified indicates that *L. texensis* phloem sap contains a very broad range of enzymes involved in various metabolic processes (e.g., glycolysis, TCA cycle, lipid biosynthesis, the pentose phosphate shunt and amino acid and nucleotide synthesis), which suggests that they might still be active in mature sieve elements. Among these processes, data presented here suggest the existence of an active glycolytic pathway as well as amino acid synthesis in sieve elements, indicating that amino acids might not only be passively transported. The 2-DE protein profile and the redox-based staining experiments also confirm the presence of redox homeostasis enzymes such as ascorbate and glutathione peroxidases, with thioredoxin h being one of the most abundant proteins in this group (Rodriguez-Medina *et al.*, 2011; Ishiwatari *et al.*, 1995; Schobert *et al.*, 1998; Walz *et al.*, 2002). These proteins constitute a mechanism to protect this plant compartment from oxidative damage, and might therefore be important for sieve element maintenance (Ishiwatari *et al.*, 1995). Finally, proteins involved in plant defence found here have been previously reported in phloem sap, including PR10 and a LRR disease resistance protein (spots 27 and 28). As a conclusion of the mapping experiment, the protein profile described in this paper resembles those reported in other species, suggesting that the protein composition of phloem sap is quite conserved between plant species.

The purity of the obtained phloem sap samples was assessed by measuring sugar concentrations and the presence of Rubisco. Sucrose was the major sugar, with hexoses being present in much lower concentrations, as expected from a sap obtained from sieve elements. From the 54 identified spots, only 4 (7%) were assigned to Rubisco; furthermore, when also considering those tentatively identified (Supporting Information Table 3.3.S1) only three additional spots

were assigned to Rubisco. The seven Rubisco spots account for 7% of the 98 identified and 3% of the total 249 spots. These percentages are in the same range as those described in other phloem sap samples obtained by the incision technique (Rodriguez-Medina *et al.*, 2011; Doering-Saad *et al.*, 2006). Also, by discarding the first droplet we tried to minimize contamination from non-phloem cells damaged at the wound site. However, it should be kept in mind that there is no bulletproof method for phloem sap isolation and that some degree of contamination from damaged cells as well as some changes in composition caused by wounding (including protein species involved in defence against insect feeding and/or in sealing processes following wounding), are inherent to this technique (Atkins, Smith and Rodriguez-Medina, 2011). Also, the nature of the phloem sap obtained by incision in certain plant species with a dual phloem transport system is still a matter of debate (Zhang *et al.*, 2012), although this does not seem to be the case in *L. texensis*.

The large majority of the polypeptides resolved by 2-DE IEF-SDS-PAGE of phloem exudates of *L. texensis* have no known relationship with metal transport, with the only exception being the Cu chaperone homolog CCH, which has been previously immunolocalized to sieve elements of *A. Thaliana* stems and could act in phloem-mediated metal allocation from senescent to young leaves (Mira, Martínez-García and Peñarrubia, 2001). A homologue of this chaperone (At3g56240) was identified in *B. napus* phloem sap (Giavalisco *et al.*, 2006), whereas in *L. albus* phloem sap this protein was not identified although its RNA was indeed detected in a cDNA library constructed from phloem sap of the same species (Rodriguez-Medina *et al.*, 2011). Other metal-binding proteins described to date in proteomic studies of phloem sap include metallothioneins found in *R. communis* and rice (Barnes *et al.*, 2004; Aki *et al.*, 2008), a putative Fe transporter protein (ITP) (Krüger *et al.*, 2002) and a ferredoxin found in *B. rapa* (Giavalisco *et al.*, 2006), as well as a Cu chaperone (CCS1-At1g12520.1) and several metalloproteases and Zn finger proteins found in *C. maxima* (Lin *et al.*, 2009). The presence of Cu chaperons involved in metal allocation in phloem sap of *Brassica* and *Lupin* species suggest that proteins may play a role in Cu binding and/or transport in phloem sap, whereas in the case of Zn and Fe no suitable proteins could be consistently detected and other molecules may be involved. It is worth mentioning that Fe and Zn have been recently found in rice phloem sap as Zn–NA and Fe-2′-DMA (Nishiyama *et al.*, 2012) indicating a role of these compounds in metal transport in phloem. Accordingly, enzymes involved in NA and 2′-DMA synthesis such as S-adenosylmethionine (SAM) are consistently present in phloem sap in all the species studied so far, including *L. texensis* (spot 43), indicating that sieve elements maintain the machinery for the synthesis of both NA and phytosiderophores.

The staining and chromatographic experiments revealed the presence of two low molecular weight Fe-binding proteins in phloem sap. Both Fe staining methods showed the presence of a protein species (spot 53 in Fig. 3.3.2A) with a molecular weight of 13.5 kDa and a p*I* of 5.6 in the 2-DE gels. This protein matched to an EST from white lupin roots that displays 51% homology to a protein annotated as phloem specific from *M. truncatula* (XP_003601185) (De Vleesschauwer, Chernin and Höfte, 2009). The peptide sequence, obtained by de novo sequencing, revealed a Glu-rich region similar to the one that has been suggested to be involved in Fe binding in the bacterium *Candida* albicans (Fang and Wang, 2002). On the other hand, a metallothionein-like protein type 2B was identified among the protein species present in a weakly retained band in the Fe-affinity chromatography, but it was probably not abundant enough to be identified in the 2-DE protein profile. The metallothionein-like protein identified has 75% homology at the amino acid level to one found in *R. communis* phloem sap (Barnes *et al.*, 2004), and transcripts of the corresponding gene have been detected in phloem-fed tissues such as flowers and first leaves of tomato and are strongly upregulated by heavy metals (Giritch *et al.*, 1998). Other metallothioneins have also been reported in rice phloem sap (Aki *et al.*, 2008). Metallothioneins are small cys-rich proteins able to bind metals (Cobbett and Goldsbrough, 2002). The presence of metallothioneins in the phloem sap of *L. texensis* (this study), rice (Aki *et al.*, 2008), and *R. communis* (Barnes *et al.*, 2004) suggests a possible conserved role in this fluid, which might be related not only to metal homeostasis but also to ROS scavenging and/or participation in plant developmental processes (Hassinen *et al.*, 2011). The metallothionein in this work was solely identified on the basis of the affinity chromatography wheremetal competition can occur, and was only observed in the weakly retained fraction. Therefore, further experiments will be needed to assess the metal specificity of this protein as well as to clarify its role in phloem sap. Another protein present in the same Fe-affinity chromatography band was a photosystem I iron–sulphur cluster that contains Fe and is likely to be involved in photosynthesis. There is no possible explanation for the occurrence of a putative component of photosystem I in phloem sap and its detection might be the result of a low level of contamination as discussed earlier, being subsequently enhanced by the affinity chromatography procedure.

The Zn affinity chromatographic experiment revealed the presence of four Zn-binding proteins in phloem sap. These proteins were retained with different strengths in the Zn affinity Hi-Trap column and subsequently eluted from the chromatographic system in different fractions. None of these species was abundant enough to be found in the 2-DE protein profiles. One of the bands (Zn1, Fig. 3.3.4B, Table 3.3.3) contained a protein with homology to an EST obtained from a phloem sap cDNA library (Rodriguez-Medina *et al.*, 2011). This EST contains a full open reading frame that displays high homology to members of a large family of LEA proteins, called dehydrins (DHNs), and in particular a 52% homology at the amino acid level with a DHN, the

ITP, which has been shown to bind Zn in vitro (Krüger *et al.*, 2002). The ITP previously reported in phloem sap of *R. communis* seedlings had a molecular weight of 17 kDa and a p*I* of 7.3, and authors suggested a role in phloem Fe transport (Krüger *et al.*, 2002); in vitro, ITP binds preferentially Fe(III) but no Fe(II) and also complexes Cu(II), Zn(II), and Mn(II). A DHN family protein has also been found in phloem sap from *C. maxima* (At2g44060), although it displayed low homology (20% at the amino acid level) to ITP. These findings altogether suggest that members of this family may bind Zn (Krüger *et al.*, 2002). Dehydrins play a fundamental role in plant response and adaptation to abiotic stresses, and multiple functions including chaperone, heat and cold protection, ion-binding, and ROS scavenging have been reported (Hanin *et al.*, 2011). The other identified Zn-binding proteins are all Zn finger proteins more likely involved in signaling. The RING-type Zn finger proteins ATL71 and RHA1B (Zn2 and Zn7 in Fig. 3.3.4B and Table 3.3.3) are ubiquitin-conjugating enzymes that play a regulatory role in protein degradation processes via the ubiquitin/26S proteasome pathway (Kosarev, Mayer and Hardtke, 2002; Serrano *et al.*, 2006), and the AN1-type zing finger protein, SAP 17 (bands Zn4 and Zn6 in Fig. 3.3.4B and Table 3.3.3), is involved in environmental stress responses (Vij and Tyagi, 2006). It is worth mentioning that these Zn finger proteins have also been identified in phloem sap of *C. maxima* by 2-D LC-MS/MS (Haebel and Kehr, 2001) but had not been identified in any of the 2-DE gel-based approaches so far, supporting that they are low abundance proteins, possibly involved in signaling and regulation. Iron- and Zn-binding protein species revealed by affinity chromatography are good candidates for further studies. However, our results do not allow establishing a role for them in metal trafficking, since the speciation of these two metals among protein and low molecular weight species has not been studied yet, and therefore their relative importance is still unknown. However, their presence in the phloem sap may indicate possible roles in signaling or oxidative stress defence that deserve further attention. Proteins identified other that the Zn-finger belong to two families (metallothioneins and DHNs) with ROS scavenging and metal binding properties, and therefore can function as antioxidants in two ways: first by depleting ROS from the phloem environment and second by sequestering free metals that induce ROS formation.

Acknowledgements

The study was supported by the Spanish Ministry of Science and Competitiveness (MINECO; grants AGL2009–09018, AGL2010–16515, and AGL2012–31988) and the Aragón Government (group A03). GL and SA were supported by FPI predoctoral fellowship from the MINECO. JK was supported by a MINECO grant (BIO2008–03432).

The authors have declared no conflict of interest.

Supporting Information for Chapter 3.3

All additional supporting information may be found in the online version of this article (doi: 10.1002/pmic.201200515).

- ***Figure 3.3.S1.*** *Membrane blots.*

- ***Figure 3.3.S2.*** *Polypeptides tentatively identified in phloem sap.*

- ***Figure 3.3.S3.*** *Manually analysed spectra of spot 53.*

- ***Figure 3.3.S4.*** *Traduced nucleotide sequence from the Lupinus albus EST (FG090187).*

- ***Table 3.3.S1.*** *Proteins tentatively identified in 2-DE IEF-SDS-PAGE gels.*

- ***Table 3.3.S2.*** *Table of BLAST results from proteins identified in phloem sap.*

- ***Table 3.3.S3.*** *Comparison of non-redundant Arabidopsis phloem proteins from Lupinus texensis with those from other plant species. The non-redundant Arabidopsis proteomes from pumpkin, rape and rice were obtained from Ref. [Lin et al,2009], and those of L. texensis by BLAST searches against the Arabidopsis database.* This Table is not included here due to the size of the file; the online version is at doi: 10.1002/pmic.201200515

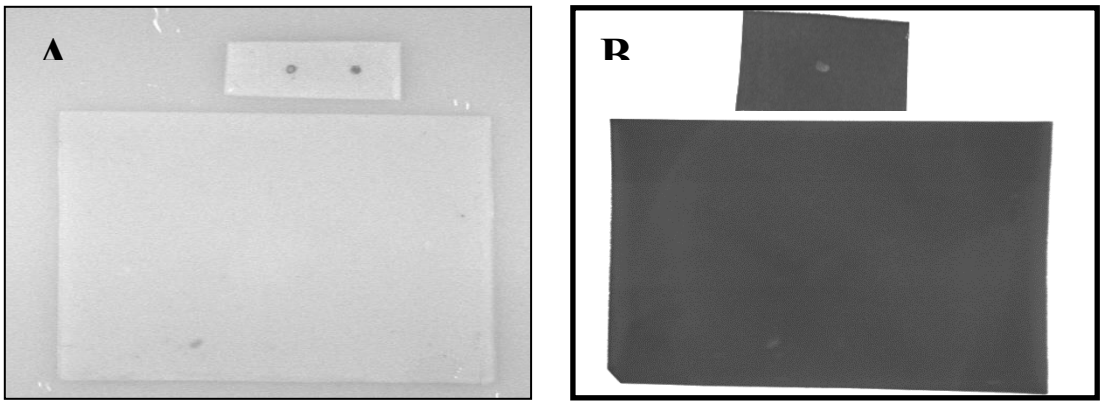

Figure 3.3.S1. *Membrane blots from gels loaded with myoglobin as standard, stained with Ferene (A) and a second method based on redox properties (B).*

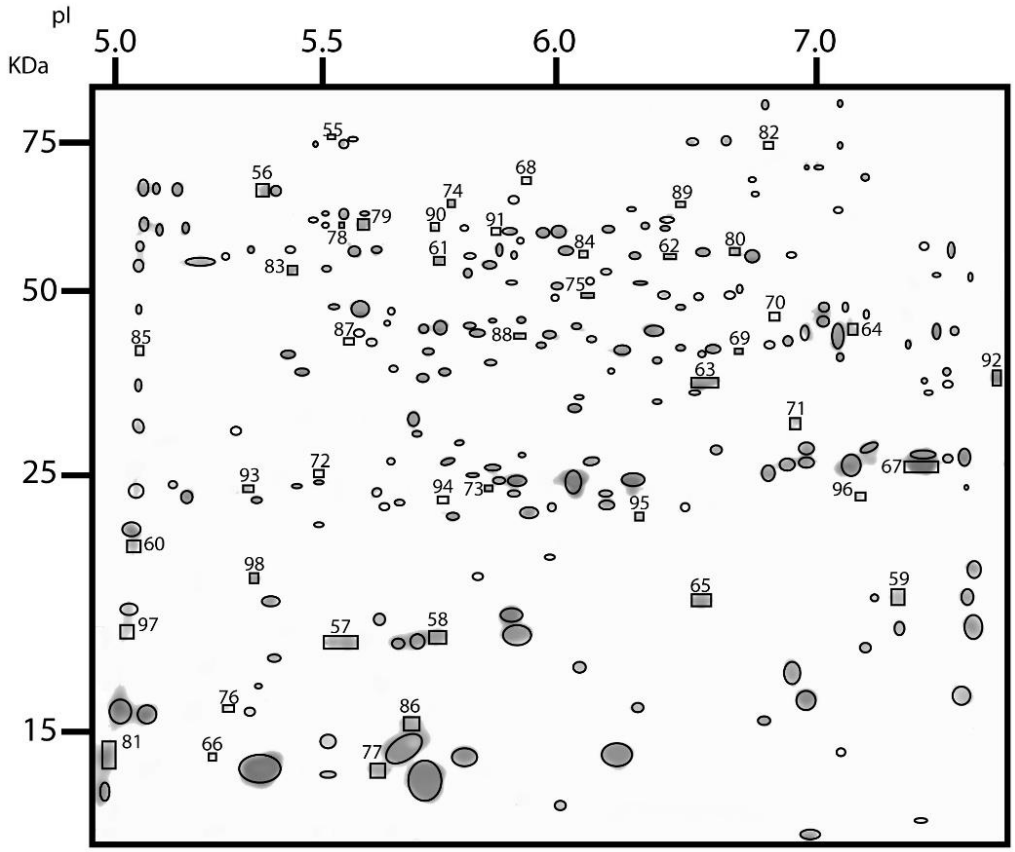

Figure 3.3.S2. *Polypeptides tentatively identified in phloem sap from Lupinus texensis. Polypeptides with only positive MASCOT scores are squared and numbered as in Supporting Information Table 3.3.S1.*

Figure 3.3.S3. *Manually analysed spectra of spot 53.*

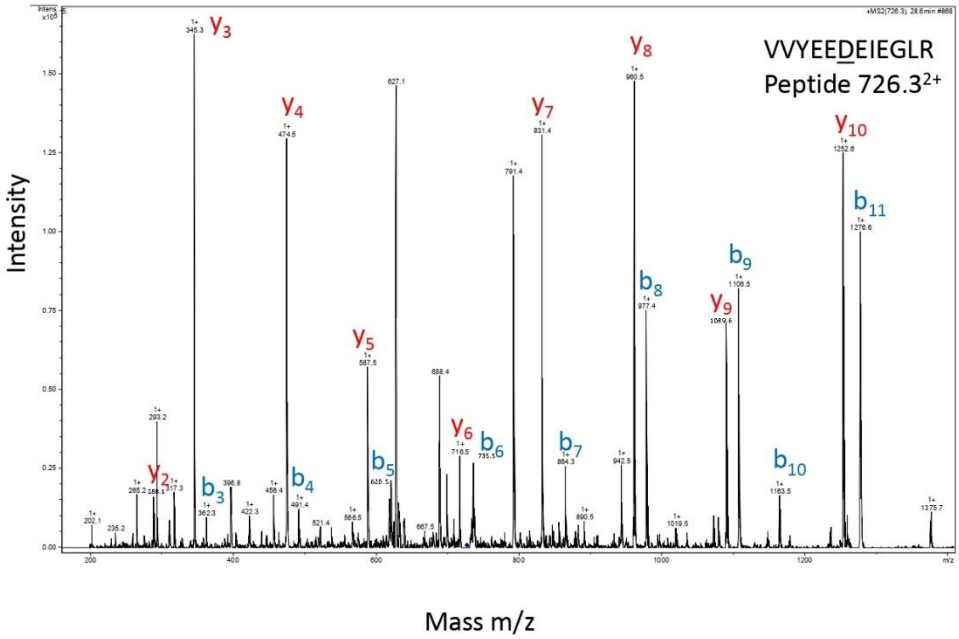

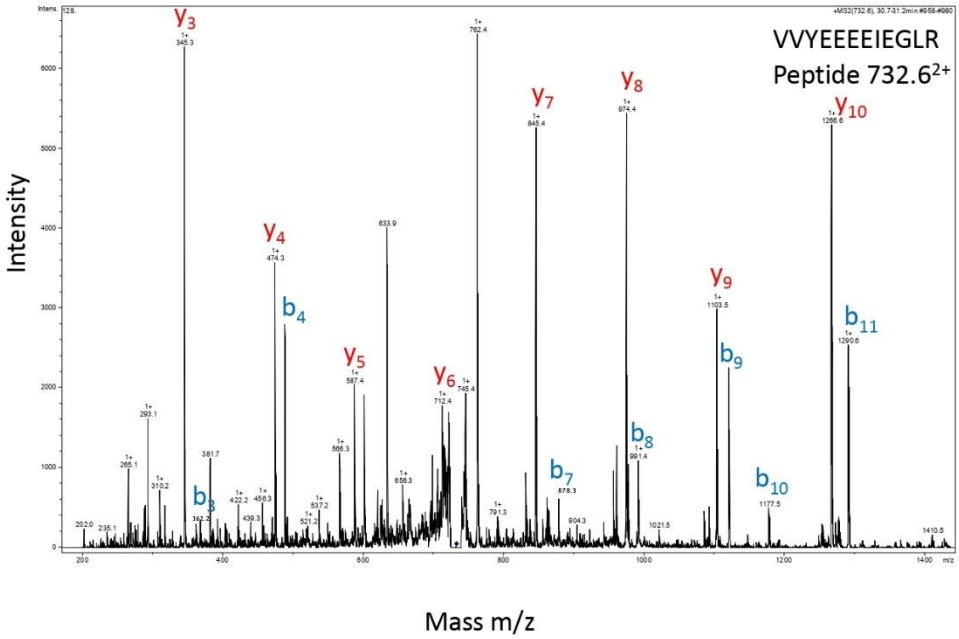

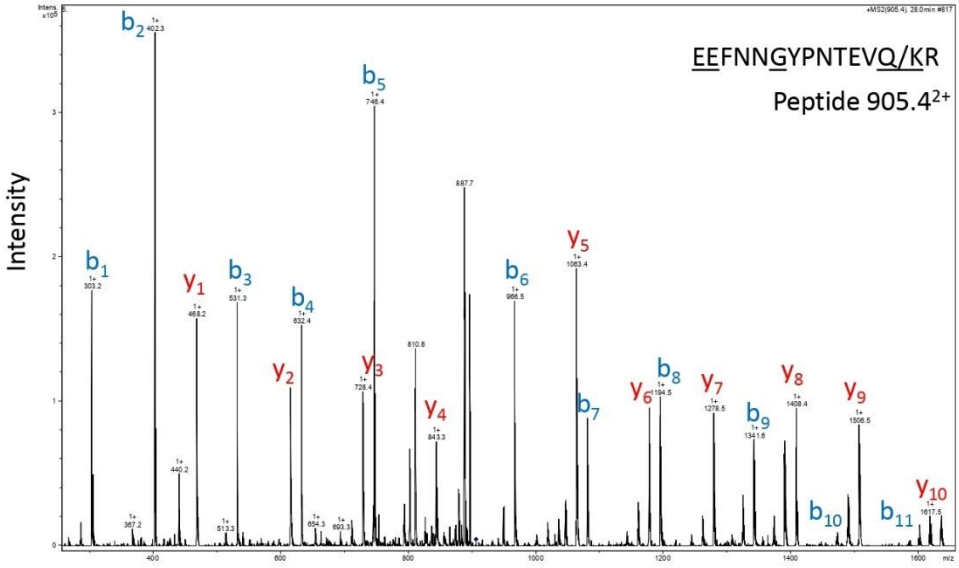
EEFNNGYPNTEVQ/KR
Peptide 905.4^{2+}
Intensity
Mass m/z

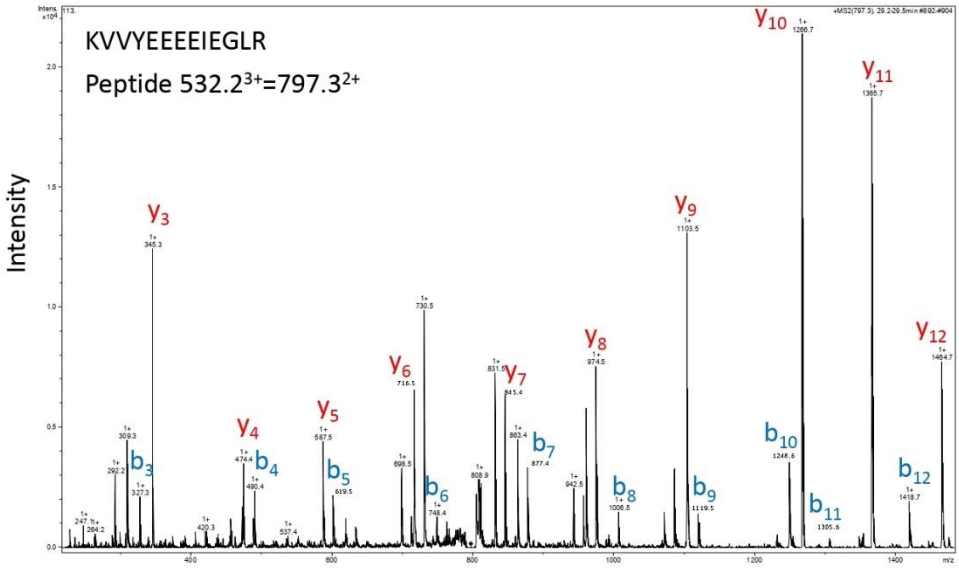
KVVYEEEEIEGLR
Peptide 532.2^{3+}=797.3^{2+}
Intensity
Mass m/z

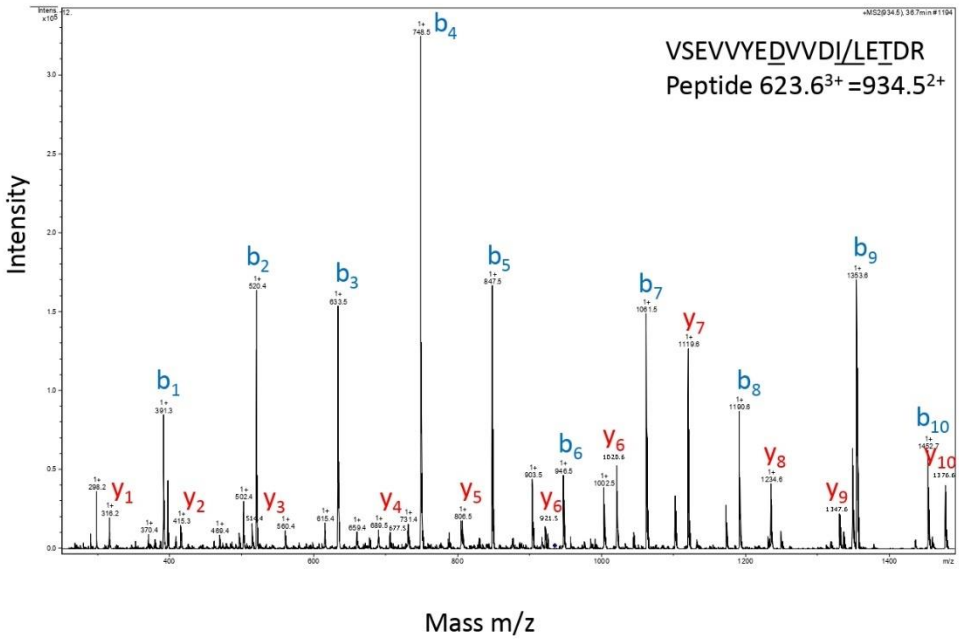
VSEVVYEDVVDI/LETDR
Peptide 623.6^{3+} =934.5^{2+}
Intensity
Mass m/z
b1
b2
b3
b4
b5
b6
b7
b8
b9
b10
y1
y2
y3
y4
y5
y6
y7
y8
y9
y10

Figure 3.3.S4. *Traduced nucleotide sequence from the Lupinus albus EST (FG090187) with deduced peptide sequences obtained with the de novo sequencing approach shown in bold (red for Mascot-assigned and black for manually assigned peptides).*

5'3' Frame 2:

```
ggggatacttgtgcatctatatttgtgaccatatccaacactacaactagaagcaataatg
  G   I   L   V   H   L   Y   L   -   P   Y   P   T   L   Q   L   E   A   I   M
gcccatttcagacctagctacaacactgaagttcacaggacttccactgtctacgatgat
 A   H   F   R   P   S   Y   N   T   E   V   H   R   T   S   T   V   Y   D   D
 E   E   F   N   N   G   Y   N   T   E   V  Q/K  R
gtttctcaatacccaaatggtcacttgaccaagaaggttgtctatgaggaggaagagatc
 V   S   Q   Y   P   N   G   H   L   T   K   K   V   V   Y   E   E   E   E   I
                                             V   V   Y   E   E   E   E   I
                                         K   V   V   Y   E   E   E   E   I
                                             V   V   Y   E   E   E   E   I
                                             V   V   Y   E   E   D   E   I
gaagggttgcgccgccacaaccaccgccaccacaaccccgaggttcgtgagagggttgaa
 E   G   L   R   R   H   N   H   R   H   H   N   P   E   V   R   E   R   V   E
 E   G   L   R
 E   G   L   R
 E   G   L   R
 E   G   L   R
gttatagaatatgagcaagtgcctgagtataacaatagggttagtgaagttgtgtatgaa
 V   I   E   Y   E   Q   V   P   E   Y   N   N   R   V   S   E   V   V   Y   E
                                             V   S   E   V   V   Y   E
gaaaatgttgtggatgttgaaagtgatcgatactaccctcgaaggaacaagggttgcatc
 E   N   V   V   D   V   E   S   D   R   Y   Y   P   R   R   N   K   G   C   I
 -   D   V   V   D  I/L  E   T   D   R   Y   Y   P   R   R   N   K   G   C   I

ttcaggaactaagatttgttgttatgtggctaatttgctaggcagaggtaccttaataat
 F   R   N   -   D   L   L   L   C   G   -   F   A   R   Q   R   Y   L   N   N
attatcaaaatcgctactgtgtggttgtaataaataaattcctgctaagcatgcagtcat
 I   I   K   I   A   T   V   W   L   -   -   I   N   S   C   -   A   C   S   H
tgtgttatcttatgttgaatattaataaataaagcttacttgtctaaaatgtatct
 C   V   I   L   C   -   I   L   I   N   K   A   Y   L   S   K   M   Y
```

Table 3.3.S1. *Proteins tentatively identified in 2-DE IEF-SDS-PAGE gels (see Supporting information Fig. 3.3.S2). Protein score is –10*Log (P), where P is the probability that the observed match is a random event. Homology identification was retained with a probability set at 95%. Function was inferred from GO biological process annotation.*

Spot	Protein	Specie	ID	Score/pep/ion	% Cv	Mw/pI th	Mw/pI exp	Function	GO (BP)
55	Cyclophilin	*Lupinus luteus*	gi|6014890	73/1/1	6	18.5/8.7	73.0/5.4	Protein folding	GO:0006457
56	70 kDa Heat shock cognate protein 3	*Vigna radiata*	gi|45331285	75/1/1	2	71.9/5.1	64.0/5.3	Protein folding	GO:0006457
57	Eukaryotic translation initiation factor 5A-2	*Solanum lycopersicum*	AAG53648.1.	49/1/1	6	17.7/5.8	17.0/5.5	Protein biosynthesis	GO:0006412
58	Eukaryotic translation initiation factor 5A-2	*Solanum lycopersicum*	AAG53648.1.	44/1/1	6	17.7/5.8	17.0/5.7	Protein biosynthesis	GO:0006412
59	Eukaryotic translation initiation factor 5A-1	*Arabidopsis thaliana*	Q9XI91	42/1/1	12	18.0/7.3	17.5/5.4	Protein biosynthesis	
60	Ubiquitin conjugating enzyme	*Solanum lycopersicum*	gi|886679	43/1/1	6	21.5/5.0	21.8/5.0	Ubiquitin-dependent proteolysis	GO:0006511
61	UDP-glucose pyrophosphorylase	*Amorpha fruticosa*	gi|17026394	54/1/1	3	51.7/6.1	51.0/5.7	Callose deposition in cell wall-pollen development	GO:0052543-GO:0009555
62	UDP-glucose 6-dehydrogenase	*Glycine max*	gi|255648377	80/1/1	2	53.8/6.6	52.4/6.3	Cell wall pectin metabolic process	GO:0052546
63	Isoflavone reductase homolog 2	*Glycine max*	gi|6573171	50/1/1	3	33.9/5.6	33.1/6.4	Lignin biosynthetic process	GO:0009807
64	Acetyl-CoA C-acyltransferase	*Arabidopsis thaliana*	gi|15238793	80/1/1	2	43.7/6.0	39.0/7.1	Isoprenoid biosynthetic process	GO:0008299
65	Cytochrome P450	*Ricinus communis*	gi|255538634	45/1/1	1	71.5/6.6	19.0/6.4	Terpene biosynthetic process	GO:0046246

66	Kaurene synthase	*Salvia miltiorrhiza*	C8XPS0	46/4/3	4	69.0/5.8	13.3/5.2	Terpene biosynthetic process	GO:0046246
67	Probable 6-phosphogluconolactonase 4	*Oryza sativa*	gi|148839656	86/1/1	4	34.5/8.5	25.0/7.4	Pentose-phosphate shunt	GO:0006098
68	Phosphoglucomutase	*Pisum sativum*	gi|12585296	58/1/1	2	63.5/5.5	65.0/5.9	Carbohydrate metabolic process	GO:0005975
69	Putative deoxyuridine triphosphatase	*Oryza sativa*	gi|31126720	44/1/1	4	23.5/8.9	37.0/6.6	dUTP metabolic process	GO:0046080
70	Aspartate aminotransferase	*Lotus corniculatus*	gi|2605932	82/1/1	6	50.2/8.9	43.2/6.8	Amino acid metabolic process	GO:0006520
71	3,5-Epimerase/4-reductase	*Brassica napus*	DY000819	82/1/1	6	19.4/5.7	29.5/6.8	Metabolic process	GO:0008152
72	Dienelactone hydrolase family protein	*Arabidopsis thaliana*	gi|15225693	77/1/1	5	26.0/5.3	24.8/5.4	Metabolic process	GO:0008152
73	Triosphosphate isomerase-like protein type I	*Gossypium hirsutum*	JG451367	72/1/1	7	18.5/7.9	24.0/5.8	Metabolic process	GO:0008152
74	V-type proton ATPase catalytic subunit A	*Daucus carota*	gi|137460	74/1/1	2	69.1/5.3	61.0/5.7	ATP biosynthetic process	GO:0006754
75	Monodehydroascorbate reductase	*Vaccinium corymbosum*	gi|163960967	74/1/1	2	47.6/5.8	47.8/6.0	Cell redox homeostasis	GO:0045454
76	CA900372 (glutaredoxin)	*Phaseolus coccineus*	CA900372	69/1/1	4	25.8/10.0	13.9/5.2	Cell redox homeostasis	GO:0045454
77	Thioredoxin	Ricinus communis	gi|1255954	53/1/1	8	13.0/5.6	13.0/5.6	Cell redox homeostasis	GO:0045454

78	Rubisco large subunit-binding protein subunit β	*Brassica napus (rape)*	gi|134104	105/1/1	6	62.8/6.6	57.5/5.5	Photosynthesis	GO:0015979
79	Rubisco large subunit-binding protein subunit β	*Brassica napus*	gi|134104	86/1/1	2	62.8/6.6	57.5/5.5	Photosynthesis	GO:0015979
80	Rubisco large chain	*Lupinus atlanticus*	CAA93928.1	68/1/1	2	50.7/6.2	52.5/6.6	Photosynthesis	GO:0015979
81	Profilin-2	*Zea mays*	gi|548597	70/1/1	9	14.2/4.9	13.3/4.9	Actin cytoskeleton organization	GO:0030036
82	GTP-binding nuclear protein Ran1	*Arabidopsis thaliana*	gi|585777	53/1/1	6	23.3/6.7	72.0/6.7	Signal transduction	GO:0007264
83	Retrotransposon protein, putative, Ty3-gypsy subclass	*Oryza sativa*	gi|77557117	54/1/1	6	15.8/8.9	50.0/5.4	DNA integration	GO:0015074
84	Retrotransposon protein, putative, Ty3-gypsy sub-class	*Oryza sativa*	gi|62733821	44/1/1	0	133.9/8.8	52.5/6.0	DNA integration	GO:0015074
85	Late embryogenesis abundant family protein	*Arabidopsis thaliana*	gi|205830697	54/1/1	4	36.2/4.7	37.0/5.0	Plant defense	GO:0006952
86	Sulfate transporter 1.1	*Arabidopsis thaliana*	BAA33932.1	33/2/1	3	70.9/9.1	13.6/5.6	Sulfate transport	GO:0008272
87	Os10g0125700	*Oryza sativa*	gi|115480968	54/1/1	0	161.8/8.2	37.05/5.5	Unknown	
88	Hypothetical protein	*Oryza sativa*	gi|57899114	44/1/1	4	17.8/11.6	38.2/5.9	Unknown	
89	Predicted protein	*Populus trichocarpa*	gi|224061597	44/1/1	0	192.9/6.0	61.5/6.4	Unknown	
90	Predicted protein	*Populus trichocarpa*	gi|224107891	43/1/1	1	124.1/6.2	57.5/5.7	Unknown	

91	Unknown	*Picea sitchensis*	gi|116789697	50/1/1	1	66.2/7.6	56.0/5.8	Unknown
92	FP032579	*Quercus robur*	FP032579	69/1/1	3	24.9/12.2	34.0/7.8	Unknown
93	Unknown	*Glycine max*	gi|255635264	72/1/1	4	24.8/5.7	24.0/5.3	Unknown
94	Predicted protein	*Micromonas sp. RCC299*	gi|255081546	51/3/3	1	269.4/5.0	23.1/5.7	Unknown
95	Putative uncharacterized protein	*Arabidopsis thaliana*	gi|3269288	54/1/1	7	22.4/6.3	22.9/6.2	Unknown
96	Hypothetical protein	*Arabidopsis lyrata*	gi|297845252	41/1/1	1	100.7/5.8	23.9/7.2	Unknown
97	Predicted protein	*Populus trichocarpa*	gi|224103499	44/1/1	1	76.6/6.0	17.5/5.0	Unknown
98	Hypothetical protein VITISV_019389	*Vitis vinifera*	gi|147843231	41/1/1	0	89.1/8.2	20.5/5.3	Unknown

Table 3.3.S2. *Table of BLAST results from proteins identified in phloem sap from L. texensis (unequivocally identified -in regular typeface- and tentatively assigned -in italics- in Tables 3.3.1 and 3.3.2, respectively; see Fig. 3.3.2A and Supporting information Fig. 3.3.S2, respectively) and L. albus (Ref. Rodriguez-Medina et al, 2011). BLAST search was performed in the NCBI website (http://blast.ncbi.nlm.nih.gov/Blast.cgi) against the Arabidopsis database (taxid:3701) on January 2013. When multiple accession numbers existed, NCBI annotations are given from the first meaningful annotation. BLAST annotations when assigned as not hit when BLAST E-values were higher than 1e-30.*

L. texensis (spot numbers as in Tables 3.3.1 and 3.3.2)				
spot	**Protein**	**ATG**	**At annotation**	**E blast**
1	HSP 70	AT5G42020	Hsc70-1	0.00e+00
2	HSP 70	AT5G02500	HSC70-1	2.00e-129
3	Groes chaperonin, putative	AT5G20720	Chaperonin 20	3.00e-112
4	Initiation factor eIF-A5	AT1G13950	Translation initiation factor eIF-5A	3.0e-96
5	Initiation factor eIF-5A2	AT1G13950	Translation initiation factor eIF-5A	1e-98
6	Eukaryotic initiation factor 5A-1	AT1G13950	Translation initiation factor eIF-5A	3.00e-100
7	Eukaryotic initiation factor 5A-5	AT1G13950	Translation initiation factor eIF-5A	2.00e-100
8	Ubiquitin-like protein	AT4G26840		
9	Ubiquitin-conjugating enzyme	AT1G78870		
10	Cysteine proteinase inhibitor	AT3G12490	Cysteine proteinase inhibitor 6	7.00e-41
11	Cysteine proteinase inhibitor	AT3G12490	Cysteine proteinase inhibitor 6	6.00e-43
12	Cysteine proteinase inhibitor	AT3G12490	Cysteine proteinase inhibitor 6	4.00e-43
13	Actin	AT5G09810	Actin 7	0.00E+00
14	Actin	AT3G12110	Actin11	0.00E+00
15	Actin depolymerizing factor 2 (ADF2)	AT3G46000	Actin depolymerizing factor 2	3.00e-92
16	Actin-depolymerizing factor 1	AT3G46010	Actin depolymerizing factor 1	7.00e-88
17	Rubisco small chain	AT1G67090	Rubisco small chain	3e-94
18	Rubisco small chain	AT1G67090	Rubisco small chain	3e-94
19	Rubisco small chain	AT1G67090	Rubisco small chain	3e-94
20	Rubisco large chain	ATCg00490	RbcL	0.00e+00
21	L-Ascorbate peroxidase	AT3G09640		

22	Glutathione peroxidase 1	AT4G11600	Glutathione peroxidase 6	8.00e-96
23	Thioredoxin	AT3G51030	Thioredoxin H1	4.00e-68
24	Thioredoxin H	AT3G51030	Thioredoxin H1	1.00e-57
25	Thioredoxin H	AT3G51030	Thioredoxin H1	7.0×10-55
26	LEA-2 protein	AT1G01470	LEA 14	1.00e-61
27	PR10.2C protein	AT1G24020	MLP-Like protein 423	9.00e-06
28	Putative LRR disease resistance protein	AT2G01210	Leucine-rich repeat transmembrane protein kinase-like protein	1.70e-01
29	Enoyl-ACP reductase	AT2G05990	Enoyl-ACP-reductase 1	0.00e+00
30	Enoyl-ACP reductase	AT2G05990	Enoyl-ACP-reductase 1	0.00e+00
31	Cytosolic phosphoglycerate kinase	AT1G79550	Phosphoglycerate kinase	0.00e+00
32	Fructose-bisphosphate aldolase	AT3G52930	Fructose-bisphosphate aldolase, classI	0.00e+00
33	Malate dehydrogenase	AT5G43330	Malate dehydrogenase	0.00e+00
34	Cytosolic malate dehydrogenase	AT5G43330	Malate dehydrogenase	3.00e-118
35	Probable 6-phosphogluconolactonase 4	AT5G24400	6-Phosphoglucolactonase 3	1.00e-121
36	Cell division cycle protein 48 homolog	AT5G03340	Cell division control protein 48	0.00e+00
37	Cell division cycle protein 48 homolog	AT5G03340	Cell division control protein 48	0.00e+00
38	Copper chaperone homolog CCH	AT3G56240	CCH	2.00e-34
39	d-3-Phosphoglycerate dehydrogenase, putative	AT4G34200	EDA9	0.00e+00
40	Uridylate kinase	AT5G26667	PYR6	1.00e-116
41	Histone H3 methyltransferase complex	AT1G51450	TRAUCO protein	2.00e-64
42	Maturase	ArthCp003	matK	2.00e-29
43	S-Adenosylmethionine synthetase	AT1G02500		
44	Lactoylglutathione lyase	AT1G11840	Gactoylglutathione lyase-like protein	6.00e-175

45	Ran-related GTP binding protein	AT5G55190	GTP-binding nuclear protein Ran-3	3.00e-118
46	Predicted protein	AT4G24280	cpHsc70-1	0.00e+00
47	Hypothetical protein	AT1G51350	Armadillo/beta-catenin-like repeats-containing protein	0.00e+00
48	Hypothetical protein VITISV_013453	-	Retroelement pol polyprotein-like	2.00e-88
49	Hypothetical protein	-		
50	Hypothetical protein	-	Putative retrotransposon polyprotein	3.00e-40
51	Conserved hypotetical protein	No hit		
52	FL852282	No hit		
53	FG090187	No hit		
54	Hypothetical protein VITISV_015790	-	Hypothetical protein	6.50e-32
55	Cyclophilin	AT2G16600	Peptidyl-prolyl cis-trans isomerase CYP19-1	6.00e-109
56	70 kDa Heat shock cognate protein 3	AT5G02500	Heat shock 70 kDa protein 1/8	0.00e+00
57	Eukaryotic translation initiation factor 5A-2	AT1G13950	Translation initiation factor eIF-5A	2.00e-99
58	Eukaryotic translation initiation factor 5A-2	AT1G13950	Translation initiation factor eIF-5A	2.00e-99
59	Eukaryotic translation initiation factor 5A-1	AT1G13950		
60	Ubiquitin conjugating enzyme	AT5G50870	Ubiquitin-conjugating enzyme E2 27	1.00e-102
61	UDP-Glucose pyrophosphorylase	AT5G17310	UTP--glucose-1-phosphate uridylyltransferase 1	0.00e+00
62	UDP-Glucose 6-dehydrogenase	AT3G29360	Putative UDP-glucose 6-dehydrogenase 1	0.00e+00
63	Isoflavone reductase homolog 2	AT4G39230	NmrA-like negative transcriptional regulator family protein	2.00e-174
64	Acetyl-CoA C-acyltransferase	AT5G47720	Acetoacetyl-CoA thiolase	
65	Cytochrome P450	AT1G75200	tRNA wybutosine-synthesizing protein 1-like protein	0.00e+00

66	Kaurene synthase	At1g79460	Ent-kaur-16-ene synthase	2.0×e-91
67	6-Phosphogluconolactonase 4, putative	AT5G24400	6-Phosphogluconolactonase	8.00e-121
68	Phosphoglucomutase	AT1G09780	Putative phosphoglucomutase	0.00e+00
69	Putative deoxyuridine triphosphatase	AT3G46940	dUTP pyrophosphatase	2.00e-71
70	Aspartate aminotransferase	AT4G31990	Aspartate aminotransferase	0.00e+00
71	3,5-Epimerase/4-reductase	AT1G63000	3,5-Epimerase/4-reductase	2.00e-116
72	Dienelactone hydrolase family protein	AT2G32520		
73	Triosphosphate isomerase-like type I	AT3G55440	Triosephosphate isomerase	2.00e-74
74	V-type proton ATPase catalytic subunit A	AT1G78900	V-type proton ATPase catalytic subunit A	0.00e+00
75	Monodehydroascorbate reductase	AT3G52880	Monodehydroascorbate reductase (NADH)	0.00e+00
76	Glutaredoxin	AT1G77370	Glutaredoxin-C3	2.00e-13
77	Thioredoxin	AT3G51030	Thioredoxin H1	4.00e-68
78	Rubisco large subunit-binding protein subunit β	AT1G55490	Rubisco large subunit-binding protein subunit beta	0.00e+00
79	Rubisco large subunit-binding protein subunit β	AT1G55490	Rubisco large subunit-binding protein subunit beta	0.00e+00
80	Rubisco large chain	ArthCp030	Rubisco large subunit-binding protein subunit beta	0.00e+00
81	Profilin-2	AT2G19760	Profilin 4	3.00e-64
82	GTP-Binding nuclear protein Ran1	AT5G55190		
83	Retrotransposon, putative, Ty3-gypsy subclass	AT1G35180	TRAM, LAG1 and CLN8 (TLC) lipid-sensing domain containing protein	2.80E+00
84	Retrotransposon, putative, Ty3-gypsy subclass	-	Putative retroelement pol polyprotein	7.00e-56
85	LEA family protein	AT4G21230	Cysteine-rich receptor-like protein kinase 27	5.1
86	Sulfate transporter 1.1	AT4G08620		

87	Os10g0125700	AT3G14460	LRR and NB-ARC domain-containing disease resistance protein	2.00e-65
88	Hypothetical protein	No hit		
89	Predicted protein	AT2G34780	Maternal effect embryo arrest 22	1.00e-110
90	Predicted protein	AT1G04300	MATH domain-containing protein	0.00e+00
91	Unknown	AT4G34200	D-3-phosphoglycerate dehydrogenase	0.00e+00
92	FP032579	No hit		
93	Unknown	AT3G48330	Protein-L-isoaspartate O-methyltransferase	1.00e-124
94	Predicted protein	No hit		
95	Predicted protein	AT4G27270	Quinone reductase family protein	
96	Hypothetical protein	AT1G22275	Synaptonemal complex protein 2	0.00e+00
97	Predicted protein	AT2G15880	Pollen-specific leucine-rich repeat extensin-like protein 3	0.00e+00
98	Hypothetical protein	AT2G28780	Hypothetical protein	0.00e+00
L. albus (spot numbers as in Ref. (Lin *et al.*, 2009)				
20,36	CAA93923	ArthCp030	RuBisCO large subunit-binding protein subunit beta	0.00e+00
40,41,42,44,70,71,72	ACL14491	AT1G02500	S-adenosylmethionine synthetase	0.00e+00
59	CAD31714	AT1G06030	PfkB-like carbohydrate kinase family protein	1.0e-143
126	ABQ41909	AT1G06680	OE23	1.0e-115
7	ACJ76774	AT1G13950	Eukaryotic translation initiation factor 5A (EIF-5A).	8.0e-99
95	Q0FZ48	AT1G16890	Ubiquitin conjugating enzyme 13b	1.0e-107
61,62	AAA87182	AT1G23740	Alkenal/one oxidoreductase	1.0e-143
21,22	BAB63949	AT1G24020	MLP-like protein 423	9.00e-06
124	XP_002281279	AT1G48630	Receptor for C kinase 1B	0.00e+00

86	NP_001046972	AT1G56070	Translation elongation factor 2-like	0.00e+00
28	BAJ33494	AT1G65480	Flowering locus, TFL1	8.0e-81
117,129	AAL71857	AT1G75270	Dehydroascorbate reductase 2	1.0e-115
100,101,102,103	O49886	AT2G16600	Cytosolic cyclophilin ROC3	1.0e+108
32	ABG88188	AT2G19770	Profilin 5	1.0e-73
84	AAM64779	AT2G21250	NAD(P)-linked oxidoreductase	0.00e+00
24,26,27	BAF34340	AT2G21660	Small glycine-rich RNA binding protein	4.0e-77
2,53,82	FG089946	AT2G26860	FBD, F-box and Leucine Rich Repeat domains containing protein	2.9
75	NP_001118453	AT2G36460	Aldolase superfamily protein	0.00e+00
35,39	CAB75428	AT2G36530	Enolase 2	0.00e+00
123	XP_002529872	AT2G37770	NADPH-dependent aldo-keto reductase 4-C9	1.0e-168
31	CAA80333	AT2G47110	Ubiquitin extension protein 6	1.0e-104
37,38,76,77,115	CAI83772	AT3G04120	Cytosolic GADPH-1	1.0e-172
74	O04300	AT3G08900	UDP-arabinose mutase 3	0.00e+00
48	ABR18607	AT3G09640	Ascorbate peroxidase 2	1.0e-151
1	Q06445	AT3G12490	Cystatin b	1.0e-41
29,96,121	ABC49719	AT3G46010	Actin-depolymerizing factor-1	4.0e-80
114	BAB40967	AT3G46440	UDP-glucuronic acid decarboxylase like	0.00e+00
33,55,108,109	CAC36986	AT3G51030	Thioredoxin H type I	2.0e-57
97	NP_566968	AT3G52560	Ubiquitin E2- 1D	0.00e+00
73	ABQ41114	AT3G52880	Monodehydroascorbate reductase 1	0.00e+00
47,66,68	ABA86966	AT3G55440	Cytosolic triose phosphate isomerase	1.0e-148

122	NP_191835	AT3G62760	Glutathione transferase	0.00e+00
94	CA410618	AT4G09320	Nucleoside diphosphate kinase 1	6.0e-89
3	AAP69867	AT4G11600	Glutathione peroxidase 6	4.0e-97
65	ABW34717	AT4G14710	Acireductone dioxygenase	1.0e-127
14,15	ACU19092	AT4G39230	Phenylcoumaran benzylic ether reductase-like	1.0e-160
63,64	BAC81649	AT5G02790	Glutathione transferase L3	1.0e-95
56,57	XP_002531678	AT5G03300	Adenosine kinase 2	0.00e+00
46	AAD03741	AT5G09810	Actin 7	0.00e+00
106	AAM65904	AT5G13120	Cyclophilin 20-2	0.00e+00
81	ABA81861	AT5G15650	UDP-arabinose mutase	0.00e+00
43,45	O64459	AT5G17310	UDP-glucose pyrophosphorylase 2	0.00e+00
51	AAQ08403	AT5G17920	Methionine synthase	0.00e+00
83	AAX86047	AT5G19780	Tubulin α5	0.00e+00
120	CAA76203	AT5G24090	Chitinase A (class III)	1.0e-118
12	AAG24884	AT5G38410	Rubisco small subunit 3B	1.0e-101
60	XP_002510414	AT5G42790	Proteasome α F1	1.0e-158
34,85	AAO15574	AT5G43330	Cytosolic malate dehydrogenase	0.00e+00
80	ABK23804	AT5G57330	Galactose mutarotase-like	1.0e-110
4	CA410380	No hit		
128	CA409832	No hit		

3.4. Effects of Fe deficiency on the protein profiles and lignin composition of stem tissues from Medicago truncatula in absence or presence of calcium carbonate

Jorge Rodríguez-Celma[1], Giuseppe Lattanzio[1], Dido Villarroya[1], Elain Gutierrez-Carbonell[1], Laura Ceballos-Laita[1], Jorge Rencoret[2], Ana Gutiérrez[2], José C. del Río[2], Michael A. Grusak[3], Anunciación Abadía[1], Javier Abadía[1] and Ana-Flor López-Millán[1]

[1]Plant Nutrition Department, Aula Dei Experimental Station (CSIC), P.O. Box 13034, E-50080, Zaragoza, Spain

2Instituto de Recursos Naturales y Agrobiología de Sevilla (CSIC), Reina Mercedes 10, E-41012 Sevilla, Spain

[3]USDA-ARS Children's Nutrition Research Center, Department of Pediatrics, Baylor College of Medicine, 1100 Bates Street, Houston, TX 77030, USA

Published in the Journal of Proteomics (2016) 140, 1-12 (doi: 10.1016/j.jprot.2016.03.017).

Additional supporting information may be found in the online version of this article at the publisher's web-site.

SUMMARY

Iron deficiency is a yield-limiting factor with major implications for crop production, especially in soils with high $CaCO_3$. Because stems are essential for the delivery of nutrients to the shoots, the aim of this work was to study the effects of Fe deficiency on the stem proteome of *Medicago truncatula*. Two-dimensional electrophoresis separation of stem protein extracts resolved 276 consistent spots in the whole experiment. Iron deficiency in absence or presence of $CaCO_3$ caused significant changes in relative abundance in 10 and 31 spots, respectively, and 80% of them were identified by mass spectrometry. Overall results indicate that Fe deficiency by itself has a mild effect on the stem proteome, whereas Fe deficiency in the presence of $CaCO_3$ has a stronger impact and causes changes in a larger number of proteins, including increases in stress and protein metabolism related proteins not observed in the absence of $CaCO_3$. Both treatments resulted in increases in cell wall related proteins, which were more intense in the presence of $CaCO_3$. The increases induced by Fe-deficiency in the lignin per protein ratio and changes in the lignin monomer composition, assessed by pyrolysis-gas chromatography–mass spectrometry and microscopy, respectively, further support the existence of cell wall alterations.

3.4.1. Introduction

Many environmental conditions, including the high pH of calcareous soils, can result in scarce Fe availability in farmlands, resulting in Fe-deficiency chlorosis and marked reductions in agricultural produce yield and quality (Mengel, 1994; Álvarez-Fernández *et al.*, 2003; Abadía *et al.*, 2011). Iron deficiency associated with soils rich in $CaCO_3$ is a major constraint for yield in economically relevant crops such as soybean grown in the upper Midwest areas of the U.S (Froechlich and Fehr, 1981; Coulombe, Chaney and Wiebold, 1984; Lin, Cianzio and Shoemaker, 1997) and fruit tree crops in Mediterranean climate areas (Barton and Abadia, 2006; Álvarez-Fernández *et al.*, 2011). When facing low soil Fe availability, plants respond by inducing root morphological and physiological changes aimed to increase the Fe uptake capacity, which vary depending on the taxonomical group (Römheld, 1987). Efforts have been devoted to deciphering this complex network in plants at the transcriptomic, proteomic and metabolomic levels (Rellán-Álvarez, Andaluz, *et al.*, 2010; Lan *et al.*, 2011; Rellán-Álvarez *et al.*, 2011; Schmidt and Buckhout, 2011; Hindt and Guerinot, 2012; López-Millán *et al.*, 2013b; Rodríguez-Celma, Lin, *et al.*, 2013). In dicotyledonous plants, root responses include an induction of the Fe-reduction based uptake machinery (Eide *et al.*, 1996; Robinson *et al.*, 1999), an enhanced proton extrusion capacity (Santi and Schmidt, 2009), the excretion of organic compounds including carboxylates, phenolics and flavins (Cesco *et al.*, 2010; Jorge Rodríguez-Celma, Vázquez-Reina, *et al.*, 2011; Rodríguez-Celma, Lin, *et al.*, 2013; Fourcroy *et al.*, 2014; Schmid *et al.*, 2014), and a reprogramming of general metabolic pathways such as the tricarboxylic acid cycle (TCA) and glycolysis to fuel the high energy requirements for Fe uptake (G. Zocchi, 2006; López-Millán *et al.*, 2009). Being an essential micronutrient, Fe must be translocated to the shoots, where it plays important roles in respiration and chlorophyll synthesis among others (Martin and H. Marschner, 1988). In the xylem pathway, complexation with citrate plays a determinant role (Durrett, Gassmann and Rogers, 2007; Rellán-Álvarez, Giner-Martínez-Sierra, *et al.*, 2010; Roschzttardtz *et al.*, 2011).

The effects of Fe deficiency are not restricted to roots and leaves, and low soil Fe availability also results in plants with reduced stem length and mass (Vasconcelos and Grusak, 2014). Plant stems provide mechanical support to the plant and are essential for the delivery of water and nutrients (e.g., minerals, sugars and amino acids) to the various plant organs (Lucas *et al.*, 2013). In addition, the vascular systems within the stem act as long distance communication channels between roots and shoots, in which hormones, micro-RNAs, peptides and proteins act as signalling molecules (Hossain and Komatsu, 2013). The dual role of these systems, including delivery of nutrients as well as signalling, makes stems crucial for the coordination of responses

to nutritional stresses at the whole plant level. However, very little information is available to date about the effects of Fe deficiency in stem tissues.

Proteomic profiling using 2-DE is an excellent tool to provide a holistic picture of changes induced by nutritional stresses (Jorrín-Novo *et al.*, 2009; Hossain and Komatsu, 2013; Liang, Tian and Liao, 2013). Indeed, changes in the protein profiles in response to Fe deficiency have already been studied in different plant tissues, mainly roots and thylakoids, using model plant species such as barrel medic (*Medicago truncatula*) (López-Millán *et al.*, 2013b). This plant species has a small diploid genome that yields manageable genetic tools, it is autogamous, has a short generation time and a prolific seed production that makes it useful as a model legume (Watson *et al.*, 2003; Benedito *et al.*, 2008; De Bruijn, 2019). Among the resources for *M. truncatula*, several reference proteomes, including that of stems, are currently available (Watson *et al.*, 2003).

In the present study, we have examined the effects of Fe deficiency on the stem protein profiles of *M. truncatula* plants submitted to Fe deficiency, and used pyrolysis-gas chromatography–mass spectrometry and microscopy to assess changes in the lignin composition of these tissues. Legumes are valuable agricultural and commercial crops that serve as important nutrient sources for both humans and animals, and a better understanding of the effects of Fe deficiency in stems, essential for the long-distance transport of Fe, may strengthen our ability to enhance Fe-efficiency responses. Two different treatments have been used to impose Fe deficiency in nutrient solution, with or without $CaCO_3$, with the aim to know whether the presence of $CaCO_3$, which is often found in Fe deficient soils, causes additional effects to those of a direct Fe shortage alone.

3.4.2. Material and methods

Plant material and growth conditions

Medicago truncatula cv. 'Jemalong' plants were grown in a controlled environment chamber with a photosynthetic photon flux density at leaf height of 350 μmol m^{-2} s^{-2} photosynthetically active radiation, 80% relative humidity and at a 16 h-23 °C/8 h-19 °C, day/night regime. Seeds were scarified by nicking the seed coat, then imbibed overnight in distilled water and germinated on filter paper for three days in darkness with full humidity. Seedlings were grown for an additional two-week period in half-strength Hoagland nutrient solution (pH 5.5) with 45 μM Fe(III)-EDTA(Terry, 1980). Plants were then transplanted to 10 L plastic buckets (six plants per bucket) containing half-strength Hoagland nutrient solution and treatments were imposed. Control plants were grown with 45 μM Fe(III)-EDTA (pH 5.5) and Fe deficient plants were grown with no added Fe (0 μM Fe), with (pH 7.7) or without (pH 5.5) 1 g

L^{-1} $CaCO_3$. After six days, stem tissues (including main stems and petioles but excluding cotyledons and leaves; Supporting Information Fig. 3.4.S1) were harvested, frozen in liquid N_2 and stored at −80 °C. Five independent batches of plants were grown and sampled for proteomic analysis. Tissues for mineral (stems including petioles, roots and leaves) and lignin (stems and petioles separately) analyses were also harvested six days after treatment onset from three plants per treatment in two independent batches of plants.

Protein extraction

For protein extraction, approximately 0.5–1 g of tissue (pooled from two plants of a given treatment), containing whole stems (including the main stems and petioles, see Supporting Information Fig. 3.4.S1) but excluding cotyledons and leaves, was ground in liquid N_2 with mortar and pestle. The tissue was homogenized in 6 mL of phenol saturated with 0.1 M Tris-HCl (pH 8.0) and containing 5 mM β-mercaptoethanol, by stirring for 30 min at 4 °C. Then, the homogenate was filtered (PVDF, 0.45 µm) and centrifuged at 5000×*g* for 15 min. The phenol phase was re-extracted for 30 min with one volume of phenol-saturated 0.1 M Tris- HCl (pH 8.0) containing 5 mM β-mercaptoethanol, and centrifuged as described above. Proteins in the phenol phase were precipitated by adding four volumes of 0.1 M ammonium acetate in cold methanol, followed by overnight incubation at −20 °C. Samples were then centrifuged at 5000×*g* for 15 min, and the pellet was washed three times with cold methanol, dried with N_2 gas and resuspended in simple rehydration buffer containing 8 M urea, 2% (w/v) CHAPS, 50 mM DTT, 2 mM PMSF and 0.2% (v/v) 3–10 ampholytes (Amersham, Uppsala, Sweden). After rehydration, samples were incubated at 38 °C for 1.5 h and then centrifuged at 15,000×*g* for 10 min at 20 °C. Samples were analyzed immediately by 2-DE. Protein concentration was measured with the Bradford method (BioRad kit), using microtiter plates in an Asys UVM 340 (Biochrom Ltd., Cambridge, U.K.) spectrophotometer and BSA as standard.

Protein 2-DE separation

Preliminary 2-DE experiments were carried out using a first dimension IEF separation with a linear pH gradient 3–10; in these conditions most of the spots were concentrated in the central region of the 2-DE gel (results not shown); therefore, to prevent protein co-migration and improve resolution a narrower pH gradient was chosen. A first dimension IEF separation was carried out on 7 cm ReadyStrip IPG Strips (BioRad) with a linear pH gradient pH 5–8 using a Protean IEF Cell (BioRad, Hercules, CA, USA). Strips were passively rehydrated for 16 h at 20 °C in 125 µL of rehydration buffer containing 60 µg of root extract proteins and a trace of bromophenol blue, and then transferred onto a strip tray. IEF was run at 20 °C, for a total of 14,000 V h (20 min with a 0–250 V linear gradient, 2 h with a 250–4000 V linear gradient and

4000 V until 10,000 V h). After IEF, strips were equilibrated for 10 min in equilibration solution I [6 M urea, 0.375 M Tris-HCl, pH 8.8, 2% (w/v) SDS, 20% (v/v) glycerol, 2% (w/v) DTT] and for another 10 min in equilibration solution II [6 M urea, 0.375 M Tris-HCl pH 8.8, 2% (w/v) SDS, 20% (v/v) glycerol and, 2.5% (w/v) iodoacetamide]. For the second dimension SDS-PAGE, equilibrated IPG strips were placed on top of vertical 12% SDS-polyacrylamide gels (8 × 10 × 0.1 cm) and sealed with melted 0.5% agarose in 50 mM Tris HCl, pH 6.8, containing 0.1% SDS. SDS-PAGE was carried out at 20 mA per gel for approximately 1.5 h, until the bromophenol blue reached the plate bottom, in a buffer containing 25 mM Tris, 192 mM glycine, and 0.1% SDS, at 4 °C. Gels were subsequently stained with colloidal Coomassie-blue G-250 (Serva, Barcelona, Spain). For each treatment, gels were made from independent whole stem samples (including petioles) preparations obtained from five different batches of plants (n=5).

Gel image and statistical analysis

Stained gels were scanned with an Epson Perfection 4990 Photo Scanner (Epson Ibérica, Barcelona, Spain) at 600 dpi, previously calibrated using the SilverFast 6 software (LaserSoft Imaging AG, Kiel, Germany) and an IT8 reference card. Spot detection, gel matching and interclass analysiswere performedwith PDQuest 8.0 software (BioRad). First, normalized spot volumes based on total intensity of valid spots were calculated for each 2-DE gel and used for statistical calculations of protein abundance; for all spots present in the gels, pI, Mr, and normalized volumes (mean values and SD) were determined. Experimental MR values were calculated by mobility comparisons with Precision Plus protein standard markers (BioRad) run in a separate lane on the SDS gel, and pI was determined by using a linear scale over the total dimension of the IPG strips. Only spots consistently present in at least 80% of the replicates (four out of five gels) from at least one class were considered and used in further analysis; missing spot volumes were estimated from the data set by a sequential K-Nearest Neighbor algorithm using an R 2.7.0 environment. After the input of missing values, a second normalization based on total intensity of valid spots per gel was used to compensate for gel replicate variations, and resulting data were used for statistical analyses. The spots were also manually checked, and consistent reproducibility between normalized spot volumes was found in the different replicates (Supporting Information Table 3.4.S1).

Univariate and multivariate statistical analyses were carried out. Spots changing in relative abundance were selected using a paired Student t-test and a significance level of $p < 0.05$. Protein response ratios were defined as the relative abundance in a given treatment divided by the relative abundance in the controls. Only proteins with mean response ratios above 2.0 or below 0.5 were considered as physiologically relevant and are discussed in this study. Principal component analysis (PCA) was carried out using Excel ad-in Multibase 2014.

Protein identification by nano-liquid chromatography-tandem mass spectrometry (nLC-ESI-MS/MS)

Consistent spots showing statistically significant differences in accumulation were excised automatically using a spot cutter EXQuest (BioRad), proteins in spots digested, and peptides separated by nano-HPLC (n-HPLC system 1200 series, Agilent Technologies, Waldbronn, Germany) as described in (Gutierrez-Carbonell *et al.*, 2013). The nano-HPLC was connected to a HCT Ultra high-capacity ion trap (Bruker Daltonics, Bremen, Germany) using a PicoTip emitter (50 μm i.d., 8 μm tip i.d., New Objective, Woburn, MA, USA) and an online nano-electrospray source. Capillary voltage was −1.8 kV in positive mode and a dry gas flow rate of 10 L min^{-1} was used with a temperature of 180 °C. MS data were acquired automatically using Hystar 3.2 software following a MS survey scan from 50 to 3000 *m/z* at a resolution of 5500. The mass window for precursor ion selection was ±0.15 *m/z* with an active exclusion after two spectra and release after 1.2 min for the one most intense peptide. MS/MS spectra were sequentially and dynamically acquired in a scan from 300 to 1500 *m/z* with a maximum accumulation time of 750 ms depending on sample concentration. The fragmentation amplitude for MS/MS was 1 V. Singly charged ions and trypsin peptides were excluded from MS/MS analysis. Peak detection, deconvolution and processing were performed with Data Analysis 3.4 (Bruker Daltonics).

Protein identification was carried out using the Mascot search engine (version 2.3.02, Matrix Science; London, UK) and the non-redundant databases NCBInr 20,120,303 (17,378,729 sequences; 5,967,463,365 residues). Search parameters were: monoisotopic mass accuracy, peptide mass tolerance ±0.2 Da, fragment mass tolerance ± 0.6 Da; one allowed missed cleavage; allowed fixed modification carbamidomethylation (Cys), and variable modification oxidation (Met). Positive identification was assigned with Mascot scores above the threshold level ($p \leq 0.05$) and at least two identified peptides with a score above homology. The list of peptides identified is shown in Supporting Information Table 3.4.S2. We used the GO biological process annotation (http://www.geneontology.org) of the individual identified proteins and UniProt database information for manual classification into functional categories.

Mineral analysis

Roots, whole stems (including petioles) and leaves were harvested from three plants per treatment, dried in a conventional oven at 60 °C and ground in a stainless steel mill. Subsamples (ca. 0.15 g dry weight) of each ground sample were digested and processed for elemental analysis as described elsewhere (Garcia and Grusak, 2015). Elemental analysis (Ca, Cu, Fe, K, Mg, Mn, Mo, Na, P, S, and Zn) was carried out using inductively coupled plasma-optical emission spectroscopy (CIROS ICP Model FCE12; Spectro, Kleve, Germany); the instrument was

calibrated daily with certified standards. Tomato leaf standards (SRM1573 A; National Institute of Standards and Technology, Gaithersburg, MD, USA) were digested and analyzed along with the *M. truncatula* samples to ensure accuracy.

Microscopy

For microscopy analysis, sections from both petioles and stems of *M. truncatula* plants grown for 6 d in the control conditions or with 0 μM Fe in the presence or absence of $CaCO_3$, were excised with a razor blade and embedded in 5% agar. Eight different petiole and stem sections from eight different plants for each treatment were analyzed. Stem and petiole transversal sections (60 μM thick) were obtained using a vibrating blade microtome (VT1000 S, Leica Microsystems GmbH). Cell walls were stained using phloroglucinol (SIGMA), and bright field and auto-fluorescence images of the transversal slices were taken with an inverted microscope (DM IL LED, Leica Microsystems GmbH) equipped with a fluorescence kit (340–380 excitation wavelength and 425 nm cut-off filter; A1 filter cube, Leica MicrosystemsGmbH) and a CCD camera (DFC 240C, Leica Microsystems GmbH).

Lignin analysis

Lignin analysis was carried out by pyrolysis-gas chromatography–mass spectrometry (Py-GC–MS) using separately petioles and stems harvested from three *M. truncatula* plants per treatment. Pyrolysis of the samples (approximately 7 mg) was performed with a 3030 μ-furnace pyrolyzer (Frontier Laboratories Ltd.) connected to an Agilent 7820 A GC using a DB-1701 fused-silica capillary column (60 m × 0.25 mm i.d., 0.25 μm film thickness) and an Agilent 5975 mass selective detector (EI at 70 eV). The pyrolysis was performed at 500 °C. The oven temperature was programmed from 45 °C (4 min) to 280 °C (10 min) at 4 °C min−1. Helium was the carrier gas (2 mL min^{-1}). Compounds were identified by comparing their mass spectra with those in the Wiley and NIST libraries and those reported in the literature(Ralph and Hatfield, 1991). Peak molar areas were calculated for the main lignin-degradation products using their characteristic mass fragment ions, the summed areas were normalized, and data from our biological replicates were averaged and expressed as percentages. The main lignin compounds and the mass fragment ions used for quantitation were: guaiacol (124), 4-methylguaiacol (*m/z* 138), 4-ethylguaiacol (*m/z* 137), 4-vinylguaiacol (*m/z* 150), eugenol (*m/z* 164), cis-isoeugenol (*m/z* 164) and trans-isoeugenol (*m/z* 164) as guaiacyl-lignin markers, and syringol (*m/z* 154), 4-methylsyringol (*m/z* 168), 4-ethylsyringol (*m/z* 167), 4-vinylsyringol (*m/z* 180), 4-allylsyringol (*m/z* 194), cis-4-propenylsyringol (*m/z* 194), and trans-4-propenylsyringol (*m/z* 194) as syringyl-lignin markers. The compounds used for quantitation of proteins and their characteristic fragment ions were phenylacetonitrile (*m/z* 117), indole (*m/z* 117), and 3-methylindole (*m/z* 130).

3.4.3. Results

Symptoms of Fe deficiency in *M. truncatula* plants included a yellowing of young leaves and a reduction of biomass, which were more intense in the treatment that included $CaCO_3$; these symptoms were described in detail in a parallel study focused to root proteomic changes (Jorge Rodríguez-Celma, Lattanzio, *et al.*, 2011).

Protein profiles

Changes in the protein profile of extracts of stems (including petioles) from Fe deficient *M. truncatula* plants grown in the absence (pH 5.5) or presence of $CaCO_3$ (pH 7.7) were studied by 2-D IEF-SDS PAGE electrophoresis. Typical real scans of 2-DE gels obtained from root protein extracts of Fe-sufficient and Fe-deficient (pH 5.5 or 7.7) plants are shown in Fig. 3.4.1A-C, respectively. The average number of detected spots (mean ± SD) was 265 ± 2, 261 ± 2 and 267 ± 2 in gels from plants grown with 45 μM Fe and 0 μM Fe in the absence or presence of $CaCO_3$; approximately 95% of spots were consistently found in all five replicates within each treatment (Supporting Information Table 3.4.S3). The total number of spots consistently detected in the whole experiment (present in at least 80% of the gels of one treatment) was 276 (Supporting Information Tables 3.4.S1 and 3.4.S3). A composite averaged virtual map containing all spots present in all 15 gels (5 per treatment) is shown in Fig. 3.4.1D.

When compared to the control plants, four and 11% of the consistent spots (10 and 31 spots, respectively) showed changes in relative abundances that were statistically significant at $p < 0.05$ and above the cut-off values for fold-change (≥2 or ≤0.5) in the 0 μM Fe treatments in the absence or presence of $CaCO_3$, respectively (these spots are marked in bold and with an asterisk in Table 3.4.1). Two of these changes (decreases in the relative abundance of spots 1 and 23) occurred irrespectively of the presence of $CaCO_3$ (Table 3.4.1 and Fig. 3.4.2B). From the total 39 spots showing physiologically relevant changes, 80% (31 spots) were reliably identified (Table 3.4.1). When a PCA analysis was run using all consistent spots, the samples from Fe-deficient plants in the presence of $CaCO_3$ were well separated, whereas those from Fe sufficient plants and Fe-deficient plants grown without $CaCO_3$ overlapped (Supplementary Information Fig. 3.4.S2A). However, when the PCA analysis was run using only those spots showing significant differences in relative abundance, samples from the three treatments were clearly separated (Supplementary Information Fig. 3.4.S2B).

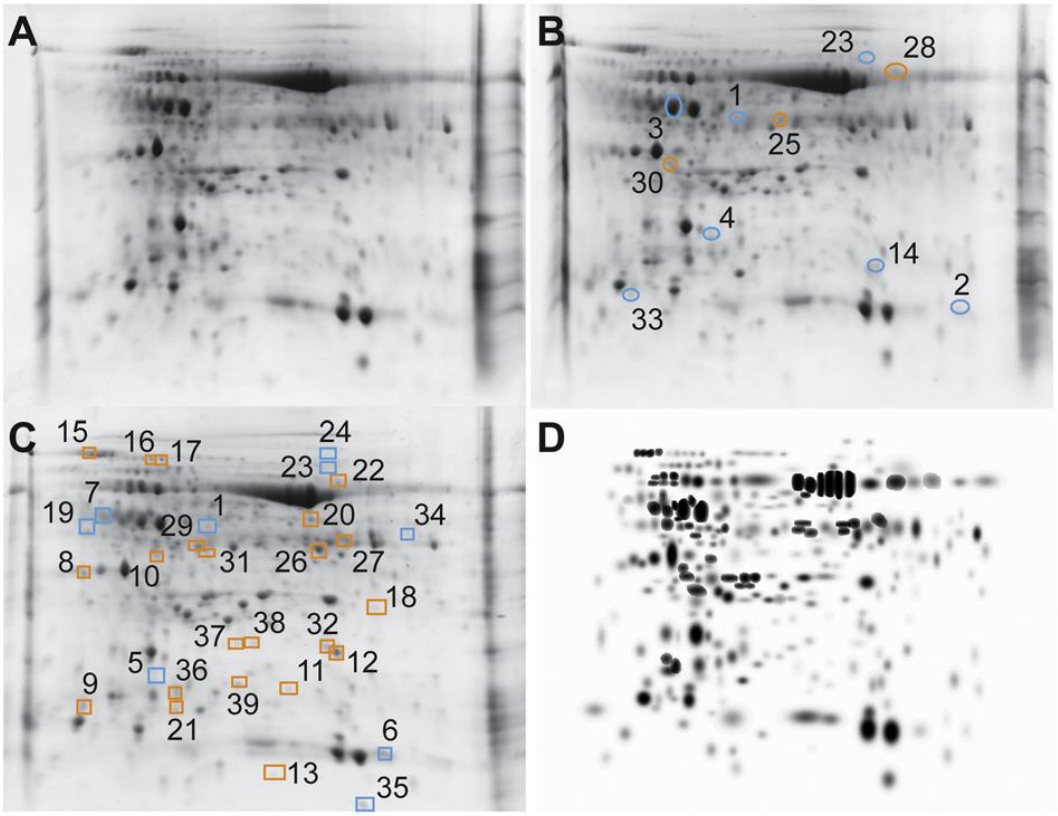

Fig. 3.4.1. *2-DE IEF-SDS PAGE protein profile maps of stem extracts from Medicago truncatula plants. Scans of typical gels from the stems of Fe-sufficient and Fe-deficient plants grown in the absence and presence of $CaCO_3$ are shown in A, B and C, respectively. To facilitate visualization of the studied spots, a virtual composite image (D) was created containing all spots present in the real gels A, B and C. In B (−Fe) and C (−Fe + $CaCO_3$), spots whose intensities decreased or increased when compared to control maps are marked with blue and orange symbols, respectively. Identified spots are labeled in B and C with the corresponding number assigned in Table 3.4.1.*

The statistical analysis of averaged maps indicated that the Fe deficiency treatment in absence of $CaCO_3$ caused significant increases ($p < 0.05$; fold-change ≥2) in relative abundance of three spots (spots 25, 28 and 30 in Table 3.4.1; orange ellipses in Fig. 3.4.1B). All of them matched reliably to known proteins and were manually classified by their GO: BP (Biological Process) annotation to general metabolism (spots 25 and 28) and phenylpropanoid metabolism (spot 30) (Fig. 3.4.2A). Five spots (spots 1–3, 14 and 23) showed significant decreases in relative abundance and two more (spots 4 and 33) were no longer detected in the 0 μM Fe treatment when compared to controls ($p < 0.05$; fold-change ≤0.5; blue ellipses in Fig. 3.4.1B), and six of them were reliably identified (spots labeled 1–4, 14 and 23 in Table 3.4.1); they were assigned to photosynthesis (spots 1–4), protein modification (spot 14) and oxidation/reduction process (spot 23) (Fig. 3.4.2A).

Changes in the whole stem protein profile were more marked when Fe deficiency was imposed in the presence of $CaCO_3$. Eighteen spots showed significant increases in relative abundance (spots 8–12, 15–18, 20, 21, 26, 27, 32, and 36–39 in Table 3.4.1) and four more were

detected *de novo* (spots 13, 22, 29 and 31 in Table 3.4.1) in the Fe deficient treatment in the presence of $CaCO_3$ when compared with the controls ($p < 0.05$; fold-change ≥2; orange rectangles in Fig. 3.4.1C). Among them, 17 were reliably identified and manually classified in the following functional categories: photosynthesis (spot 8), defense and oxidative stress (spots 9–13), protein metabolism (spots 15–18, 20 and 21), oxidation/reduction processes (spot 22), general metabolism (spots 26 and 27) and secondary metabolism (spots 29 and 31) (Table 3.4.1, Fig. 3.4.2A). Six spots showed significant decreases in relative abundance (spots 1, 6, 7, 23, 24 and 35 in Table 3.4.1) and three more (spots 5, 19 and 34 in Table 3.4.1) were no longer detected ($p < 0.05$; fold-change ≤0.5; blue rectangles in Fig. 3.4.1C). Among them, seven spots were identified and assigned to photosynthesis (spots 1 and 5–7), translation (spot 19), and oxidation-reduction process (spots 23 and 24) (Fig. 3.4.2A).

The information on the significant changes (p b 0.05; fold-change ≥2 or ≤0.5) in protein abundance as a result of both Fe deficiency treatments is summarized in a Venn diagram (Fig. 3.4.2B), using the same color code than that used in Fig. 3.4.1 (orange and blue numbers for increases and increases in relative abundance, respectively). Two spots (spots 1 and 23 in Table 3.4.1) changed significantly and above the cut-off values in both Fe-deficiency treatments.

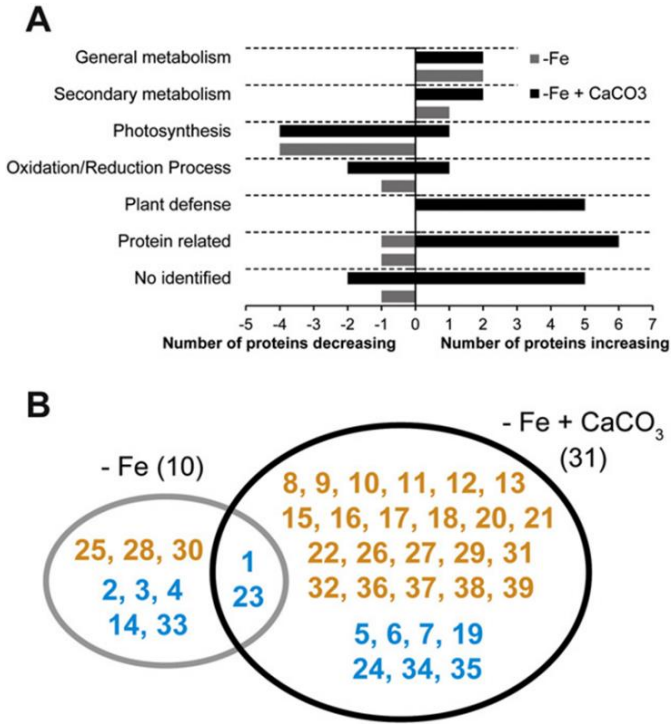

Fig. 3.4.2. *A. Number of identified spots changing as a result of Fe deficiency, organized in metabolic pathways. Pathways related to the identified proteins were integrated according to the UniProt database and GO annotation. B. Venn diagram depicting proteins with changes in abundance as a result of the Fe deficiency treatments. Numbers indicate spots as in Table 3.4.1. Orange and blue color numbers indicate increases (including new appearances) and decreases (including disappearances) in spot abundance as a result of Fe deficiency, respectively.*

Table 3.4.1. *Proteins identified in 2-D IEF-SDS PAGE gels. In the−Fe vs+Fe and−Fe + $CaCO_3$ vs+Fe columns, spots showing statistically significant changes (t-Student's test, p < 0.05) and above the biological relevant cut-off values (fold ≥2 or fold≤0.5) are marked in bold with an asterisk, and spots showing significant changes in relative abundance but with fold-changes outside the cut-off values are marked only in bold. For some spots, fold changes outside the threshold cut off values (p < 0.05 and/or fold ≥2 or fold ≤0.5) are indicated in normal typeface in a given treatment when they were significant in the other treatment. Spots were analyzed by LC-MS/MS and positive identification was retained with Mascot scores (Sc) above the threshold levels (p b 0.05) and at least two identified peptides with a ion score above homology (ion/pep). Function was inferred from GO and UniProt entry annotation. "new" and "lost" indicate spots that have been newly detected or no longer detected in the −Fe treatments.*

Spot n	UniProt Identifier	Protein description	Species	Mascot output (Sc/ion/pep)	Sq %	theor Mw/pI	exp Mw/pI	-Fe vs +Fe	-Fe+$CaCO_3$ vs +Fe	GO:BP
Photosynthesis										
1	Q40073	Rubisco activase A	*H. vulgare*	162/2/2	8	47/8.6	44/6.2	**0.2***	**0.1***	Photosynthesis (GO:0015979)/ATP binding (GO:0005524
2	B7FMC2	Rubisco small chain 3A	*M. truncatula*	343/10/6	44	20/8.7	16/7.3	**0.2***	**0.7**	Photosynthesis (GO:0015979)/ C fixation (GO:0015977)
3	A0A072UZ59	Rubisco activase	*M. truncatula*	975/53/15	45	48.0/6.9	43/5.7	**0.5***	**0.6**	Photosynthesis (GO:0015979)/Reductive pentose-phosphate cycle (GO:0019253)
4	P28459	Rubisco largechain	*V. acerifolium*	62/2/2	4	53/6.1	25/5.9	**Lost***	0.7	Photosynthesis (GO:0015979)/Reductive pentose-phosphate cycle (GO:0019253)
5	B7FGU7	Cytochrome b6-f complex iron- sulfur subunit	*M. truncatula*	156/2/2	11	24/7.6	23/5.9	0.3	**Lost***	Photosynthetic electron transport chain (GO:0009767)

Table 3.4.1 (continued)

Spot n	UniProt Identifier	Protein description	Species	Mascot output (Sc/ion/pep)	Sq %	theor Mw/pI	exp Mw/pI	-Fe vs +Fe	-Fe+$CaCO_3$ vs +Fe	GO:BP
6	KEH21532	Rubisco small chain	*M. truncatula*	275/14/6	37	20.4/8.7	16/7.6	0.2	**0.2***	Photosynthesis (GO:0015979)/ C fixation (GO:0015977)
7	Q8GTY4	Rubisco activase	*M. sativa*	480/10/6	39	30/5.6	43/5.4	1.8	**0.5***	Photosynthesis (GO:0015979)/ATP binding (GO:0005524)
8	P14226	Oxygen-evolving enhancer protein 1	*P. sativum*	141/3/3	13	35/6.25	30/5.2	**1.5**	**2.2***	Photosynthesis (GO:0015979)/Photosystem II stabilization (GO:0042549)
Defense/Response to oxidative stress										
9	B7FKA0	Polyketide cyclase/dehydraseand lipid transporter	*M. truncatula*	148/3/3	24	18/5.1	20/5.5	0.9	**2.1***	Defense response (GO:0006952)/ mRNA modification (GO:0016556)
10	A6XJ26	Thioredoxin reductase	*M. truncatula*	155/2/2	7	40/6.9	34/5.8	1.4	**2.8***	Removal of superoxide radicals (GO:0019430)
11	Q56VU1	Glutathione peroxidase 1	*L. japonicus*	125/3/2	9	26/8.8	22/6.7	2.9	**3.7***	Response to oxidative stress (GO:0006979)
12	B6ZHC0	PR-5b protein	*G. max*	159/3/2	17	27/6.3	27/7.0	2.8	**12.4***	Phatogenesis related
13	A0A072TXU 3	Glutaredoxin C4	*M. truncatula*	108/2/2	34	11.4/6.5	14/6.6	new	**new***	Cell redox homeostasis (GO:0045454)

Table 3.4.1 (continued)

Protein-related process										
14	B7FF81	Ubiquitin-conjugating enzyme	*M. truncatula*	77/2/2	14	17/6.2	20/7.1	**0.4***	0.9	Protein ubiquitination (GO:0016567)
Spot n	**UniProt Identifier**	**Protein description**	**Species**	**Mascot output (Sc/ion/pep)**	**Sq %**	**theor Mw/pI**	**exp Mw/pI**	**-Fe vs +Fe**	**-Fe+$CaCO_3$ vs +Fe**	**GO:BP**
15	P49118	78 kDa Glucose-regulated protein homolog	*S. lycopersicu m*	367/5/4	13	41/8.5	74/5.4	1.4	**2.1***	Potein folding (GO:0006457)
16	G7JU14	Heat shock 70 kDa Protein	*M. truncatula*	887/16/13	24	72/5.9	70/5.8	1.2	**2.3***	Potein folding (GO:0006457)
17	P37900	Heat shock 70 kDa protein. mitochondrial	*P. sativum*	241/6/4	8	72/5.8	70/5.8	1.2	**2.5***	Potein folding (GO:0006457)
18	P38548	GTP-binding nuclear protein Ran/TC4	*V. faba*	175/5/4	19	25.6/6.4	29/7.3	lost	**6.1***	Small GTPase mediated signal transduction (GO:0007264)/ protein transport (GO:0015031)
19	XM_003594608	30S Ribosomal protein S1	*M. truncatula*	297/5/5	18	44.9/5.2	44/5.3	1.0	**lost***	Translation (GO:0006412)
20	D7KCE2	Elongation factor Tu	*A. lyrata*	366/10/6	15	49/6.6	43/6.8	1.1	**2.8***	Translational elongation (GO:0006414)
21	G7LE33	40S Ribosomal protein S12	*M. truncatula*	218/6/5	51	15.6/5.5	20/6.0	0	**22.9***	Translation (GO:0006412)

Table 3.4.1 (continued)

Oxidation/reduction process										
22	O81413	Ferric leghemoglobin reductase-2	*G. max*	278/7/6	14	53/6.9	51/7.0	nd	**new***	Cell redox homeostasis (GO:0045454)

Spot n	**UniProt Identifier**	**Protein description**	**Species**	**Mascot output (Sc/ion/pep)**	**Sq %**	**theor Mw/pI**	**exp Mw/pI**	**-Fe vs +Fe**	**-Fe+$CaCO_3$ vs +Fe**	**GO:BP**
23	G7JL79	Ferredoxin-nitrite reductase	*M. truncatula*	223/4/4	9	65.8/6.5	64/7.0	**0.2***	**0.3***	Nitrate transport (GO:0015706)/ Cysteine biosynthetic process (GO:0019344)/ Oxidation-reduction process (GO:0055114**)**
24	G7J8R4	NADH-ubiquinone oxidoreductase 75 kDa subunit	*M. truncatula*	310/5/5	8	82/7.1	74/7.0	0.7	**0.4***	Respiratory chain complex I (GO:0045271)/ Proteasome corecomplex assembly (GO:0080129)/ Oxidation-reduction process (GO:0055114)/ ATP synthesis coupled electron transport (GO:0042773)/ Response to oxidative stress (GO:0006979)/ Gravitropism (GO:0009630)

Table 3.4.1 (continued)

Metabolism										
25	Q9FT00	Malate dehydrogenase 2	*C.arietinum*	71/2/2	8	36/5.9	43/6.4	**4.8***	2.5	Tricarboxylic acid cycle (GO:0006099)/ Carbohydrate metabolic process (GO:0005975)
26	O48904	Malate dehydrogenase precursor	*M. sativa*	541/12/7	24	36/8.8	36/6.9	1.0	**2.6***	Tricarboxylic acid cycle (GO:0006099)/ Carbohydrate metabolic process (GO:0005975)
Spot n	**UniProt Identifier**	**Protein description**	**Species**	**Mascot output (Sc/ion/pep)**	**Sq %**	**theor Mw/pI**	**exp Mw/pI**	**-Fe vs +Fe**	**-Fe+$CaCO_3$ vs +Fe**	**GO:BP**
27	B7FJQ4	Malate dehydrogenase	*M. truncatula*	351/11/5	13	36/6.1	42/7.1	2.2	**2.7***	Tricarboxylic acid cycle (GO:0006099)/ Carbohydrate metabolic process (GO:0005975)
28	A9YWS0	Serine-hydroxymethyl-transferase	*M. truncatula*	87/2/2	7	58/8.4	52/7.2	**3.1***	**1.5**	Serine (GO:0006563) and glycine (GO:0006544) metabolic process /One C metabolism (GO:0006730)/ methylation (GO:0032259)

Table 3.4.1 (continued)

Secondary metabolism										
29	B7FHV0	Phenylcoumaran benzylic ether reductase-like protein Fi1	*M.truncatula*	358/6/6	27	33.9/5.6	42/6.1	nd	**new***	Oxidation-reduction process (GO:0055114) / Phenylpropanoid metabolic process (GO:0009698)
30	B7FIC1	Putative O-methyltransferase	*M. truncatula*	114/4/4	23	28/5.4	30/5.7	**3.8***	4.6	Methylation (GO:0032259)/ Phenylpropanoid metabolic process (GO:0009698)/ Cysteine biosynthetic process (GO:0019344)
31	Q45FF2	Pyridoxal biosynthesis protein PDX1.3	*M. truncatula*	334/8/4	16	34/5.6	35/6.2	nd	new*	Pyridoxal phosphate biosynthetic process (GO:0042823)
Spot n	**UniProt Identifier**	**Protein description**	**Species**	**Mascot output (Sc/ion/pep)**	**Sq %**	**theor Mw/pI**	**exp Mw/pI**	**-Fe vs +Fe**	**-Fe+$CaCO_3$ vs +Fe**	**GO:BP**
Not Identified										
32		not identified					27/6.9	**1.4**	**2.3***	
33		not identified					17/5.5	**lost***	1.1	
34		not identified					43/7.5	0.4	**lost***	
35		not identified					13/7.1	0.7	**0.4***	
36		not identified					22/5.9	1.0	**2.0***	
37		not identified					28/6.3	1.7	**2.3***	
38		not identified					28/6.5	1.0	**2.4***	
39		not identified					23/6.4	1.2	**3.2***	

Mineral analysis

Mineral analysis was carried out in whole stem samples (including stems and petioles). The stem dry weights from Fe-deficient plants grown in both conditions were approximately 24% lower than that of the Fe-sufficient controls (Fig. 3.4.3A). Iron concentration in stems of Fe-deficient plants grown in the absence of $CaCO_3$ did not change when compared to controls, whereas in Fe-deficient plants grown in the presence of $CaCO_3$ the Fe concentration was 54% lower than in Fe-sufficient controls (Fig. 3.4.3B). The total Fe content in stems was lower in both Fe deficiency treatments when compared to controls, due to the lower stem dry weights in the absence of Fe (Supporting Information Fig. 3.4.S3). Stem concentrations of Zn, Cu and Mn from Fe-deficient plants grown in the absence of $CaCO_3$ were 90, 100 and 60% higher, respectively, than those in the Fe-sufficient controls, whereas the concentrations of Ni, Mo, Co and B did not change significantly (Fig. 3.4.3B). The presence of $CaCO_3$ in the zero-Fe solution did not lead to significant changes in the concentrations of Zn, Cu, Mn, Ni, Mo Co and B when compared to the Fe-sufficient controls (Fig. 3.4.3B).

With regard to macronutrient concentrations, in whole stems of Fe-deficient plants grown in the absence of CaCO3 the only significant change was a 50% increase in Mg concentration when compared to Fe-sufficient controls (Fig. 3.4.3C). In the presence of $CaCO_3$, increases in Mg (140%), and Ca (28%) concentrations and a decrease in K concentration (10%) were found when compared to those in Fe-sufficient controls (Fig. 3.4.3C).

The mineral composition of leaves and roots was also determined (Supporting Information Fig. 3.4.S4). In roots, Fe concentration was lower than in controls in both Fe deficiency treatments, whereas Zn and Cu concentrations increased in the absence of $CaCO_3$ and Ni concentration increased in the presence of $CaCO_3$. In leaves, Fe concentration only decreased in the presence of $CaCO_3$. Regarding other micronutrients in leaves, results were similar to those described above for stems, with Zn, Cu, Mn and also Ni concentrations being higher in the Fe-deficiency treatment in the absence of $CaCO_3$ than in Fe-sufficient controls, and similar to controls or only slightly higher in the presence of $CaCO_3$ (Supporting Information Fig. 3.4.S4). The trends observed for changes in macronutrient concentrations in leaves and roots as a result of both Fe deficiency treatments were quite similar to those observed in stems (Supporting Information Fig. 3.4.S4). The only significant changes in macronutrient root concentrations occurred in Fe-deficient plants in the presence of $CaCO_3$, and included an increase in Ca and decreases in P and S concentrations (Supporting Information Fig. 3.4.S4). In leaves, Fe deficiency increased Ca and Mg concentrations, with the increases being larger in the presence of $CaCO_3$.

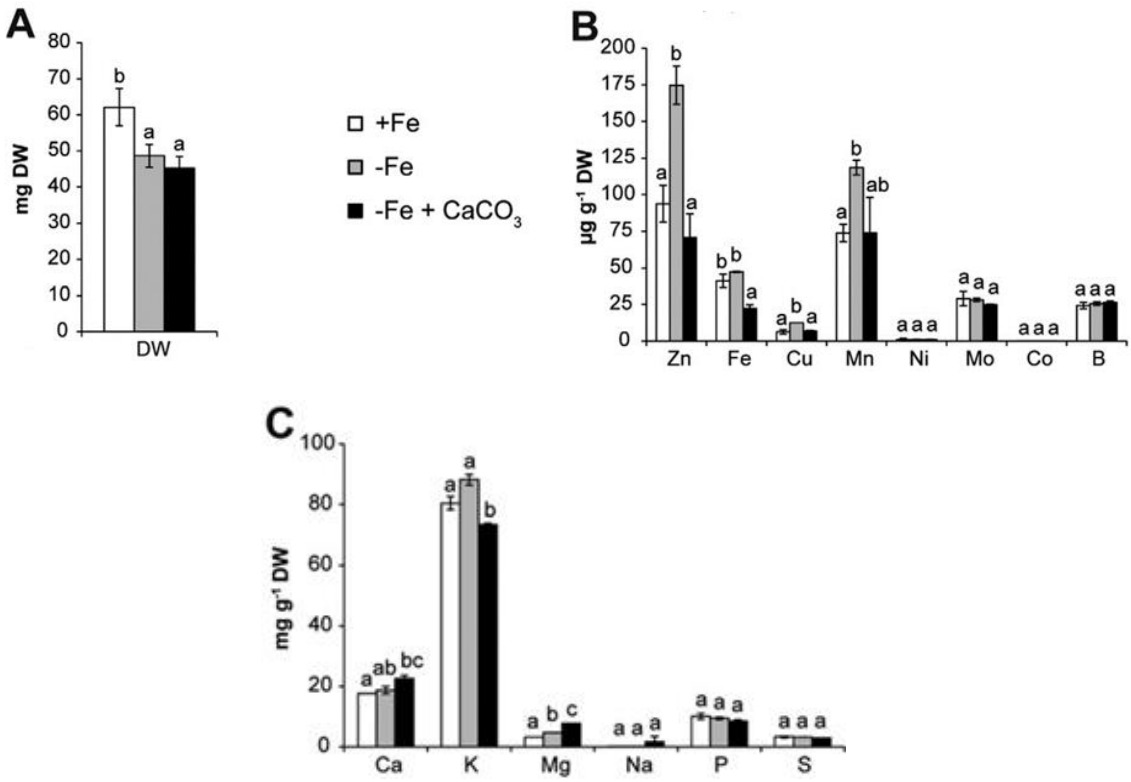

Fig. 3.4.3. *Mineral composition of stems, including petioles, as affected by Fe deficiency. A: dry mass (DW, in mg per plant); B: micronutrient concentrations (in µg g^{-1} DW), and C: macronutrient concentrations (in mg g^{-1} DW) of stems (including petioles) of Medicago truncatula plants grown for six days in Fe-sufficient (white columns) and Fe-deficient conditions (grey columns for plants grown in the absence of $CaCO_3$ and black columns for plants grown in the presence of $CaCO_3$). Data are means ± SE (n = 3; from one batch of plants with three samples per treatment). Columns marked with the same letter are not significantly different at the $p \leq 0.05$ probability level.*

Microscopy of petiole and stem sections

In order to study possible cell wall changes, lignin was localized in sections of stems and petioles using autofluorescence and phloroglucinol staining. In Fe-sufficient petioles, the blue autofluorescence signal was mainly detected in xylem vessels and sclerenchyma tissue (Fig. 3.4.4A). When compared to controls, Fe-deficient petioles from plants grown in the absence of $CaCO_3$ showed a slightly lower autofluorescence intensity in both xylem vessel and sclerenchyma tissue (Fig. 3.4.4B), whereas in petiole sections from Fe-deficient plants grown in the presence of $CaCO_3$, the autofluorescence signal intensity decreased in xylem vessels when compared to both sclerenchyma and controls (Fig. 3.4.4C). This decrease in autofluorescence occurred especially in the innermost part of xylem vessels, where blue autofluorescence was barely observed and instead a greenish color was detected (Fig. 3.4.4C).

When phloroglucinol staining was used, lignin distribution in Fe-sufficient petioles was similar to that found using autofluorescence, but the staining was more intense in the sclerenchyma (deep red) than in xylem vessels (almost black) (Fig. 3.4.4D). Phloroglucinol

staining of Fe-deficient petioles from plants grown in the absence of $CaCO_3$ yielded an intense coloration in xylem vessels similar to that observed in Fe-sufficient controls and little staining in the sclerenchyma (Fig. 3.4.4E). In petiole sections from Fe-deficient plants grown in the presence of $CaCO_3$, phloroglucinol staining was intense and even higher than that observed in controls in both xylem vessels and sclerenchyma (Fig. 3.4.4F).

Stems of Fe-sufficient plants showed a clear blue autofluorescence in the xylem vessels and a more diffuse one in the cortex, and similar results were observed when phloroglucinol was used for lignin staining (Supporting Information Fig. 3.4.S5). Stems from Fe deficient plants showed similar autofluorescence and staining patterns to those of controls, irrespective of the presence of $CaCO_3$ in the nutrient solution (Supporting Information Fig. 3.4.S5).

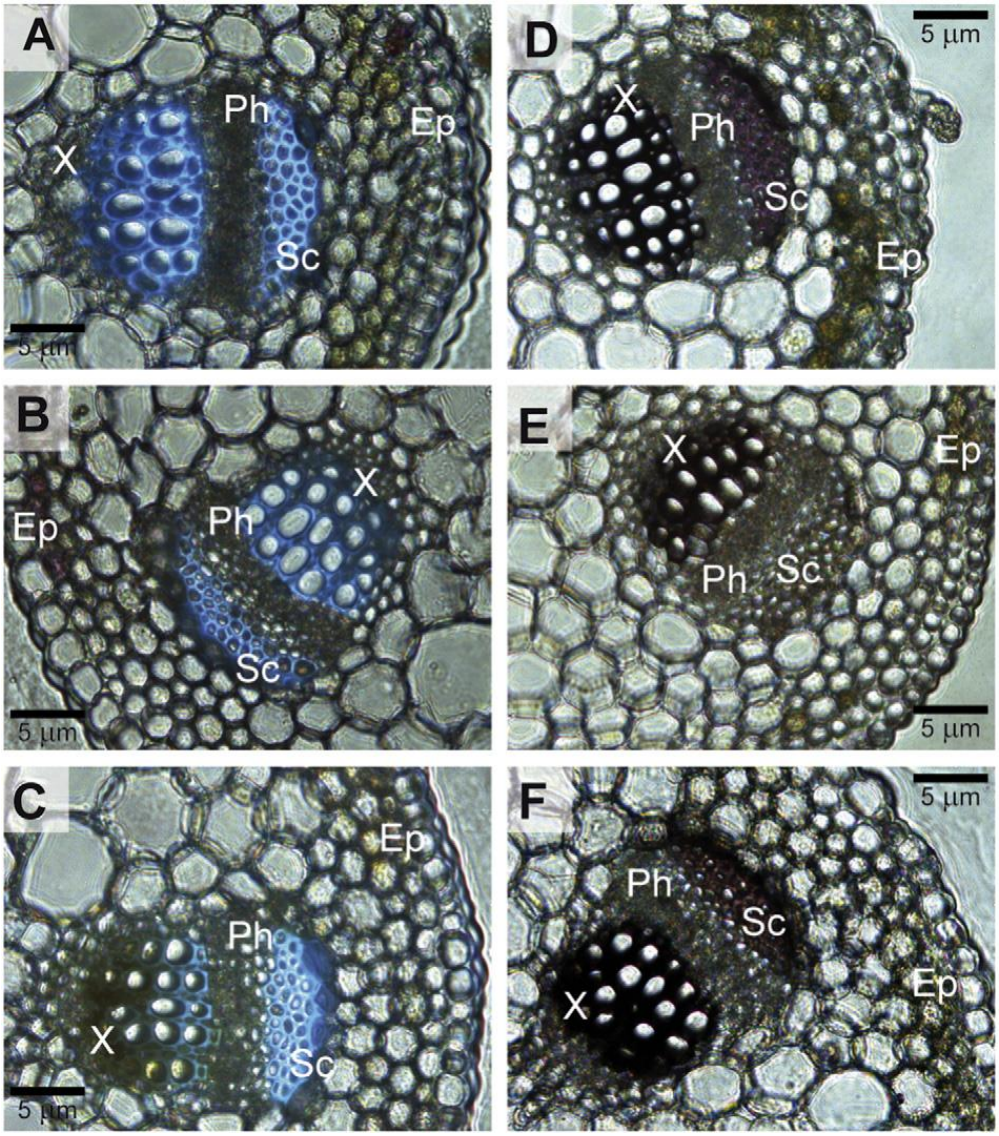

Fig.3.4.4. *Microscopy analyses of Fe-deficient petioles. Micrographs of petiole sections (10×): autofluorescence (A–C) and phloroglucinol staining (D–F) from Fe-sufficient plants (A and D) and Fe-deficient plants grown in the absence (B and E) and presence of $CaCO_3$ (C and F). X: xylem; Ph: phloem; C: cortex; Ep: epidermis, and Sc: sclerenchyma. Transversal petiole slices, 60 µm thick, were obtained using a vibrating blade microtome.*

Lignin analysis

The lignin composition (relative molar abundances of G- and S-lignin derived markers and S/G ratios) of both stems and petioles samples was studied by Py-GC/MS. The percentages of protein markers relative to the lignin markers (lignin/protein ratio) were also estimated.

In petioles, the lignin per protein ratio increased 20 and 110% in the Fe deficiency treatment in the absence and presence of $CaCO_3$, respectively, when compared to the Fe-sufficient controls (Table 3.4.2). The total relative abundance of S- and G- lignin markers and the S/G ratio in petioles from both Fe deficiency treatments were similar to those of controls but significantly different between them (Table 3.4.2). However, the relative molar abundances for most of the specific G lignin markers (six of the seven compounds measured) in Fe-deficient samples presented statistically significant differences (two compounds increased and four compounds decreased with Fe deficiency) with those of control samples (Table 3.4.2). The relative molar abundances of specific S-lignin markers changed in at least one of the Fe-deficiency treatments in four of the seven measured compounds when compared to control petioles (Table 3.4.2).

On the other hand, very few changes in the stem lignin parameters were found with Fe deficiency. The lignin per protein ratios, relative molar abundances of G- and S-lignin derived markers and S/G ratios were similar in the Fe-deficient samples, irrespective of the presence of $CaCO_3$, to those found in Fe-sufficient controls (Table 3.4.2).

Table 3.4.2. *Relative molar abundance of G- and S-lignin derived markers, S/G ratio, percentage of protein markers and lignin/protein ratio in stems and petioles of Fe-sufficient and Fe-deficient plants grown in the absence and presence of $CaCO_3$, as estimated by Py-GC/MS. Data are means ± SD of four biological replicates. Different letters within the same row and tissue indicate statistically significant differences using the Student's t-test and $p < 0.05$.*

Compounds	Petioles			Stems		
	+Fe	-Fe	-Fe+$CaCO_3$	+Fe	-Fe	-Fe+$CaCO_3$
G-lignin markers						
Guaiacol	19.5 ± 0.5 a	24.7 ± 2.1 b	23.9 ± 2.2 b	25.6 ± 1.5 a	27.5 ± 2.1 a	26.2 ± 1.8 a
4-Methylguaiacol	3.4 ± 0.2 b	3.1 ± 0.2 a	3.0 ± 0.1 a	3.3 ± 0.4 a	3.4 ± 0.1 a	3.2 ± 0.1 a
4-Ethylguaiacol	4.0 ± 0.7 a	6.4 ± 0.2 b	6.5 ± 0.9 b	6.4 ± 0.4 a	7.1 ± 0.3 b	7.0 ± 0.7 ab
4-Vinylguaiacol	44.2 ± 2.4 c	36.2 ± 2.0 a	40.7 ± 2.4 b	23.5 ± 1.4 a	24.2 ± 1.2 a	25.2 ± 1.9 a
Eugenol	1.9 ± 0.2 b	1.4 ± 0.2 a	1.1 ± 0.3 a	1.0 ± 0.1 a	1.1 ± 0.1 a	1.1 ± 0.2 a
cis-Isoeugenol	1.5 ± 0.0 b	1.2 ± 0.2 a	1.0 ± 0.2 a	1.2 ± 0.1 a	1.2 ± 0.1 a	1.3 ± 0.1 a
trans-Isoeugenol	7.1 ± 0.2 a	7.0 ± 0.3 a	6.1 ± 0.9 a	6.4 ± 0.5 a	6.7 ± 0.7 a	7.1 ± 0.6 a
Total G compounds	**81.6 ± 1.3 ab**	**80.1 ± 1.2 a**	**82.3 ± 1.3 b**	**67.5 ± 3.6 a**	**71.0 ± 1.6 a**	**71.1 ± 1.0 a**
S-lignin markers						
Syringol	7.8 ± 0.6 a	9.1 ± 0.5 b	7.8 ± 0.9 a	15.2 ± 1.7 b	13.9 ± 0.5 b	12.8 ± 0.5 a
4-Methylsyringol	1.3 ± 0.1 b	1.2 ± 0.1 ab	1.0 ± 0.2 a	2.1 ± 0.1 b	1.7 ± 0.1 a	1.6 ± 0.1 a
4-Ethylsyringol	1.1 ± 0.2 a	1.6 ± 0.1 b	1.7 ± 0.3 b	3.2 ± 0.5 a	2.7 ± 0.2 a	2.9 ± 0.2 a
4-Vinylsyringol	5.7 ± 0.3 b	5.4 ± 0.4 ab	4.7 ± 0.6 a	8.0 ± 0.9 b	6.7 ± 0.5 a	6.7 ± 0.4 a
4-Allylsyringol	0.5 ± 0.1 a	0.4 ± 0.0 a	0.4 ± 0.1 a	0.5 ± 0.1 a	0.5 ± 0.1 ab	0.6 ± 0.0 b
cis-4-Propenylsyringol	0.3 ± 0.1 a	0.3 ± 0.1 a	0.3 ± 0.0 a	0.6 ± 0.1 a	0.5 ± 0.1 a	0.7 ± 0.1 a
trans-4-Propenylsyringol	1.7 ± 0.3 a	1.1 ± 0.1 a	1.8 ± 0.2 a	3.0 ± 0.4 a	3.0 ± 0.5 ab	3.7 ± 0.2 b
Total S compounds	**18.4 ± 1.3 ab**	**19.9 ± 1.2 b**	**17.7 ± 1.3 a**	**32.5 ± 3.6 a**	**29.0 ± 1.6 a**	**28.9 ± 1.0 a**
S/G ratio	**0.2 ± 0.0 ab**	**0.3 ± 0.0 b**	**0.2 ± 0.0 a**	**0.5 ± 0.1 a**	**0.4 ± 0.0 a**	**0.4 ± 0.0 a**
Protein markers*						
Phenylacetonitrile	42.9 ± 6.3 c	28.5 ± 5.5 b	12.9 ± 5.0 a	8.7 ± 1.8 b	9.3 ± 3.0 b	5.2 ± 1.4 a
Indole	138.0 ± 20.5 b	120.5 ± 16.0 b	76.7 ± 17.8 a	45.0 ± 5.2 a	57.2 ± 18.0 a	46.8 ± 15.8 a
3-Methylindole	35.9 ± 7.9 b	18.9 ± 4.1 a	15.1 ± 2.5 a	8.6 ± 1.3 a	10.0 ± 3.4 a	10.9 ± 2.8 a
Total protein markers*	**216.8 ± 32.5 c**	**167.9 ± 25.1 b**	**104.7 ± 24.8 a**	**62.4 ± 8.2 a**	**76.5 ± 24.1 a**	**62.9 ± 19.9 a**
Lignin/Protein ratio	**0.5 ± 0.1 a**	**0.6 ± 0.1 b**	**1.0 ± 0.2 c**	**1.6 ± 0.2 a**	**1.4 ± 0.3 a**	**1.7 ± 0.4 a**

* protein-markers calculated as percentage of total lignin markers (G+S)

3.4.4. Discussion

In the present study we have characterized the differences in the protein profiles of whole stems (including petioles) from *M. truncatula* plants grown in hydroponics in two different Fe deficiency conditions, in the presence and absence of $CaCO_3$, with the aim of shedding light into processes that may be relevant in Fe deficiency induced modifications in this tissue. It should be noted that the individual specific effects of Fe deficiency and $CaCO_3$ in the proteome of stems from Fe-deficient plants grown in the presence of $CaCO_3$ cannot be discriminated using the current experimental approach. The presence of $CaCO_3$ along with Fe(III)-EDTA as an Fe source causes Fe precipitation and immobilization, therefore making unfeasible its use as a control.

Overall results from the protein profiling indicate that Fe deficiency in the presence of $CaCO_3$ has a more pronounced impact on the stem proteome than the lack of Fe alone, since a larger number of spots (31) displayed differences in relative accumulation in the presence of $CaCO_3$ than in its absence (10). This stronger effect is also supported on one hand by the fact that the functional category containing the most spots that increased in relative abundance (five) in Fe-deficient plants grown in the presence of $CaCO_3$ was the defense and stress category, whereas in the absence of $CaCO_3$ no proteins from this category were found to increase significantly (Fig. 3.4.2A and Table 3.4.1). A similar situation was described in the proteomic profiling of roots of in the same plant species (Jorge Rodríguez-Celma, Lattanzio, *et al.*, 2011); this is not only the result of the lack of Fe and the presence of $CaCO_3$, but also of a combination of factors including the basic pH of the growing solution which impairs Fe mobilization in the root apoplast (Mengel, 1994; Zuo *et al.*, 2007; Martínez-Cuenca *et al.*, 2013). Furthermore, the presence of $CaCO_3$ may alter the pH of plant fluids such as the xylem sap and apoplastic fluid causing changes in the chemical speciation of Fe and therefore in Fe availability (Kosegarten, Hoffmann and Mengel, 1999; Lopez-Millan, Morales, Abadia, *et al.*, 2000; Nikolic and Römheld, 2002). On the other hand, the functional category containing most of the spots decreasing in relative abundance was photosynthesis, with six proteins decreasing in relative abundance in the presence of $CaCO_3$ (four of them above and two below the biological cut-off value) in comparison with the four decreasing in the absence of $CaCO_3$. The decreases in the relative abundance of the photosynthesis related proteins affect different isoforms of the Rubisco activase (spots 1, 3 and 7; Supporting Information Fig. 3.4.S6A), the large (spot 4) and small chains (spots 2 and 6) of Rubisco, and the iron-sulfur subunit of the cytochrome b6-f complex (spot 5),which imply a decreased carbon fixation capacity and are in agreement with the well-known Fe deficiency induced impairment of the photosynthetic processes (Martin and H. Marschner, 1988). All proteins identified in the stress and defense category increased in abundance, and were related either to general defense [polyketide cyclase/ dehydratase (spot 9) and PR-5b (spot 12)] or to defense against oxidative

stress [thioredoxin reductase (spot 10), glutathione peroxidase 1 (spot 11) and glutaredoxin C4 (spot 13)]. The polyketide cyclase/dehydratase contains a Betv1 domain and belongs to family 10 of plant pathogenesis-related proteins (PR-10; UniProt annotation) and PR-5b belongs to the thaumatin superfamily (Lytle *et al.*, 2009), both with yet unknown functions. However, some members of PR5 subfamily have been described to play distinctive roles in the defense system that protects against high-salt stress or osmotic imbalance (Tachi *et al.*, 2009), which is also likely to occur in the Fe-deficiency treatment in the presence of $CaCO_3$. The same PR5b protein showed increases in abundance in roots of *M. truncatula* plants grown in the presence of $CaCO_3$ (Jorge Rodríguez-Celma, Lattanzio, *et al.*, 2011).Interestingly, a proteomic study on *Beta vulgaris* roots submitted to several levels of Zn toxicity, which also causes induced Fe-deficiency, found that some Bet v1 proteins, including some PR-10, increased in abundance in rootswhen Zn supply increased (Gutierrez-Carbonell *et al.*, 2013). Therefore, we could speculate that the increases measured in both pathogenesis related proteins in the $CaCO_3$ treatment might be related to osmotic stress caused by both metal imbalances and the presence of $CaCO_3$. On the other hand, increases in proteins related to defense against oxidative stress including thioredoxin reductase (spot 10) and those associated with glutathione metabolism, such as the glutathione peroxidase (spot 11) and the glutaredoxin C4 (spot 13), found in this study, have been reported to increase upon Fe deficiency in different root proteome studies (López-Millán *et al.*, 2013b) and are probably associated with the redox imbalances caused by the lack of Fe. The existence of osmotic and redox unbalances in the high pH treatment is also supported by the *de novo* detection of a pyridoxal biosynthesis protein (spot 31). Pyridoxal, or vitamin B6, is a singlet oxygen quencher and may play a role in osmotic or salt tolerance as well as in oxidative stress resistance (Chen and Xiong, 2005; Tambasco-Studart *et al.*, 2005).

Changes in the protein-related category also indicate a Fe deficiency driven stress situation which was more severe in the presence of $CaCO_3$. Relative increases were observed in three proteins of the heat shock 70 kDa (HSP70) family whose members have direct functions in managing stress situations by preventing misfolded or damaged proteins to aggregate or by facilitating their disposal by interacting with ubiquitin ligases (Lüders, Demand and Höhfeld, 2000). One of the HSP70 (spot 15) increased in both Fe-deficiency treatments (although below the threshold level in the absence of $CaCO_3$), and its *Arabidopsis* counterpart (AtBIP1; At5g28540) is involved in the ER degradation of misfolded proteins (TAIR, https://www.arabidopsis.org/). The decrease measured in the ubiquitin-conjugating enzyme (spot 14) which belongs to the E2 class performing the second step in the ubiquitination pathway (UniProt annotation) may also suggest a role of the ubiquitin-dependent catabolic pathway in the Fe deficiency response. The other two HSP70 (spots 16 and 17) increased only in the presence of $CaCO_3$ and are most likely isoforms of the same protein given their localization in the 2-DE gel

(Supporting Information Fig. 3.4.S6B). These proteins blast to the same *Arabidopsis* orthologue (AtHsp70–10, At5g09590) that has been suggested to play an important role in the regulation of the Fe-S assembly pathway in mitochondria (Leaden, Busi and Gomez-Casati, 2014). Their increases may be related to the decreases measured in Fe-S cluster proteins, including the NADH-ubiquinone reductase (spot 24) of the respiratory chain complex I, the Fe-S subunit of the cytochrome b6f complex (spot 5) and the ferredoxin nitrite reductase (spot 23). On the other hand, significant changes in the protein translation machinery were only observed in the Fe deficiency treatment in the presence of $CaCO_3$, affecting two structural components of the ribosome (spots 19 and 21) and an elongation factor (spot 20). Changes in the abundance of some components of the ribosome induced by Fe deficiency have been described in *Arabidopsis* roots and authors speculated that these changes can control mRNA preference and bias translation efficiency towards specific sets of genes (Lan *et al.*, 2011; Lan, Li and Schmidt, 2012; Rodríguez-Celma, Chun Pan, *et al.*, 2013), but they also may indicate the need of de novo synthesis of Fe-deficiency effector proteins. The fact that these changes are only observed in the presence of $CaCO_3$ reinforces the strong effect of this treatment in the stem proteome.

Several lines of evidence support that Fe deficiency causes alterations in the cell wall of stem tissues, especially in the presence of $CaCO_3$. First, the increases in relative abundance measured in two protein species involved in the phenylpropanoid biosynthesis pathway: the phenylcoumaran benzylic ether reductase (PCBER, spot 29) and a putative O-methyltrasferase similar to the caffeoyl-CoA O-methyltransferase 1 (spot 30). PCBER has been shown to be one of the most abundant proteins in the xylem of poplar (Gang *et al.*, 1999) that participates in lignan synthesis (Vander Mijnsbrugge *et al.*, 2000) and the O-methyltrasferase probably plays a role in the methylation steps necessary for the biosynthesis of monolignols, the lignin precursors (Do *et al.*, 2007). Their increases suggest that Fe deficiency may cause changes in lignification. A second line of evidence is provided by the lignin Py-GC/MS analysis of the petioles, which showed a small but significant relative increase in the lignin per protein ratio in Fe-deficient petioles when compared to the controls, which was more intense in the presence than in the absence of $CaCO_3$ (Table 3.4.2). Finally, the microscopy study of petiole sections also indicates stronger alterations in plants grown in the presence than in the absence of $CaCO_3$. In petioles from plants grown in the presence of CaCO3, phloroglucinol staining indicates an increase in lignin in the inner part of the xylem vessels (Fig. 3.4.4F), and the shift towards a green color in the autofluorescence signal in the same area suggests the existence of changes in lignin composition (Fig. 3.4.4C); similar shifts in autofluorescence have been associated elsewhere with changes in lignin composition (Djikanović *et al.*, 2012). When Fe-deficient plants were grown in the absence of $CaCO_3$, changes in the micrograph images relative to the controls were less marked (Fig. 3.4.4B,E). Conversely to what occurs in the petioles, in the case of the stems from Fe-deficient plants the lignin/protein

ratio, the lignin composition and the autofluorescence and phloroglucinol micrographs did not differ from those of control plants, and this is likely due to the fact that these stems were developed before the onset of Fe deficiency.

Overall, cell wall-related changes observed in petioles of plants grown in the presence of $CaCO_3$ should led to an increase in cell wall rigidity, especially in the xylem vessels. Changes in cell wall composition resulting in increased lignification have been described to occur upon mineral imbalances, for instance in the roots of Fe-deficient pear and quince cultivars (Donnini *et al.*, 2009), and have also been suggested as a detoxification strategy for excess Cd in roots (Lux *et al.*, 2011; Redjala *et al.*, 2011). Modification in cell wall related proteins have also been described in proteomic studies of Fe-deficient roots (López-Millán *et al.*, 2013b). It has been hypothesized that increased lignification may provide a protective barrier to avoid the lateral transport and distribution of minerals by decreasing the permeability of the cell wall (Higuchi, 1981). In leaves, Fe deficiency also elicits structural changes in morphology, including a reduction of the leaf xylem vessel size, which could disturb normal stomatal functioning (Fernández *et al.*, 2008; Eichert *et al.*, 2010).

Other effects of Fe deficiency in the stem protein profiles included increases in several spots identified as malate dehydrogenase (spots 25–27 in Table 3.4.1 and Supporting Information Fig. 3.4.S6C) and in a serinehydroxymethyl-transferase (spot 28) in both treatments that were also described in the proteome of Fe-deficient *M. truncatula* roots (Jorge Rodríguez-Celma, Lattanzio, *et al.*, 2011). Increases in both proteins have been reported in physiological and proteomic studies on Fe deficiency in roots and leaves (Abadía *et al.*, 2002; López-Millán *et al.*, 2013b) and results from this study indicate this may be a common response throughout plant organs.

Mineral analyses indicate the existence of alterations in micro- and macronutrient balances as a result of Fe deficiency. Although the stem Fe concentrations did not decrease significantly in Fe-deficient plants grown in the absence of $CaCO_3$, Fe content decreases occurred in both Fe deficiency treatments (Fig. 3.4.3, Supporting Information Fig. 3.4.S3). The decrease in stem Fe concentration in the presence of $CaCO_3$ was accompanied at the proteomic level by decreases in relative abundance of three Fe containing proteins related to energy production: a subunit of a NADH-ubiquinone oxidoreductase (spot 24), the ferredoxin-nitrite reductase (spot 23), and the cytochrome b6-f complex (spot 5). Decreases in abundance in Fe-containing, energy related proteins have been widely described in different proteomic studies as a result of Fe shortage (López-Millán *et al.*, 2013b), and this could ultimately account for the reduction in stem mass.

3.4.5. Conclusions

A summary of the proteomic results is shown in Fig. 3.4.5. Overall results indicate that Fe deficiency by itself has a mild effect on the stem proteome of *M. truncatula* plants, mainly affecting photosynthesis-related proteins. However, Fe deficiency in the presence of $CaCO_3$ has a stronger impact on the proteome, including a general increase in stress and protein metabolism related proteins not observed in Fe-deficient plants grown without $CaCO_3$, as well as a larger number of photosynthesis related proteins decreasing. These results probably indicate the existence of mineral and osmotic unbalances. Iron deficiency also elicited significant increases in cell wall related proteins and in the lignin per protein ratio, which were more intense in the presence of $CaCO_3$. Changes in the lignin S and G monomer composition induced by Fe-deficiency and the microscopy study of petiole sections further confirm the existence of alterations in cell walls of petiole tissues. These results suggest that Fe-deficient plants, especially those grown in the presence of $CaCO_3$ as occurs in many arable soils, present an increased lignification and a probable lower capacity of cell walls to interact with ions in the xylem fluid, which ultimately may affect solute transport and distribution to the leaves.

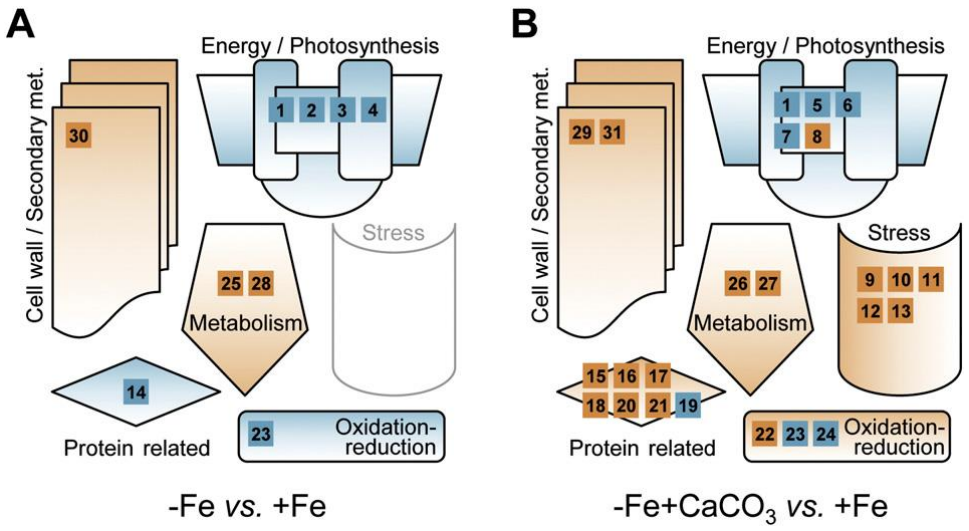

Fig. 3.4.5. *Changes inmetabolic pathways as affected by Fe deficiency without (A) andwith $CaCO_3$ (B) when compared to Fe-sufficient plants. Pathways related to the identified proteins were integrated according to the GO annotation. A statistical Student t-test was performed to show relevant changes between samples. Orange symbols mark newly detected and proteins with increased relative abundance compared to controls (using a two-fold threshold change). The same threshold (decreases larger than 50%) was selected for proteins with decreased relative abundance (blue symbols). Numbers correspond to those in Table 3.4.1.*

Acknowledgements

Work supported by the Spanish Ministry of Science and Competitiveness (MINECO; projects AGL2012-31988, AGL2011-25379 and AGL2013-42175-R, co-financed by FEDER), the Aragón Government (group A03), and the US Department of Agriculture, Agricultural Research Service (under Agreement number 58-6250-0-008 to MAG). Support was obtained by contracts I3P-CSIC (JRC), FPI-MINECO (GL and LC-L), JAE-PRE-CSIC (EG-C) and JAE-DOC-CSIC (JR), co-financed by the European Social Fund. Authors thank A. Calviño for assistance in growing and harvesting plants. The contents of this publication do not necessarily reflect the views or policies of the US Department of Agriculture, nor does mention of trade names, commercial products, or organizations imply endorsement by the US Government.

Supporting Information for Chapter 3.4

All additional supporting information may be found in the online version of this article (doi: 10.1016/j.jprot.2016.03.017).

- ***Figure 3.4.S1.*** *Tissue sampling.*

- ***Figure 3.4.S2.*** *PCA analysis.*

- ***Figure 3.4.S3.*** *Mineral contents in leaves and roots.*

- ***Figure 3.4.S4.*** *Mineral concentrations in leaves and roots.*

- ***Figure 3.4.S5.*** *Autofluorescence and staining patterns.*

- ***Figure 3.4.S6.*** *Differential protein expression.*

- ***Table 3.4.S1.*** *Univariate statistical analysis of 2-DE gels. Spot volumes in all samples (15 gels, 3 treatments and 5 biological replicates) are listed in columns C-Q. Column A shows spot identifier assigned by the PDQuest v.8.0 software and column B shows spots with changes statistically significant ($p \leq 0.05$) and above the cut-off values numbered as in Table 3.4.1. t-Student test values, fold changes, mean values and standard deviations are shown in columns R-S, T-V, V-X and Y-AA, respectively.* This Table is not included here due to the size of the files; doi: 10.1002/pmic.20120051.

- ***Table 3.4.S2.*** *List of peptides identified.*

- ***Table 3.4.S3.*** *Summary of the 2-DE protein profiling results.*

Figure 3.4.S1. *Tissue sampling: protein extract from stem tissues (including main stems and petioles but excluding cotyledons and leaves*

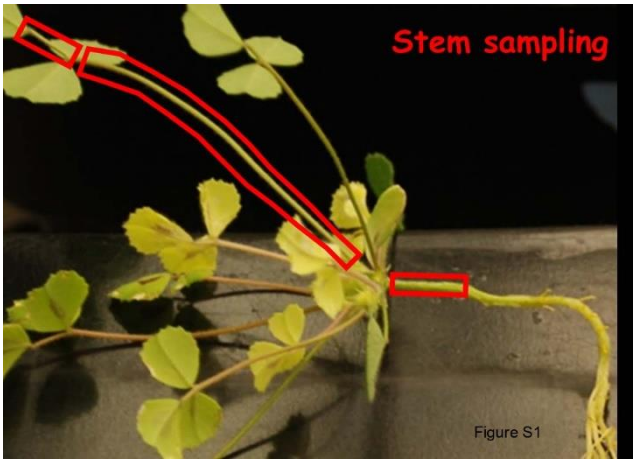

Figure 3.4.S2. *PCA analysis was run using all consistent spots, the samples from Fe-deficient plants in the presence of $CaCO_3$ were well separated, whereas those from Fe sufficient plants and Fe-deficient plants grown without $CaCO_3$ overlapped (Fig. 3.4.S2A). However, when the PCA analysis was run using only those spots showing significant differences in relative abundance, samples from the three treatments were clearly separated (Fig. 3.4.S2B).*

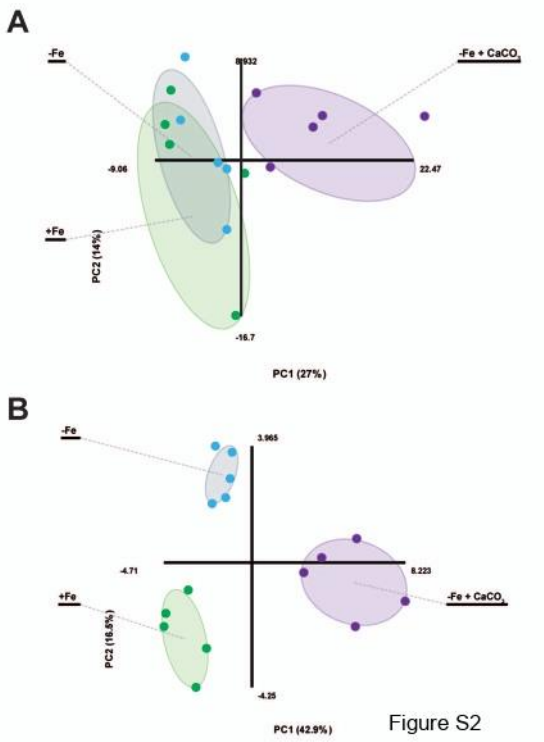

Figure 3.4.S3. *Mineral analyses indicate the existence of alterations in micro- and macronutrient balances as a result of Fe deficiency.*

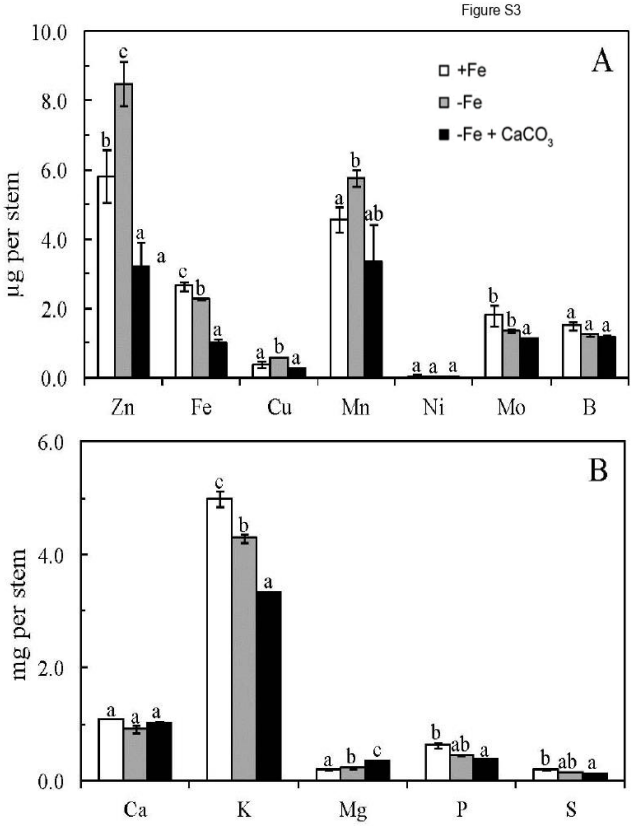

Figure 3.4.S4. *The mineral composition of leaves and roots.*

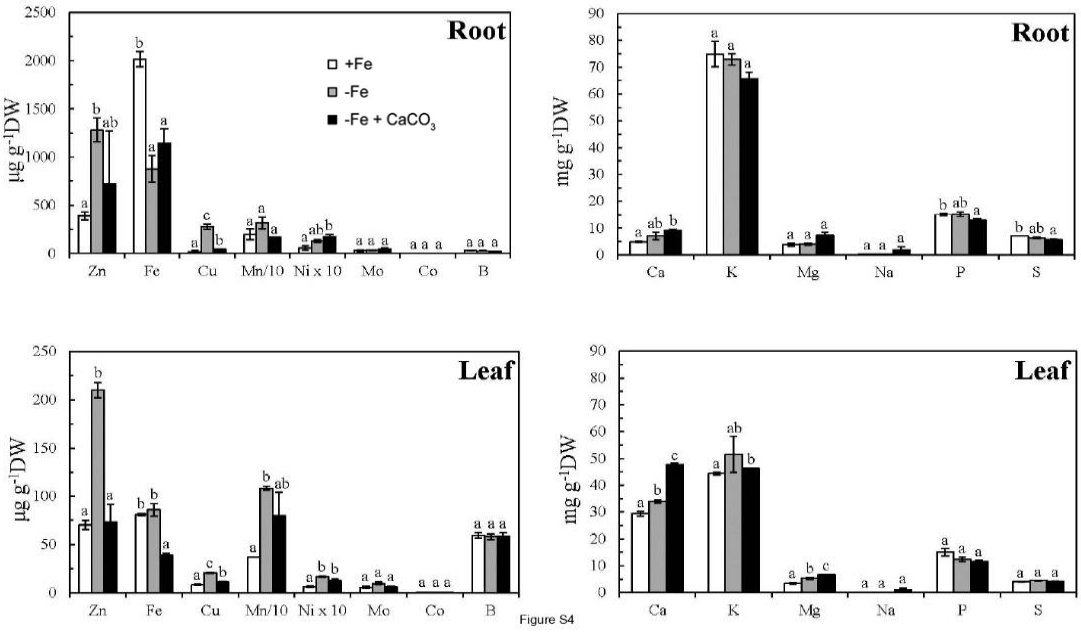

Figure 3.4.S5. *Stems of Fe-sufficient plants showed a clear blue autofluorescence in the xylem vessels and a more diffuse one in the cortex, and similar results were observed when phloroglucinol was used for lignin staining. Stems from Fe deficient plants showed similar autofluorescence and staining patterns to those of controls, irrespective of the presence of $CaCO_3$ in the nutrient solution.*

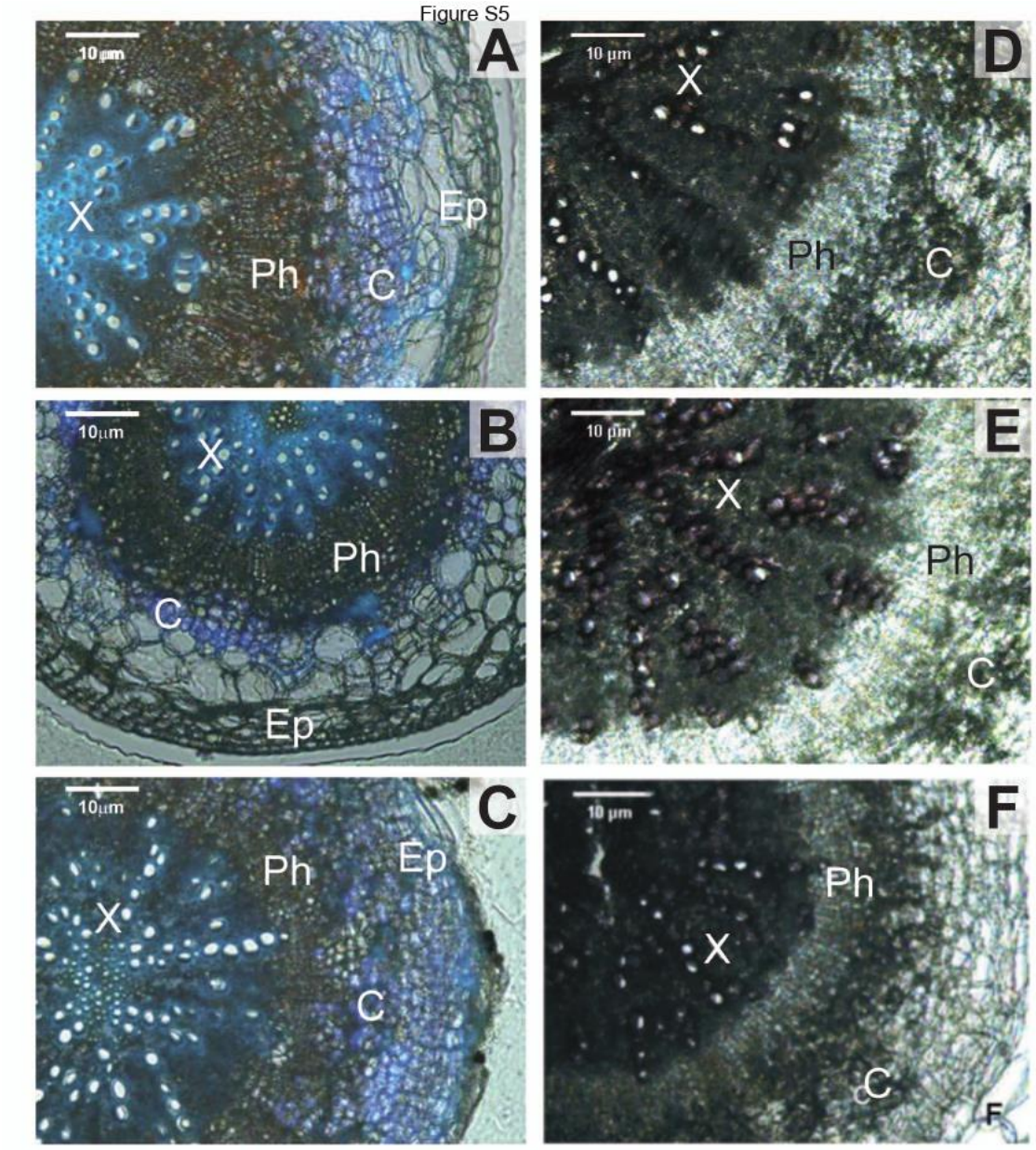

Figure 3.4.S6. *Differential protein expression in the 2-DE gels. A: The decreases in the relative abundance of the photosynthesis related proteins affect different isoforms of the Rubisco activase (spots 1, 3 and 7); B: HSP70 (spots 16 and 17) increased only in the presence of $CaCO_3$ and are most likely isoforms (spot 15) of the same protein given their localization; C: Malate dehydrogenase (spots 25–27) and serinehydroxymethyl-transferase (spot 28) increase during Fe deficiency, in both treatments.*

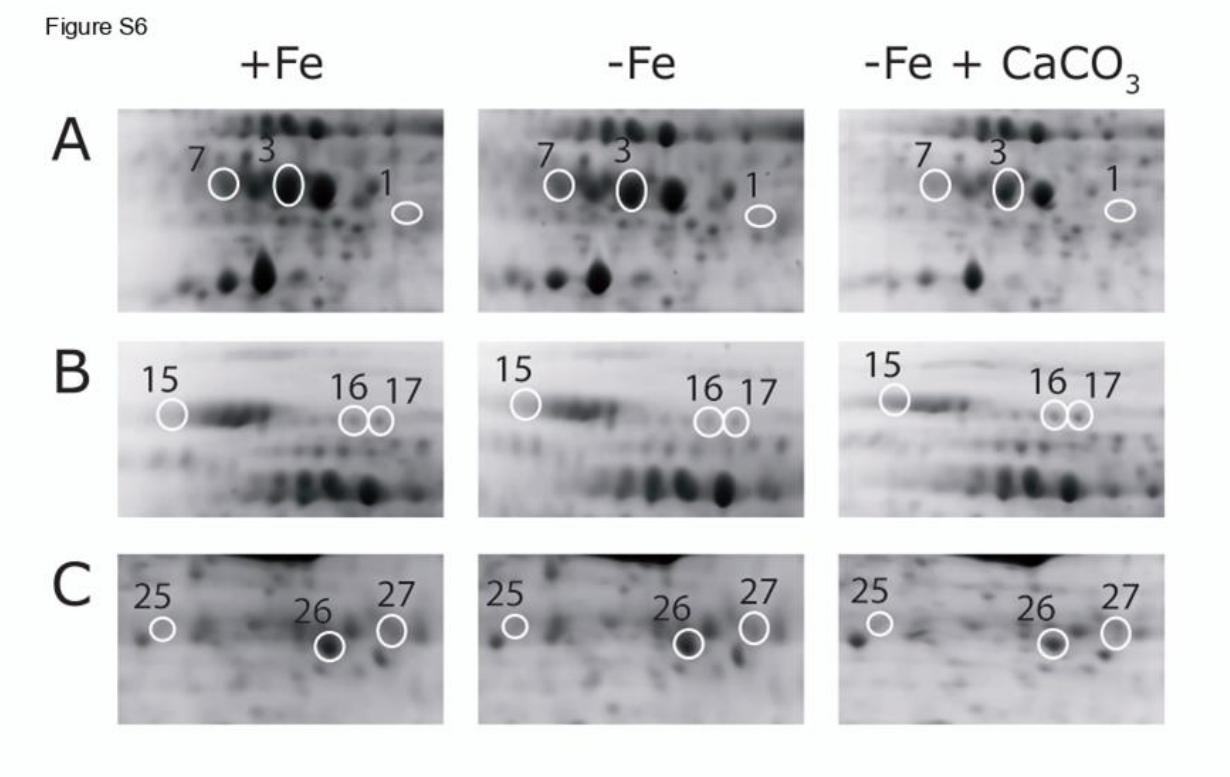

Table 3.4.S2. *The list of peptides identified: we used the GO biological process annotation (http://www.geneontology.org) of the individual identified proteins and UniProt database information for manual classification into functional categories.*

Spot n	SSP	UniProt Identifier	Protein description	Sequence	Ions score
1	5502	Q40073	Rubisco activase A	K.GLAYDISDDQQDITR.G	97
				K.MGINPIMMSAGELESGNAGE PAK.L + 3 Oxidation (M)	65
2	8007	B7FMC2	Rubisco small chain 3A	K.FETLSYLPPLTR.E	47
				K.GWVACLEFETEK.G	96
				R.ENHSSPGYYDGR.Y	43
				K.LPLFGATDASQVLK.E	52
				K.ELDEVVVAYPNAFVR.I	47
				R.QVQCISFIAHTPEVY.-	59

Spot n	SSP	UniProt Identifier	Protein description	Sequence	Ions score
3	2605	A0A072UZ59	Rubisco activase	R.GLAYDISDDQQDITR.G	52
				K.QYNFDNTMDGFYIAPAFMD K.L + 2 Oxidation (M)	32
				K.NFLTLPNIK.V	41
				K.VPLILGVWGGK.G	10
				K.SFQAELVFAK.M	25
				K.MGINPIMMSAGELESGNAGE PAK.L + 3 Oxidation (M)	54
				K.MCCLFINDLDAGAGR.M + Oxidation (M)	59
				R.VPIIVTGNDFSTLYAPLIR.D	49
				K.IVDTFPGQSIDFFGALR.A	50
				K.WVSGVGIETIGK.K	67
				K.DGPPVFEQPK.M	65
				K.LLEYGNMLVSEQENVK.R + Oxidation (M)	60
				K.LLEYGNMLVSEQENVKR.V + Oxidation (M)	55
				K.YLEGAALGDANQDAIK.E	78
4	3104	P28459	Rubisco large chain	R.EITLGFVDLLR.D	62
				R.EGNEVIRYASK.W	2
5	3106	B7FGU7	Cytochrome b6-f complex iron-sulfur subunit	K.DAVGNDVVAAEWLK.S	83
				K.GDPTYLVVESDR.T	73
6	8013	KEH21532	Rubisco small chain	K.FETLSYLPPLTR.E	37
				K.EVEYLIR.K	27
				R.ENHSSPGYYDGR.Y	14
				K.LPLFGATDASQVLK.E	81
				K.ELDEVVVAYPNAFVR.I	56
				R.IIGFDNVR.Q	60
7	603	Q8GTY4	Rubisco activase	K.MGINPIMMSAGELESGNAGE PAK.L + Oxidation (M)	82
				K.MCCLFINDLDAGAGR.M + Oxidation (M)	108
				R.VPIIVTGNDFSTLYAPLIR.D	47
				K.IVDTFPGQSIDFFGALR.A	58
				K.LLEYGNMLVSEQENVK.R + Oxidation (M)	97
				K.YLEGAALGDANQDAIK.E	87
8	402	P14226	Oxygen-evolving enhancer protein 1	R.LTFDEIQSK.T	44
				K.GTGTANQCPTIDGGVDSFSF KPGK.Y	47
				K.IQGVWYAQLES.-	50

Spot n	SSP	UniProt Identifier	Protein description	Sequence	Ions score
9	103	B7FKA0	Polyketide cyclase/dehydrase and lipid transporter	R.HFTYAEGSQLAK.S	46
				K.VSNDIPDPSIVK.N	35
				K.NFIEVDEYVQSLAA.-	66
10	3408	A6XJ26	Thioredoxin reductase	K.FGTEIFTETVSK.V	52
				R.TVEADSVIVATGAVAK.R	103
11	6104	Q56VU1	Glutathione peroxidase 1	R.GNDVNLGDYK.G	69
				R.YAPTTSPLSIEK.D	56
12	7202	B6ZHC0	PR-5b protein	R.GQTWNLWVNPGTAMAR.I + Oxidation (M)	84
				R.CHDSYSYPQDDPTSTFTCPAGSNYK.V	75
13	6004	A0A072TXU3	Glutaredoxin C4	K.EIVSSNPVVVFSK.S	74
				K.AVELDSESDGSEIQGALAQWTGQR.T	34
14	7102	B7FF81	Ubiquitin-conjugating enzyme	R.EYSMEDILTQLK.K Oxidation (M)	47
				K.LVQPPEGTYF.-	30
15	907	P49118	78 kDa Glucose-regulated protein homolog	K.DAGVIAGLNVAR.I	93
				R.IINEPTAAAIAYGLDK.K	114
				R.FEELNNDLFR.K	63
				K.NQIDEIVLVGGSTR.I	98
16	2905	G7JU14	Heat shock 70 kDa protein	R.QAVTNPTNTLFGTK.R	80
				K.APNGDAWVEINK.Q	94
				K.MKETAEAYLGK.T + Oxidation (M)	42
				K.AVVTVPAYFNDAQR.Q	64
				K.FEALVNNLIER.T	71
				K.DVDEVLLVGGMTR.V + Oxidation (M)	84
				K.VQEVVSEIFGK.S	68
				K.SQVFSTAADNQTQVGIK.V	93
				K.SLGEFDLVGIPPAPR.G	31
				R.SSGGLSDDEINNMVK.E + Oxidation (M)	79
				K.NSADTSIYSIEK.S	79
				K.EIENSVSDLR.T	61
				R.TAMEGESVDEIK.T + Oxidation (M)	42
17	3901	P37900	Heat shock 70 kDa protein. mitochondrial	R.QAVTNPTNTLFGTK.R	65
				K.AVVTVPAYFNDAQR.Q	53
				K.DVDEVLLVGGMTR.V + Oxidation (M)	80
				K.SLGEFDLVGIPPAPR.G	43

Spot n	SSP	UniProt Identifier	Protein description	Sequence	Ions score
18	8205	P38548	GTP-Binding nuclear protein Ran/TC4	K.LVIVGDGGTGK.T	40
				R.HLTGEFEK.K	27
				R.VCENIPIVLCGNK.V	63
				K.NLQYYEISAK.S	45
19	606	XM_003594608	30S Ribosomal protein S1	R.NAPMEGVSFTLDQFTETLEK.Y + Oxidation (M)	46
				K.STAYLPLYEASLYK.L	74
				K.GGVVAEVEGLK.G	51
				K.SPGEEIIEFEVPLK.F	76
				R.ISDIVTVLQPGDTLK.V	49
20	7601	D7KCE2	Elongation factor Tu	K.AVAFDEIDK.A	31
				K.VDAVDDPELLELVEMELR.E	112
				R.ELLSFYK.F	16
				K.FPGDDIPIIR.G	71
				R.GSALSALQGTNEEIGR.K	111
				K.VELPENVK.M	25
21	3107	G7LE33	40S Ribosomal protein S12	K.HAAQLCVLAEDCDQPDYVK.L	35
				K.ALCAEHSVSLLTVPNAK.T	36
				K.TLGEWAGLCK.I	55
				K.VTGCSCVVVK.D	57
				K.DFGEEHEAYNVVLQHVK.S	35
22	7805	O81413	Ferric leghemoglobin reductase-2	K.GIEGLFK.K	28
				K.VVGVDTSGDGVK.L	39
				K.AEEDGVACVEYIAGK.V	43
				K.AIDNAEGLVK.I	63
				R.VCHAHPTMSEAVK.E + Oxidation (M)	32
				K.EAAMATYDKPIHI.- + Oxidation (M)	24
23	7804	G7JL79	Ferredoxin-nitrite reductase	R.GVTLPDVPEILK.G	52
				K.GLAEVGLTSLQSGMDNVR.N + Oxidation (M)	51
				K.LEALLNEPLLK.D	61
				K.ATEGVDIFLGGR.I	62
24	7909	G7J8R4	NADH-Ubiquinone oxidoreductase 75 kDa subunit	R.GSGEEIGTYVEK.L	27
				R.LNEDINEEWISDK.T	70
				K.ADAFLLVGTQPR.V	51
				K.FVYLMGADDTNLDK.I + Oxidation (M)	109
				R.LPYDTIGGVR.A	55

Spot n	SSP	UniProt Identifier	Protein description	Sequence	Ions score
25	5507	Q9FT00	Malate dehydrogenase 2	K.MELVDAAFPLLK.G Oxidation (M)	42
				K.VLVVANPANTNALILK.E]	30
26	7502	O48904	Malate dehydrogenase precursor	R.SQVTGYAGEDELGK.A	67
				K.ALEGADVVIIPAGVPR.K	112
				K.SLATAISK.Y	53
				R.LFGVTTLDVVR.A	89
				R.TQDGGTEVVTAK.A	66
				K.NGVEEILGLGSLSDFEK.Q	105
				K.QGLENLK.S	49
27	7509	B7FJQ4	Malate dehydrogenase	R.LNVQVSDVK.N	25
				K.MELVDAAFPLLK.G + Oxidation (M)	60
				K.IVQGLSIDEFSR.K	66
				K.LDLTAEELSEEK.N	92
				K.KLDLTAEELSEEK.N	109
28	8801	A9YWS0	Serine-hydroxymethyltransferase	K.QLNSSLEEIDPEIADIIELEK.A	50
				K.LKDFVETLQSSSYVQSEISK.L	37
29	4408	B7FHV0	Phenylcoumaran benzylic ether reductase-like protein Fi1	K.VGLAQMLR.G + Oxidation (M)	66
				R.GGVIMDVVNAEQAR.I + Oxidation (M)	99
				R.MSDPQLIK.E + Oxidation (M)	50
				K.GEAGTGNIIEAVR.H	76
				R.NMDEDEVFTFAK.K + Oxidation (M)	64
				K.IGAPYDLVMQTK.Q + Oxidation (M)	61
30	2306	B7FIC1	Putative O-methyltransferase	K.NTMEIGVYTGYSLLATALAIP EDGK.I Oxidation (M)	18
				K.ENYELGLPVIK.K	51
				R.EGPALPVLDEMIK.D+ Oxidation (M)	18
				R.DFVLELNK.A	27
31	4406	Q45FF2	Pyridoxal biosynthesis protein PDX1.3	R.GGVIMDVVNAEQAR.I	100
				K.GEAGTGNIIEAVR.H	84
				R.NMDEDEVFTFAK.K	85
				K.IGAPYDLVMQTK.Q	65

Table 3.4.S3. *Summary of the 2-DE protein profiling results. Stem (including petioles) fresh weight (g stem^{-1}), percentage of petioles in the proteomic sample which includes petioles and stems, protein yield (µg protein g^{-1} stem FW), average number of spots, number of spots changing significantly in relative abundance (t-test at $p \leq 0.05$) and above a two-fold threshold, and number of spots newly detected, showing increased and decreased relative abundance and no longer detected. Numbers in brackets indicate identified proteins.*

	+Fe	**-Fe**	**-Fe+$CaCO_3$**
Fresh weight stem including petioles (g^{-1} stem)	0.65 ± 0.24	0.50 ± 0.12	0.39 ± 0.13
% petioles (g FW [petiole] g^{-1} FW [petiole and stem])	57 ± 3	58 ± 2	57 ± 3
Protein yield (µg protein g^{-1} FW stem including petioles)	632 ± 187	806± 243	800 ± 407
Number of spots	265 ± 2	261± 2	267 ± 2
Number of consistent spots	272		
	-Fe *vs.* +Fe	**-Fe+$CaCO_3$ *vs.* +Fe**	
Spots with significant intensity changes (p<0.05; fold ≥ 2 or ≤ 0.5)	10	31	
Number of new spots	0	4 (4)	
Number of spots with increased abundance	3(3)	18 (13)	
Number of spots with decreased abundance	5 (5)	6 (5)	
Number of lost spots	2 (1)	3 (2)	

Capítulo 4

DISCUSIÓN GENERAL

A lo largo de esta Tesis Doctoral, se han estudiado los fenómenos relacionados con homeostasis de Fe en varias especies vegetales utilizadas como modelo (patrones *Prunus dulcis* × *Prunus persica*, *Lupinus texensis* y *Medicago truncatula*). La aplicación de un enfoque proteómico mediante el análisis de diferentes tejidos, como tallo, raíz y savia de floema, ha arrojado luz sobre procesos específicos afectados por la deficiencia de Fe en estos tejidos.

Esta aproximación analítica ha permitido obtener una visión global sobre los diferentes perfiles proteicos y de los procesos metabólicos implicados en la deficiencia de hierro. Además de análisis proteómicos clásicos, basados en la electroforesis bidimensional en geles (2DE-PAGE), se han sentado las bases para el uso de una nueva tecnología experimental: MALDI-*Mass Spectrometry Imaging* (MALDI-MSI). Esta nueva herramienta, poco empleada en plantas, ha demostrado ser un potente aliado en el análisis de la distribución espacial de metabolitos y proteínas en los diferentes tejidos vegetales.

En este apartado se lleva a cabo la discusión integral de los resultados obtenidos en los diferentes estudios realizados, mediante la utilización de técnicas proteómicas y de nuevas tecnologías, como el MALDI-MSI, para elucidar los mecanismos relacionados con la nutrición en las plantas. Se pone el foco sobre la homeostasis del Fe, y en particular sobre sus efectos a nivel de la expresión de proteínas y de las alteraciones metabólicas inducidas. El trabajo pretende describir los cambios causados a nivel fisiológico por los estreses de Fe, incluyendo tanto su deficiencia como su reposición. Para ello, se han utilizado varias plantas modelo para el análisis de diferentes sub-proteomas (savia de floema, tallo y raíz), con el fin de obtener una visión global de los fenómenos relacionados con la homeostasis de este metal y de los mecanismos que se activan en los tejidos responsables de la absorción y el transporte del Fe en las plantas. La discusión está organizada siguiendo los objetivos planificados.

4.1. Aplicando nuevas tecnologías, el MALDI-Mass Spectrometry Imaging (MALDI-MSI): optimización de los parámetros analíticos al empleo de muestras vegetales

Esta primera parte del trabajo consistió en la optimización de protocolos de preparación de muestra que permitieran analizar la distribución espacial de pequeñas moléculas, utilizando crio-disecciones de granos inmaduros de cebada (*Hordeum vulgare*) y de raíz de tabaco (*Nicotiana tabacum*) cultivados en condiciones control.

Tanto en el caso de los granos de cebada como en el de las raíces de tabaco, el procedimiento debía preservar, en la medida de lo posible, la estructura tridimensional de estas muestras, que son complejas y comprenden diferentes tipos de tejido (por ejemplo, tejidos parenquimáticos, colenquimáticos y vasculares). Durante la fase inicial del desarrollo vegetal, el grano de cebada contiene una elevada proporción de agua, lo que hace que la preparación de las muestras sea bastante sencilla. Sin embargo, los granos más maduros contienen mucha menos agua libre, por lo que su seccionamiento (crio-disección) requiere una atención especial. Los objetivos específicos fueron la optimización de los protocolos empleados, en cuanto a: la preparación de las secciones de tejido; la elección de la matriz y la aplicación de la misma; y los parámetros de adquisición del MALDI-MSI y posterior análisis de datos.

Preparación de las secciones de tejido

La preparación de la muestra es especialmente delicada cuando hay un conjunto de tejidos altamente diferenciados. Convencionalmente, la mayoría de los cortes empleados para el MALDI-MSI tienen un grosor de entre 10 y 20 µm (Goodwin, Pennington and Pitt, 2008; Amstalden van Hove, Smith and Heeren, 2010). Sin embargo, el grosor óptimo de los cortes depende en gran medida del tipo de tejido investigado.

Para realizar los cortes de tejido se empleó un criotomo convencional. No se pudo seguir los procedimientos histológicos estándar, como los empleados en la preparación de cortes para inmuno-tinción o tinción con colorantes, debido a que la incrustación en compuestos poliméricos, como la resina sintética (HM20), o el uso del medio OCT (*optimal cutting temperature*), dan lugar a fenómenos de supresión de la ionización de los analitos durante las mediciones por espectrometría de masas (MS). Por lo tanto, en lugar de embeberlas, las muestras se fijaron en la orientación deseada con una pequeña gota de medio de fijación en el bloque de corte del instrumento (criotomo). El uso de secciones congeladas no embebidas en medio de fijación requiere un alto grado de competencia técnica. Para la fijación, se testaron dos compuestos, OCT y agua (hielo). Se realizaron una serie de cortes transversales tanto de las raíces principales y laterales del tabaco como de los granos de cebada cosechados a

diferentes DAP (para más detalles, véase Fig. 3.1.1a,b). Resultó imposible evitar la supresión de la ionización por la contaminación con OCT en los granos de cebada menores de 6 DAP y en las secciones longitudinales de las raíces de tabaco, por lo que se prefirió el agua (hielo) como medio de fijación. Este hecho dio lugar a un grado apreciable de difusión de los analitos durante la fase de la descongelación del tejido, que se hace visible como una mancha alrededor de la sección (para más detalles, véase Fig. 3.1.1c,d). Otros métodos, como es la fijación con película adhesiva (utilizado con éxito para el análisis de granos de arroz) (Kawamoto, 2003; Zaima, 2012), resultaron ser poco práctico para el tamaño reducido de las muestras utilizadas en el presente trabajo.

Otro parámetro importante a la hora de optimizar la producción de secciones es el grosor de las mismas. La influencia del grosor de la sección de la raíz en el resultado de la técnica del MALDI-MSI se puede observar en la Fig. 3.1.2a, que muestra imágenes de cuatro iones de aducción molecular detectados en secciones transversales de 35, 45 y 55 µm de una raíz lateral de tabaco. Cuando el grosor de corte fue superior a 45 µm se observó una notable disminución de la señal (sensibilidad), especialmente al analizar los patrones de distribución en la raíz central de tabaco. La pérdida de señal del espectro de masas en esta región de la raíz probablemente refleja los efectos de absorción de la matriz, ya que las intensidades de la señal para la corteza de la raíz eran bastante independientes del grosor de la muestra. Para las muestras de tabaco de 8 semanas se consiguieron obtener secciones transversales de la raíz principal de 55 µm, y para la raíz lateral secciones longitudinales de 55 µm y transversales de 40 µm (Fig 3.1.1). En ambos casos, estas secciones son más gruesas que las utilizadas habitualmente para los experimentos de MALDI-MSI, pero fueron necesarias para evitar la ruptura del tejido causada por los grandes espacios intercelulares de la corteza del parénquima. Para los granos jóvenes de cebada (1-7 DAP), los cortes de 20 µm fueron eficaces en la preservación de la estructura del tejido, pero a medida que el grano se desarrollaba, la acumulación de almidón (asociada a una pérdida de contenido de agua) obligó a aumentar el grosor de la criosección hasta 30-40 µm (Fig. 3.1.1a). El aumento del grosor de la sección tuvo un efecto negativo en la intensidad de la señal de MS, debido a la mayor absorción de la matriz por el tejido, por lo que la preparación de secciones de los granos de cebada se fijó en 30 µm. A diferencia de lo observado en raíz, hubo menos efectos de matriz dependientes del tipo de tejido para los granos de cebada, y la estructura del grano, menos frágil, permitió el uso de secciones más delgadas.

Elección de la matriz y aplicación de la misma

Para nuestro trabajo seleccionamos las llamadas "esponjas protónicas", un tipo de matriz introducida por Shroff y Svatoš (Shroff and Svatoš, 2009), como son HCCA, DHB, DMAN y DTCB. Debido a su fuerte basicidad, este tipo de matrices es útil para el análisis por MS de aniones en modo negativo. De las matrices probadas, la matriz DHB dio los resultados mejores resultados, debido a la

estrategia de aplicación de la matriz, el *background* derivado de la misma (*Supporting Information* Fig. 3.1.S1) y la reproducibilidad de los espectros de MALDI-MSI obtenidos (Fig. 3.1.5).

Uno de los aspectos más complejos del MALDI-MSI está relacionado con la reproducibilidad en la aplicación de la matriz utilizada para el análisis (Gustafsson, McColl and Hoffmann, 2008). Las técnicas de deposición de la matriz más utilizadas son la pulverización con un simple aerógrafo o el uso de un instrumento específicamente diseñado para obtener la vaporización vibracional de la matriz. Nosotros adoptamos este último enfoque, basado en un instrumento Image-Prep de Bruker, que es capaz de aplicar una serie de capas de matriz, con un periodo de incubación y secado entre cada paso de deposición. Se obtuvieron capas reproducibles con HCCA, DCTB y DHB. Sin embargo, la matriz DMAN no pudo depositarse por vaporización vibracional, ya que su química impide una formación adecuada de cristales. Para conseguir una reproducibilidad óptima, era necesario el uso de placas de pulverización nuevas. Un enfoque alternativo a la pulverización, que consigue una resolución de 10-100 µm, hubiera sido el uso de la tecnología de microchips (con una resolución espacial de <20 µm) o la sublimación (con una resolución de 1 µm), que consiguen una mejor resolución espacial (Agar *et al.*, 2010; Kaletaş *et al.*, 2009).

Un parámetro critico a tener en cuenta a la hora de una correcta elección de la matriz es la presencia de señales derivadas de dicha matriz en MALDI-MSI. La matriz emite señales y estas son causadas por la fragmentación de la misma y/o la formación de *clusters*. Dentro el proceso de evaluación de los datos provenientes de la técnica del MALDI-MSI, es muy importante poder discernir entre las señales provenientes de la matriz y los picos generados por la muestra. Por esta razón, en cada experimento de MSI se incluye la medición también de una región espacial tomada como referencia o "blanco" que está ocupada sólo por la matriz. La comparación de las señales de masas (expresadas como *m/z*; masa/carga) es crucial durante el análisis de los datos. En este proceso se superponen los espectros de masas acumulados durante el experimento y se comparan los picos en ambas regiones de medición (blanco *vs.* muestra), permitiendo substraer las señales provenientes de las muestras retirando las interferencias provenientes de la misma matriz, seleccionando así el patrón único de señales que provienen sólo del tejido. Para ello, se estudiaron los espectros de masas obtenidos con cada una de las matrices utilizadas. HCCA, DHB, DMAN y DTCB se compararon en modo de ionización positiva y negativa. Se llegó a la conclusión de que para nuestro estudio el DHB era la mejor opción en modo de ionización positiva, generando el menor número de interferencias asociadas con la fragmentación de DHB y la formación de clústeres con las señales generadas a partir de nuestros tejidos. El uso de este compuesto tiene la limitación de que muchas de las señales en la región de bajo rango de masas (*m/z* <400 Da) podrían estar relacionadas con el mismo DHB, por lo que era necesario sustraerlas durante el proceso de evaluación de datos (Fig. 3.1.3). También se han introducido otros reactivos que mejoran la ionización, como son las nanopartículas de plata u oro (Hua *et al.*, 2007; Wu *et al.*, 2009), y los coloides

y el grafito (Svatoš, 2010). Estos compuestos parecen tener ventajas en la detección de lípidos, y tienden a producir menos señales y de menor intensidad, mejorando así la resolución espacial de la técnica. Sin embargo, el uso de estas matrices requiere la optimización de los protocolos de aplicación y tener muy en cuenta el tipo de compuesto/diana que se quiere analizar.

Parámetros de MALDI-MSI y análisis de datos

Reproducibilidad

La reproducibilidad de los resultados mediante el MALDI-MSI se refleja en la obtención de un patrón consistente de distribución de valores de *m/z* independientemente del experimento. En nuestro caso, las distribuciones espaciales de metabolitos derivadas de MALDI-MSI se verificaron tanto mediante réplicas biológicas como comparando los resultados de secciones longitudinales y transversales de diferentes partes de la semilla de cebada. Se realizaron al menos tres réplicas para obtener patrones de distribución espacial y temporal. Así es posible describir la disposición específica de las moléculas tanto histológicamente como en un contexto de desarrollo fisiológico de la planta. Además, los espectros MALDI-MSI de extractos de tejidos de granos de cebada disecados manualmente revelaron valores de *m/z* con el mismo patrón de distribución que el detectado por los experimentos MALDI-MSI.

Resolución de la imagen

Uno de los parámetros clave de la técnica MALDI-MSI es la resolución en la imagen. La mayor parte de la literatura de MALDI-MSI en material vegetal describía resoluciones espaciales en el rango de 100-200 µm (Kaspar *et al.*, 2011). Las excepciones son una investigación de semillas de berenjena con una resolución de 25 µm (Goto-Inoue, Setou and Zaima, 2010), y un estudio de la flor, el tallo y la raíz de *A. thaliana* con resoluciones de medición de 12, 25 y 50 µm (Jun *et al.*, 2010). La resolución espacial más alta obtenida en material vegetal, 10 µm, se logró con *A. thaliana* e *Hypericum* mediante espectrometría de masas de ionización láser en el rango de luz UV, sin utilizar matriz y para el análisis de las distribuciones espacial de metabolitos secundarios, que absorben en el UV (Hölscher *et al.*, 2009).

La resolución de la imagen dependerá tanto del tamaño real de la muestra, como de la capacidad de procesamiento de datos. En nuestro caso, el tamaño de las secciones longitudinales del grano de cebada aumenta desde una longitud de 2 mm a los 2 DAP (con un diámetro de 1 mm), hasta una longitud de >10 mm a los 14 DAP (con y un diámetro de 3 mm). Por lo tanto, dependiendo del tamaño de la muestra, se deben adaptar las resoluciones de medición al MS no sólo para extraer información biológicamente relevante, sino también para limitar el tamaño del conjunto de datos. La resolución buscada en la medida también depende del tipo de tejido a utilizar. Así, las distribuciones de metabolitos en los granos de cebada aparecen a nivel de tejido más que a nivel unicelular, y los niveles de

metabolitos en una célula única varían mucho desde los granos muy jóvenes (1-6 DAP) hasta los granos en la etapa de llenado de semillas o hasta la maduración completa (7-20 DAP). Algunos tejidos requieren una adquisición de la señal con una mayor resolución que otros; por ejemplo, la capa de aleurona (agrupación proteica) sólo tiene dos o tres capas de células de espesor (Garrett *et al.*, 2011). En consecuencia, la resolución espacial adoptada para los granos de 1-6 DAP fue de 10-20 µm y, para los de 7-20 DAP, de 20-35 µm (*Supplementary Information* Tabla 3.1.S1).

Análisis de los datos de MS

Una vez completada la recogida de datos de MS, los mismos son procesados y visualizados para su evaluación, analizando la distribución de las distintas masas medidas y sus intensidades y llevando a cabo una comparación estadística. Existen varios paquetes de software para MALDI-MSI (tanto de código abierto como comerciales) que ofrecen algoritmos de procesamiento de datos obtenidos y su análisis estadístico (Kaspar *et al.*, 2011), pero todavía no se dispone de un software para la sustracción del *background* de la matriz en el rango bajo de *m/z*. Esta escala de datos está más allá de la capacidad analítica de los programas informáticos utilizados, subrayando la necesidad de un desarrollo a nivel de software en este sentido, como sería por ejemplo el programa de análisis BioMap (http://www.maldi-msi.org/). Otro factor limitante a la hora de analizar estadísticamente los conjuntos de datos de MALDI-MSI es la capacidad de estos paquetes de software diseñados *ad hoc*, que a veces no son capaces de manejar grandes conjuntos de datos, lo que hace necesaria una reducción de datos crudos totales, a costa de la resolución de las imágenes espaciales. En resumen, del número de espectros individuales adquirido durante el análisis dependerá de la calidad de la resolución de las imágenes, y una reducción de datos implicará una pérdida de resolución. El número de espectros adquiridos rutinariamente en nuestros experimentos varió de 2500 a 18000 por sección de tejido (*Supplementary Information* Tabla 3.1.S1). Se utilizó el software FlexImaging tanto para la evaluación de la suma de los espectros del conjunto completo de los datos obtenidos como para visualizar imágenes de iones múltiples y de iones seleccionados dentro de las crio-secciones de tejido. La sustracción de la línea de base se incluyó en la adquisición de datos, pero no fue posible realizar una sustracción adicional de la señal derivada de la matriz utilizada. Por lo tanto, los espectros provenientes del tejido tuvieron que ser comparados manualmente con los espectros derivados solamente de la matriz utilizada.

Identificación de los metabolitos

Es necesario un gran esfuerzo para la identificación de los compuestos detectados con MALDI-MSI. Para conseguir valores de *m/z* con la mayor exactitud posible es necesario hacer mediciones manuales en la superficie del tejido. Para clasificar los productos en función de la *m/z* medida se utilizaron varias bases de datos en línea (http://metlin.scripps.edu/), KNApSack (http://kanaya.naist.jp/KNApSAcK/) y Lipidomics Gateway (http://www.lipidmaps.org/), así como

datos de la literatura. En algunos casos, se obtuvo información adicional mediante análisis por MS/MS (MALDI TOF/TOF). Por ejemplo, el espectro de fragmentación del ion molecular *m/z* 520,4 encontrado en el tejido del grano de cebada generó iones hijos de *m/z* 104 y 184. La fragmentación *in silico* de 2 fosfatidilcolinas, como L-α-phosphatidylcholine (PC) y L-α-lysophosphatidylcholine (LPC) producen iones hijos de *m/z* 104 y 184 y una pérdida neutra de *m/z* 59 (Xu *et al.*, 2009; Garrett *et al.*, 2011; Murphy and Gaskell, 2011). Una comparación con el espectro MS/MS de *m/z* 520.4 de la solución estándar de LPC mostró los mismos iones, por lo que se concluyó que ambas fosfatidilcolinas correspondían a lo encontrado en las muestras de cebada.

Sin embargo, la precisión de masa de la instrumentación MALDI-TOF/TOF es aún insuficiente en la actualidad para determinar las fórmulas moleculares de los compuestos seleccionados, y por ello sigue siendo necesario un análisis dirigido basado en la cromatografía de gases-espectrometría de masas (GC-MS) y/o LC-MS para lograr una identificación concluyente. Todavía se requieren mejoras en el software analítico para mejorar la exactitud de la masa de los espectros acumulados y para evitar los desplazamientos de los picos durante la adquisición simultánea de diferentes regiones de interés en la criosección del tejido. En nuestro protocolo, el instrumento se calibró en el modo de ionización positiva con PEG200 + 600 antes del inicio de una adquisición automática, ya que la calibración entre mediciones individuales no estaba admitida en el software propietario del equipo. El desarrollo de soluciones de software para la calibración externa durante las ejecuciones automáticas de MALDI-MSI sigue siendo una gran prioridad.

Evolución de la técnica

En los últimos años se ha avanzado mucho en la aplicación del MALDI-MSI en plantas. Muchos trabajos se han centrado en la mejoría de los aspectos generales de la instrumentación, los enfoques analíticos y la preparación de muestras (Berin A. Boughton *et al.*, 2016). También se han hecho grandes avances para realizar un análisis de datos más eficiente y eficaz, mejorando notablemente las resoluciones espaciales de las imágenes obtenidas (Heyman and Dubery, 2016). A pesar de los esfuerzos, la información relativa a los métodos de preparación de muestras para los tejidos vegetales es todavía limitada (Dong *et al.*, 2016) en comparación con los tejidos animales. Este trabajo pretende contribuir en abrir nuevas perspectivas en el estudio de la distribución de las pequeñas moléculas en plantas (Matros and Mock, 2013), poniendo de manifiesto el enorme potencial de las técnicas de MSI combinadas con el análisis metabolómico, con la ventaja adicional de generar también información crucial sobre la distribución espacial de los metabolitos. El desarrollo del MSI para su uso en la metabolómica de las plantas se encuentra en un momento emocionante y la posibilidad de nuevos e interesantes descubrimientos son muy evidentes (Heyman and Dubery, 2016).

En la última década, se ha demostrado que el MSI permite visualizar la distribución espacial de analitos tales como lípidos, proteínas, péptidos y secuencias de ADN, determinando las coordenadas exactas de dichos compuestos en el tejido vegetal (Susniak *et al.*, 2020). La posibilidad de utilizar junto al MALDI espectrómetros de masas de alta resolución ha permitido una mayor sensibilidad e importantes mejoras en los límites de detecciones de los compuestos (Susniak *et al.*, 2020). Un reciente estudio ha utilizado el MSI para estudio de raíces de espárrago. En dicho estudio han conseguido estudiar las diferentes distribuciones espaciales de metabolitos específicos de exudados, tejidos externos (epidermis y exodermis) e internos (corteza y tejido vascular) de la raíz, identificando hasta 263 metabolitos distintos en las tres fracciones (Döll *et al.*, 2021). En el mismo experimento, además del perfil metabólico se investigaron las características del proteoma del tejido externo e interno de la raíz mediante la técnica del *label-free proteomics*, permitiendo identificar y cuantificar al mismo tiempo la abundancia relativa de las proteínas, pudiendo afirmar que los proteomas eran espacialmente muy distintos (Döll *et al.*, 2021), de acuerdo con las diferencias fundamentales entre sus funciones y estructuras.

A pesar de todo esto, la técnica del MSI sigue teniendo las mismas limitaciones encontradas en esta Tesis Doctoral, ya que sigue siguiendo una técnica compleja en comparación con las más accesibles de LC-MS para el análisis de pequeñas moléculas, con las que se pierde toda la información sobre la distribución espacial de compuestos. La preparación de muestras biológicas de tejido vegetal sigue siendo muy difícil de trabajar debido a su heterogeneidad de la muestra, y puede ser un factor limitante para un usuario no entrenado (Susniak *et al.*, 2020). Además, el uso de las técnicas de descongelación a la hora de preparar las sesiones de tejido puede provocar un cierto desplazamiento de los metabolitos (Sturtevant *et al.*, 2021), así como generar ligeros cambios en los perfiles metabólicos de las muestras (Susniak *et al.*, 2020). La correcta elección de la matriz y/o el desarrollo de nuevas matrices, en función del tipo de tejido y planta utilizada para cada experimento, sigue siendo un factor crucial para la detección de las moléculas, reduciendo las interferencias provenientes de la misma matriz y aumentando al mismo tiempo la sensibilidad de la señal (Sun *et al.*, 2020). Por último, la elección de los parámetros de análisis por MALDI-MSI, el procesado de los datos crudos mediante plataformas de software dedicados (Sturtevant *et al.*, 2021) y la interpretación de estos resultados requiere de ciertos conocimientos y un buen grado de experiencia (Susniak *et al.*, 2020).

4.2. Efectos de la deficiencia de Fe y su reabastecimiento en el proteoma radicular de un patrón híbrido de melocotón y almendro (*P. dulcis* × *P. persica*)

En este capítulo se han evaluado los cambios en los perfiles proteicos de la raíz de un patrón híbrido de *Prunus* GF 677 cultivado en hidroponía, en presencia de una deficiencia de Fe y también a corto plazo tras el reabastecimiento de Fe. Como aproximación se han utilizado técnicas de proteómica diferencial usando geles bidimensionales de poliacrilamida (2-DE). Mediante esta técnica se consiguió detectar de un modo consistente 355 manchas (o "spots"), un número que está en el rango de otros estudios similares (Rellán-Álvarez, Andaluz, *et al.*, 2010; Rodríguez-Celma *et al.*, 2010; Jorge Rodríguez-Celma, Lattanzio, *et al.*, 2011). Las proteínas identificadas indican que las vías metabólicas más afectadas por la deficiencia de Fe (-Fe) son las de estrés, defensa y metabolismo de los hidratos de carbono. Tras el reabastecimiento a corto plazo de Fe (-FeR), las vías de estrés y defensa siguen representando la mayor parte de los cambios, observándose también una cierta acumulación de proteínas relacionadas con la glucólisis y el metabolismo del N (Fig. 3.2.6).

Cambios en las raíces deficientes en Fe

La deficiencia de Fe provocó cambios significativos en la abundancia relativa de aproximadamente un 5% de las proteínas detectadas (17 spots). Este porcentaje es menor que los encontrados en estudios previos similares de 2-DE que describen cambios con la deficiencia de Fe en remolacha azucarera, tomate, pepino y *M. truncatula* (un 13, 11, 14 y 7% del total, respectivamente) (Li *et al.*, 2008; Donnini *et al.*, 2010; Rellán-Álvarez, Andaluz, *et al.*, 2010; Jorge Rodríguez-Celma, Lattanzio, *et al.*, 2011). Este bajo número de cambios puede estar asociado a los peculiares efectos de la deficiencia de Fe en las plantas leñosas (ver más adelante) (Jiménez *et al.*, 2009), a la tolerancia especialmente alta a la deficiencia de Fe descrita previamente para este portainjerto (patrón) (Cinelli, Iacona and Tamantini, 2004) o a ambas razones a la vez. Otros resultados también reflejan la alta tolerancia a la deficiencia de Fe de este patrón hibrido, que en condiciones de deficiencia de Fe muestra valores de índice SPAD y de las tasas de fotosíntesis que son relativamente altos (Jiménez *et al.*, 2009, 2011).

Cuando se comparan los cambios en el perfil proteico de la raíz del híbrido de *Prunus* GF 677, afectados por la deficiencia de Fe con los previamente registrados en otras especies no leñosas, se observan bastantes diferencias. Quizá la diferencia más llamativa es la ausencia de incrementos importantes en la expresión de proteínas implicadas en el ciclo TCA (el ciclo del ácido tricarboxílico) y en la ruta metabólica de las pentosas-fosfato (Fig. 3.2.6A). En las raíces del GF 677, sólo dos especies de proteínas asociadas a estos procesos mostraron un aumento en su abundancia debido a la deficiencia de Fe: la enolasa (spot 28) y la alcohol deshidrogenasa (spot 29). El aumento observado en la glicólisis es, por tanto, moderado. Ya habían sido descrito con anterioridad aumentos en ambas enzimas en las

raíces de varias especies no leñosas sometidas a deficiencia de Fe (Lopez-Millan, Morales, Andaluz, *et al.*, 2000; Thimm *et al.*, 2001; López-Millán *et al.*, 2009; Donnini *et al.*, 2010), siempre acompañados de otras del TCA y la PEPC. Merece la pena mencionar que en las raíces del GF 677, el aumento de la actividad de la PEPC en condiciones de deficiencia de Fe es de sólo 4 veces, un valor mucho menor que el aumento de entre 10 y 60 veces encontrado en las especies no leñosas (Abadía *et al.*, 2002; Jiménez *et al.*, 2011). En este portainjerto, el cambio de piruvato hacia un metabolismo anaeróbico podría ser más relevante que la extensiva reprogramación metabólica descrita para especies no leñosas (Barton and Abadia, 2006; Vigani, 2012). Esto encaja con los aumentos relativamente pequeños que se observaron en los carboxilatos en la raíz de este portainjerto tras la escasez de Fe (Jiménez *et al.*, 2011). El aumento de la concentración de los niveles de sacarosa en la raíz encontrado en este genotipo (Jiménez *et al.*, 2011) apoya también el cambio metabólico hacia la fermentación.

Una segunda diferencia importante entre este híbrido de *Prunus* y las plantas no leñosas, es que las proteínas relacionadas con el estrés representan una gran parte (50%) de las especies proteicas que muestran cambios significativos en su abundancia (estando un 33 y un 17% implicadas en el estrés oxidativo y la defensa de la planta, respectivamente; Fig. 3.2.6A). En plantas no leñosas, los cambios en el metabolismo del C y del N representaron las mayores diferencias (Li *et al.*, 2008; Donnini *et al.*, 2010; Rellán-Álvarez, Andaluz, *et al.*, 2010; Jorge Rodríguez-Celma, Lattanzio, *et al.*, 2011). La principal respuesta a la deficiencia de Fe en este portainjerto consiste por tanto más en una estrategia de defensa que en una reprogramación metabólica. Las enzimas relacionadas con el estrés oxidativo que mostraron cambios significativos en las raíces deficientes en Fe fueron las peroxidasas (spots 1,4,5), la galactosa deshidrogenasa (spots 3) y la MnSOD (spot 2). El estrés oxidativo es una consecuencia común de la deficiencia de Fe en todo el reino vegetal (Iturbe-Ormaetxe *et al.*, 1995; Zaharieva, Gogorcena and Abadía, 2004), incluidos los árboles frutales (Molassiotis *et al.*, 2006), habiéndose asociado el nivel de elicitación de los mecanismos de defensa con la tolerancia a la deficiencia de Fe (Molassiotis *et al.*, 2006; M'sehli *et al.*, 2009). Los aumentos de las concentraciones de Mn en la raíz encontrados en GF677 tras la escasez de Fe (Jiménez, 2006) pueden estar tras el aumento de abundancia relativa encontrado en la Mn-superóxido dismutasa (MnSOD). Sin embargo, los incrementos en la actividad de esta peroxidasa parecen estar más relacionados con modificaciones en la pared celular que con la tolerancia al estrés oxidativo, llevando a un incremento en la lignificación de la raíz. Esta hipótesis se ve reforzada por la disminución de la β-glucosidasa (spot 40), una exo-celulasa con especificidad para sustratos β-D-glucósido. Se ha descrito un proceso similar de lignificación de la raíz impulsado por la peroxidasa en peras y membrillos deficientes en Fe (M'sehli *et al.*, 2009).

Dentro de las proteínas afectadas por el estrés asociado con la deficiencia de Fe se incluyen dos proteínas alergénicas, Pru av 1 y Pru du 1.04, y una glutatión S-transferasa. Se sabe que la abundancia de las proteínas alergénicas aumenta en caso de estrés biótico o abiótico, siendo algunas de ellas proteínas de transferencia de lípidos, aunque las funciones específicas en el metabolismo de las plantas

son todavía poco conocidas (Scheurer *et al.*, 1997; Sánchez-Monge *et al.*, 1999). Las glutatión S-transferasas conjugan el glutatión con productos citotóxicos, y la disminución encontrada en este trabajo en condiciones de deficiencia de Fe es similar a la encontrada raíces de tomate (Li *et al.*, 2008), pero contrasta con los aumentos observados en las raíces de *M. truncatula*, que es una especie acumuladora de flavinas. En las raíces de remolacha, también productora de flavinas, se encontraron aumentos en los depósitos de glutatión en situación de deficiencia de Fe (Zaharieva and Abadía, 2003; Zaharieva, Gogorcena and Abadía, 2004). También se detectó un aumento en la abundancia relativa de una proteína putativa relacionada con la biosíntesis de fenazinas debido a la deficiencia de Fe. Las fenazinas son un gran grupo de compuestos heterocíclicos que contienen N y que son producidos por una gran variedad de bacterias que sirven como transportadores de electrones capaces de modificar la homeostasis de la reacciones redox de las células (Mavrodi *et al.*, 2010; Pierson and Pierson, 2010).

Cambios a corto plazo tras el reabastecimiento de Fe (*resupply;-FeR*) en comparación con las plantas condiciones de suficiencia de Fe

El reabastecimiento con Fe produjo en 24 h cambios en la abundancia relativa de un 10% de las proteínas detectadas en los extractos de raíz. Como ya ocurre en las raíces sometidas a deficiencia de Fe, las categorías más representadas fueron las de estrés oxidativo y defensa, constituyendo un 45% del total de cambios detectados (con el 24 y el 21% implicados en el estrés oxidativo y los mecanismos de defensa de la planta, respectivamente; Fig. 3.2.6B). La mayoría de las proteínas mostraron cambios en la misma dirección (aumentos o disminuciones de la abundancia relativa) a los medidos en las plantas deficientes en Fe, sugiriendo un mantenimiento de las respuestas, al menos durante esas primeras 24h. También se mantuvo la disminución de la abundancia relativa de la β-glucosidasa (spot 40), lo que sugiere que las modificaciones de la pared celular pueden seguir existiendo poco después tras el reabastecimiento de Fe.

Varios tipos de proteínas asociadas al metabolismo del N disminuyeron tras el reabastecimiento de Fe a corto plazo (-FeR). Es notable que la glutamina sintetasa (GS, spot 24) mostró la mayor disminución en la abundancia relativa (10 veces) tras la reposición de Fe. Esta enzima citosólica es clave en el control del uso del N dentro de la célula (Eisenberg *et al.*, 2000). La fuerte disminución en la abundancia relativa de GS tras el reabastecimiento de Fe (-FeR) sugiere que esta enzima podría ser uno de los primeros indicadores del estado nutricional del Fe, respondiendo a la disminución de las necesidades de compuestos a base de N tras añadir Fe. Los aumentos en el factor de traducción 5A (spot 20) y en una proteína ribosomal 40S (spot 21) indican que la síntesis *de novo* de proteínas aumenta en respuesta a la reposición de Fe.

Con respecto al metabolismo del C, las disminuciones de dos enzimas de la vía glicolítica y del metabolismo del piruvato (enolasa y dihidrolipoamida acetiltransferasa) y el aumento de una proteína de la ruta metabólica de las pentosas fosfato (ribosa 5-P-isomerasa, spot 32) indican que la ligera

reprogramación del metabolismo del C inducida por la deficiencia de Fe ya se está desactivando poco después tras el reabastecimiento de Fe (Fig. 3.2.6B).

Otros de los cambios que merecen ser mencionados en las raíces GF 677 en condiciones de reabastecimiento de Fe, con respecto a las plantas controles, son los cambios a nivel de expresión en direcciones opuestas (aumentos/disminuciones) en las abundancias relativas de dos quinonas reductasas (spots 33 y 34, respectivamente), que sugieren la aparición de un mecanismo compensatorio. Este cambio de tendencia a nivel de la expresión proteica se observa también en las raíces en condiciones de deficiencia de Fe respecto a las plantas controles.

Cambios tras el reabastecimiento a corto plazo en comparación con las plantas deficientes en Fe

La comparación entre las raíces reabastecidas de Fe y las plantas deficientes en dicho elemento, indica claramente que las plantas reabastecidas de Fe siguen comportándose mayoritariamente como las plantas deficientes de Fe, ya que sólo ocho proteínas mostraron cambios en su abundancia relativa. Estas proteínas pueden considerarse como las primeras en responder al estado nutricional de Fe.

Cinco proteínas aumentaron en abundancia relativa en las plantas reabastecidas con Fe frente a las deficientes. Dos de ellas, relacionadas con la biosíntesis y el transporte de proteínas, aumentaron en abundancia relativa, apoyando que la síntesis *de novo* de proteínas es uno de los primeros pasos dentro de la recuperación del estrés. El aumento de una proteína en la ruta metabólica de las pentosas fosfato reflejaría la necesidad de energía y del poder reductor para este proceso. Sin embargo, el aumento de la abundancia relativa de una peroxidasa y del alérgeno Pru du 1,04 implica que las plantas se enfrentan a un estrés adicional.

Al centrarnos en las tres proteínas que mostraron disminuciones en su abundancia relativa, el mayor cambio se observó en la glutamina sintetasa, confirmando su sensibilidad al estado del Fe en la planta y la disminución de las necesidades de reciclaje de N. La desactivación de los cambios metabólicos también se ve apoyada por la disminución de la enzima dihidrolipoamida acetiltransferasa. Finalmente, la chalcona sintasa, una enzima que cataliza la síntesis de metabolitos derivados de la chalcona, acetonas aromáticas, en la vía de los fenilpropanoides (PAL), disminuyó en abundancia cuando se produjo el reabastecimiento con Fe. Esta enzima puede estar implicada en mecanismos de defensa y en el papel de protección contra el estrés oxidativo (Haraguchi *et al.*, 1998; Choi, Kim and Kim, 2010) y además está implicada en la biosíntesis de la lignina. Esto se ha visto que se produce también en las raíces en condiciones de deficiencia de Fe después del reabastecimiento a corto plazo de Fe, apuntando que esta enzima (o la vía PAL) podría tener un papel en la respuesta temprana de recuperación a este tipo de estrés. En el futuro será necesario estudiar los efectos del reabastecimiento de Fe a largo plazo en los procesos de reverdecimiento de las plantas.

4.3. Caracterización del proteoma de la savia del floema de Lupinus texensis y estudio de las proteínas implicadas en la unión con el Fe y el Zn

El objetivo de este capítulo fue la caracterización del perfil proteico de la savia del floema de *Lupinus texensis*, con especial atención a las proteínas que unen Fe y Zn. Se eligió *L. texensis* como planta modelo, dada la sencillez para obtener exudados de los tubos cribosos (Carella *et al.*, 2016; Rodríguez-Celma *et al.*, 2016; Ogden *et al.*, 2020; Liu *et al.*, 2021) Para minimizar la contaminación procedente de la incisión, se descartó la primera gota exudada. A pesar de las precauciones, siempre existe un cierto grado de contaminación de las células dañadas, y también puede haber algunos cambios en la composición del exudado causados por la herida (incluidas especies proteicas involucradas en mecanismos de defensa contra la alimentación de los insectos y/o en los procesos de sellado después de la herida) (Atkins, Smith and Rodriguez-Medina, 2011). La naturaleza de la savia del floema obtenida por incisión en ciertas especies de plantas con un sistema de transporte de floema dual sigue siendo objeto de debate (Zhang *et al.*, 2012), aunque este no es el caso de *L. texensis*. Otros métodos de extracción de floema utilizan insectos (áfidos) o utilizan EDTA como facilitador (Liu *et al.*, 2021b).

La pureza de las muestras de savia del floema obtenidas se evaluó midiendo las concentraciones de azúcar y la presencia de Rubisco. La sacarosa fue el azúcar mayoritario, estando las hexosas presentes en concentraciones mucho menores, tal y como se esperaba de una savia obtenida a partir de elementos cribosos. De todas las proteínas identificadas, sólo 4 (7%) se asignaron a Rubisco, y si se tienen en cuenta todas las especies proteicas detectadas, pero no identificadas este porcentaje baja al 3%. Estos porcentajes están en el mismo rango que los descritos en otras muestras de savia del floema obtenidas mediante la técnica de incisión (Doering-Saad *et al.*, 2006; Rodriguez-Medina *et al.*, 2011).

El enfoque proteómico 2-DE nos permitió encontrar 249 polipéptidos en el floema de *L. texensis*, de los cuales se identificaron 54 (22%). Estos resultados son similares a los reportados en *L. albus*, donde se detectaron 200 manchas de las cuales se identificaron 52 de ellas (26%) (Rodriguez-Medina *et al.*, 2011), y en *Brassica napus*, con 600 manchas de las cuales se identificaron 135 (23%) (Giavalisco *et al.*, 2006). La distribución de las proteínas según el proceso biológico en el que están involucradas en *L. texensis* (Fig. 3.3.2B) es muy similar al reportado para *L. albus*, siendo el metabolismo general (24%) y la modificación/*turnover* de proteínas (19%) los grupos que contienen un mayor número de proteínas, seguidos por la homeostasis redox (9%), la defensa (7%) y los componentes estructurales celulares (7%). Los experimentos de tinción y de cromatografía de afinidad con iones metálicos inmovilizados (IMAC) revelaron la presencia en la savia del floema de dos proteínas de bajo peso molecular que se unen al Fe y cuatro proteínas de unión al Zn.

Mapeo 2-DE de las proteínas presentes en el floema de *L. texensis*

Una visión general de las proteínas identificadas indica que la savia del floema de *L. texensis* contiene una gama muy amplia de enzimas implicadas en varios procesos metabólicos (por ejemplo, la glicólisis, el ciclo del TCA, la biosíntesis de lípidos, la derivación de las pentosas fosfato y la síntesis de aminoácidos y nucleótidos), lo que sugiere que todavía podrían estar activas en los elementos de tamiz maduros. Entre estos procesos, los datos obtenidos sugieren la existencia de una vía glicolítica activa, así como síntesis de aminoácidos en los elementos cribosos, lo que indica que los aminoácidos podrían no ser transportados únicamente de forma pasiva. También confirman la presencia de enzimas de homeostasis redox como la ascorbato peroxidasa y la glutatión peroxidasa, siendo la tiorredoxina H una de las proteínas reductoras más abundantes de este grupo (Ishiwatari *et al.*, 1995; Schobert *et al.*, 1998; Walz *et al.*, 2002; Rodriguez-Medina *et al.*, 2011). Estas proteínas constituyen un mecanismo de protección de este compartimento vegetal frente al daño oxidativo, por lo que podrían ser importantes para el mantenimiento de los elementos cribosos (Ishiwatari *et al.*, 1995). Por último, también se han encontrado proteínas implicadas en los mecanismos de defensa de la planta, como son la PR10 y una proteína de resistencia a la enfermedad LRR (spots 27 y 28).

Para poner en contexto el mapeo del floema de *L. texensis*, se han comparamos los resultados con los obtenidos en la bibliografía para otras especies vegetales (calabaza, colza y arroz), utilizando como referencia el proteoma no redundante del floema de *Arabidopsis* (Giavalisco *et al.*, 2006; Buhtz *et al.*, 2008; Lin *et al.*, 2009). Esta comparación (Fig. 3.3.2C), muestra la presencia de 13 proteínas identificadas en nuestro estudio que no se han reportado previamente en estas especies. De ellas, las más interesantes son una histona metiltransferasa (spot 41) y una maturasa (spot 42). La presencia en la savia del floema de *L. texensis* de especies de proteínas implicadas en el procesamiento de RNA/DNA es coherente con la propuesta de la existencia de una red de señalización basada en el RNA a nivel de planta completa (Lough and Lucas, 2006; Atkins, Smith and Rodriguez-Medina, 2011). Ambas proteínas se identificaron en spots de baja intensidad, lo cual encaja con un posible rol en procesos de señalización. En otras especies también se han identificado proteínas de unión al RNA, como los factores de iniciación eucarióticos y la proteína de unión al ran-GTP, lo que apoyaría la existencia de dicha red de regulación vía floema (Supplementary Information Tabla 3.3.S3). Además, la presencia de una histona metiltransferasa podría sugerir un papel en la regulación epigenética en la savia del floema de *L. texensis*. La presencia de una proteína de unión a las histonas en la savia del floema de la calabaza (Lin *et al.*, 2009) también proporciona soporte a esta hipótesis.

Hay un grupo de proteínas que se han encontrado de forma sistemática en la savia del floema de especies mono- y dicotiledóneas, y que apoyaría que los elementos enucleados del tubo cribosos mantienen ciertos componentes y funciones celulares básicos. Entre ellas se encuentran varios factores de iniciación eucariotas (spots 4-7), lo que les daría la capacidad de síntesis de proteínas; la presencia

de actina y factores de despolimerización de actina (spots 13 y 15); la presencia de dos proteínas relacionadas con la ubiquitina (spots 8 y 9), que les dotaría de la maquinaria necesaria para la degradación de proteínas a través de la vía de la ubiquitina/proteasoma (proteasoma 26S); y el hallazgo de una enzima glicolítica como la fructosa bifosfato aldolasa (spot 32) en todas las especies de dicotiledóneas analizadas, que apoya la existencia de un metabolismo activo de carbohidratos y alimenta el debate sobre el papel de los azúcares reductores en la savia del floema (Van Bel and Hess, 2008; Lin *et al.*, 2009; Rodriguez-Medina *et al.*, 2011). También están presentes las cisteína-proteinasas, que en nuestro estudio fueron tres de los spots más intensos (spots 10-12), que podrían jugar un papel en la estabilidad de las proteínas en el floema (Giavalisco *et al.*, 2006; Rodriguez-Medina *et al.*, 2011), lo que sugiere un papel conservado entre las especies vegetales. Asimismo, la presencia de S-adenosilmetionina sintetasa (spot 43) en todas las especies de dicotiledóneas analizadas puede estar relacionada con la síntesis de nicotianamina, un quelante para el que se ha propuesto un papel esencial en la translocación de metales en el floema (Curie *et al.*, 2009), y que también puede proporcionar grupos metilo para la modificación de proteínas.

Como conclusión del experimento de mapeo, el perfil proteico descrito en este trabajo se asemeja a los reportados en otras especies, lo que sugiere que la composición proteica de la savia del floema está conservada. Es importante subrayar que desde la realización de este estudio los avances metodológicos en el campo de la proteómica han permitido arrojar luz no sólo sobre la composición proteica de estos fluidos vegetales, incrementando su mapeado, sino también sobre su funcionalidad (Rodríguez-Celma *et al.*, 2016). Un reciente estudio reciente ha conseguido identificar >2500 proteínas de savia de floema de tomate, sugiriendo que en este compartimento hay muchas vías biológicas involucradas más allá de las reportadas en estudios anteriores (Ogden *et al.*, 2020).

Análisis de las proteínas que unen Fe y Zn en el floema de *L. texensis*

La gran mayoría de los polipéptidos resueltos por 2-DE IEF-SDS-PAGE en los exudados del floema de *L. texensis* no tienen ninguna relación conocida con el transporte de metales, con la única excepción del homólogo de la chaperona de Cu CCH. Dado que homólogos de esta proteína han sido también detectados en *Arabidopsis*, *B. napus* y *L. albus*, podría actuar en el reparto de metales mediado por el floema desde las hojas senescentes a las hojas jóvenes (Mira, Martínez-García and Peñarrubia, 2001). Otras proteínas de unión a metales descritas hasta la fecha en estudios proteómicos de la savia del floema incluyen las metalotioneínas encontradas en *Ricinus communis* y *Oryza sativa* (Barnes *et al.*, 2004; Aki *et al.*, 2008), una proteína putativa transportadora de Fe (ITP) (Krüger *et al.*, 2002) y una ferredoxina encontrada en *B. rapa* (Giavalisco *et al.*, 2006), así como una chaperona de Cu (CCS1-At1g12520.1) y varias metaloproteasas y proteínas Zn *finger* encontradas en *C. máxima* (Lin *et al.*, 2009).

Los experimentos de tinción y de cromatografía de afinidad revelaron la presencia de dos proteínas de bajo peso molecular que se unen al Fe en la savia del floema. Ambos métodos de tinción de Fe (tinción con Ferene S y tinción basada en propriedades redox) mostraron la presencia de una especie de proteína (spot 53 en la Fig.3.3.2A) con un peso molecular de 13,5 kDa y un pI de 5,6 en los geles 2-DE. La identificación por espectrometría de masas de esta proteína dio como resultado un EST de raíces de *Lupinus albus* L. que muestra un 51% de homología con una proteína anotada como específica del floema de *M. truncatula* (XP_003601185) (De Vleesschauwer, Chernin and Höfte, 2009).

Después de la publicación de nuestros resultados, se volvió a analizar las secuencias obtenida por secuenciación *de novo* (Supplementary Information Fig. 3.3.S4) mediante una búsqueda por homología mediante el algoritmo blastp (protein-protein BLAST; https://blast.ncbi.nlm.nih.gov/Blast.cgi) contra la base de dato de NCBI *Lupinus* (taxid:3869). La búsqueda dio como resultado la identificación de una proteína especifica de *Lupinus albus* (*hypothetical protein Lalb_Chr08g0236771*; GenBank: KAE9608537.1). Contrastando la identificación en el repositorio UniProt la proteína aparece como una *uncharacterized protein* de *L. albus* (A0A6A5MEV3_LUPAL) relacionada con la familia de proteínas específicas de floema según la clasificación de la base de datos PANTHER (PTHR38224; https://www.pantherdb.org/). Se trata de una proteína de 104 aminoácidos con una gran cantidad de glutamatos (16), histidinas (7) y aspartartatos (4), aminoácidos normalmente actúan como ligandos en quelación de metales. Estos residuos podrían formar un complejo de unión con el hierro mediante interacciones electrostáticas o de coordinación con enlaces de hidrogeno (Walters, Esfandi and Tsopmo, 2018). Según la base de datos AlphaFold (https://alphafold.com/; AFBD *accension* AF-A0A6A5MEV3-F1), la estructura tridimensional de la proteína de *L. albus* aparece organizada en 4 semielices/cadenas aparentemente desorganizadas, pero quizá la unión de ese cofactor metálico sea necesaria para adoptar una estructura definida.

Por otra parte, en una tenue banda retenida en la cromatografía de afinidad al Fe se identificó una proteína similar a la metalotioneína tipo 2B entre las especies proteicas presentes. La proteína identificada tiene un 75% de homología a nivel de aminoácidos con una proteína encontrada en la savia del floema de *R. communis* (Barnes *et al.*, 2004), y los transcritos del gen correspondiente se han detectado en tejidos alimentados por floema, como son las flores y las primeras hojas del tomate, y están fuertemente regulados por los metales pesados (Giritch *et al.*, 1998). También se ha informado de la presencia de otras en la savia del floema de *O. sativa* (Aki *et al.*, 2008). Las metalotioneínas son pequeñas proteínas ricas en Cys (cisteína) capaces de unirse a los metales (Cobbett and Goldsbrough, 2002). La presencia de metalotioneínas en la savia del floema de *L. texensis* (este estudio), *O. sativa* (Aki *et al.*, 2008) y *R.* communis (Barnes *et al.*, 2004) sugiere un posible papel conservado en este fluido, que podría estar relacionado no sólo con la homeostasis de los metales, sino también con la eliminación de ROS y/o la participación en los procesos de desarrollo de la planta (Hassinen *et al.*,

2011). La metalotioneína de este trabajo se identificó únicamente sobre la base de la cromatografía de afinidad, donde puede producirse una competencia de metales, y sólo se observó débilmente en la fracción retenida. Por lo tanto, serían necesarios más experimentos para evaluar la especificidad metálica de esta proteína, así como para aclarar su papel en la savia del floema. Otra proteína presente en la misma banda de cromatografía de afinidad de Fe era un *cluster* de hierro-azufre del Fotosistema I que contiene Fe y que probablemente esté implicado en la fotosíntesis. No hay ninguna explicación posible para la aparición de un componente putativo del Fotosistema I en la savia del floema y su detección podría ser el resultado de contaminación, como se ha comentado anteriormente, que pudiera haberse potenciado posteriormente por el procedimiento de cromatografía de afinidad utilizado.

El experimento de cromatografía de afinidad de Zn reveló la presencia de cuatro proteínas de unión al Zn en la savia del floema. Estas proteínas fueron retenidas con diferente fuerza en la columna Hi-Trap de afinidad al Zn y posteriormente se eluyeron en diferentes fracciones de la columna cromatográfica. Ninguna de estas especies fue lo suficientemente abundante como para poder ser detectada en los perfiles proteicos del 2-DE. Una de las bandas (Zn1, Fig. 3.3.4B, Tabla 3.3.3) contenía una proteína homologa a una EST (L.alb_phloem_01; GenBank: GW583364.1) obtenida de una biblioteca de cDNA de savia del floema (Rodriguez-Medina *et al.*, 2011). Esta EST contiene un marco de lectura abierto completo que muestra una alta homología con miembros de una gran familia de proteínas LEA, llamadas deshidrinas (DHNs), y en particular una homología del 52% a nivel de aminoácidos con una DHN, la ITP, que ha demostrado unirse al Zn in vitro (Krüger *et al.*, 2002). La ITP que se había descrito anteriormente en la savia del floema de las plántulas de *R. communis* tenía un peso molecular de 17 kDa y un pI de 7,3, y los autores sugirieron que desempeñaba un papel en el transporte de Fe en el floema (Krüger *et al.*, 2002); in vitro, la ITP se une preferentemente al Fe(III) pero no al Fe(II) y también forma complejos con Cu(II), Zn(II) y Mn(II). También se ha encontrado una proteína de la familia DHN en la savia del floema de *C. maxima* (At2g44060), aunque mostró una baja homología (20% a nivel de aminoácidos) con la ITP. Las deshidrinas desempeñan un papel fundamental en la respuesta y la adaptación de las plantas a los estreses abióticos, y se han descrito múltiples funciones para ellas, incluyendo la de chaperona, la protección contra el calor y el frío, la unión de iones y la eliminación de ROS (Hanin *et al.*, 2011). Las otras proteínas de unión a Zn identificadas son todas proteínas *Zinc finger* que probablemente están implicadas en los mecanismos de señalización. Las proteínas *Zinc finger* de tipo RING ATL71 y RHA1B (Zn2 y Zn7 en la Fig. 3.3.4B y la Tabla 3.3.3) son enzimas conjugadoras de ubiquitina que desempeñan un papel regulador en los procesos de degradación de proteínas a través de la vía de la ubiquitina/Proteasoma (proteasoma 26S) (Kosarev, Mayer and Hardtke, 2002; Serrano *et al.*, 2006), y la proteína *Zinc finger* de tipo AN1, SAP 17 (bandas Zn4 y Zn6 en la Fig. 3.3.4B y la Tabla 3.3.3), está implicada en las respuestas al estrés ambiental (Vij and Tyagi, 2006). Vale la pena mencionar que estas proteínas *Zinc finger* también han sido identificadas en la savia del floema de *C. maxima* por 2-DE LC-MS/MS (Haebel and Kehr, 2001)

pero no habían sido identificadas en ninguno de los enfoques basados en gel 2-D hasta ahora, apoyando que son proteínas de baja abundancia, posiblemente involucradas en la señalización y regulación.

Las especies de proteínas que se unen al Fe y al Zn reveladas por la cromatografía de afinidad son buenas candidatas para futuros estudios. Sin embargo, nuestros resultados no permiten establecer un papel para ellas en el tráfico de metales, ya que la especiación de estos dos metales entre las proteínas y las especies de bajo peso molecular no se ha estudiado todavía, y por tanto su importancia relativa es aún desconocida. Además, su presencia en la savia del floema puede indicar posibles papeles en la señalización o en la defensa contra el estrés oxidativo que merecen mayor atención.

4.4. Efectos de la deficiencia de Fe en los perfiles proteicos y la composición de lignina del tallo de Medicago truncatula en ausencia o presencia de carbonato cálcico

En este objetivo se estudiaron tallos completos, incluidos los peciolos, de *M. truncatula* cultivada en hidroponía en condiciones control (+Fe) y de deficiencias de Fe en presencia y ausencia de $CaCO_3$ (-Fe+$CaCO_3$ y -Fe respectivamente). Este tratamientos no sólo comprenden la falta de Fe y la presencia de $CaCO_3$, sino también otros factores como un pH básico, el cual dificulta la movilización de Fe en el apoplasto de la raíz (Mengel, 1994; Zuo *et al.*, 2007; Martínez-Cuenca *et al.*, 2013). Además, la presencia de $CaCO_3$ también puede alterar el pH de los fluidos de la planta, incluyendo la savia del xilema y el fluido apoplástico, pudiendo provocar cambios en la especiación química del Fe, y por tanto en la disponibilidad del mismo (Kosegarten, Hoffmann and Mengel, 1999; Lopez-Millan, Morales, Abadia, *et al.*, 2000; Nikolic and Römheld, 2002). Los extractos proteicos obtenidos en las tres condiciones de cultivo utilizadas se han analizado mediante proteómica diferencial basada en geles bidimensionales (2-DE PAGE). El análisis mineral indicó la existencia de alteraciones en los equilibrios de micro- y macro-nutrientes como resultado de ambos tratamientos de deficiencia de Fe (Fig. 3.4.3, *Supporting Information* Fig. 3.4.S3).

Cambios en el perfil proteico

Los resultados generales de los perfiles proteicos indican que la deficiencia de Fe en presencia de $CaCO_3$ tiene un impacto más pronunciado en el proteoma del tallo que la deficiencia de Fe en solitario, ya que un mayor número de spots (31 *vs.* 10) mostraron diferencias en abundancia relativa. En este tratamiento, la categoría funcional que mostró un mayor número de spots con aumentos en abundancia relativa (cinco) fue la de defensa y estrés, mientras que en ausencia de $CaCO_3$ no se encontró ningún aumento significativo en esta categoría (Fig. 3.4.2A y Tabla 3.4.1). Las proteínas identificadas están relacionadas con la defensa general [policétido ciclasa/deshidratasa (spot 9) y PR-5b (spot 12)] o con la defensa contra el estrés oxidativo [tiorredoxina reductasa (spot 10), glutatión peroxidasa 1 (spot 11) y glutaredoxina C4 (spot 13)]. Se ha descrito que algunos miembros de la subfamilia PR5 desempeñan funciones específicas en el sistema de defensa frente al estrés por alta salinidad o desequilibrio osmótico (Tachi *et al.*, 2009), lo que probablemente ocurre también en el tratamiento de deficiencia de Fe en presencia de $CaCO_3$. Una situación similar se describió para el proteoma de raíz de la misma especie (Jorge Rodríguez-Celma, Lattanzio, *et al.*, 2011). La misma proteína PR5b mostró aumentos de expresión en las raíces de plantas de *M. truncatula* cultivadas en presencia de $CaCO_3$ (Jorge Rodríguez-Celma, Lattanzio, *et al.*, 2011). Además, un estudio proteómico sobre las raíces de *Beta vulgaris* sometidas a varios niveles de toxicidad por Zn, que también provoca una inducción de la deficiencia de Fe, encontró que algunas proteínas Bet v1, incluyendo algunas PR-10, aumentaron en

abundancia en las raíces con el suministro de Zn (Gutierrez-Carbonell *et al.*, 2013). Por lo tanto, se podría especular que los aumentos en ambas proteínas observados en el tratamiento con $CaCO_3$ podrían estar relacionados con un estrés osmótico causado tanto por los desequilibrios de Fe como por la presencia de $CaCO_3$. Por otro lado, aumentos en proteínas relacionadas con mecanismos de defensa frente al estrés oxidativo como los observados en este trabajo, incluyendo la tiorredoxina reductasa (spot 10) y otras asociadas con el metabolismo del glutatión, como son la glutatión peroxidasa (spot 11) y la glutaredoxina C4 (spot 13), también se han descrito en diferentes estudios sobre el proteoma de raíz de plantas deficientes en Fe (López-Millán *et al.*, 2013b). Dichos aumentos están probablemente asociados con desequilibrios redox causados por la falta de Fe. La existencia de tales desequilibrios también se ve apoyada por la detección *de novo* de una proteína de biosíntesis de piridoxal (spot 31). El piridoxal, o vitamina B6, es un amortiguador de oxígeno singlete (estado excitado del oxígeno molecular) y puede desempeñar un papel en la tolerancia osmótica o a la salinidad, así como en la resistencia al estrés oxidativo (Chen and Xiong, 2005; Tambasco-Studart *et al.*, 2005).

Por otra parte, la categoría funcional que contiene la mayoría de los spots que disminuyen en abundancia relativa en ambos tratamientos es la de fotosíntesis, con seis proteínas que disminuyen en presencia de $CaCO_3$ y cuatro que disminuyen en su ausencia. Las proteínas identificadas incluyen isoformas de la Rubisco activasa (spots 1, 3 y 7; *Supporting Information* Fig. 3.4.S6A), las cadenas grandes (spot 4) y pequeñas (spots 2 y 6) de la Rubisco, y la subunidad hierro-azufre (Fe-S) del complejo citocromo b6-f (spot 5). Estos descensos implican una disminución de la capacidad de fijación de carbono y está en línea con el conocido deterioro de los procesos fotosintéticos inducido por la deficiencia de Fe (Martin and H. Marschner, 1988).

También se observaron aumentos relativos en tres proteínas de la familia de choque térmico de 70 kDa (HSP70), las cuales están implicadas en la gestión de situaciones de estrés, impidiendo que las proteínas mal plegadas o dañadas se agreguen y facilitando su eliminación mediante la interacción con ubiquitina ligasas (Lüders, Demand and Höhfeld, 2000). Una de dichas HSP70 (spot 15) aumentó en ambos tratamientos de deficiencia de Fe, y su homólogo en *Arabidopsis* (AtBIP1; At5g28540) está implicado en la degradación en el retículo endoplasmático (RE) de las proteínas mal plegadas (TAIR, https://www.arabidopsis.org/). La disminución observada en la enzima conjugadora de ubiquitina (spot 14), que pertenece a la clase E2 y realiza el segundo paso en la vía de ubiquitinación (UniProt, https://www.uniprot.org/), también puede sugerir un papel de la vía catabólica dependiente de la ubiquitina en la respuesta a la deficiencia de Fe. Las otras dos HSP70 (manchas 16 y 17) aumentaron únicamente en presencia de $CaCO_3$ y muy probablemente son isoformas de la misma proteína, dada su localización en el gel 2-DE (*Supporting Information* Fig. 3.4.S6B). Su ortólogo en *Arabidopsis* (AtHsp70-10, At5g09590) juega un papel importante en la regulación de la vía de ensamblaje del Fe-S en la mitocondria (Leaden, Busi and Gomez-Casati, 2014). Estos aumentos pueden estar relacionados

con los descensos observados en las proteínas del clúster Fe-S, incluyendo la NADH-ubiquinona reductasa (spot 24) del complejo I de la cadena respiratoria mitocondrial, la subunidad Fe-S del complejo del citocromo b6f (spot 5) y la ferredoxina nitrito reductasa (spot 23). Por otro lado, se observaron cambios significativos en la maquinaria de traducción de proteínas en el tratamiento de deficiencia de Fe en presencia de $CaCO_3$, afectando a dos componentes estructurales del ribosoma (spots 19 y 21) y a un factor de elongación (spot 20). Se han descrito cambios en la abundancia de algunos componentes del ribosoma inducidos por la deficiencia de Fe en raíces de *Arabidopsis*, y se ha especulado que dichos cambios podrían controlar la preferencia del mRNA y orientar la eficiencia de la traducción hacia conjuntos de genes específicos (Lan *et al.*, 2011; Lan, Li and Schmidt, 2012; Rodríguez-Celma, Chun Pan, *et al.*, 2013), aunque también pueden indicar la necesidad de síntesis *de novo* de algunas proteínas efectoras de la deficiencia de Fe. El hecho de que estos cambios sólo se observen en presencia de $CaCO_3$ subraya el fuerte efecto de este tratamiento en el proteoma del tallo.

Otros efectos de la deficiencia de Fe en los perfiles proteicos del tallo son aumentos en varios spots identificados como malato deshidrogenasa (spots 25-27 en la Tabla 3.4.1 y en la *Supporting Information* Fig. 3.4.S6C) y en una serina-hidroximetil-transferasa (spots 28) en ambos tratamientos. Estos cambios también se han descrito en el proteoma de raíz de plantas de *M. truncatula* deficientes en Fe (Jorge Rodríguez-Celma, Lattanzio, *et al.*, 2011). También se han descrito aumentos de ambas proteínas en estudios fisiológicos y proteómicos sobre la deficiencia de Fe en raíz y y hoja (Abadía *et al.*, 2002; López-Millán *et al.*, 2013b) y los resultados de este estudio indican que ésta puede ser una respuesta común en todos los órganos de la planta.

Efectos en la pared celular

Varias líneas de evidencia apoyan que la deficiencia de Fe causa alteraciones en la pared celular de los tejidos del tallo, especialmente en presencia de $CaCO_3$. En primer lugar, los aumentos en la abundancia relativa observados para dos especies proteicas implicadas en la vía de biosíntesis de fenilpropanoides, la fenilcumarato bencílico éter reductasa (PCBER, spot 29) y una O-metiltrasferasa putativa similar a la cafeoil-CoA O-metiltransferasa 1 (spot 30). Se ha demostrado que la PCBER es una de las proteínas más abundantes en savia del xilema del álamo (Gang *et al.*, 1999), la cual participa en la síntesis de lignanos (Vander Mijnsbrugge *et al.*, 2000), mientras que la O-metiltrasferasa probablemente desempeña un papel en los pasos de metilación necesarios para la biosíntesis de monolignoles, los precursores de la lignina (Do *et al.*, 2007). Los incrementos relativos de dichas especies proteicas sugieren que la deficiencia de Fe puede causar cambios en la lignificación.

El análisis de lignina Py-GC/MS de los peciolos mostró un pequeño pero significativo aumento en la proporción de lignina/proteína en los peciolos deficientes en Fe, que fue más intenso en presencia (-Fe+$CaCO_3$) que en ausencia de $CaCO_3$ (Tabla 3.4.2). El estudio microscópico de las secciones de

peciolo también indicó una mayor alteración en las plantas cultivadas en presencia de $CaCO_3$ que en su ausencia. En los peciolos de las plantas cultivadas en presencia de $CaCO_3$, la tinción con floroglucinol indicó un aumento de la lignina en la parte interna de los vasos del xilema (Fig. 3.4.4F), mientras que el cambio hacia un color verde en la señal de autofluorescencia en la misma zona sugiere la existencia de cambios en la composición de la lignina (Fig. 3.4.4C). Cambios similares en autofluorescencia han sido asociados en otros estudios con cambios en la composición de la lignina (Djikanović *et al.*, 2012). El tratamiento en ausencia de $CaCO_3$ provocó cambios menos marcados (Fig. 3.4.4B, E). Al contrario de lo que ocurre en los peciolos, en el caso de los tallos de las plantas deficientes en Fe la relación lignina/proteína, la composición de la lignina y las micrografías de autofluorescencia y floroglucinol no fueron diferentes respecto las observadas en las plantas control, debido probablemente a que el desarrollo de estos tejidos había sido anterior al inicio de la deficiencia de Fe.

Los cambios relacionados con la pared celular observados en los peciolos de las plantas cultivadas en presencia de $CaCO_3$ podrían indicar un aumento de la rigidez de la pared celular, especialmente en los vasos del xilema. Se ha descrito que cuando hay desequilibrios minerales hay cambios en la composición de la pared celular que resultan en un aumento de la lignificación, por ejemplo en las raíces de cultivares de pera y membrillo deficientes en Fe (Donnini *et al.*, 2009). También se ha sugerido que ésta sea una estrategia de desintoxicación en el caso de un exceso de Cd en las raíces (Lux *et al.*, 2011; Redjala *et al.*, 2011). Por otro lado, se han descrito modificaciones en proteínas relacionadas con la pared celular en estudios del proteoma de raíces deficientes en Fe (López-Millán *et al.*, 2013b). Este aumento de la lignificación podría proporcionar una barrera protectora para evitar el transporte lateral y la distribución de minerales, como consecuencia de la disminución de la permeabilidad de la pared celular (Higuchi, 1981).

Evolución de la metodología empleada en los apartados 4.2, 4.3 y 4.4

Es importante resaltar el cambio de tendencia en los estudios proteómicos en plantas hacia el uso de técnicas de espectrometría de masas (MS) de alta resolución, como es la técnica del *shotgun proteomics* (Ceballos-laita *et al.*, 2020), utilizando geles 1-DE de poliacrilamida (SDS-PAGE) como método de fraccionamiento, seguido de un análisis LC/MS-MS en lugar de una separación de las muestras en geles 2-DE. La proteómica diferencial clásica basada en geles (2-DE SDS-PAGE) ha sido muy empleada para evaluar los cambios de perfiles proteicos en plantas. Sin embargo, esta aproximación tiene sus limitaciones, como son el bajo número de proteínas de interés identificadas, la experiencia técnica (destreza) necesaria para generar geles bidimensionales de calidad y el tiempo empleado en el análisis estadístico de las imágenes (Nilo-Poyanco *et al.*, 2021).

La proteómica basada en el *shotgun* ha demostrado ser en los últimos años una herramienta robusta capaz de ampliar notablemente el número de proteínas identificadas y proporcionar así más

información sobre las vías y los procesos biológicos, permitiendo profundizar aún más en el conocimiento de los proteomas en plantas (Nilo-Poyanco *et al.*, 2021). No obstante, podemos afirmar que los dos enfoques proteómicos, ya sean basados en gel (2-DE) o no, siguen siendo herramientas útiles para entender las respuestas que las plantas desarrollan cuando se enfrentan a un estrés por metales (Ceballos-laita *et al.*, 2020).

Recientes investigaciones sobre la deficiencia de micronutrientes en plantas afirman que hoy en día las técnicas de proteómica diferencial basadas en geles bidimensionales de poliacrilamida (2-DE PAGE) sigue siendo una potente herramienta (Ali *et al.*, 2020) para investigar los cambios a nivel proteico en situación de estrés. La tendencia hoy en día es combinar los resultados de la proteómica diferencial basada en geles (2-DE) seguida del análisis compartido basado en técnicas de espectrometría de masas de alta resolución (MS/MS). Esta combinación de técnicas (Ali *et al.*, 2020) puede ayudar a identificar nuevas dianas proteicas que determinen si estos micronutrientes afectan o no a otras vías metabólicas, lo que permitirá comprender adecuadamente los mecanismos relacionados con el estrés en plantas de cultivo.

Capítulo 5

CONCLUSIONES

1. La técnica de la desorción láser asistida por matriz acoplada a la espectrometría de masas por imagen (MALDI-MSI) es una potente herramienta que permite analizar la distribución espacial de metabolitos en criosecciones de granos inmaduros de cebada (*Hordeum vulgare*) y raíces de tabaco (*Nicotiana tabacum*).
2. La optimización del proceso de preparación de la muestra es crítica para obtener unos resultados fiables usando la técnica MALDI-MSI.
3. Una vez establecido un protocolo experimental apropiado, el MALDI-MSI proporciona una herramienta rápida, precisa y altamente selectiva para la evaluación de la distribución espacial de una gran variedad de compuestos.
4. Las principales respuestas provocadas por la deficiencia de hierro en un híbrido de *Prunus* GF677 (*P. dulcis* × *P. persica*) cultivado en hidroponía están asociadas a la oxidación y al estrés general, en contraste con lo descrito en las especies herbáceas, cuya principal adaptación es la reprogramación metabólica del C/N.
5. La alta tolerancia a la deficiencia de Fe del portainjerto GF 677 está relacionada con su capacidad para provocar una sólida respuesta de defensa tanto contra el estrés general como contra el oxidativo.
6. El floema de plantas mono- y dicotiledóneas contiene proteínas que desempeñan un papel central en la función celular, implicadas en la síntesis de proteínas y el metabolismo activo de carbohidratos, lo que apoya la existencia de estas rutas de forma activa en las células de los tubos cribosos.
7. El floema de *L. texensis* contiene dos proteínas de bajo peso molecular que se unen al Fe: una metalotioneína tipo B2 y un *cluster* de hierro-azufre del Fotosistema I; y cuatro proteínas de unión al Zn: una perteneciente a la familia de la deshidrinas y tres proteínas del tipo *Zinc finger* (metalotioneninas).
8. En el floema de *L. texensis* hemos identificado la proteína de *L. albus* (A0A6A5MEV3_LUPAL) y demostrado que une hierro, posiblemente a través de sus multiples glutamatos (16), histidinas (6) y aspártatos (4).
9. La deficiencia de hierro afecta levemente la expresión proteica en el tallo de *M. truncatula*, especialmente en las proteínas fotosintéticas. La presencia de $CaCO_3$ intensifica la respuesta, elevando la expresión de proteínas vinculadas al estrés y al metabolismo proteico.
10. En el tallo de *M. truncatula*, la deficiencia de hierro provoca aumentos significativos en las proteínas relacionadas con la síntesis y modificación de la pared celular y en la ratio lignina/proteína, siendo estos cambios más pronunciados en presencia de $CaCO_3$.

BIBLIOGRAFÍA

Abadía, J. *et al.* (2002) 'Organic acids and Fe deficiency: A review', *Plant and Soil*, 241(1), pp. 75–86. Available at: https://doi.org/10.1023/A:1016093317898.

Abadía, J. *et al.* (2004) 'Technologies for the diagnosis and remediation of Fe deficiency', *Soil Science and Plant Nutrition*, 50(7), pp. 965–971. Available at: https://doi.org/10.1080/00380768.2004.10408562.

Abadía, J. *et al.* (2011) 'Towards a knowledge-based correction of iron chlorosis', *Plant Physiology and Biochemistry*, 49(5), pp. 471–482. Available at: https://doi.org/10.1016/j.plaphy.2011.01.026.

Abdallah, C. *et al.* (2012) 'Gel-based and gel-free quantitative proteomics approaches at a glance', *International Journal of Plant Genomics*, 2012. Available at: https://doi.org/10.1155/2012/494572.

Abdul-Khalek, N. *et al.* (2023) 'Insight on physicochemical properties governing peptide MS1 response in HPLC-ESI-MS/MS: A deep learning approach', *Computational and Structural Biotechnology Journal*, 21, pp. 3715–3727. Available at: https://doi.org/10.1016/J.CSBJ.2023.07.027.

Aebersold, R. and Mann, M. (2003) 'Mass spectrometry-based proteomics', *Nature*, 422(6928), pp. 198–207. Available at: https://doi.org/10.1038/nature01511.

Aebersold, R. and Mann, M. (2016) 'Mass-spectrometric exploration of proteome structure and function', *Nature*. Nature Publishing Group, pp. 347–355. Available at: https://doi.org/10.1038/nature19949.

Agar, N.Y.R. *et al.* (2010) 'Tissue preparation for the in situ MALDI MS imaging of proteins, lipids, and small molecules at cellular resolution', *Methods in Molecular Biology*, 656, pp. 415–431. Available at: https://doi.org/10.1007/978-1-60761-746-4_24.

Agrawal, G.K. *et al.* (2011) *Plant organelle proteomics: Collaborating for optimal cell function*, *Mass Spectrometry Reviews*. John Wiley & Sons, Ltd. Available at: https://onlinelibrary.wiley.com/doi/full/10.1002/mas.20301 (Accessed: 18 November 2023).

Aizat, W.M. and Hassan, M. (2018) 'Proteomics in systems biology', in *Advances in Experimental Medicine and Biology*. Springer New York LLC, pp. 31–49. Available at: https://doi.org/10.1007/978-3-319-98758-3_3.

Ajith, A. *et al.* (2022) 'Mass Spectrometry Imaging for Spatial Chemical Profiling of Vegetative Parts of Plants', *Plants*. Multidisciplinary Digital Publishing Institute, p. 1234. Available at: https://doi.org/10.3390/plants11091234.

Aki, T. *et al.* (2008) 'Nano scale proteomics revealed the presence of regulatory proteins including three FT-like proteins in phloem and xylem saps from rice', *Plant and Cell Physiology*, 49(5), pp. 767–790. Available at: https://doi.org/10.1093/pcp/pcn049.

Al-Amrani, S. *et al.* (2021) 'Proteomics: Concepts and applications in human medicine', *World Journal of Biological Chemistry*, 12(5), pp. 57–69. Available at: https://doi.org/10.4331/wjbc.v12.i5.57.

Alexandrov, T. (2012) 'MALDI imaging mass spectrometry: statistical data analysis and current computational challenges.', *BMC bioinformatics*. Available at: https://doi.org/10.1186/1471-2105-13-s16-s11.

Ali, A. *et al.* (2020) 'Proteomic Studies of Micronutrient Deficiency and Toxicity', *Plant Micronutrients*, pp. 257–284. Available at: https://doi.org/10.1007/978-3-030-49856-6_11.

Álvarez-Fernández, A. *et al.* (2003) 'Effects of Fe deficiency chlorosis on yield and fruit quality in peach (Prunus persica L. Batsch)', *Journal of Agricultural and Food Chemistry*, 51(19), pp. 5738–5744. Available at: https://doi.org/10.1021/jf034402c.

Álvarez-Fernández, A. *et al.* (2011) 'Effects of moderate and severe iron deficiency chlorosis on fruit yield, appearance and composition in pear (Pyrus communis L.) and peach (Prunus persica (L.) Batsch)', *Environmental and Experimental Botany*, 71(2), pp. 280–286. Available at: https://doi.org/10.1016/j.envexpbot.2010.12.012.

Álvarez-Fernández, A. *et al.* (2014) 'Metal species involved in long distance metal transport in plants', *Frontiers in Plant Science*, 5(MAR). Available at: https://doi.org/10.3389/FPLS.2014.00105/FULL.

Amagliani, L. *et al.* (2017) 'Composition and protein profile analysis of rice protein ingredients', *Journal of Food Composition and Analysis*, 59, pp. 18–26. Available at: https://doi.org/10.1016/j.jfca.2016.12.026.

Amantonico, A., Urban, P.L. and Zenobi, R. (2010) 'Analytical techniques for single-cell metabolomics: State of the art and trends', *Analytical and Bioanalytical Chemistry*, 398(6), pp. 2493–2504. Available at: https://doi.org/10.1007/s00216-010-3850-1.

Amstalden van Hove, E.R., Smith, D.F. and Heeren, R.M.A. (2010) 'A concise review of mass spectrometry imaging', *Journal of Chromatography A*, 1217(25), pp. 3946–3954. Available at: https://doi.org/10.1016/j.chroma.2010.01.033.

Anderson, E.R. *et al.* (2009) 'An examination of the MASC social anxiety scalein a non-referred sample of adolescents', *Journal of Anxiety Disorders*, 23(8), pp. 1098–1105. Available at: https://doi.org/10.1016/j.janxdis.2009.07.013.

Arif, Y. *et al.* (2020) 'Salinity induced physiological and biochemical changes in plants: An omic approach towards salt stress tolerance', *Plant Physiology and Biochemistry*, 156, pp. 64–77. Available at: https://doi.org/10.1016/J.PLAPHY.2020.08.042.

Aslam, B. *et al.* (2017a) *No Title*, *Journal of Chromatographic Science*. Oxford Academic. Available at: https://dx.doi.org/10.1093/chromsci/bmw167 (Accessed: 13 November 2023).

Aslam, B. *et al.* (2017b) 'Proteomics: Technologies and their applications', *Journal of Chromatographic Science*. Oxford Academic, pp. 182–196. Available at: https://doi.org/10.1093/chromsci/bmw167.

Atkins, C.A., Smith, P.M.C. and Rodriguez-Medina, C. (2011) 'Macromolecules in phloem exudates-a review', *Protoplasma*, 248(1), pp. 165–172. Available at: https://doi.org/10.1007/s00709-010-0236-3.

Awad, H., Khamis, M.M. and El-Aneed, A. (2015) 'Mass Spectrometry, Review of the Basics: Ionization', *Applied Spectroscopy Reviews*, 50(2), pp. 158–175. Available at: https://doi.org/10.1080/05704928.2014.954046.

Baerenfaller, K. *et al.* (2008) 'Genome-scale proteomics reveals Arabidopsis thaliana gene models and proteome dynamics', *Science*, 320(5878), pp. 938–941. Available at: https://doi.org/10.1126/SCIENCE.1157956/SUPPL_FILE/BAERENFALLER.SOM.PDF.

Barnes, A. *et al.* (2004) 'Determining protein identity from sieve element sap in Ricinus communis L. by quadrupole time of flight (Q-TOF) mass spectrometry', *Journal of Experimental Botany*, 55(402), pp. 1473–1481. Available at: https://doi.org/10.1093/jxb/erh161.

Barton, L.L. and Abadia, J. (2006) *Iron nutrition in plants and Rhizospheric microorganisms*, *Iron Nutrition in Plants and Rhizospheric Microorganisms*. Available at: https://doi.org/10.1007/1-4020-4743-6.

Bashir, K. *et al.* (2006) 'Cloning and characterization of deoxymugineic acid synthase genes from graminaceous plants', *Journal of Biological Chemistry*, 281(43), pp. 32395–32402. Available at: https://doi.org/10.1074/jbc.M604133200.

Bashir, K. *et al.* (2016) 'Regulating subcellular metal homeostasis: The key to crop improvement', *Frontiers in Plant Science*, 7(AUG2016), p. 204298. Available at: https://doi.org/10.3389/FPLS.2016.01192/BIBTEX.

Batailler, B. *et al.* (2012) 'Soluble and filamentous proteins in Arabidopsis sieve elements', *Plant, Cell and Environment*, 35(7), pp. 1258–1273. Available at: https://doi.org/10.1111/j.1365-3040.2012.02487.x.

Bateman, A. *et al.* (2023) 'UniProt: the Universal Protein Knowledgebase in 2023', *Nucleic Acids Research*, 51(D1), pp. D523–D531. Available at: https://doi.org/10.1093/NAR/GKAC1052.

Benedito, V.A. *et al.* (2008) 'A gene expression atlas of the model legume Medicago truncatula', *Plant Journal*, 55(3), pp. 504–513. Available at: https://doi.org/10.1111/j.1365-313X.2008.03519.x.

Beretov, J. *et al.* (2014) 'Proteomics for breast cancer urine biomarkers', in *Advances in Clinical Chemistry*. Elsevier, pp. 123–167. Available at: https://doi.org/10.1016/B978-0-12-800094-6.00004-2.

Bian, Y. *et al.* (2021a) 'Identification of 7 000-9 000 Proteins from Cell Lines and Tissues by Single-Shot Microflow LC-MS/MS', *Analytical Chemistry*, 93(25), pp. 8687–8692. Available at: https://doi.org/10.1021/ACS.ANALCHEM.1C00738/SUPPL_FILE/AC1C00738_SI_002.XLSX.

Bian, Y. *et al.* (2021b) 'Identification of 7 000-9 000 Proteins from Cell Lines and Tissues by Single-Shot Microflow LC-MS/MS', *Analytical Chemistry*, 93(25), pp. 8687–8692. Available at: https://doi.org/10.1021/acs.analchem.1c00738.

Bjellqvist, B. *et al.* (1982) 'Isoelectric focusing in immobilized pH gradients: Principle, methodology and some applications', *Journal of Biochemical and Biophysical Methods*, 6(4), pp. 317–339. Available at: https://doi.org/10.1016/0165-022X(82)90013-6.

Blum, H., Beier, H. and Gross, H.J. (1987) 'Improved silver staining of plant proteins, RNA and DNA in polyacrylamide gels', *Electrophoresis*, 8(2), pp. 93–99. Available at: https://doi.org/10.1002/elps.1150080203.

Borlotti, A., Vigani, G. and Zocchi, G. (2012) 'Iron deficiency affects nitrogen metabolism in cucumber (Cucumis sativus L.) plants', *BMC Plant Biology*, 12, p. 189. Available at: https://doi.org/10.1186/1471-2229-12-189.

Boughton, B.A. *et al.* (2016) 'Mass spectrometry imaging for plant biology: a review', *Phytochemistry Reviews*, 15(3), pp. 445–488. Available at: https://doi.org/10.1007/s11101-015-9440-2.

Brais, C.J. *et al.* (2021) 'RECENT ADVANCES IN INSTRUMENTAL APPROACHES TO TIME-OF-FLIGHT MASS SPECTROMETRY', *Mass Spectrometry Reviews*. John Wiley & Sons, Ltd, pp. 647–669. Available at: https://doi.org/10.1002/mas.21650.

De Bruijn, F.J. (2019) 'Medicago truncatula proteomics: Introduction', *The Model Legume Medicago truncatula*, 73, pp. 1068–1069. Available at: https://doi.org/10.1002/9781119409144.ch137.

Brumbarova, T. *et al.* (2008) 'A proteomic study showing differential regulation of stress, redox regulation and peroxidase proteins by iron supply and the transcription factor FER', *Plant Journal*, 54(2), pp. 321–334. Available at: https://doi.org/10.1111/j.1365-313X.2008.03421.x.

Buchberger, A.R. *et al.* (2018) 'Mass Spectrometry Imaging: A Review of Emerging Advancements and Future Insights', *Analytical Chemistry*, 90(1), pp. 240–265. Available at: https://doi.org/10.1021/ACS.ANALCHEM.7B04733/ASSET/IMAGES/ACS.ANALCHEM.7B04733.SOCIAL.JPEG_V03.

Buhtz, A. *et al.* (2008) 'Identification and characterization of small RNAs from the phloem of Brassica napus', *Plant Journal*, 53(5), pp. 739–749. Available at: https://doi.org/10.1111/j.1365-313X.2007.03368.x.

Burnum, K.E., Frappier, S.L. and Caprioli, R.M. (2008) 'Matrix-assisted laser desorption/ionization imaging mass spectrometry for the investigation of proteins and peptides', *Annual Review of Analytical Chemistry*, 1(1), pp. 689–705. Available at: https://doi.org/10.1146/annurev.anchem.1.031207.112841.

Burrell, M.M., Earnshaw, C.J. and Clench, M.R. (2007) 'Imaging Matrix Assisted Laser Desorption Ionization Mass Spectrometry: A technique to map plant metabolites within tissues at high spatial resolution', *Journal of Experimental Botany*, 58(4), pp. 757–763. Available at: https://doi.org/10.1093/jxb/erl139.

Camps-Valls, G. and Morgan Chalk, A. (2011) 'Bioinformatics and Computational Biology', in S. Rajasekaran (ed.) *Encyclopedia of Data Warehousing and Mining, Second Edition*. Springer-Verlag, pp. 282–294. Available at: https://doi.org/10.4018/9781605660103.ch026.

Cannon, W.B. (1929) 'Organization for Physiological Homeostasis', *Physiological Reviews*, 9(3), pp. 399–431. Available at: https://doi.org/10.1152/physrev.1929.9.3.399.

Caprioli, R.M., Farmer, T.B. and Gile, J. (1997) 'Molecular Imaging of Biological Samples: Localization of Peptides and Proteins Using MALDI-TOF MS', *Analytical Chemistry*, 69(23), pp. 4751–4760. Available at: https://doi.org/10.1021/ac970888i.

Carella, P. *et al.* (2016) 'Comparative proteomics analysis of phloem exudates collected during the induction of systemic acquired resistance', *Plant Physiology*, 171(2), pp. 1495–1510. Available at: https://doi.org/10.1104/pp.16.00269.

Carpentler, S.C. *et al.* (2008) 'Proteome analysis of non-model plants: A challenging but powerful approach', *Mass Spectrometry Reviews*, 27(4), pp. 354–377. Available at: https://doi.org/10.1002/MAS.20170.

Castañeda, V., González, E.M. and Wienkoop, S. (2021) 'Phloem Sap Proteins Are Part of a Core Stress Responsive Proteome Involved in Drought Stress Adjustment', *Frontiers in Plant Science*, 12, p. 625224. Available at: https://doi.org/10.3389/fpls.2021.625224.

Ceballos-Laita, L. *et al.* (2022) 'Effects of Fe and Mn Deficiencies on the Root Protein Profiles of Tomato (Solanum lycopersicum) Using Two-Dimensional Electrophoresis and Label-Free Shotgun Analyses', *International Journal of Molecular Sciences*, 23(7), p. 3719. Available at: https://doi.org/10.3390/IJMS23073719/S1.

Ceballos-laita, L. *et al.* (2020) 'Effects of excess manganese on the xylem sap protein profile of tomato (Solanum lycopersicum) as revealed by shotgun proteomic analysis', *International Journal of Molecular Sciences*, 21(22), pp. 1–28. Available at: https://doi.org/10.3390/ijms21228863.

Cesco, S. *et al.* (2010) 'Release of plant-borne flavonoids into the rhizosphere and their role in plant nutrition', *Plant and Soil*, 329(1), pp. 1–25. Available at: https://doi.org/10.1007/s11104-009-0266-9.

Chaurand, P., Schwartz, S.A., *et al.* (2004) 'Integrating Histology and Imaging Mass Spectrometry', *Analytical Chemistry*, 76(4), pp. 1145–1155. Available at: https://doi.org/10.1021/AC0351264.

Chaurand, P., Sanders, M.E., *et al.* (2004) 'Proteomics in diagnostic pathology: Profiling and imaging proteins directly in tissue sections', *American Journal of Pathology*, 165(4), pp. 1057–1068. Available at: https://doi.org/10.1016/S0002-9440(10)63367-6.

Chaurand, P. and Caprioli, R.M. (2002) 'Direct Profiling and Imaging of Peptides and Proteins from Mammalian Cells and Tissue Sections by Mass Spectrometry', *Electrophoresis*, 23(18), p. 3125.

Chaurand, P., Schwartz, S.A. and Caprioli, R.M. (2004) 'Assessing Protein Patterns in Disease Using Imaging Mass Spectrometry', *J. Proteome Res.*, 3(2), p. 245.

Chen, H. and Xiong, L. (2005) 'Pyridoxine is required for post-embryonic root development and tolerance to osmotic and oxidative stresses', *Plant Journal*, 44(3), pp. 396–408. Available at: https://doi.org/10.1111/j.1365-313X.2005.02538.x.

Chen, J. *et al.* (2023) 'Spatial lipidomics and metabolomics of multicellular tumor spheroids using MALDI-2 and trapped ion mobility imaging', *Talanta*, 265, p. 124795. Available at: https://doi.org/10.1016/J.TALANTA.2023.124795.

Chen, S. and Harmon, A.C. (2006) 'Advances in plant proteomics', *PROTEOMICS*, 6(20), pp. 5504–5516. Available at: https://doi.org/10.1002/PMIC.200600143.

Chen, Y.L. *et al.* (2019) 'An improved scoring method for the identification of endogenous peptides based on the Mascot MS/MS ion search', *Analyst*, 144(9), pp. 3045–3055. Available at: https://doi.org/10.1039/C8AN02141D.

Choi, S.H., Kim, Y.W. and Kim, S.G. (2010) 'AMPK-mediated GSK3β inhibition by isoliquiritigenin contributes to protecting mitochondria against iron-catalyzed oxidative stress', *Biochemical Pharmacology*, 79(9), pp. 1352–1362. Available at: https://doi.org/10.1016/j.bcp.2009.12.011.

Cinelli, F., Iacona, C. and Tamantini, I. (2004) 'Nutritional (Fe-Mn) interactions in "Big Top" peach plants as influenced by the rootstock and by the soil CaCO3 concentration', *Soil Science and Plant Nutrition*, 50(7), pp. 1097–1102. Available at: https://doi.org/10.1080/00380768.2004.10408580.

Cinelli, F. and Loreti, F. (2004) 'Evaluation of some plum rootstocks in relation to lime-induced chlorosis by hydroponic culture', *Acta Horticulturae*, 658, pp. 421–427. Available at: https://doi.org/10.17660/ActaHortic.2004.658.62.

Cobbett, C. and Goldsbrough, P. (2002) 'Phytochelatins and metallothioneins: Roles in heavy metal detoxification and homeostasis', *Annual Review of Plant Biology*, 53, pp. 159–182. Available at: https://doi.org/10.1146/annurev.arplant.53.100301.135154.

Colombo, C. *et al.* (2014) 'Review on iron availability in soil: Interaction of Fe minerals, plants, and microbes', *Journal of Soils and Sediments*, 14(3), pp. 538–548. Available at: https://doi.org/10.1007/S11368-013-0814-Z.

Cornett, D.S. *et al.* (2006) 'A novel histology-directed strategy for MALDI-MS tissue profiling that improves throughput and cellular specificity in human breast cancer', *Molecular and Cellular Proteomics*, 5(10), pp. 1975–1983. Available at: https://doi.org/10.1074/mcp.M600119-MCP200.

Coulombe, B.A., Chaney, R.L. and Wiebold, W.J. (1984) 'Bicarbonate Directly Induces Iron Chlorosis in Susceptible Soybean Cultivars', *Soil Science Society of America Journal*, 48(6), pp. 1297–1301. Available at: https://doi.org/10.2136/sssaj1984.03615995004800060019x.

Cox, J. and Mann, M. (2007) 'Is Proteomics the New Genomics?', *Cell*, 130(3), pp. 395–398. Available at: https://doi.org/10.1016/j.cell.2007.07.032.

Cui, M., Cheng, C. and Zhang, L. (2022) 'High-throughput proteomics: a methodological mini-review', *Laboratory Investigation*. Elsevier, pp. 1170–1181. Available at: https://doi.org/10.1038/s41374-022-00830-7.

Curie, C. *et al.* (2001) 'Maize yellow stripe1 encodes a membrane protein directly involved in Fe(III) uptake', *Nature*, 409(6818), pp. 346–349. Available at: https://doi.org/10.1038/35053080.

Curie, C. *et al.* (2009) 'Metal movement within the plant: Contribution of nicotianamine and yellow stripe 1-like transporters', *Annals of Botany*, 103(1), pp. 1–11. Available at: https://doi.org/10.1093/aob/mcn207.

Dafoe, N.J. *et al.* (2009) 'Analysis of the poplar phloem proteome and its response to leaf wounding', *Journal of Proteome Research*, 8(5), pp. 2341–2350. Available at: https://doi.org/10.1021/pr800968r.

De Vleesschauwer, D., Chernin, L. and Höfte, M.M. (2009) 'Differential effectiveness of Serratia plymuthica IC1270-induced systemic resistance against hemibiotrophic and necrotrophic leaf pathogens in rice', *BMC Plant Biology*, 9, p. 1. Available at: https://doi.org/10.1186/1471-2229-9-9.

Deeken, R. *et al.* (2008) 'Identification of Arabidopsis thaliana phloem RNAs provides a search criterion for phloem-based transcripts hidden in complex datasets of microarray experiments', *Plant Journal*, 55(5), pp. 746–759. Available at: https://doi.org/10.1111/j.1365-313X.2008.03555.x.

Dell'Orto, M. *et al.* (2000) 'Development of Fe-deficiency responses in cucumber (Cucumis sativus L.) roots: Involvement of plasma membrane H+-ATPase activity', *Journal of Experimental Botany*, 51(345), pp. 695–701. Available at: https://doi.org/10.1093/jxb/51.345.695.

Dinneny, J.R. *et al.* (2008) 'Cell identity mediates the response of Arabidopsis roots to abiotic stress', *Science*, 320(5878), pp. 942–945. Available at: https://doi.org/10.1126/science.1153795.

Dinneny, J.R. (2010) 'Analysis of the salt-stress response at cell-type resolution', *Plant, Cell and Environment*, 33(4), pp. 543–551. Available at: https://doi.org/10.1111/j.1365-3040.2009.02055.x.

Djikanović, D. *et al.* (2012) 'Structural Differences Between Lignin Model Polymers Synthesized from Various Monomers', *Journal of Polymers and the Environment*, 20(2), pp. 607–617. Available at: https://doi.org/10.1007/s10924-012-0422-9.

Do, C.T. *et al.* (2007) 'Both caffeoyl Coenzyme A 3-O-methyltransferase 1 and caffeic acid O-methyltransferase 1 are involved in redundant functions for lignin, flavonoids and sinapoyl malate biosynthesis in Arabidopsis', *Planta*, 226(5), pp. 1117–1129. Available at: https://doi.org/10.1007/s00425-007-0558-3.

Doering-Saad, C. *et al.* (2006) 'A phloem-enriched cDNA library from Ricinus: Insights into phloem function', *Journal of Experimental Botany*, 57(12), pp. 3183–3193. Available at: https://doi.org/10.1093/jxb/erl082.

Döll, S. *et al.* (2021) 'Tissue-specific signatures of metabolites and proteins in asparagus roots and exudates', *Horticulture Research*, 8(1), pp. 1–14. Available at: https://doi.org/10.1038/s41438-021-00510-5.

Dong, Q. *et al.* (2005) 'Comparative EST Analyses in Plant Systems', *Methods in Enzymology*, 395, pp. 400–418. Available at: https://doi.org/10.1016/S0076-6879(05)95022-2.

Dong, Y. *et al.* (2016) 'Sample preparation for mass spectrometry imaging of plant tissues: A review', *Frontiers in Plant Science*, 7(FEB2016), p. 60. Available at: https://doi.org/10.3389/fpls.2016.00060.

Donnini, S. *et al.* (2009) 'Differential responses in pear and quince genotypes induced by Fe deficiency and bicarbonate', *Journal of Plant Physiology*, 166(11), pp. 1181–1193. Available at: https://doi.org/10.1016/j.jplph.2009.01.007.

Donnini, S. *et al.* (2010) 'Proteomic characterization of iron deficiency responses in Cucumis sativus L. roots', *BMC Plant Biology*, 10, p. 268. Available at: https://doi.org/10.1186/1471-2229-10-268.

Donnini, S., Dell'Orto, M. and Zocchi, G. (2011) 'Oxidative stress responses and root lignification induced by Fe deficiency conditions in pear and quince genotypes', *Tree Physiology*, 31(1), pp. 102–113. Available at: https://doi.org/10.1093/treephys/tpq105.

Dreisewerd, K. *et al.* (1995) 'Influence of the Laser Intensity and Spot Size on the Desorption of Molecules and Ions in Matrix-Assisted Laser-Desorption Ionization with a Uniform Beam Profile', *Int. J. Mass Spectrom. Ion Processes*, 141(2), p. 127.

Dupree, E.J. *et al.* (2020) *A critical review of bottom-up proteomics: The good, the bad, and the future of this field*, *Proteomes*. Multidisciplinary Digital Publishing Institute. Available at: https://doi.org/10.3390/proteomes8030014.

Durrett, T.P., Gassmann, W. and Rogers, E.E. (2007) 'The FRD3-mediated efflux of citrate into the root vasculature is necessary for efficient iron translocation', *Plant Physiology*, 144(1), pp. 197–205. Available at: https://doi.org/10.1104/pp.107.097162.

Dyballa, N. and Metzger, S. (2009) 'Fast and sensitive colloidal coomassie G-250 staining for proteins in polyacrylamide gels', *Journal of visualized experiments : JoVE* [Preprint], (30). Available at: https://doi.org/10.3791/1431.

Eichert, T. *et al.* (2010) 'Effects of iron chlorosis and iron resupply on leaf xylem architecture, water relations, gas exchange and stomatal performance of field-grown peach (Prunus persica)', *Physiologia Plantarum*, 138(1), pp. 48–59. Available at: https://doi.org/10.1111/j.1399-3054.2009.01295.x.

Eide, D. *et al.* (1996) 'A novel iron-regulated metal transporter from plants identified by functional expression in yeast', *Proceedings of the National Academy of Sciences of the United States of America*, 93(11), pp. 5624–5628. Available at: https://doi.org/10.1073/pnas.93.11.5624.

Eisenberg, D. *et al.* (2000) 'Structure-function relationships of glutamine synthetasesre', *Biochimica et Biophysica Acta - Protein Structure and Molecular Enzymology*, 1477(1–2), pp. 122–145. Available at: https://doi.org/10.1016/S0167-4838(99)00270-8.

El-Aneed, A., Cohen, A. and Banoub, J. (2009) 'Mass Spectrometry, Review of the Basics: Electrospray, MALDI, and Commonly Used Mass Analyzers', *Applied Spectroscopy Reviews*, 44(3), pp. 210–230. Available at: https://doi.org/10.1080/05704920902717872.

Enomoto, Y. *et al.* (2007) 'Long-distance signals positively regulate the expression of iron uptake genes in tobacco roots', *Planta*, 227(1), pp. 81–89. Available at: https://doi.org/10.1007/s00425-007-0596-x.

Evert, R.F. and Elements, S. (1990) *Comparative Structure, Induction and Development, Springer-Verlag*. Berlin: Springer-Verlag.

Fang, H.M. and Wang, Y. (2002) 'Characterization of iron-binding motifs in Candida albicans high-affinity iron permease CaFtr1p by site-directed mutagenesis', *Biochemical Journal*, 368(2), pp. 641–647. Available at: https://doi.org/10.1042/BJ20021005.

Fenn, J.B. *et al.* (1989) 'Electrospray Ionization for Mass Spectrometry of Large Biomolecules', *Science*, 246(4926), pp. 64–71. Available at: https://doi.org/10.1126/SCIENCE.2675315.

Fernández, V. *et al.* (2008) 'Leaf structural changes associated with iron deficiency chlorosis in field-grown pear and peach: Physiological implications', *Plant and Soil*, 311(1–2), pp. 161–172. Available at: https://doi.org/10.1007/s11104-008-9667-4.

Fey, S.J. and Larsen, P.M. (2001) '2D or not 2D', *Current Opinion in Chemical Biology*, 5(1), pp. 26–33. Available at: https://doi.org/10.1016/S1367-5931(00)00167-8.

Fiehn, O. (2003) 'Metabolic networks of Cucurbita maxima phloem', *Phytochemistry*, 62(6), pp. 875–886. Available at: https://doi.org/10.1016/S0031-9422(02)00715-X.

Fisher, D.B., Wu, Y. and Ku, M.S.B. (1992) 'Turnover of soluble proteins in the wheat sieve tube', *Plant Physiology*, 100(3), pp. 1433–1441. Available at: https://doi.org/10.1104/pp.100.3.1433.

Fourcroy, P. *et al.* (2014) 'Involvement of the ABCG37 transporter in secretion of scopoletin and derivatives by Arabidopsis roots in response to iron deficiency', *New Phytologist*, 201(1), pp. 155–167. Available at: https://doi.org/10.1111/nph.12471.

Froechlich, D.M. and Fehr, W.R. (1981) ' Agronomic Performance of Soybeans with Differing Levels of Iron Deficiency Chlorosis on Calcareous Soil 1 ', *Crop Science*, 21(3), pp. 438–441. Available at: https://doi.org/10.2135/cropsci1981.0011183x002100030021x.

Fuchs, P. *et al.* (2020) 'Single organelle function and organization as estimated from Arabidopsis mitochondrial proteomics', *The Plant Journal*, 101(2), pp. 420–441. Available at: https://doi.org/10.1111/TPJ.14534.

G. Zocchi (2006) 'Metabolic changes in iron-stressed dicotyledoneus plants', in J.A. (Eds. in: L.L. Barton (ed.) *Iron Nutrition in Plants and Rhizospheric Microorganisms*. Dordrecht: Springer, pp. 359–370.

Gang, D.R. *et al.* (1999) 'Evolution of plant defense mechanisms: Relationships of phenylcoumaran benzylic ether reductases to pinoresinol-lariciresinol and isoflavone reductases', *Journal of Biological Chemistry*, 274(11), pp. 7516–7527. Available at: https://doi.org/10.1074/jbc.274.11.7516.

Garcia, C.B. and Grusak, M.A. (2015) 'Mineral accumulation in vegetative and reproductive tissues during seed development in Medicago truncatula', *Frontiers in Plant Science*, 6(AUG), p. 622. Available at: https://doi.org/10.3389/fpls.2015.00622.

Gardel, M.L. *et al.* (2008) 'Chapter 19 Mechanical Response of Cytoskeletal Networks', in J.C. Correia and H.W. Detrich (eds) *Methods in Cell Biology*. Academy Press, pp. 487–519. Available at: https://doi.org/10.1016/S0091-679X(08)00619-5.

Garden, R.W. and Sweedler, J. V. (1999) 'Heterogeneity within MALDI Samples As Revealed by Mass Spectrometric Imaging', *Analytical Chemistry*, 72(1), pp. 30–36. Available at: https://doi.org/10.1021/AC9908997.

Garden, R.W. and Sweedler, J. V (2000) 'Heterogeneity Within MALDI Samples as Revealed by Mass Spectrometric Imaging', *Anal. Chem.*, 72(1), p. 30.

Garg, M. *et al.* (2018) 'Biofortified Crops Generated by Breeding, Agronomy, and Transgenic Approaches Are Improving Lives of Millions of People around the World', *Frontiers in Nutrition*, 5, p. 301899. Available at: https://doi.org/10.3389/FNUT.2018.00012/BIBTEX.

Garrett, T.J. *et al.* (2011) 'Lipid analysis of flat-mounted eye tissue by imaging mass spectrometry with identification of contaminants in preservation', *Analytical and Bioanalytical Chemistry*, 401(1), pp. 103–113. Available at: https://doi.org/10.1007/s00216-011-5044-x.

Gessel, M.M., Norris, J.L. and Caprioli, R.M. (2014) *MALDI imaging mass spectrometry: Spatial molecular analysis to enable a new age of discovery*, *Journal of Proteomics*. Elsevier. Available at: https://doi.org/10.1016/j.jprot.2014.03.021.

Giavalisco, P. *et al.* (2006) 'Towards the proteome of Brassica napus phloem sap', *Proteomics*, 6(3), pp. 896–909. Available at: https://doi.org/10.1002/pmic.200500155.

Giorgi, M. *et al.* (2005) 'The rootstock effects on plant adaptability, production, fruit quality, and nutrition in the peach (cv. 'Suncrest')', *Scientia Horticulturae*, 107(1), pp. 36–42. Available at: https://doi.org/10.1016/j.scienta.2005.06.003.

Giritch, A. *et al.* (1998) 'Structure, expression and chromosomal localisation of the metallothionein-like gene family of tomato', *Plant Molecular Biology*, 37(4), pp. 701–714. Available at: https://doi.org/10.1023/A:1006001701919.

Gogorcena, Y. *et al.* (2001) 'Characterization of the responses of cork oak (Quercus suber) to iron deficiency', *Tree Physiology*, 21(18), pp. 1335–1340. Available at: https://doi.org/10.1093/treephys/21.18.1335.

Gogorcena, Y., Abadía, J. and Abadía, A. (2000) 'Induction of in vivo root ferric chelate reductase activity in fruit tree rootstock', *Journal of Plant Nutrition*, 23(1), pp. 9–21. Available at: https://doi.org/10.1080/01904160009381993.

Gogorcena, Y., Abadía, J. and Abadía, A. (2004) 'A new technique for screening iron-efficient genotypes in peach rootstocks: Elicitation of root ferric chelate reductase by manipulation of external iron concentrations', *Journal of Plant Nutrition*, 27(10), pp. 1701–1715. Available at: https://doi.org/10.1081/LPLA-200026406.

Gonzalo, M.J., Moreno, M.Á. and Gogorcena, Y. (2011) 'Physiological responses and differential gene expression in Prunus rootstocks under iron deficiency conditions', *Journal of Plant Physiology*, 168(9), pp. 887–893. Available at: https://doi.org/10.1016/j.jplph.2010.11.017.

Goodwin, R.J.A., Pennington, S.R. and Pitt, A.R. (2008) 'Protein and peptides in pictures: Imaging with MALDI mass spectrometry', *Proteomics*, 8(18), pp. 3785–3800. Available at: https://doi.org/10.1002/pmic.200800320.

Görg, A. *et al.* (1995) 'Two-dimensional polyacrylamide gel electrophoresis with immobilized pH gradients in the first dimensin (IPG-Dalt): The state of the art and the controversy of vertical versus horizontal systems', *ELECTROPHORESIS*, 16(1), pp. 1079–1086. Available at: https://doi.org/10.1002/elps.11501601183.

Görg, A., Weiss, W. and Dunn, M.J. (2004) 'Current two-dimensional electrophoresis technology for proteomics', *PROTEOMICS*, 4(12), pp. 3665–3685. Available at: https://doi.org/10.1002/PMIC.200401031.

Goto-Inoue, N., Setou, M. and Zaima, N. (2010) 'Visualization of spatial distribution of γ-aminobutyric acid in eggplant (Solanum melongena) by matrix-assisted laser desorption/ionization imaging mass spectrometry', *Analytical Sciences*, 26(7), pp. 821–825. Available at: https://doi.org/10.2116/analsci.26.821.

Groseclose, M.R. *et al.* (2007) 'Identification of proteins directly from tissue: In situ tryptic digestions coupled with imaging mass spectrometry', *Journal of Mass Spectrometry*, 42(2), pp. 254–262. Available at: https://doi.org/10.1002/jms.1177.

Gusev, A.I. *et al.* (1995) 'Imaging of Thin-Layer Chromatograms Using Matrix-Assisted Laser Desorption/Ionization Mass Spectrometry', *Analytical Chemistry*, 67(24), pp. 4565–4570. Available at: https://doi.org/10.1021/ac00120a021.

Gustafsson, J.O.R., McColl, S.R. and Hoffmann, P. (2008) 'Imaging Mass Spectrometry (IMS) and its Application to Murine Tissues', *Journal of Proteomics & Bioinformatics*, S2(01), pp. 172–173. Available at: https://doi.org/10.4172/jpb.s1000128.

Gutierrez-Carbonell, E. *et al.* (2013) 'Changes induced by zinc toxicity in the 2-DE protein profile of sugar beet roots', *Journal of Proteomics*, 94, pp. 149–161. Available at: https://doi.org/10.1016/j.jprot.2013.09.002.

Haag, A.M. (2016) 'Mass analyzers and mass spectrometers', in *Advances in Experimental Medicine and Biology*. Springer New York LLC, pp. 157–169. Available at: https://doi.org/10.1007/978-3-319-41448-5_7.

Haebel, S. and Kehr, J. (2001) 'Erratum: Matrix-assisted laser desorption/ionization time of flight mass spectrometry peptide mass fingerprints and post source decay: A tool for the identification and analysis of phloem proteins from Cucurbita maxima Duch. separated by two-dimensional p', *Planta*, 214(2), p. 332. Available at: https://doi.org/10.1007/s00425-001-0695-z.

Halder, T. *et al.* (2022) 'Wheat Proteomics for Abiotic Stress Tolerance and Root System Architecture: Current Status and Future Prospects', *Proteomes 2022, Vol. 10, Page 17*, 10(2), p. 17. Available at: https://doi.org/10.3390/PROTEOMES10020017.

Hanin, M. *et al.* (2011) 'Plant dehydrins and stress tolerance: Versatile proteins for complex mechanisms', *Plant Signaling and Behavior*, 6(10), pp. 1503–1509. Available at: https://doi.org/10.4161/psb.6.10.17088.

Hankin, J. *et al.* (2007) 'Sublimation as a method of matrix application for mass spectrometric imaging', *ACS Publications*, 18(9), pp. 1646–1652. Available at: https://doi.org/10.1016/j.jasms.2007.06.010.

Haraguchi, H. *et al.* (1998) 'Antioxidative and superoxide scavenging activities of retrochalcones in Glycyrrhiza inflata', *Bioorganic and Medicinal Chemistry*, 6(3), pp. 339–347. Available at: https://doi.org/10.1016/S0968-0896(97)10034-7.

Harris, W.R., Sammons, R.D. and Grabiak, R.C. (2012) 'A speciation model of essential trace metal ions in phloem', *Journal of Inorganic Biochemistry*, 116, pp. 140–150. Available at: https://doi.org/10.1016/j.jinorgbio.2012.07.011.

Hassinen, V.H. *et al.* (2011) 'Plant metallothioneins - metal chelators with ROS scavenging activity?', *Plant Biology*, 13(2), pp. 225–232. Available at: https://doi.org/10.1111/j.1438-8677.2010.00398.x.

Hayashi, H. *et al.* (2000) 'Proteins in the sieve element-companion cell complexes: Their detection, localization and possible functions', *IMF Occasional Papers*, 27(189), pp. 489–496.

Henzel, W.J., Watanabe, C. and Stults, J.T. (2003) 'Protein identification: The origins of peptide mass fingerprinting', *Journal of the American Society for Mass Spectrometry*, 14(9), pp. 931–942. Available at: https://doi.org/10.1016/S1044-0305(03)00214-9.

Heyman, H.M. and Dubery, I.A. (2016) 'The potential of mass spectrometry imaging in plant metabolomics: a review', *Phytochemistry Reviews*, 15(2), pp. 297–316. Available at: https://doi.org/10.1007/s11101-015-9416-2.

Higuchi, K. *et al.* (1999) 'Cloning of nicotianamine synthase genes, novel genes involved in the biosynthesis of phytosiderophores', *Plant Physiology*, 119(2), pp. 471–479. Available at: https://doi.org/10.1104/pp.119.2.471.

Higuchi, T. (1981) 'Biosynthesis of Lignin', in *Plant Carbohydrates II*. Berlin Heidelberg: Springer, pp. 194–224. Available at: https://doi.org/10.1007/978-3-642-68234-6_9.

Hindt, M.N. and Guerinot, M. Lou (2012) 'Getting a sense for signals: Regulation of the plant iron deficiency response', *Biochimica et Biophysica Acta - Molecular Cell Research*, 1823(9), pp. 1521–1530. Available at: https://doi.org/10.1016/j.bbamcr.2012.03.010.

Ho, C.S. *et al.* (2003) 'Electrospray Ionisation Mass Spectrometry: Principles and Clinical Applications', *The Clinical Biochemist Reviews*, 24(1), p. 3. Available at: /pmc/articles/PMC1853331/ (Accessed: 19 November 2023).

Hölscher, D. *et al.* (2009) 'Matrix-free UV-laser desorption/ionization (LDI) mass spectrometric imaging at the single-cell level: Distribution of secondary metabolites of Arabidopsis thaliana and Hypericum species', *Plant Journal*, 60(5), pp. 907–918. Available at: https://doi.org/10.1111/j.1365-313X.2009.04012.x.

Holzscheiter, M.H. (1995) 'A brief history in time of ion traps and their achievements in science', *Physica Scripta*, 1995(T59), pp. 69–76. Available at: https://doi.org/10.1088/0031-8949/1995/T59/009.

Horn, P.J. and Chapman, K.D. (2023) 'Imaging plant metabolism in situ', *Journal of Experimental Botany* [Preprint]. Available at: https://doi.org/10.1093/JXB/ERAD423.

Hossain, Z. and Komatsu, S. (2013) 'Contribution of proteomic studies towards understanding plant heavy metal stress response', *Frontiers in Plant Science*, 3(JAN). Available at: https://doi.org/10.3389/fpls.2012.00310.

Hu, J., Rampitsch, C. and Bykova, N. V. (2015) 'Advances in plant proteomics toward improvement of crop productivity and stress resistance', *Frontiers in Plant Science*, 6(APR), p. 132865. Available at: https://doi.org/10.3389/FPLS.2015.00209/BIBTEX.

Hua, L. *et al.* (2007) 'Silver nanoparticles as matrix for laser desorption/ionization mass spectrometry of peptides', *Journal of Nanoparticle Research*, 9(6), pp. 1133–1138. Available at: https://doi.org/10.1007/s11051-007-9244-4.

Humphery-Smith, I. (2015) 'The 20th anniversary of proteomics and some of its origins', *Proteomics*, 15(11), pp. 1773–1776. Available at: https://doi.org/10.1002/PMIC.201400582.

Husi, H. and Albalat, A. (2014) 'Proteomics', in *Handbook of Pharmacogenomics and Stratified Medicine*. Academic Press, pp. 147–179. Available at: https://doi.org/10.1016/B978-0-12-386882-4.00009-8.

Inoue, H. *et al.* (2003) 'Three rice nicotianamine synthase genes, OsNAS1, OsNAS2, and OsNAS3 are expressed in cells involved in long-distance transport of iron and differentially regulated by iron', *Plant Journal*, 36(3), pp. 366–381. Available at: https://doi.org/10.1046/j.1365-313X.2003.01878.x.

Inoue, H. *et al.* (2008) 'Identification and localisation of the rice nicotianamine aminotransferase gene OsNAAT1 expression suggests the site of phytosiderophore synthesis in rice', *Plant Molecular Biology*, 66(1–2), pp. 193–203. Available at: https://doi.org/10.1007/S11103-007-9262-8.

Ishimaru, Y. *et al.* (2006) 'Rice plants take up iron as an Fe3+-phytosiderophore and as Fe2+', *Wiley Online LibraryY Ishimaru, M Suzuki, T Tsukamoto, K Suzuki, M Nakazono, T Kobayashi, Y WadaThe Plant Journal, 2006•Wiley Online Library*, 45(3), pp. 335–346. Available at: https://doi.org/10.1111/j.1365-313X.2005.02624.x.

Ishiwatari, Y. *et al.* (1995) 'Thioredoxin h is one of the major proteins in rice phloem sap', *Planta*, 195(3), pp. 456–463. Available at: https://doi.org/10.1007/BF00202605.

Iturbe-Ormaetxe, I. *et al.* (1995) 'Activated oxygen and antioxidant defences in iron-deficient pea plants', *Plant, Cell & Environment*, 18(4), pp. 421–429. Available at: https://doi.org/10.1111/j.1365-3040.1995.tb00376.x.

Jiménez, S. (2006) *Selección de patrones frutales de hueso tolerantes a la clorosis férrica. Aspectos nutricionales y metabólicos*, *Dialnet*. University of Zaragoza. Available at: https://digital.csic.es/handle/10261/9629 (Accessed: 17 September 2021).

Jiménez, S. *et al.* (2008) 'Tolerance response to iron chlorosis of Prunus selections as rootstocks', *HortScience*, 43(2), pp. 304–309. Available at: https://doi.org/10.21273/hortsci.43.2.304.

Jiménez, S. *et al.* (2009) 'Elemental 2-D mapping and changes in leaf iron and chlorophyll in response to iron re-supply in iron-deficient GF 677 peach-almond hybrid', *Plant and Soil*, 315(1–2), pp. 93–106. Available at: https://doi.org/10.1007/s11104-008-9735-9.

Jiménez, S. *et al.* (2011) 'Metabolic response in roots of Prunus rootstocks submitted to iron chlorosis', *Journal of Plant Physiology*, 168(5), pp. 415–423. Available at: https://doi.org/10.1016/j.jplph.2010.08.010.

Jones, E.A. *et al.* (2012) 'Imaging mass spectrometry statistical analysis', *Journal of Proteomics*, 75(16), pp. 4962–4989. Available at: https://doi.org/10.1016/J.JPROT.2012.06.014.

Joo, W.A. *et al.* (2007) 'Comparison of search engine contributions in protein mass fingerprinting for protein identification', *Biotechnology and Bioprocess Engineering*, 12(2), pp. 125–130. Available at: https://doi.org/10.1007/BF03028637.

Jorrin-Novo, J. V. *et al.* (2019) 'Gel electrophoresis-based plant proteomics: Past, present, and future. Happy 10th anniversary Journal of Proteomics!', *Journal of Proteomics*, 198, pp. 1–10. Available at: https://doi.org/10.1016/J.JPROT.2018.08.016.

Jorrín-Novo, J. V. *et al.* (2009) 'Plant proteomics update (2007-2008): Second-generation proteomic techniques, an appropriate experimental design, and data analysis to fulfill MIAPE standards, increase plant proteome coverage and expand biological knowledge', *Journal of Proteomics*, 72(3), pp. 285–314. Available at: https://doi.org/10.1016/j.jprot.2009.01.026.

Jorrín-Novo, J. V. *et al.* (2015) 'Fourteen years of plant proteomics reflected in Proteomics: Moving from model species and 2DE-based approaches to orphan species and gel-free platforms', *PROTEOMICS*, 15(5–6), pp. 1089–1112. Available at: https://doi.org/10.1002/PMIC.201400349.

Jorrin Novo, J. V. (2021) 'Proteomics and plant biology: contributions to date and a look towards the next decade', *Expert Review of Proteomics*, 18(2), pp. 93–103. Available at: https://doi.org/10.1080/14789450.2021.1910028.

Josic, D. and Kovac, S. (2010) 'Reversed-Phase High Performance Liquid Chromatography of Proteins', *Current Protocols in Protein Science*, 61(1), pp. 8.7.1-8.7.22. Available at: https://doi.org/10.1002/0471140864.PS0807S61.

Jun, J.H. *et al.* (2010) 'High-spatial and high-mass resolution imaging of surface metabolites of arabidopsis thaliana by laser desorption-ionization mass spectrometry using colloidal silver', *Analytical Chemistry*, 82(8), pp. 3255–3265. Available at: https://doi.org/10.1021/ac902990p.

Jurchen, J.C.J.J.C. *et al.* (2005) 'MALDI-MS imaging of features smaller than the size of the laser beam', *Journal of the American Society for Mass Spectrometry*, 16(10), pp. 1654–1659. Available at: https://doi.org/10.1016/j.jasms.2005.06.006.

Kaletaş, B.K. *et al.* (2009) 'Sample preparation issues for tissue imaging by imaging MS', *Proteomics*, 9(10), pp. 2622–2633. Available at: https://doi.org/10.1002/pmic.200800364.

Karas, M. *et al.* (1987) 'Matrix-Assisted Ultraviolet-Laser Desorption of Nonvolatile Compounds', *Int. J. Mass Spectrom. Ion Processes*, 78, p. 53.

Karas, M. *et al.* (1989) 'Laser Desorption/Ionization Mass Spectrometry of Proteins of Mass 100 000 to 250 000 Dalton', *Angewandte Chemie International Edition in English*, 28(6), pp. 760–761. Available at: https://doi.org/10.1002/anie.198907601.

Kaspar, S. *et al.* (2010) 'Protein analysis of laser capture micro-dissected tissues revealed cell-type specific biological functions in developing barley grains', *Analytical and Bioanalytical Chemistry*, 398(7–8), pp. 2883–2893. Available at: https://doi.org/10.1007/s00216-010-4120-y.

Kaspar, S. *et al.* (2011) 'MALDI-imaging mass spectrometry - An emerging technique in plant biology', *Proteomics*, 11(9), pp. 1840–1850. Available at: https://doi.org/10.1002/pmic.201000756.

Kaufmann, K. *et al.* (2011) 'Proteomics insights into plant signaling and development', *Proteomics*, 11(4), pp. 744–755. Available at: https://doi.org/10.1002/pmic.201000418.

Kaur, B. *et al.* (2021) 'Omics for the Improvement of Abiotic, Biotic, and Agronomic Traits in Major Cereal Crops: Applications, Challenges, and Prospects', *Plants 2021, Vol. 10, Page 1989*, 10(10), p. 1989. Available at: https://doi.org/10.3390/PLANTS10101989.

Kawamoto, T. (2003) 'Use of a new adhesive film for the preparation of multi-purpose fresh-frozen sections from hard tissues, whole-animals, insects and plants', *Archives of Histology and Cytology*, 66(2), pp. 123–143. Available at: https://doi.org/10.1679/aohc.66.123.

Khoranhlai, K.K. (2015) 'Advances in Proteomics and Bioinformatics in Agriculture Research and Crop Improvement', *Journal of Proteomics & Bioinformatics*, 08(03), pp. 39–048. Available at: https://doi.org/10.4172/jpb.1000351.

Klose, J. (1975) 'Protein mapping by combined isoelectric focusing and electrophoresis of mouse tissues - A novel approach to testing for induced point mutations in mammals', *Human Genetics*, 26(3), pp. 231–243. Available at: https://doi.org/10.1007/BF00281458/METRICS.

Kobayashi, T., Nozoye, T. and Nishizawa, N.K. (2019) 'Iron transport and its regulation in plants.', *Free radical biology & medicine*, 133, pp. 11–20. Available at: https://doi.org/10.1016/j.freeradbiomed.2018.10.439.

Koçak, E., Eylem, C.C. and Nemutlu, E. (2023) 'Liquid chromatography in proteomics research', in *Liquid Chromatography: Applications*. Elsevier, pp. 331–356. Available at: https://doi.org/10.1016/B978-0-323-99969-4.00028-0.

Kondo, T. *et al.* (2006) 'A plant peptide encoded by CLV3 identified by in situ MALDI-TOF MS analysis', *Science*, 313(5788), pp. 845–848. Available at: https://doi.org/10.1126/science.1128439.

Kosarev, P., Mayer, K.F.X. and Hardtke, C.S. (2002) 'Evaluation and classification of RING-finger domains encoded by the Arabidopsis genome.', *Genome biology*, 3(4), p. 16. Available at: https://doi.org/10.1186/gb-2002-3-4-research0016.

Kosegarten, H.U., Hoffmann, B. and Mengel, K. (1999) 'Apoplastic pH and Fe3+ reduction in intact sunflower leaves', *Plant Physiology*, 121(4), pp. 1069–1079. Available at: https://doi.org/10.1104/pp.121.4.1069.

Krüger, C. *et al.* (2002) 'A metal-binding member of the late embryogenesis abundant protein family transports iron in the phloem of Ricinus communis L.', *Journal of Biological Chemistry*, 277(28), pp. 25062–25069. Available at: https://doi.org/10.1074/jbc.M201896200.

Kruse, R. and Sweedler, J. V (2003) 'Spatial Profiling Invertebrate Ganglia Using MALDI MS', *J. Am. Soc. Mass Spectrom.*, 14(7), p. 752.

Lan, P. *et al.* (2011) 'ITRAQ protein profile analysis of arabidopsis roots reveals new aspects critical for iron homeostasis', *Plant Physiology*, 155(2), pp. 821–834. Available at: https://doi.org/10.1104/pp.110.169508.

Lan, P., Li, W. and Schmidt, W. (2012) 'Complementary proteome and transcriptome profiling in phosphate-deficient arabidopsis roots reveals multiple levels of gene regulation', *Molecular and Cellular Proteomics*, 11(11), pp. 1156–1166. Available at: https://doi.org/10.1074/mcp.M112.020461.

Leaden, L., Busi, M. V. and Gomez-Casati, D.F. (2014) 'The mitochondrial proteins AtHscB and AtIsu1 involved in Fe-S cluster assembly interact with the Hsp70-type chaperon AtHscA2 and modulate its catalytic activity', *Mitochondrion*, 19(PB), pp. 375–381. Available at: https://doi.org/10.1016/j.mito.2014.11.002.

Leung, S.-M. and Pitts, R.L. (2008) 'A Novel Approach Using MALDI-TOF/TOF Mass Spectrometry and Prestructured Sample Supports (AnchorChip Technology) for Proteomic Profiling and Protein Identification', in. Humana Press, pp. 57–70. Available at: https://doi.org/10.1007/978-1-60327-047-2_4.

Li, C. *et al.* (2021) 'Towards Higher Sensitivity of Mass Spectrometry: A Perspective From the Mass Analyzers', *Frontiers in Chemistry*. Frontiers Media S.A., p. 813359. Available at: https://doi.org/10.3389/fchem.2021.813359.

Li, J. *et al.* (2008) 'Proteomic response to iron deficiency in tomato root', *Proteomics*, 8(11), pp. 2299–2311. Available at: https://doi.org/10.1002/pmic.200700942.

Li, J. *et al.* (2012) 'Matrix assisted ionization: New aromatic and nonaromatic matrix compounds producing multiply charged lipid, peptide, and protein ions in the positive and negative mode observed directly from surfaces', *Journal of the American Society for Mass Spectrometry*, 23(10), pp. 1625–1643. Available at: https://doi.org/10.1007/s13361-012-0413-z.

Li, Z. *et al.* (2015) 'Protein Dynamics in Young Maize Root Hairs in Response to Macro- and Micronutrient Deprivation', *Journal of Proteome Research*, 14(8), pp. 3362–3371. Available at: https://doi.org/10.1021/ACS.JPROTEOME.5B00399/SUPPL_FILE/PR5B00399_SI_002.ZIP.

Liang, C., Tian, J. and Liao, H. (2013) 'Proteomics dissection of plant responses to mineral nutrient deficiency', *Proteomics*, 13(3–4), pp. 624–636. Available at: https://doi.org/10.1002/pmic.201200263.

Lin, M.K. *et al.* (2009) 'Analysis of the pumpkin phloem proteome provides insights into angiosperm sieve tube function', *Molecular and Cellular Proteomics*, 8(2), pp. 343–356. Available at: https://doi.org/10.1074/mcp.M800420-MCP200.

Lin, S., Cianzio, S. and Shoemaker, R. (1997) 'Mapping genetic loci for iron deficiency chlorosis in soybean', *Molecular Breeding*, 3(3), pp. 219–229. Available at: https://doi.org/10.1023/A:1009637320805.

Liu, Y. *et al.* (2021) 'Unraveling the roles of vascular proteins using proteomics', *Molecules*, 26(3), p. 667. Available at: https://doi.org/10.3390/molecules26030667.

Lopez-Millan, A.F., Morales, F., Abadia, A., *et al.* (2000) 'Effects of iron deficiency on the composition of the leaf apoplastic fluid and xylem sap in sugar beet. Implications for iron and carbon transport', *Plant Physiology*, 124(2), pp. 873–884. Available at: https://doi.org/10.1104/pp.124.2.873.

Lopez-Millan, A.F., Morales, F., Andaluz, S., *et al.* (2000) 'Responses of sugar beet roots to iron deficiency. Changes in carbon assimilation and oxygen use?', *Plant Physiology*, 124(2), pp. 885–897. Available at: https://doi.org/10.1104/pp.124.2.885.

López-Millán, A.F., Morales, F., Abadía, A., *et al.* (2001) 'Changes induced by Fe deficiency and Fe resupply in the organic acid metabolism of sugar beet (Beta vulgaris) leaves', *Physiologia Plantarum*, 112(1), pp. 31–38. Available at: https://doi.org/10.1034/j.1399-3054.2001.1120105.x.

López-Millán, A.F., Morales, F., Gogorcena, Y., *et al.* (2001) 'Iron resupply-mediated deactivation of Fe-deficiency stress responses in roots of sugar beet', *Australian Journal of Plant Physiology*, 28(3), pp. 171–180. Available at: https://doi.org/10.1071/pp00105.

López-Millán, A.F. *et al.* (2009) 'Metabolic responses in iron deficient tomato plants', *Journal of Plant Physiology*, 166(4), pp. 375–384. Available at: https://doi.org/10.1016/j.jplph.2008.06.011.

López-Millán, A.F. *et al.* (2013) 'Iron deficiency in plants: An insight from proteomic approaches', *Frontiers in Plant Science*, 4(JUL), p. 254. Available at: https://doi.org/10.3389/fpls.2013.00254.

Lough, T.J. and Lucas, W.J. (2006) 'Integrative plant biology: Role of phloem long-distance macromolecular trafficking', *Annual Review of Plant Biology*, 57, pp. 203–232. Available at: https://doi.org/10.1146/annurev.arplant.56.032604.144145.

Lucas, W.J. *et al.* (2013) 'The Plant Vascular System: Evolution, Development and Functions', *Journal of Integrative Plant Biology*, 55(4), pp. 294–388. Available at: https://doi.org/10.1111/jipb.12041.

Lucas, W.J., Yoo, B.C. and Kragler, F. (2001) 'RNA as a long-distance information macromolecule in plants', *Nature Reviews Molecular Cell Biology*, 2(11), pp. 849–857. Available at: https://doi.org/10.1038/35099096.

Lüders, J., Demand, J. and Höhfeld, J. (2000) 'The ubiquitin-related BAG-1 provides a link between the molecular chaperones Hsc70/Hsp70 and the proteasome', *Journal of Biological Chemistry*, 275(7), pp. 4613–4617. Available at: https://doi.org/10.1074/jbc.275.7.4613.

Lux, A. *et al.* (2011) 'Cadmium induces hypodermal periderm formation in the roots of the monocotyledonous medicinal plant Merwilla plumbea', *Annals of Botany*, 107(2), pp. 285–292. Available at: https://doi.org/10.1093/aob/mcq240.

Luxembourg, S.L. *et al.* (2004) 'High-Spatial Resolution Mass Spectrometric Imaging of Peptide and Protein Distributions on a Surface', *Analytical Chemistry*, 76(18), pp. 5339–5344. Available at: https://doi.org/10.1021/AC049692Q.

Lytle, B.L. *et al.* (2009) 'Structures of two Arabidopsis thaliana major latex proteins represent novel helix-grip folds', *Proteins: Structure, Function and Bioinformatics*, 76(1), pp. 237–243. Available at: https://doi.org/10.1002/prot.22396.

M'sehli, W. *et al.* (2009) 'Variability of metabolic responses and antioxidant defence in two lines of Medicago ciliaris to Fe deficiency', *Plant and Soil*, 320(1–2), pp. 219–230. Available at: https://doi.org/10.1007/s11104-008-9887-7.

Macnicol, R.D. and Beckett, P.H.T. (1985) 'Critical tissue concentrations of potentially toxic elements', *Plant and Soil*, 85(1), pp. 107–129. Available at: https://doi.org/10.1007/BF02197805/METRICS.

Mai, H.J. and Bauer, P. (2016) 'From the proteomic point of view: Integration of adaptive changes to iron deficiency in plants', *Current Plant Biology*, 5, pp. 45–56. Available at: https://doi.org/10.1016/J.CPB.2016.02.001.

Maia, M. *et al.* (2022) 'Grapevine leaf MALDI-MS imaging reveals the localisation of a putatively identified sucrose metabolite associated to Plasmopara viticola development', *Frontiers in Plant Science*, 13, p. 1012636. Available at: https://doi.org/10.3389/FPLS.2022.1012636/BIBTEX.

March, R.E. (1999) 'Ion Trap Mass Spectrometers', in *Encyclopedia of Spectroscopy and Spectrometry*. Elsevier, pp. 1000–1009. Available at: https://doi.org/10.1006/rwsp.2000.0143.

Marentes, E. and Grusak, M.A. (1998) 'Mass determination of low-molecular-weight proteins in phloem sap using matrix-assisted laser desorption/ionization time-of-flight mass spectrometry', *Journal of Experimental Botany*, 49(322), pp. 903–911. Available at: https://doi.org/10.1093/jxb/49.322.903.

Martin, M.H. and Marschner, H. (1988) *The Mineral Nutrition of Higher Plants.* 2nd edn, *The Journal of Ecology*. 2nd edn. London: Academic Press. Available at: https://doi.org/10.2307/2260650.

Martínez-Cuenca, M.R. *et al.* (2013) 'Bicarbonate blocks iron translocation from cotyledons inducing iron stress responses in Citrus roots', *Journal of Plant Physiology*, 170(10), pp. 899–905. Available at: https://doi.org/10.1016/j.jplph.2013.01.012.

Mascini, N.E. and Heeren, R.M.A. (2012) 'Protein identification in mass-spectrometry imaging', *TrAC Trends in Analytical Chemistry*, 40, pp. 28–37. Available at: https://doi.org/10.1016/J.TRAC.2012.06.008.

Matros, A. and Mock, H.P. (2013) 'Mass spectrometry based imaging techniques for spatially resolved analysis of molecules', *Frontiers in Plant Science*, 4(APR), p. 89. Available at: https://doi.org/10.3389/fpls.2013.00089.

Mavrodi, D. V. *et al.* (2010) 'Diversity and evolution of the Phenazine Biosynthesis Pathways', *Applied and Environmental Microbiology*, 76(3), pp. 866–879. Available at: https://doi.org/10.1128/AEM.02009-09.

McDonnell, L.A. *et al.* (2012) 'Going forward: Increasing the accessibility of imaging mass spectrometry', *Journal of Proteomics*, 75(16), pp. 5113–5121. Available at: https://doi.org/10.1016/J.JPROT.2012.05.016.

McHugh, L. and Arthur, J.W. (2008) 'Computational methods for protein identification from mass spectrometry data', *PLoS Computational Biology*, 4(2), p. e12. Available at: https://doi.org/10.1371/journal.pcbi.0040012.

McWhite, C.D. *et al.* (2020) 'A Pan-plant Protein Complex Map Reveals Deep Conservation and Novel Assemblies', *Cell*, 181(2), pp. 460-474.e14. Available at: https://doi.org/10.1016/j.cell.2020.02.049.

Mengel K., Kosegarten H., K.E.A. (2001) *Principles of Plant Nutrition*, *Principles of Plant Nutrition*. Springer Netherlands. Available at: https://doi.org/10.1007/978-94-010-1009-2.

Mengel, K. (1994) 'Iron availability in plant tissues-iron chlorosis on calcareous soils', *Plant and Soil*, 165(2), pp. 275–283. Available at: https://doi.org/10.1007/BF00008070.

Mengel, K. and Geurtzen, G. (1986) 'Iron chlorosis on calcareous soils. alkaline nutritional condition as the cause for the chlorosis', *Journal of Plant Nutrition*, 9(3–7), pp. 161–173. Available at: https://doi.org/10.1080/01904168609363434.

Mergner, J. and Kuster, B. (2022) *Plant Proteome Dynamics*, *Annual Review of Plant Biology*. Annual Reviews. Available at: https://doi.org/10.1146/annurev-arplant-102620-031308.

Vander Mijnsbrugge, K. *et al.* (2000) 'Phenylcoumaran benzylic ether reductase, a prominent poplar xylem protein, is strongly associated with phenylpropanoid biosynthesis in lignifying cells', *Planta*, 211(4), pp. 502–509. Available at: https://doi.org/10.1007/s004250000326.

Mira, H., Martínez-García, F. and Peñarrubia, L. (2001) 'Evidence for the plant-specific intercellular transport of the Arabidopsis copper chaperone CCH', *Plant Journal*, 25(5), pp. 521–528. Available at: https://doi.org/10.1046/j.1365-313x.2001.00985.x.

Mitulović, G. and Mechtler, K. (2006) 'HPLC techniques for proteomics analysis—a short overview of latest developments', *Briefings in Functional Genomics*, 5(4), pp. 249–260. Available at: https://doi.org/10.1093/BFGP/ELL034.

Molassiotis, A. *et al.* (2006) 'Effects of 4-month Fe deficiency exposure on Fe reduction mechanism, photosynthetic gas exchange, chlorophyll fluorescence and antioxidant defense in two peach rootstocks differing in Fe deficiency tolerance', *Journal of Plant Physiology*, 163(2), pp. 176–185. Available at: https://doi.org/10.1016/j.jplph.2004.11.016.

Morales, J. *et al.* (2022) 'A joint NCBI and EMBL-EBI transcript set for clinical genomics and research', *Nature 2022 604:7905*, 604(7905), pp. 310–315. Available at: https://doi.org/10.1038/s41586-022-04558-8.

Moreno-Gordaliza, E. *et al.* (2017) 'MALDI-LTQ-Orbitrap mass spectrometry imaging for lipidomic analysis in kidney under cisplatin chemotherapy', *Talanta*, 164, pp. 16–26. Available at: https://doi.org/10.1016/j.talanta.2016.11.026.

Mori, S. and Nishizawa, N. (1987) 'Methionine as a dominant precursor of phytosiderophores in graminaceae plants', *Plant and Cell Physiology*, 28(6), pp. 1081–1092. Available at: https://academic.oup.com/pcp/article-abstract/28/6/1081/1940234 (Accessed: 11 November 2023).

Mullen, A.K. *et al.* (2005) 'Determination of agrochemical compounds in soya plants by imaging matrix-assisted laser desorption/ionisation mass spectrometry', *Rapid Communications in Mass Spectrometry*, 19(18), pp. 2507–2516. Available at: https://doi.org/10.1002/rcm.2078.

Müller, W.H. *et al.* (2021) 'Imaging lipids in biological samples with surface-assisted laser desorption/ionization mass spectrometry: A concise review of the last decade', *Progress in Lipid Research*, 83, p. 101114. Available at: https://doi.org/10.1016/J.PLIPRES.2021.101114.

Münch, E. (1932) *Die Stoffbewegungen in der Pflanze*, *Protoplasma*. Jena: Fischer, G. Available at: https://doi.org/10.1007/bf01610295.

Murphy, R.C. and Gaskell, S.J. (2011) 'New applications of mass spectrometry in lipid analysis', *Journal of Biological Chemistry*, 286(29), pp. 25427–25433. Available at: https://doi.org/10.1074/jbc.R111.233478.

Mustroph, A. *et al.* (2009) 'Profiling translatomes of discrete cell populations resolves altered cellular priorities during hypoxia in Arabidopsis', in *Proceedings of the National Academy of Sciences of the United States of America*. USA, pp. 18843–18848. Available at: https://doi.org/10.1073/pnas.0906131106.

Nadler, W.M. *et al.* (2017) 'MALDI versus ESI: The Impact of the Ion Source on Peptide Identification', *Journal of Proteome Research*, 16(3), pp. 1207–1215. Available at: https://doi.org/10.1021/ACS.JPROTEOME.6B00805/SUPPL_FILE/PR6B00805_SI_001.PDF.

Nahar, L., Onder, A. and Sarker, S.D. (2020) 'A review on the recent advances in HPLC, UHPLC and UPLC analyses of naturally occurring cannabinoids (2010–2019)', *Phytochemical Analysis*, 31(4), pp. 413–457. Available at: https://doi.org/10.1002/PCA.2906.

Nakanishi, H. *et al.* (2000) 'Two dioxygenase genes, Ids3 and Ids2, from Hordeum vulgare are involved in the biosynthesis of mugineic acid family phytosiderophores', *Plant Molecular Biology*, 44(2), pp. 199–207. Available at: https://doi.org/10.1023/A:1006491521586.

Nathan, A.J. and Scobell, A. (2012) 'How China sees America', in *Foreign Affairs*. Jena, Germany, pp. 1689–1699. Available at: https://doi.org/10.1017/CBO9781107415324.004.

Nikolic, M. and Römheld, V. (2002) 'Does high bicarbonate supply to roots change availability of iron in the leaf apoplast?', *Plant and Soil*, 241(1), pp. 67–74. Available at: https://doi.org/10.1023/A:1016029024374.

Nilo-Poyanco, R. *et al.* (2021) 'Shotgun proteomics of peach fruit reveals major metabolic pathways associated to ripening', *BMC Genomics*, 22(1), pp. 1–29. Available at: https://doi.org/10.1186/s12864-020-07299-y.

Nishiyama, R. *et al.* (2012) 'Identification of Zn-nicotianamine and Fe-2′-deoxymugineic acid in the phloem sap from rice plants (Oryza sativa L.)', *Plant and Cell Physiology*, 53(2), pp. 381–390. Available at: https://doi.org/10.1093/pcp/pcr188.

Nolting, D., Malek, R. and Makarov, A. (2019) 'Ion traps in modern mass spectrometry', *Mass Spectrometry Reviews*. John Wiley & Sons, Ltd, pp. 150–168. Available at: https://doi.org/10.1002/mas.21549.

O'Farrell, P.H. (1975) 'High resolution two dimensional electrophoresis of proteins', *Journal of Biological Chemistry*, 250(10), pp. 4007–4021. Available at: https://doi.org/10.1016/s0021-9258(19)41496-8.

Ogden, A.J. *et al.* (2020) 'Phloem exudate protein profiles during drought and recovery reveal abiotic stress responses in tomato vasculature', *International Journal of Molecular Sciences*, 21(12), pp. 1–20. Available at: https://doi.org/10.3390/ijms21124461.

Omid, A. *et al.* (2007) 'Characterization of phloem-sap transcription profile in melon plants', *Journal of Experimental Botany*, 58(13), pp. 3645–3656. Available at: https://doi.org/10.1093/jxb/erm214.

Oparka, K.J. and Santa Cruz, S. (2000) 'The great escape: Phloem transport and unloading of macromolecules', *Annual Review of Plant Biology*, 51(26), pp. 323–347. Available at: https://doi.org/10.1146/annurev.arplant.51.1.323.

Pandey, A. and Mann, M. (2000) 'Proteomics to study genes and genomes', *Nature 2000 405:6788*, 405(6788), pp. 837–846. Available at: https://doi.org/10.1038/35015709.

Panicker, R.C., Chattopadhaya, S. and Yao, S.Q. (2006) 'Advanced analytical tools in proteomics', *Analytica Chimica Acta*. Elsevier, pp. 69–79. Available at: https://doi.org/10.1016/j.aca.2005.05.060.

Pappin, D.J.C., Hojrup, P. and Bleasby, A.J. (1993) 'Rapid identification of proteins by peptide-mass fingerprinting', *Current Biology*, 3(6), pp. 327–332. Available at: https://doi.org/10.1016/0960-9822(93)90195-T.

Patton, W.F. (2000) 'A thousand points of light: The application of fluorescence detection technologies to two-dimensional gel electrophoresis and proteomics', *Electrophoresis*, pp. 1123–1144. Available at: https://doi.org/10.1002/(SICI)1522-2683(20000401)21:6<1123::AID-ELPS1123>3.0.CO;2-E.

Peng, J. and Gygi, S.P. (2001) 'Proteomics: the move to mixtures', *Journal of Mass Spectrometry*, 36(10), pp. 1083–1091. Available at: https://doi.org/10.1002/JMS.229.

Pérez-Míguez, R. *et al.* (2019) 'Separation and identification of peptides in hydrolysed protein extracts from edible macroalgae by HPLC-ESI-QTOF/MS', *Algal Research*, 39, p. 101465. Available at: https://doi.org/10.1016/J.ALGAL.2019.101465.

Perkins, D.N. *et al.* (1999) 'Probability-based protein identification by searching sequence databases using mass spectrometry data', in *Electrophoresis*, pp. 3551–3567. Available at: https://doi.org/10.1002/(SICI)1522-2683(19991201)20:18<3551::AID-ELPS3551>3.0.CO;2-2.

Pierson, L.S. and Pierson, E.A. (2010) 'Metabolism and function of phenazines in bacteria: Impacts on the behavior of bacteria in the environment and biotechnological processes', *Applied Microbiology and Biotechnology*, 86(6), pp. 1659–1670. Available at: https://doi.org/10.1007/s00253-010-2509-3.

Price, D. (2023) *Time-of-Flight Mass Spectrometry The Early Years as Chronicled by the European Time-of-Flight Symposia*. Available at: https://pubs.acs.org/doi/abs/10.1021/bk-1994-0549.ch001%0Ahttps://pubs.acs.org/sharingguidelines (Accessed: 19 November 2023).

Rabilloud, T. (1998) 'Use of thiourea to increase the solubility of membrane proteins in two-dimensional electrophoresis', *ELECTROPHORESIS*, 19(5), pp. 758–760. Available at: https://doi.org/10.1002/ELPS.1150190526.

Ralph, J. and Hatfield, R.D. (1991) 'Pyrolysis-Gc-Ms Characterization of Forage Materials', *Journal of Agricultural and Food Chemistry*, 39(8), pp. 1426–1437. Available at: https://doi.org/10.1021/jf00008a014.

Redjala, T. *et al.* (2011) 'Relationship between root structure and root cadmium uptake in maize', *Environmental and Experimental Botany*, 71(2), pp. 241–248. Available at: https://doi.org/10.1016/j.envexpbot.2010.12.010.

Rellán-Álvarez, R., Andaluz, S., *et al.* (2010) 'Changes in the proteomic and metabolic profiles of Beta vulgaris root tips in response to iron deficiency and resupply', *BMC Plant Biology*, 10, p. 120. Available at: https://doi.org/10.1186/1471-2229-10-120.

Rellán-Álvarez, R., Giner-Martínez-Sierra, J., *et al.* (2010) 'Identification of a Tri-Iron(III), Tri-Citrate Complex in the Xylem Sap of Iron-Deficient Tomato Resupplied with Iron: New Insights into Plant Iron Long-Distance Transport', *Plant and Cell Physiology*, 51(1), pp. 91–102. Available at: https://doi.org/10.1093/pcp/pcp170.

Rellán-Álvarez, R., López-Gomollón, S., *et al.* (2011) 'Development of a new high-performance liquid chromatography-electrospray ionization time-of-flight mass spectrometry method for the determination of low molecular mass organic acids in plant tissue extracts', *Journal of Agricultural and Food Chemistry*, 59(13), pp. 6864–6870. Available at: https://doi.org/10.1021/jf200482a.

Rellán-Álvarez, R., El-Jendoubi, H., *et al.* (2011) 'Metabolite profile changes in xylem sap and leaf extracts of strategy I plants in response to iron deficiency and resupply', *Frontiers in Plant Science*, 2(OCT), p. 66. Available at: https://doi.org/10.3389/fpls.2011.00066.

Rellán-Álvarez, R., Abadía, J. and Álvarez-Fernández, A. (2008) 'Formation of metal-nicotianamine complexes as affected by pH, ligand exchange with citrate and metal exchange. A study by electrospray ionization time-of-flight mass spectrometry', *Rapid Communications in Mass Spectrometry*, 22(10), pp. 1553–1562. Available at: https://doi.org/10.1002/rcm.3523.

Reyzer, M.L. *et al.* (2003) 'Direct analysis of drug candidates in tissue by matrix-assisted laser desorption/ionization mass spectrometry', *Journal of Mass Spectrometry*, 38(10), pp. 1081–1092. Available at: https://doi.org/10.1002/jms.525.

Riffle, M. and Eng, J.K. (2009) 'Proteomics data repositories', *Proteomics*, 9(20), pp. 4653–4663. Available at: https://doi.org/10.1002/pmic.200900216.

Righetti, P.G. *et al.* (2005) 'Prefractionation techniques in proteome analysis: The mining tools of the third millennium', *ELECTROPHORESIS*, 26(2), pp. 297–319. Available at: https://doi.org/10.1002/ELPS.200406189.

Righetti, P.G., Castagna, A. and Herbert, B. (2001) 'Prefractionation techniques - In - Proteome analysis', *Analytical Chemistry*. American Chemical Society, pp. 320 A-326 A. Available at: https://doi.org/10.1021/AC012465T.

Robinson, N.J. *et al.* (1999) 'A ferric-chelate reductase for iron uptake from soils', *Nature*, 397(6721), pp. 694–697. Available at: https://doi.org/10.1038/17800.

Robinson, S. *et al.* (2007) 'Localization of water-soluble carbohydrates in wheat stems using imaging matrix-assisted laser desorption ionization mass spectrometry', *New Phytologist*, 173(2), pp. 438–444. Available at: https://doi.org/10.1111/j.1469-8137.2006.01934.x.

Rodríguez-Celma, J. *et al.* (2010) 'Changes induced by two levels of cadmium toxicity in the 2-DE protein profile of tomato roots', *Journal of Proteomics*, 73(9), pp. 1694–1706. Available at: https://doi.org/10.1016/j.jprot.2010.05.001.

Rodríguez-Celma, J., Vázquez-Reina, S., *et al.* (2011) 'Characterization of flavins in roots of Fe-deficient strategy i plants, with a focus on Medicago truncatula', *Plant and Cell Physiology*, 52(12), pp. 2173–2189. Available at: https://doi.org/10.1093/pcp/pcr149.

Rodríguez-Celma, J., Lattanzio, G., *et al.* (2011) 'Root responses of Medicago truncatula plants grown in two different iron deficiency conditions: Changes in root protein profile and riboflavin Biosynthesis', *Journal of Proteome Research*, 10(5), pp. 2590–2601. Available at: https://doi.org/10.1021/pr2000623.

Rodríguez-Celma, J., Lin, W.D., *et al.* (2013) 'Mutually exclusive alterations in secondary metabolism are critical for the uptake of insoluble iron compounds by arabidopsis and Medicago truncatula', *Plant Physiology*, 162(3), pp. 1473–1485. Available at: https://doi.org/10.1104/pp.113.220426.

Rodríguez-Celma, J., Chun Pan, I., *et al.* (2013) 'The transcriptional response of Arabidopsis leaves to Fe deficiency', *Frontiers in Plant Science*, 4(JUL), p. 276. Available at: https://doi.org/10.3389/fpls.2013.00276.

Rodríguez-Celma, J. *et al.* (2016) 'Plant fluid proteomics: Delving into the xylem sap, phloem sap and apoplastic fluid proteomes', *Biochimica et Biophysica Acta - Proteins and Proteomics*, 1864(8), pp. 991–1002. Available at: https://doi.org/10.1016/j.bbapap.2016.03.014.

Rodríguez-Celma, J. *et al.* (2019) 'Hemerythrin E3 ubiquitin ligases as negative regulators of iron homeostasis in plants', *Frontiers in Plant Science*, 10, p. 437974. Available at: https://doi.org/10.3389/FPLS.2019.00098/BIBTEX.

Rodriguez-Medina, C. *et al.* (2011) 'Macromolecular composition of phloem exudate from white lupin (Lupinus albus L.)', *BMC Plant Biology*, 11(1), p. 36. Available at: https://doi.org/10.1186/1471-2229-11-36.

Rohner, T.C., Staab, D. and Stoeckli, M. (2005) 'MALDI mass spectrometric imaging of biological tissue sections', *Mechanisms of Ageing and Development*, 126(1), pp. 177–185. Available at: https://doi.org/10.1016/j.mad.2004.09.032.

Rombolà, A.D. and Tagliavini, M. (2006) 'Iron nutrition of fruit tree crops', *Iron Nutrition in Plants and Rhizospheric Microorganisms*, pp. 61–83. Available at: https://doi.org/10.1007/1-4020-4743-6_3.

Römheld, V. (1987) 'Different strategies for iron acquisition in higher plants', *Physiologia Plantarum*, 70(2), pp. 231–234. Available at: https://doi.org/10.1111/j.1399-3054.1987.tb06137.x.

Römheld, V. and Marschner, H. (1986) 'Evidence for a Specific Uptake System for Iron Phytosiderophores in Roots of Grasses', *Plant Physiology*, 80(1), pp. 175–180. Available at: https://doi.org/10.1104/pp.80.1.175.

Roschzttardtz, H. *et al.* (2011) 'The FRD3 citrate effluxer promotes iron nutrition between symplastically disconnected tissues Throughout Arabidopsis development', *Plant Cell*, 23(7), pp. 2725–2737. Available at: https://doi.org/10.1105/tpc.111.088088.

Rubakhin, S.S., Greenough, W.T. and Sweedler, J. V (2003) 'Spatial Profiling with MALDI MS: Distribution of Neuropeptides Within Single Neurons', *Anal. Chem.*, 75(20), p. 5374.

Rychert, J. (2019) 'Benefits and Limitations of MALDI-TOF Mass Spectrometry for the Identification of Microorganisms', *Journal of Infectiology and Epidemiology*, 2(4), pp. 1–5. Available at: https://doi.org/10.29245/2689-9981/2019/4.1142.

Saito, K. and Matsuda, F. (2010) 'Metabolomics for functional genomics, systems biology, and biotechnology', *Annual Review of Plant Biology*, 61, pp. 463–489. Available at: https://doi.org/10.1146/annurev.arplant.043008.092035.

Salviati, E., Sommella, E. and Campiglia, P. (2022) 'MALDI–mass spectrometry imaging: the metabolomic visualization', in *Metabolomics Perspectives: From Theory to Practical Application*. Academic Press, pp. 535–551. Available at: https://doi.org/10.1016/B978-0-323-85062-9.00015-5.

Sánchez-Monge, R. *et al.* (1999) 'Lipid-transfer proteins are relevant allergens in fruit allergy', *Journal of Allergy and Clinical Immunology*, 103(3 II), pp. 514–519. Available at: https://doi.org/10.1016/s0091-6749(99)70479-3.

Santi, S. and Schmidt, W. (2009) 'Dissecting iron deficiency-induced proton extrusion in Arabidopsis roots', *New Phytologist*, 183(4), pp. 1072–1084. Available at: https://doi.org/10.1111/j.1469-8137.2009.02908.x.

Sarabia, L.D. *et al.* (2018) 'High-mass-resolution MALDI mass spectrometry imaging reveals detailed spatial distribution of metabolites and lipids in roots of barley seedlings in response to salinity stress', *Metabolomics*, 14(5), pp. 1–16. Available at: https://doi.org/10.1007/S11306-018-1359-3/TABLES/2.

Scheurer, S. *et al.* (1997) 'Molecular cloning, expression and characterization of Pru a 1, the major cherry allergen', *Molecular Immunology*, 34(8–9), pp. 619–629. Available at: https://doi.org/10.1016/S0161-5890(97)00072-2.

Schmid, N.B. *et al.* (2014) 'Feruloyl-CoA 6′-Hydroxylase1-dependent coumarins mediate iron acquisition from alkaline substrates in Arabidopsis', *Plant Physiology*, 164(1), pp. 160–172. Available at: https://doi.org/10.1104/pp.113.228544.

Schmidt, W. and Buckhout, T.J. (2011) 'A hitchhiker's guide to the Arabidopsis ferrome', *Plant Physiology and Biochemistry*, 49(5), pp. 462–470. Available at: https://doi.org/10.1016/j.plaphy.2010.12.001.

Schobert, C. *et al.* (1998) 'Identification of immunologically related proteins in sieve-tube exudate collected from monocotyledonous and dicotyledonous plants', *Planta*, 206(2), pp. 245–252. Available at: https://doi.org/10.1007/s004250050396.

Schützendübel, A. and Polle, A. (2002) 'Plant responses to abiotic stresses: heavy metal-induced oxidative stress and protection by mycorrhization', *Journal of Experimental Botany*, 53(372), pp. 1351–1365. Available at: https://doi.org/10.1093/JEXBOT/53.372.1351.

Schwartz, S.A. *et al.* (2005) 'Proteomic-based prognosis of brain tumor patients using direct-tissue matrix-assisted laser desorption ionization mass spectrometry', *Cancer Research*, 65(17), pp. 7674–7681. Available at: https://doi.org/10.1158/0008-5472.CAN-04-3016.

Schwartz, S.A. and Caprioli, R.M. (2010) *Imaging mass spectrometry: Viewing the future*, *Methods in Molecular Biology*. Edited by S.S. Rubakhin and J. V Sweedler. New York, NY, USA: Humana Press. Available at: https://doi.org/10.1007/978-1-60761-746-4_1.

Schwartz, S.A., Reyzer, M.L. and Caprioli, R.M. (2003) 'Direct tissue analysis using matrix-assisted laser desorption/ionization mass spectrometry: Practical aspects of sample preparation', *Journal of Mass Spectrometry*, 38(7), pp. 699–708. Available at: https://doi.org/10.1002/jms.505.

Serrano, M. *et al.* (2006) 'The ATL gene family from Arabidopsis thaliana and Oryza sativa comprises a large number of putative ubiquitin ligases of the RING-H2 type', *Journal of Molecular Evolution*, 62(4), pp. 434–445. Available at: https://doi.org/10.1007/s00239-005-0038-y.

Shah, T.R. and Misra, A. (2011) 'Proteomics', in *Challenges in Delivery of Therapeutic Genomics and Proteomics*. Elsevier, pp. 387–427. Available at: https://doi.org/10.1016/B978-0-12-384964-9.00008-6.

Shi, Y. *et al.* (2004) 'The role of liquid chromatography in proteomics.', *Journal of chromatography. A*, 1053(1–2), pp. 27–36.

Shojima, S. *et al.* (1989) 'Biosynthesis of nicotianamine in the suspension-cultured cells of tobacco (Nicotiana megalosiphon)', *Biology of Metals*, 2(3), pp. 142–145. Available at: https://doi.org/10.1007/BF01142552.

Shojima, S. *et al.* (1990) 'Biosynthesis of Phytosiderophores In Vitro Biosynthesis of 2′-Deoxymugineic Acid from l-Methionine and Nicotianamine', *academic.oup.comS Shojima, NK Nishizawa, S Fushiya, S Nozoe, T Irifune, S MoriPlant Physiology, 1990•academic.oup.com*, 93, pp. 1497–1503. Available at: https://academic.oup.com/plphys/article-abstract/93/4/1497/6085424 (Accessed: 11 November 2023).

Shroff, R. *et al.* (2008) 'Nonuniform distribution of glucosinolates in Arabidopsis thaliana leaves has important consequences for plant defense', in *Proceedings of the National Academy of Sciences of the United States of America*. USA, pp. 6196–6201. Available at: https://doi.org/10.1073/pnas.0711730105.

Shroff, R. and Svatoš, A. (2009) 'Proton sponge: A novel and versatile MALDI matrix for the analysis of metabolites using mass spectrometry', *Analytical Chemistry*, 81(19), pp. 7954–7959. Available at: https://doi.org/10.1021/ac901048z.

Sinha, A. and Mann, M. (2020) 'A beginner's guide to mass spectrometry–based proteomics', *The Biochemist*, 42(5), pp. 64–69. Available at: https://doi.org/10.1042/BIO20200057.

Smith, L.M. *et al.* (2013) 'Proteoform: A single term describing protein complexity', *Nature Methods*. Nature Publishing Group, pp. 186–187. Available at: https://doi.org/10.1038/nmeth.2369.

Spengler B., Hubert M., K.R. (1994) 'MALDI ion imaging and biological ion imaging with a new scanning UV-laser microprobe', *Proc. 42nd Annual Conf. Mass Spectrom. and Allied Topics*, p. 1041. Available at: https://scholar.google.com/scholar_lookup?title=MALDI Ion Imaging and Biological Ion Imaging with a New Scanning UV-Laser Microprobe&publication_year=1994&author=B. Spengler&author=M. Hubert&author=R. Kaufmann (Accessed: 26 November 2023).

Spengler, B. and Hubert, M. (2002) 'Scanning Microprobe Matrix-Assisted Laser Desorption Ionization (SMALDI) Mass Spectrometry: Instrumentation for Submicrometer Resolved LDI and MALDI Surface Analysis', *J. Am. Soc. Mass Spectrom.*, 13(6), p. 735.

Stoeckli, M. *et al.* (2001) 'Imaging mass spectrometry: A new technology for the analysis of protein expression in mammalian tissues', *Nature Medicine*, 7(4), pp. 493–496. Available at: https://doi.org/10.1038/86573.

Stoeckli, M. *et al.* (2002) 'Molecular Imaging of Amyloid β-Peptides in Mouse Brain Sections Using Mass Spectrometry', *Anal. Biochem.*, 311(1), p. 33.

Sturtevant, D. *et al.* (2021) 'In situ localization of plant lipid metabolites by matrix-assisted laser desorption/ionization mass spectrometry imaging (MALDI-MSI)', *Methods in Molecular Biology*, 2295, pp. 417–438. Available at: https://doi.org/10.1007/978-1-0716-1362-7_24.

Sun, C. *et al.* (2020) 'Development of a high-coverage matrix-assisted laser desorption/ionization mass spectrometry imaging method for visualizing the spatial dynamics of functional metabolites in Salvia miltiorrhiza Bge', *Journal of Chromatography A*, 1614. Available at: https://doi.org/10.1016/j.chroma.2019.460704.

Susniak, K. *et al.* (2020) 'Recent developments in MALDI MSI application in plant tissue analysis', *Acta Biochimica Polonica*, 67(3), pp. 277–281. Available at: https://doi.org/10.18388/abp.2020_5394.

Suzuki, M. *et al.* (2021) 'Development of a mugineic acid family phytosiderophore analog as an iron fertilizer', *Nature Communications*, 12(1). Available at: https://doi.org/10.1038/s41467-021-21837-6.

Svatoš, A. (2010) 'Mass spectrometric imaging of small molecules', *Trends in Biotechnology*, pp. 425–434. Available at: https://doi.org/10.1016/j.tibtech.2010.05.005.

Svatoš, A. and Mock, H.P. (2013) 'MALDI Mass Spectrometric Imaging of Plants', *The Handbook of Plant Metabolomics*, pp. 93–110. Available at: https://doi.org/10.1002/9783527669882.CH5.

Tabet, J.C. and Cotter, R.J. (1984) 'Laser Desorption Time-of-Flight Mass Spectrometry of High Mass Molecules', *Analytical Chemistry*, 56(9), pp. 1662–1667. Available at: https://doi.org/10.1021/ac00273a028.

Tachi, H. *et al.* (2009) 'Molecular characterization of a novel soybean gene encoding a neutral PR-5 protein induced by high-salt stress', *Plant Physiology and Biochemistry*, 47(1), pp. 73–79. Available at: https://doi.org/10.1016/j.plaphy.2008.09.012.

Tagliavini, M. and Rombolà, A.D. (2001) 'Iron deficiency and chlorosis in orchard and vineyard ecosystems', *European Journal of Agronomy*, 15(2), pp. 71–92. Available at: https://doi.org/10.1016/S1161-0301(01)00125-3.

TAIR (no date) *TAIR - Home Page*. Available at: https://www.arabidopsis.org/ (Accessed: 3 October 2021).

Takagi, Sei-ichi Ichi (1976) 'Naturally occurring iron-chelating compounds in oat- and rice-root washings', *Soil Science and Plant Nutrition*, 22(4), pp. 423–433. Available at: https://doi.org/10.1080/00380768.1976.10433004.

Takagi, S.I., Nomoto, K. and Takemoto, T. (1984) 'Physiological Aspect of Mugineic Acid, A Possible Phytosiderophore of Graminaceous Plants', *Journal of Plant Nutrition*, 7(1–5), pp. 469–477. Available at: https://doi.org/10.1080/01904168409363213.

Takahashi, M. *et al.* (1999) 'Cloning two genes for nicotianamine aminotransferase, a critical enzyme in iron acquisition (strategy II) in graminaceous plants', *Plant Physiology*, 121(3), pp. 947–956. Available at: https://doi.org/10.1104/pp.121.3.947.

Takahashi, M. *et al.* (2003) 'Role of nicotianamine in the intracellular delivery of metals and plant reproductive development', *Plant Cell*, 15(6), pp. 1263–1280. Available at: https://doi.org/10.1105/tpc.010256.

Tambasco-Studart, M. *et al.* (2005) 'Vitamin B6 biosynthesis in higher plants', *Proceedings of the National Academy of Sciences of the United States of America*, 102(38), pp. 13687–13692. Available at: https://doi.org/10.1073/pnas.0506228102.

Tauseef, A. *et al.* (2021) 'Proteomic Profile Mapping and Differential Expression of Protein in Ovarian Cancer', *Sains Malaysiana*, 50(12), pp. 3667–3681. Available at: https://doi.org/10.17576/jsm-2021-5012-17.

Terry, N. (1980) 'Limiting Factors in Photosynthesis', *Plant Physiology*, 65(1), pp. 114–120. Available at: https://doi.org/10.1104/pp.65.1.114.

Thiel, J. *et al.* (2008) 'Different hormonal regulation of cellular differentiation and function in nucellar projection and endosperm transfer cells: A microdissection-based transcriptome study of young barley grains', *Plant Physiology*, 148(3), pp. 1436–1452. Available at: https://doi.org/10.1104/pp.108.127001.

Thiel, J. *et al.* (2009) 'Amino acid metabolism at the maternal-filial boundary of young barley seeds: A microdissection-based study', *Planta*, 230(1), pp. 205–213. Available at: https://doi.org/10.1007/s00425-009-0935-1.

Thikekar, A.K. *et al.* (2023) 'A review on-analytical tools in proteomics', *Journal of Proteins and Proteomics*, 14(3), pp. 201–221. Available at: https://doi.org/10.1007/s42485-023-00108-6.

Thimm, O. *et al.* (2001) 'Response of Arabidopsis to iron deficiency stress as revealed by microarray analysis', *Plant Physiology*, 127(3), pp. 1030–1043. Available at: https://doi.org/10.1104/pp.010191.

Thompson, G.A. and Schulz, A. (1999) 'Macromolecular trafficking in the phloem', *Trends in Plant Science*, 4(9), pp. 354–360. Available at: https://doi.org/10.1016/S1360-1385(99)01463-6.

Tian, L. *et al.* (2009) 'Transcript and proteomic analysis of developing white lupin (Lupinus albus L.) roots', *BMC Plant Biology*, 9(1), p. 1. Available at: https://doi.org/10.1186/1471-2229-9-1.

Todd, P.J. *et al.* (2001) 'Organic Ion Imaging of Biological Tissue with Secondary Ion Mass Spectrometry and Matrix-Assisted Laser Desorption/Ionization', *J. Mass Spectrom.*, 36(4), p. 355.

Tripathi, D.K. *et al.* (2018) 'Acquisition and homeostasis of Iron in higher plants and their probable role in abiotic stress tolerance', *Frontiers in Environmental Science*, 5(FEB), p. 86. Available at: https://doi.org/10.3389/fenvs.2017.00086.

Tsukagoshi, H., Busch, W. and Benfey, P.N. (2010) 'Transcriptional regulation of ROS controls transition from proliferation to differentiation in the root', *Cell*, 143(4), pp. 606–616. Available at: https://doi.org/10.1016/j.cell.2010.10.020.

Tubert-Brohman, I. *et al.* (2013) 'Improved docking of polypeptides with glide', *Journal of Chemical Information and Modeling*, 53(7), pp. 1689–1699. Available at: https://doi.org/10.1021/ci400128m.

Turbett, G.R. and Sellner, L.N. (1997) 'The use of optimal cutting temperature compound can inhibit amplification by polymerase chain reaction', *Diagnostic Molecular Pathology*, 6(5), pp. 298–303. Available at: https://doi.org/10.1097/00019606-199710000-00009.

Turgeon, R. (2010) 'The puzzle of phloem pressure', *Plant Physiology*, 154(2), pp. 578–581. Available at: https://doi.org/10.1104/pp.110.161679.

Tyers, M. and Mann, M. (2003) 'From genomics to proteomics', *Nature 2003 422:6928*, 422(6928), pp. 193–197. Available at: https://doi.org/10.1038/nature01510.

UNIPROT (no date) *UniProt - Home Page*. Available at: https://www.uniprot.org/ (Accessed: 3 October 2021).

Vadivel, A.K.A. (2015) 'Gel-based proteomics in plants: Time to move on from the tradition', *Frontiers in Plant Science*, 6(MAY), pp. 1–4. Available at: https://doi.org/10.3389/FPLS.2015.00369/BIBTEX.

Van Bel, A.J.E. (2003) 'The phloem, a miracle of ingenuity', *Plant, Cell and Environment*, 26(1), pp. 125–149. Available at: https://doi.org/10.1046/j.1365-3040.2003.00963.x.

Van Bel, A.J.E. and Hess, P.H. (2008) 'Hexoses as phloem transport sugars: The end of a dogma?', *Journal of Experimental Botany*, 59(2), pp. 261–272. Available at: https://doi.org/10.1093/jxb/erm294.

Varkonyi-Gasic, E. *et al.* (2010) 'Characterisation of microRNAs from apple (Malus domestica 'Royal Gala') vascular tissue and phloem sap.', *BMC plant biology*, 10, p. 159. Available at: https://doi.org/10.1186/1471-2229-10-159.

Vasconcelos, M.W. and Grusak, M.A. (2014) 'Morpho-physiological parameters affecting iron deficiency chlorosis in soybean (Glycine max L.)', *Plant and Soil*, 374(1–2), pp. 161–172. Available at: https://doi.org/10.1007/s11104-013-1842-6.

Vert, G. *et al.* (2002) 'IRT1, an Arabidopsis transporter essential for iron uptake from the soil and for plant growth', *Plant Cell*, 14(6), pp. 1223–1233. Available at: https://doi.org/10.1105/tpc.001388.

Vigani, G. (2012) 'Discovering the role of mitochondria in the iron deficiency-induced metabolic responses of plants', *Journal of Plant Physiology*, 169(1), pp. 1–11. Available at: https://doi.org/10.1016/j.jplph.2011.09.008.

Vigani, G., Maffi, D. and Zocchi, G. (2009) 'Iron availability affects the function of mitochondria in cucumber roots', *New Phytologist*, 182(1), pp. 127–136. Available at: https://doi.org/10.1111/j.1469-8137.2008.02747.x.

Vij, S. and Tyagi, A.K. (2006) 'Genome-wide analysis of the stress associated protein (SAP) gene family containing A20/AN1 zinc-finger(s) in rice and their phylogenetic relationship with Arabidopsis', *Molecular Genetics and Genomics*, 276(6), pp. 565–575. Available at: https://doi.org/10.1007/s00438-006-0165-1.

Walker, J.M. (2010) 'Methods in Molecular Biology: Mass Spectrometry Imaging Principles and Protocols', in S.S. Rubakhin and J. V Sweedler (eds) *Mass Spectrometry Imaging Principles and Protocols*. Humana Press, pp. 1–481.

Walters, M.E., Esfandi, R. and Tsopmo, A. (2018) 'Potential of Food Hydrolyzed Proteins and Peptides to Chelate Iron or Calcium and Enhance their Absorption', *Foods 2018, Vol. 7, Page 172*, 7(10), p. 172. Available at: https://doi.org/10.3390/FOODS7100172.

Walz, C. *et al.* (2002) 'Evidence for the presence and activity of a complete antioxidant defence system in mature sieve tubes', *Plant Journal*, 31(2), pp. 189–197. Available at: https://doi.org/10.1046/j.1365-313X.2002.01348.x.

Walz, C. *et al.* (2004) 'Proteomics of curcurbit phloem exudate reveals a network of defence proteins', *Phytochemistry*, 65(12), pp. 1795–1804. Available at: https://doi.org/10.1016/j.phytochem.2004.04.006.

Wang, J. *et al.* (2023) 'MALDI mass spectrometry in food carbohydrates analysis: A review of recent researches', *Food Chemistry*. Elsevier, p. 133968. Available at: https://doi.org/10.1016/j.foodchem.2022.133968.

Wang, J.Y. *et al.* (2010) 'Proteomics approach to identify differentially expressed proteins induced by iron deficiency in roots of Malus', *Pakistan Journal of Botany*, 42(5), pp. 3055–3064.

Wang, X. *et al.* (2023) 'Editorial: Insight into plant spatial omics: mass spectrometry imaging', *Frontiers in Plant Science*. Frontiers Media SA, p. 1273010. Available at: https://doi.org/10.3389/fpls.2023.1273010.

Wang, Y. *et al.* (2018) 'A "soft" and "hard" Ionization Method for Comprehensive Studies of Molecules', *Analytical Chemistry*, 90(24), pp. 14095–14099. Available at: https://doi.org/10.1021/acs.analchem.8b04437.

Wasinger, V.C. *et al.* (1995) 'Progress with gene-product mapping of the Mollicutes: Mycoplasma genitalium', *ELECTROPHORESIS*, 16(1), pp. 1090–1094. Available at: https://doi.org/10.1002/elps.11501601185.

Watson, B.S. *et al.* (2003) 'Mapping the proteome of barrel medic (Medicago truncatula)', *Plant Physiology*, 131(3), pp. 1104–1123. Available at: https://doi.org/10.1104/pp.102.019034.

Weschke, W. *et al.* (2000) 'Sucrose transport into barley seeds: Molecular characterization of two transporters and implications for seed development and starch accumulation', *Plant Journal*, 21(5), pp. 455–467. Available at: https://doi.org/10.1046/j.1365-313X.2000.00695.x.

White, P.J. and Brown, P.H. (2010) 'Plant nutrition for sustainable development and global health', *Annals of Botany*, 105(7), pp. 1073–1080. Available at: https://doi.org/10.1093/AOB/MCQ085.

Wilkins, M.R. *et al.* (1996) 'From Proteins to Proteomes: Large Scale Protein Identification by Two-Dimensional Electrophoresis and Arnino Acid Analysis', *Bio/Technology 1996 14:1*, 14(1), pp. 61–65. Available at: https://doi.org/10.1038/nbt0196-61.

Williams, K.L. *et al.* (2014) 'A Sydney proteome story', *Journal of Proteomics*. Elsevier, pp. 13–23. Available at: https://doi.org/10.1016/j.jprot.2014.04.006.

Wilson, S.R. *et al.* (2015) 'Nano-LC in proteomics: recent advances and approaches', *http://dx.doi.org/10.4155/bio.15.92*, 7(14), pp. 1799–1815. Available at: https://doi.org/10.4155/BIO.15.92.

Wittek, O., Jahreis, B. and Römpp, A. (2023) 'MALDI MS Imaging of Chickpea Seeds (Cicer arietinum) and Crab's Eye Vine (Abrus precatorius) after Tryptic Digestion Allows Spatially Resolved Identification of Plant Proteins', *Analytical Chemistry*, 26, p. 19. Available at: https://doi.org/10.1021/acs.analchem.3c02428

Wu, H.P. *et al.* (2009) 'Gold Nanoparticles as Assisted Matrices for the Detection of Biomolecules in a High-Salt Solution through Laser Desorption/Ionization Mass Spectrometry', *Journal of the American Society for Mass Spectrometry*, 20(5), pp. 875–882. Available at: https://doi.org/10.1016/j.jasms.2009.01.002.

Wu, Y. *et al.* (2023) 'Technology development trend of electrospray ionization mass spectrometry for single-cell proteomics', *TrAC Trends in Analytical Chemistry*, 159, p. 116913. Available at: https://doi.org/10.1016/J.TRAC.2022.116913.

Xiong, X. *et al.* (2012) 'Data processing for 3D mass spectrometry imaging', *ACS Publications*, 23(6), pp. 1147–1156. Available at: https://doi.org/10.1007/s13361-012-0361-7.

Xu, F. *et al.* (2009) 'Use of liquid chromatography/tandem mass spectrometry and online databases for identification of phosphocholines and lysophosphatidylcholines in human red blood cells', *Rapid Communications in Mass Spectrometry*, 23(19), pp. 3243–3254. Available at: https://doi.org/10.1002/rcm.4246.

Xu, Z.R. *et al.* (2024) 'Mitigating cadmium accumulation in dicotyledonous vegetables by iron fertilizer through inhibiting Fe transporter IRT1-mediated Cd uptake', *Chemosphere*, 346, p. 140559. Available at: https://doi.org/10.1016/J.CHEMOSPHERE.2023.140559.

Yamashita, M. and Fenn, J.B. (1984) 'Electrospray Ion-Source—Another Variation on the Free-Jet Theme', *J. Phys. Chem.*, 88(20), p. 4451.

Yanagisawa, K. *et al.* (2003) 'Proteomic Patterns of Tumor Subsets in Non-Small-Cell Lung Cancer', *Lancet*, 362(9382), p. 433.

Yang, J. and Caprioli, R.M. (2011) 'Matrix sublimation/recrystallization for imaging proteins by mass spectrometry at high spatial resolution', *Analytical Chemistry*, 83(14), pp. 5728–5734. Available at: https://doi.org/10.1021/AC200998A/ASSET/IMAGES/MEDIUM/AC-2011-00998A_0008.GIF.

Yoo, B.C. *et al.* (1979) 'A systemic small RNA signaling system in plants', *Plant Cell 2004*, 16.

Yuan, J.Q. *et al.* (2008) 'New triterpene glucosides from the roots of Rosa laevigata Michx', *Molecules*, 13(9), pp. 2229–2237. Available at: https://doi.org/10.3390/molecules13092229.

Zaharieva, T.B. and Abadía, J. (2003) 'Iron deficiency enhances the levels of ascorbate, glutathione, and related enzymes in sugar beet roots', *Protoplasma*, 221(3–4), pp. 269–275. Available at: https://doi.org/10.1007/s00709-002-0051-6.

Zaharieva, T.B., Gogorcena, Y. and Abadía, J. (2004) 'Dynamics of metabolic responses to iron deficiency in sugar beet roots', *Plant Science*, 166(4), pp. 1045–1050. Available at: https://doi.org/10.1016/j.plantsci.2003.12.017.

Zaima, N., Goto-Inoue, N., *et al.* (2010) 'Application of imaging mass spectrometry for the analysis of Oryza sativa rice', *Rapid Communications in Mass Spectrometry*, 24(18), pp. 2723–2729. Available at: https://doi.org/10.1002/rcm.4693.

Zaima, N., Hayasaka, T., *et al.* (2010) 'Matrix-assisted laser desorption/ionization imaging mass spectrometry', *International Journal of Molecular Sciences*, 11(12), pp. 5040–5055. Available at: https://doi.org/10.3390/ijms11125040.

Zaima, N. (2012) 'Application of matrix-assisted laser desorption/ionization imaging mass spectrometry for the analysis of Oryza sativa rice', *Rice: Production, Consumption and Health Benefits*, 24, pp. 175–182.

Zanetti, M.E. *et al.* (2005) 'Immunopurification of polyribosomal complexes of Arabidopsis for global analysis of gene expression', *Plant Physiology*, 138(2), pp. 624–635. Available at: https://doi.org/10.1104/pp.105.059477.

Zardecki, C. *et al.* (2022) 'PDB-101: Educational resources supporting molecular explorations through biology and medicine', *Protein Science*, 31(1), pp. 129–140. Available at: https://doi.org/10.1002/pro.4200.

Zengin, T. *et al.* (2017) 'A Smart Way for Talking With Proteins; Proteomics', *MOJ Proteomics & Bioinformatics*, 5(3), p. 160. Available at: https://doi.org/10.15406/mojpb.2017.05.00160.

Zhang, C. *et al.* (2012) 'The origin and composition of cucurbit "Phloem" exudate', *Plant Physiology*, 158(4), pp. 1873–1882. Available at: https://doi.org/10.1104/pp.112.194431.

Zhang, H. *et al.* (1999) 'Combining Solid-Phase Preconcentration, Capillary Electrophoresis and Off-Line Matrix-Assisted Laser Desorption/Ionization Mass Spectrometry: Intracerebral Metabolic Processing of Peptide E in Vivo', *J. Mass Spectrom.*, 34(4), p. 377.

Zhang, H. *et al.* (2022) 'Abiotic stress responses in plants', *Nature Reviews Genetics*, 23(2), pp. 104–119. Available at: https://doi.org/10.1038/s41576-021-00413-0.

Zhang, W. and Chait, B.T. (2000) 'ProFound: An expert system for protein identification using mass spectrometric peptide mapping information', *Analytical Chemistry*, 72(11), pp. 2482–2489. Available at: https://doi.org/10.1021/ac991363o.

Zhang, X. *et al.* (2022) 'Physiological and proteomic dissection of the rice roots in response to iron deficiency and excess', *Journal of Proteomics*, 267, p. 104689. Available at: https://doi.org/10.1016/J.JPROT.2022.104689.

Zhu, R. *et al.* (2017) 'Glycoprotein Enrichment Analytical Techniques: Advantages and Disadvantages', in *Methods in Enzymology*. Academic Press, pp. 397–429. Available at: https://doi.org/10.1016/bs.mie.2016.11.009.

Zhu, X. *et al.* (2022) 'Advances in MALDI Mass Spectrometry Imaging Single Cell and Tissues', *Frontiers in Chemistry*, 9, p. 782432. Available at: https://doi.org/10.3389/FCHEM.2021.782432/BIBTEX.

Zuo, Y. *et al.* (2007) 'Bicarbonate concentration as affected by soil water content controls iron nutrition of peanut plants in a calcareous soil', *Plant Physiology and Biochemistry*, 45(5), pp. 357–364. Available at: https://doi.org/10.1016/j.plaphy.2007.03.017.

ANEXOS

Anexo I

OTRAS PUBLICACIONES

En este Anexo se indican un total de siete (7) publicaciones científicas en revistas SCI en las que he colaborado activamente, todas ellas relacionadas con las temáticas tratadas en esta Tesis Doctoral. Estos trabajos han formado parte en distintas Tesis Doctorales dentro de las líneas de investigaciones del Grupo de Fisiología de Estrés Abiótico en Plantas:

1) Gutierrez-Carbonell E, **Lattanzio G**, Albacete A, Rios JJ, Kehr J, Abadía A, Grusak MA, Abadía J, López-Millán AF **(2015)** Effects of Fe deficiency on the protein profile of *Brassica napus* phloem sap. **Proteomics** 15, 3835–3853. **Q1 IF: 4.079** (doi: 10.1002/pmic.201400464).

2) Ceballos-Laita L, Gutierrez-Carbonell E, **Lattanzio G**, Vázquez S, Contreras-Moreira B, Abadía A, Abadía J, López-Millán AF **(2015)** Protein profile of *Beta vulgaris* leaf apoplastic fluid and changes induced by Fe deficiency and Fe resupply. **Frontiers in Plant Science** 6, 145. **Q1 IF: 4.495** (doi:10.3389/fpls.2015.00145).

3) Gutierrez-Carbonell E, Takahashi D, **Lattanzio G**, Rodríguez-Celma J, Soll J, Philippar K, Kehr J, Uemura M, Abadía J, López-Millán A **(2014)** The distinct functional roles of the inner and outer chloroplast envelope of pea (*Pisum sativum*) as revealed by proteomic approaches. **Journal of Proteome Research** 13, 2941–2953. **Q1 IF: 4.173** (doi: 10.1021/pr500106s).

4) Basa B, **Lattanzio G**, Solti Á, Tóth B, Abadía J, Fodor F, Sárvári É **(2014)** Changes induced by cadmium stress and iron deficiency in the composition and organization of thylakoid complexes in sugar beet (*Beta vulgaris* L.). **Environmental Experimental Botany** 101, 1-11. **Q1 IF: 3.359** (doi: 10.1016/j.envexpbot.2013.12.026).

5) Gutierrez-Carbonell E, **Lattanzio G**, Sagardoy R, Rodríguez-Celma J, Ríos JJ, Matros A, Abadía A, Abadía J,López-Millán A-F **(2013)** Changes induced by zinc toxicity in the 2-DE protein profile of sugar beet roots. **J Proteomics** 94, 149-161. **Q1 IF: 3.973** (doi: 10.1016/j.jprot.2013.09.002).

6) Sudre D, Gutierrez-Carbonell E, **Lattanzio G**, Rellán-Álvarez R, Gaymard F, Wohlgemuth G, Fiehn O, Álvarez-Fernández A, Zamarreño AM, Bacaicoa E, Duy D, García-Mina JM, Abadía J, Philippar K, López-Millán AF, Briat JF **(2013)** Iron-dependent modifications of the flower transcriptome, proteome, metabolome and hormonal content in an Arabidopsis ferritin mutant. **Journal of Experimental Botany** 64, 2665-2688. **Q1 IF: 5.794** (doi: 10.1093/jxb/ert112).

7) Rodríguez-Celma J, **Lattanzio G**, Grusak MA, Abadía A, Abadía J, López-Millán AF **(2011)** Root responses of *Medicago truncatula* plants grown in two different iron deficiency conditions: changes in root protein profile and riboflavin biosynthesis. **Journal of Proteome Research** 10:2590-2601. **Q1** **IF: 5.113** (doi: 10.1021/pr2000623).

Anexo II

CURRICULUM VITAE

Apellidos: **Lattanzio** Nombre: **Giuseppe**

Datos personales

Fecha de nacimiento:	21-04-1976
NIE:	X9168479N
Sexo:	Varón
Dirección postal:	Calle Cineasta José María Beltrán, 15 7ºA 50018, Zaragoza
Móvil:	656646685
Correo electrónico:	giuseppe.lattanzio@gmail.com

Situación profesional actual

Organismo:	Instituto Aragonés de Ciencias de la Salud (IACS)
Dpto.:	Unidad de Proteómica
Categoría profesional:	Técnico Superior de Apoyo a la Investigación
Fecha de inicio:	enero 2013-actual

Formación Académica

Titulación Superior	**Centro**	**Fecha**
Licenciado en Química y Tecnología Farmacéuticas	Universidad de Bolonia, Italia	Jul. 2007

Máster	**Centro**	**Fecha**
Química	Universidad de Granada, España	Jul. 2008

Actividades anteriores de carácter científico profesional

Puesto	**Institución**	**Fechas**
Técnico Superior de apoyo a la investigación	Unidad de Proteómica; Instituto Aragonés de Ciencias de la Salud (IACS), Zaragoza	Ene. 2013-actual
Becario Predoctoral (Beca FPI-MINECO BES-2008-005834)	Dpto. de Nutrición Vegetal; Estación Experimental de Aula Dei (EEAD-CSIC), Zaragoza	Nov. 2008-Dic. 2012
Técnico de apoyo a la investigación	Dpto. Química Analítica; Universidad de Granada	Abr. 2008-Sept. 2008

Idiomas (R = regular, B = bien, C = correctamente)

Idioma	Habla	Lee	Escribe
Italiano	Nativo		
Español	C	C	C
Ingles	R	R	R

Participación en Proyectos de I+D financiados en Convocatorias públicas

Análisis del impacto de la historia de esporulación en la dinámica de germinación resucitación en esporos de B. subtilis

ENTIDAD FINANCIADORA: MCIN (Plan Nacional de Investigación)
DURACION DESDE: 2019 HASTA: 2022
INVESTIGADOR PRINCIPAL: Elisa Gayán Ordás (UNIZAR)

Metalomica vegetal: una aproximación a la homeostasis de metales en plantas mediante espectrometría de masas integrada (AGL2010-16515)
ENITIDAD FINANCIADORA: MICINN (Plan Nacional de Investigación)
DURACION DESDE: 2010 HASTA: 2013
INVESTIGADOR PRINCIPAL: Javier Abadía (EEAD-CSIC)

Homeostasis y transporte de Hierro – mejorando la productividad y crecimiento de las plantas (EUI2008-03618)

ENTIDAD FINANCIADORA: MICINN (Programa Nacional de Internacionalización de la I+D)
DURACION DESDE: 2009 HASTA: 2012
INVESTIGADOR PRINCIPAL: Javier Abadía (EEAD-CSIC)

Grupo Consolidado DGA (A03)
ENTIDAD FINANCIADORA: Diputación General de Aragón
DURACION DESDE: 2003 HASTA: 2011
INVESTIGADOR PRINCIPAL: Javier Abadía (EEAD-CSIC)

Estudios sobre la homeostasis de metales en plantas (AGL2007-61948)

ENTIDAD FINANCIADORA: MEC (Plan Nacional de Investigación)
DURACION DESDE: 2007 HASTA: 2010
INVESTIGADOR PRINCIPAL: Javier Abadía (EEAD-CSIC)

Estancias en Centros extranjeros y nacionales

CENTRO: **CSIC Estación Experimental de Aula Dei (EEAD)**
TUTOR: Prof. Javier Abadía Bayona
LOCALIDAD: Zaragoza PAIS: España
AÑO: 2008 DURACION: 1 mes
TEMA: Análisis de proteómica relacionada con la homeostasis de metales en plantas

CENTRO: **Universidad de Verona**
TOTOR: Dra. Daniela Cecconi
LOCALIDAD: Verona PAIS: Italia
AÑO: 2009 DURACION: 2 semanas
TEMA: Técnicas de separación de proteínas (electroforesis mono y bidimensional) e identificación de proteínas mediante Espectrometría de Masas (*Bottom-up proteomics*)

CENTRO: ***Leibniz Institute of Plant Genetics and Crop Plant Research***
TUTOR: Prof. Hans-Peter Mock
LOCALIDAD: Gatersleben PAIS: Alemania
AÑO: 2010 DURACION: 3 meses
TEMA: Identificación de proteínas mediante Espectrometría de Masas (*Bottom-up proteomics*); Distribución y localización espacial de metabolitos (*MALDI Imaging mass spectrometry*)

CENTRO: ***Leibniz Institute of Plant Genetics and Crop Plant Research***
TUTOR: Prof. Hans-Peter Mock
LOCALIDAD: Gatersleben PAIS: Alemania
AÑO: 2012 DURACION: 3 meses
TEMA: Distribución y localización espacial de metabolitos (*MALDI Imaging mass spectrometry*)

CENTRO: ***Macquarie University***
TUTOR: Prof. Paul H. Haynes
LOCALIDAD: Sydney PAIS: Australia
AÑO: 2012 DURACION: 2 meses
TEMA: Identificación de proteínas en mezclas complejas mediante Espectrometría de Masas (*Shotgun proteomics*) y estadística aplicada a Espectrometría de Masas

Artículos en Revistas Internacionales SCI

Publicaciones

1. Freire V, **Lattanzio G**, Orera I, Mañas P, Cebrián G. Component release after exposure of Staphylococcus aureus cells to pulsed electric fields (2021). **Innovative Food Science & Emerging Technologies** 74:102838 (doi: 10.1016/j.ifset.2021.102838). **Q1 IF: 7.104**

2. Rodríguez-Celma J, **Lattanzio G**, Villarroya D, Gutierrez-Carbonell E, Ceballos-Laita L, Rencoret J, Gutiérrez A, del Río JC, Grusak MA, Abadía A, Abadía J, López-Millán AF (2016) Effects of Fe deficiency on the protein profiles and lignin composition of stem tissues from *Medicago truncatula* in absence or presence of calcium carbonate. **Journal of Proteomics** 140, 1-12 (doi: 10.1016/j.jprot.2016.03.017). **Q1 IF: 3.867**

3. Gutierrez-Carbonell E, **Lattanzio G**, Albacete A, Rios JJ, Kehr J, Abadía A, Grusak MA, Abadía J, López-Millán AF (2015) Effects of Fe deficiency on the protein profile of *Brassica napus* phloem sap. **Proteomics** 15, 3835–3853 (doi: 10.1002/pmic.201400464). **Q1 IF: 4.079**

4. Ceballos-Laita L, Gutierrez-Carbonell E, **Lattanzio G**, Vázquez S, Contreras-Moreira B, Abadía A, Abadía J.López-Millán AF (2015) Protein profile of *Beta vulgaris* leaf apoplastic fluid and changes induced by Fe deficiency and Fe resupply. **Frontiers in Plant Science** 6, 145 (doi: 10.3389/fpls.2015.00145). **Q1 IF: 4.495**

5. Basa B, **Lattanzio G**, Solti Á, Tóth B, Abadía J, Fodor F, Sárvári É (2014) Changes induced by cadmium stress and iron deficiency in the composition and organization of thylakoid complexes in sugar beet (*Beta vulgaris* L.). **Environmental Experimental Botany** 101, 1-11. (doi: 10.1016/j.envexpbot.2013.12.026). **Q1 IF: 3.359**

6. Gutierrez-Carbonell E, Takahashi D, **Lattanzio G**, Rodríguez-Celma J, Soll J, Philippar K, Kehr J, Uemura M.Abadía J, López-Millán A (2014) The distinct functional roles of the inner and outer chloroplast envelope of pea (*Pisum sativum*) as revealed by proteomic approaches. **Journal of Proteome Research** 13, 2941–2953 (doi: 10.1021/pr500106s). **Q1 IF: 4.245**

7. Gutierrez-Carbonell E, **Lattanzio G**, Sagardoy R, Rodríguez-Celma J, Ríos JJ, Matros A, Abadía A, Abadía J.López-Millán A-F (2013) Changes induced by zinc toxicity in the 2-DE protein profile of sugar beet roots. **Journal of Proteomics** 94, 149-161. (doi: 10.1016/j.jprot.2013.09.002). **Q1 IF: 3.973**

8. **Lattanzio G**, Andaluz S, Matros A, Calvete JJ, Kehr J, Abadía A, Abadía J, López-Millán AF (2013) Protein profile of *Lupinus texensis* phloem sap exudates: searching for Fe and Zn containing proteins. **Proteomics** 13, 2283-2296 (doi: 10.1002/pmic.201200515). **Q1 IF: 4.399**

9. Rodríguez-Celma J, **Lattanzio G**, Jiménez S, Briat JF, Abadía J, Abadía A, Gogorcena Y, López-Millán AF (2013) Changes induced by Fe deficiency and Fe resupply in the root protein profile of a peach-almond hybrid rootstock. **Journal of Proteome Research** 12, 1162–1172 (doi: 10.1021/pr300763c). **Q1 IF: 5.001**

10. Sudre D, Gutierrez-Carbonell E, **Lattanzio G**, Rellán-Álvarez R, Gaymard F, Wohlgemuth G, Fiehn O, Álvarez-Fernández A, Zamarreño AM, Bacaicoa E, Duy D, García-Mina JM, Abadía J, Philippar K, López-Millán AF, Briat JF (2013) Iron-dependent modifications of the flower transcriptome, proteome, metabolome and hormonal content in an *Arabidopsis* ferritin mutant. **Journal of Experimental Botany** 64, 2665-2688 (doi: 10.1093/jxb/ert112). **Q1 IF: 5.794**

11. Manuela Peukert, Andrea Matros, **Giuseppe Lattanzio**, Stephanie Kaspar, Javier Abadía, Hans-Peter Mock (2012) Spatially resolved analysis of small molecules by matrix-assisted laser desorption/ionization mass spectrometric imaging (MALDI-MSI). **New Phytologist** 193, 806-815. (doi: 10.1111/j.1469-8137.2011.03970.x) **Q1 IF: 6.736**

12. Rodríguez-Celma J, Lattanzio G, Grusak MA, Abadía A, Abadía J, López-Millán AF (2011) Root responses of *Medicago truncatula* plants grown in two different iron deficiency conditions: changes in root protein profile and riboflavin biosynthesis. **Journal of Proteome Research** 10:2590-2601. (doi: 10.1111/ 10.1021/pr2000623) **Q1 IF: 5.113**

13. **Giuseppe Lattanzio**, Ana Mª García-Campaña, Jorge J. Soto–Chinchilla, Laura Gámiz–Gracia, Stefano Girotti (2008) Chemiluminescence determination of sulphadiazine in drugs by flow injection analysis using the peroxyoxalate reaction in micellar medium. **Journal of Pharmaceutical and Biomedical Analysis**: 46, 381–385. (doi: 10.1111/ 10.1016/j.jpba.2007.09.027) **Q1 IF: 2.629**

Resúmenes extendidos

1. **Giuseppe Lattanzio**, Ana Mª García-Campaña, Jorge J. Soto–Chinchilla, Laura Gámiz–Gracia, Stefano Girotti (2006) Use of flow injection analysis coupled with chemiluminescence detection for quality control of sulphadiazine in pharmaceuticals **Luminescence**: The Journal of Biological and Chemical Luminescence: 21, 347-349. **Q4 IF: 0.874**

Contribuciones a Congresos

2020 23ª Reunión Anual Asociación Española de Gastroenterología, Madrid, España

(15) Elena Piazuelo, Federico Sopeña, Samanta Arechavaleta, Irene Orera, Alberto Cebollada, Pilar Roncalés, María Luisa Hernáez, Giuseppe Lattanzio, Pilar Vadillo, Eduardo Chueca, Mª Asunción García-González, Angel Lanas. *Caracterización de los cambios en el proteóma plaquetario asociados al desarrollo de cáncer colorrectal.* (Poster)

2013 *5th Congress of the Spanish Proteomics Society* Barcelona, España

(14) Gutierrez-Carbonell EF, Takahashi D, Lattanzio G, Philippar K, Uemura M, Abadía J, López-Millán AF. *Proteomic profiles of Pisum sativum inner and outer chloroplast envelope membranes* (Poster)

(13) Giuseppe Lattanzio, Sofía Andaluz, Anunciación Abadía, Javier Abadía, Ana-Flor López-Millán. *Protein profile of Lupinus texensis phloem sap exudates: searching for Fe and Zn containing proteins* (Poster)

(12) Gutierrez-Carbonell EF, Takahashi D, Lattanzio G, Rodíguez-Celma J, Duy D, Philippar K, Kehr J, Uemura M, Abadía J, López-Millán AF. Proteomic profiles of Pisum sativum inner and outer chloroplast envelope membranes (Poster)

2012 III Jornadas de Jóvenes Investigadores en Proteómica, Santiago de Compostela, España

(11) Elain F. Gutierrez-Carbonell*, Giuseppe Lattanzio*, Jorge Rodriguez-Celma, Daniela Duy, Julia Kehr, Katrin Philippar, Ana Flor López-Millán, Javier Abadía. *Caracterización del proteoma de las envolturas interna y externa de cloroplasto de Pisum sativum* (Asistencia/Comunicación oral)

2012 *Plant Science Student Conference*, IPK Gatersleben, Germany

(10) Elain F. Gutierrez-Carbonell*, Giuseppe Lattanzio*, Jorge Rodriguez-Celma, Daniela Duy, Julia Kehr, Katrin Philippar, Ana Flor López-Millán, Javier Abadía. *Proteomic profiling of Inner and Outer Chloroplast Membranes* (Asistencia/Comunicación oral)

16th International Symposium on Iron Nutrition and Interactions in Plants Amherst, Massachusetts, USA

(9) Gutierrez-Carbonell E*, Lattanzio G*, Rellán-Álvarez, Sudre, Gaymard, Fiehn O, Abadía J, Álvarez-Fernández A, López-Millán AF, Briat JF. *Changes in flower protein and metabolite profiles in an Arabidopsis ferritin null mutant* (Poster)

(8) Rodríguez-Celma J*, Lattanzio G*, Jímenez S, Abadía J, Abadía A, Gorgorcena G, López-Millán AF. *Changes induced by Fe deficiency and Fe resupply in the protein profile of GF677 Prunus amygdalo x persica roots* (Poster)

XIV Simposio Hispano-Luso de Nutrición Mineral de las Plantas, Madrid, España

(7) Elain Gutiérrez-Carbonell*, Giuseppe Lattanzio*, Jorge Rodríguez-Celma, Ruth Sagardoy, Anunciación Abadía, Javier Abadía, Ana-Flor López-Millán. Cambios en los perfiles proteicos de raíz de plantas de Beta vulgaris cultivadas en distintas concentraciones de Zn (Poster)

(6) Gutierrez-Carbonell E*, Lattanzio G*, Rellán-Álvarez R, Sudre D, Gaymard F, Fiehn O, Abadía J, Álvarez-Fernández A, López-Millán AF, Briat JF. *Changes in flower protein and metabolite profiles in an Arabidopsis ferritin null mutant* (Poster)

2011 *The 3rd International Symposium on Frontiers in Agriculture Proteome Research: Contribution of proteomics technology in agricultural sciences*, Tsukuba, Japan

(5) Jorge RODRÍGUEZ-CELMA, Elain GUTIERREZ-CARBONELL, Giuseppe LATTANZIO, Julia KEHR, Anunciación ABADÍA, Ana-Flor LÓPEZ-MILLÁN, Javier ABADÍA. *Changes in the Medicago truncatula Stem Protein Profile as a Result of Fe Deficiency* (Presentación oral)

2011 XIX Reunión de la Sociedad Española de Fisiología Vegetal (SEFV) y XII Congreso Hispano-Luso de Fisiología Vegetal, Castelló de la Plana, España

(4) Elain Gutierrez-Carbonell, Jorge Rodríguez-Celma, Daniela Duy, Giuseppe Lattanzio, Ana Flor López-Millán, Katrin Philippar, Javier Abadía. *Chloroplast envelope proteomics* (Poster)

(3) Jorge Rodríguez-Celma, Giuseppe Lattanzio, Rubén Rellán, Anunciación Abadía, Javier Abadía, Ana Flor López-Millán. *Root proteomics and heavy metal homeostasis: Fe and Cd in the focus* (Comunicación oral)

2010 II Jornadas Bienales de Jóvenes Investigadores en Proteómica (SEProt), Córdoba, España (Asistencia)

15th International Symposium on Iron Nutrition and Interactions in Plants (ISINIP), Budapest, Hungría (Asistencia)

2009 *COST FA0603 WG1 MEETING: Technical aspects inherent to Plant Proteomics Classical and novel approaches in Plant Proteomics*, Viterbo, Italia (Asistencia)

XVIII Reunión de la Sociedad Española de Fisiología Vegetal (SEFV) y XI Congreso Hispano-Luso de Fisiología Vegetal, Zaragoza, España (Asistencia)

2007 VII Reunión Científica de la Sociedad Española de Cromatografía y Técnicas Afines (SECyTA), Granada, España (Asistencia)

2006 *The XII International Symposium on Luminescence Spectrometry*, Lugo, España

(2) Giuseppe Lattanzio, Ana Mª García-Campaña, Jorge J. Soto–Chinchilla, Laura Gámiz–Gracia, Stefano Girotti. *Use of flow injection analysis coupled with chemiluminescence detection for quality control of sulphadiazine in pharmaceuticals* (Asistencia/Poster)

2005 XXVIII Minicongreso de farmacología, Madrid, España

(1) Giuseppe Lattanzio. Fármacos inhibidores de la vasopresina. (Asistencia/Comunicación oral)

Docencia universitaria

Categoría: Personal asociado (Profesor asociado)
Régimen dedicación: General
Organismo/Empresa: Universidad de Zaragoza
Lugar: Dpto. Bioquímica y Biología Molecular, Facultad de Ciencias
Actividad: Docencia en “Bioquímica de la Nutrición” (60 horas)
Año académico: 2019-20

Categoría: Colaborador extraordinario (POD)
Régimen dedicación: General
Organismo/Empresa: Universidad de Zaragoza

Lugar: Dpto. Bioquímica y Biología Molecular, Facultad de Ciencias
Actividad: Docencia en "Técnicas avanzadas en biología molecular y celular" (2 horas);
Año académico: 2019-20

Categoría: Colaborador extraordinario (POD)
Régimen dedicación: General
Organismo/Empresa: Universidad de Zaragoza
Lugar: Dpto. Bioquímica y Biología Molecular, Facultad de Ciencias
Actividad: Docencia en "Biotecnología Clínica" (2 horas)
Año académico: 2019-20

Divulgación científica y organización de eventos

Colaborador en la realización y participación en los talleres científicos con motivo del "Dia Internación de la Mujer y la Niña en la Ciencia" en el CEIP III de Cuarte, Zaragoza, 10 de febrero de 2020

Colaborador en la realización y participación de los laboratorios científicos (Unidad de Proteomica) dentro del proyecto FECYT "Ciencias con sentidos" en ETOPIA Centro de arte y Tecnología, Zaragoza 3 de mayo de 2019

Investigación" dentro del European Researcher´s Nigth en el CaixaForum, Zaragoza 6 de noviembre de 2019

Colaborador en la realización y participación en el Taller científico dentro del proyecto FECYT "InvestIACS" en el Auditorio de Cuarte de Huerva, Zaragoza 20 de septiembre de 2018

Colaborador en la realización y participación en el Taller científico dentro del proyecto FECYT "InvestIACS" en el Centro Itaca de Andorra, Teruel 15 de noviembre de 2018

Colaborador en la realización y participación en el Taller científico de "La aventura de la Investigación" dentro del European Researcher´s Nigth en el CaixaForum, Zaragoza 6 de noviembre de 2019

Colaborador en la realización y participación en el Taller científico de "Proteínas" dentro del European Researcher´s Nigth en el CaixaForum, Zaragoza 28 de septiembre de 2018

Participación en la actividad de divulgación organizada por la Delegación del CSIC en Aragón durante las Jornadas de Puertas Abiertas en la Estación Experimental del Aula Dei, Zaragoza 18 de octubre 2011

Colaboración en las labores de organización del I Workshop de la Sociedad Española de Espectrometría de Masas (SEEM); 16 de octubre del 2007

Colaboración en las labores de organización de la VII reunión Científica de la sociedad Española de Cromatografía y Técnicas Afines (SECyTA); 17-19 de octubre del 2007

Cursos

Curso de "Formación en Prevención de riesgos Laborales" de la empresa Mas Prevención, Zaragoza mayo de 2023 (50h)

Curso de "PREVENCIÓN DE RIESGOS LABORALES PERSONAL ÁREA BIOLOGÍA CELULAR" de la Universidad de Zaragoza, junio 2020 (7 h)

Curso de "Introducción a la Bioinformática" de la Universidad Nacional de Educación a Distancia (UNED); diciembre 2019 - mayo 2020 (180 h)

Curso de "La publicación científica" de la Universidad de Zaragoza; abril y mayo 2020 (6 h)

Curso de "Bioseguridad. Nivel Básico" del Instituto Aragonés de Ciencias de la Salud (IACS); Zaragoza, 23-25 de octubre de 2019 (24 h)

Curso de "Química Forense" en el Colegio Oficial de Químicos de Zaragoza, Zaragoza 26- noviembre y diciembre de 2018 (25 h)

Curso de "Soporte vital básico y manejo del DESA (desfibrilador semiautomático)" en el IACS, Zaragoza 27-28 de septiembre de 2018 (8 h)

Curso de "Eksigent nano-micro LC 400 Systems" (HPLC) de la empresa SCIEX en Instituto Aragonés de Ciencias de la Salud (IACS); 03 de mayo 2018 (2 h)

Curso de "Reanimación cardiopulmonar (RCP), en el IACS, Zaragoza 2 de junio de 2017 (3h)

Curso de "Formación en Prevención de riesgos Laborales" de la empresa Mas Prevención, Zaragoza octubre de 2015 (30h)

Curso de "PROTEOMICS INFORMATICS: MASCOT; MAXQUANT; PROGENESIS AND SKYLINE. Pre-congress course", de la Human Proteome Organization (HUPO), Madrid, 3 y 4 de octubre de 2014 (15 h)

Curso de "I statistics for Proteomics Course" de la Red española de laboratorios de investigación en proteómica (Proteored), Madrid, 15-17 de diciembre de 2010 (16 h)

Summer School "Mineral Nutrition in photosynthetic organisms: molecular, physiological and ecological aspects", Acquafredda di Maratea (PZ) Italia, 17-20 de junio de 2009

Curso de "Introduction to Protein Biochemistry" dentro del programa de Doctorado en Bioquímica de la Universidad de Zaragoza; junio de 2009 (40 h)

Curso de "Bioquímica y Fisiología Vegetal" en la Facultad de Ciencias de la Universidad de Zaragoza en el segundo cuadrimestre del curso académico 2008-2009 (60 h)

Curso de "Español (lengua y cultura)" de la Universidad de Salamanca, octubre de 2004 (30 h)

Otros méritos

Pertenencia a Grupos de Investigación

Miembro colaborador del Grupo Consolidado de Biología Estructural (B18)	2020-actual

Pertenencia a Sociedades Científicas

SECyTA: Sociedad Española de Cromatografía y Técnicas Afines	2008-2012
SEProt: Sociedad Española de Proteómica Sociedad Española	2008-actual

Becas y ayudas de carácter competitivo

Beca SeProt "Estancias de Investigación" en el *Dept of Chemistry and Biomolecular Sciences, Macquarie* University, Sydney, Australia (2012)

Beca FPI "Estancias Breves" (FPI-MICINN) en el *Leibniz Institute of Plant Genetics and Crop Plant Research* (IPK), Gatersleben, Alemania (2012)

Beca FPI "Estancias Breves" (FPI-MICINN) en el *Leibniz Institute of Plant Genetics and Crop Plant Research* (IPK), Gatersleben, Alemania (2010)

Beca de colaboración por un periodo de investigación en el Departamento de Química Analítica, en la Facultad de Ciencia de la Universidad de Granada, España (2007-08)

Beca "Erasmus" en la facultad de Farmacia de la Universidad de Salamanca, España (2004-05)